Nano Engineered Surfaces to Control Biological Response

by

Rahul M Visalakshan

BSc Biotechnology, MSc Biotechnology and Management

A thesis submitted for the degree of

DOCTOR OF PHILOSOPHY (PhD)

School of Engineering, University of South Australia, Mawson Lakes, SA 5095, Australia

Future Industries Institute, University of South Australia, Mawson Lakes, SA 5095, Australia



University of
South Australia

May 2019

Contents

I. List of Publications ..... *ix*
a. Manuscripts Published ix
b. Manuscripts Under Revision ix
c. Manuscripts Under Preparation and Revision xi
II. List of Conference Presentations and Awards ..... *xi*
III. Awards ..... *xii*
IV. Grants ..... *xii*
V. Cover Images ..... *xiii*
VI. Summary ..... *xv*
VII. Declaration ..... *xix*
VIII. Acknowledgments ..... *xxi*
Chapter 1. Introduction and Literature Review 23
1.1. Introduction *24*
1.1.1. Biomaterials 25
1.1.2. Foreign Body Response to Biomaterial Implant 25
1.1.3. Biomaterial Immune Responses 27
1.1.4. Immune cell responses 27
1.1.5. Biomaterial - Protein-Cell Interactions 28
1.1.5.1. Protein-Surface Interactions *28*
1.1.5.2. Protein Conformational Changes *29*
1.1.5.3. Protein-Cell Interaction *31*
1.1.6. Surface Properties 32
1.1.6.1. Chemical Modification *32*
1.1.6.2. Plasma Polymerization *36*
1.1.6.3. Nano-Structural Modification *38*
1.2. Research Gap *40*
1.3. Hypothesis and Aims *41*
1.3.1. Hypothesis 41
1.3.2. Aims 42
1.3.2.1 Material Aspect *42*
1.3.2.2. Biological Response *42*
1.4. Research Outcome as Research Manuscripts (structure of the thesis) 42
Chapter 2. Downstream Influences of Oxazoline Plasma Polymerisation Conditions on Chemical and Biological Interactions 45

2.1. Abstract *48*
2.2. Introduction *48*
2.3. Experimental *50*
2.3.1. Materials 50
2.3.2. Methods 50
Plasma polymerisation *50*
Gold nanoparticle synthesis *50*
Thickness measurement *50*
Immobilization of gold nanoparticles *51*
Atomic Force Microscopy (AFM) imaging *51*
Cell culture *51*
2.4. Results and Discussion *52*
2.4.1. Thickness changes as a function of plasma polymerisation parameters ... 52
2.4.2. Stability of coatings 54
2.4.3. Gold nanoparticle binding reaction of PPOX films 55
2.4.4. Biocompatibility and cell proliferation 56
2.5. Conclusion *58*
2.6. Acknowledgements *58*
2.7. Presenting Author Biography *58*
2.8. Copy Right Permission *59*
Chapter 3. Creating Nano-Engineered Biomaterials with Well-Defined Surface Descriptors 61
3.1. Table of Contents (TOC) Graphic *63*
3.2. Abstract *64*
3.3. Introduction *64*
3.4. Materials and Methods *67*
3.4.1. Materials 67
3.4.1.1. Surface Preparation *67*
3.4.1.2. Gold Nanoparticle Synthesis *67*
3.4.1.3 Immobilization of GNPs *68*
3.4.1.4. Surface Characterization *68*
X-ray Photo Spectroscopy (XPS) 68
Thickness Measurement 68
Transmission Electron Microscopy (TEM) 68
Atomic Force Microscopy (AFM) 68
Surface Charge Analysis 69
Time-of-Flight Secondary Mass Spectrometry (ToF-SIMS) 69
3.5. Result and Discussion *69*

3.5.1. GNPs Deposition on the Model Surface....69
3.5.2 Role of Diffusion and Interaction Energy on the GNPs Binding to the Surface 71
3.5.3. Effect of pH....74
3.5.4. Well-defined Nanotopography with Equal Nanoparticle Density....77
3.5.5. Creating Uniform Surface Chemistry While Preserving Nanotopography...78
3.6. Conclusion.... 81
3.7. Acknowledgments 82
3.8. Associated Content.... 83
SI 3.9. Supporting Information 83
SI 3.10. Copy Right Permission.... 85
Chapter 4. Nanotopography-Induced Unfolding of Fibrinogen Modulates Leukocyte Binding and Activation.... 87
4.1. TOC.... 90
4.2. Abstract 91
4.3. Introduction.... 91
4.4. Results and Discussion 93
4.4.1. Model Surface with Well-Defined Nanotopography and Surface Chemistry 93
4.4.2 Fibrinogen Adsorption on Surfaces with and Without Nanotopography....96
4.4.3 Effect of Surface Nanotopography on the Conformation of Adsorbed Fibrinogen 99
4.4.4 Fibrinogen Unfolding and Mac-1 Receptor Binding 101
4.4.5 Nanotopography-Induced Unfolding of Fibrinogen Modulates THP-1 Leukocyte Binding and Activation 102
4.5. Conclusion.... 107
4.6. Experimental Section.... 108
4.6.1. Plasma Polymerization 108
4.6.2. Gold Nanoparticle Synthesize....108
4.6.3. Immobilization of Gold NPs and Overcoating....108
4.6.4. Atomic Force Microscopy (AFM)....109
4.6.5. X-ray Photoelectron Spectroscopy (XPS) 109
4.6.6. ToF-SIMS 109
4.6.7. Micro BCA 110
4.6.8. Quartz Crystal Microbalance with Dissipation (QCM-D)....110
4.6.9. Circular Dichroism Spectroscopy (CD)....111
4.6.10. Probing unfolding with antibody ELISA 111
4.6.11. In vitro Cell Culture 112
4.6.12. Selective Binding and Mac-1 Receptors Expression 112
4.6.13. Immune responses 112

4.7. Supporting Information ... *113*
4.8. Acknowledgments ... *113*
4.9. Conflict of Interest ... *113*
SI 4.10. Supporting Information ... *113*
SI 4.11. Copy Right Permission ... *116*
SI 4.12. Cover Image Published in the Journal ... *118*
Chapter 5. Hydrophobicity Mediated Serum Protein Adsorption Regulates Inflammatory Consequences to Biomaterial Surfaces ... **119**
5.1. Abstract ... *122*
Keywords: ... **122**
5.2. Introduction ... *122*
5.3. Experimental Section ... *134*
5.4. Supporting Information ... *134*
5.5. Acknowledgements ... *134*
SI 5.6. Materials ... *134*
SI 5.6.1. Materials for Plasma Polymerization ... 134
SI 5.6.2. Materials for Protein Corona Studies ... 134
SI 5.6.3. Materials for Immune Studies ... 134
SI 5.7. Supporting Materials and Methods ... *135*
SI. 5.7.1. Methods ... 135
SI 5.7.1.1. Surface Preparation ... *135*
Plasma Polymerization ... 135
SI 5.7.1.2. Surface Characterization ... *135*
X-Ray Photoelectron Spectroscopy (XPS) ... 135
Water Contact Angle ... 135
Zeta Potential Measurement ... 136
Ellipsometry ... 136
SI 5.7.1.3. Serum Protein Adsorption Studies ... *136*
Protein Corona Formation and Quantification ... 136
SDS Polyacrylamide Gel Electrophoresis (SDS PAGE) ... 136
Liquid-Chromatography Mass-Spectrometry (LC-MS) Analysis ... 137
SI 5.7.1.4. Immune response studies ... *137*
SI 5.7.1.5 Statistical Analysis. ... *137*
SI 5.8. Supporting Figures and Tables ... *138*
SI 5.9. Copy Right Permission ... *152*
Chapter 6. Tailor-Engineered Modulation of Macrophages Differentiation by Geometric and Chemical Features in Nanoporous Substrates ... **153**
6.1. TOC ... *154*

6.2. Abstract *155*
6.3. Introduction *155*
6.4. Materials and Methods *157*
6.4.1. Materials 157
6.4.2. Fabrication of Nanoporous Materials 157
6.4.3. Plasma Polymerization 158
6.4.4. Scanning Electron Microscopy 158
6.4.5. X-Ray Photoelectron Spectroscopy 158
6.4.6. Cell Culture 158
6.4.7. Inflammatory response of macrophage 159
6.4.8. Statistical Analysis 159
6.5. Results *159*
6.5.1. Fabrication of uniformly overcoated NAA substrates 159
6.5.2. Characterization of Surface Chemistry 163
6.5.3. Inflammatory responses (pro-inflammatory and anti-inflammatory) on different chemistry and nanoporosity 163
6.6. Discussion *166*
6.7. Conclusion *168*
6.8. Acknowledgment *168*
SI 6.9. Supporting Information *169*
SI 6.9.1. Macrophage Cell Count 169
Chapter 7. Nanoparticle Shape Influence on Protein Corona Formation 171
7.2. Introduction *172*
7.3. Result and Discussion *174*
7.4. Acknowledgement *179*
SI 7.5. Supplementary Information *179*
SI 7.5.1. Synthesis of SBA-15-130st (rod) 180
SI 7.5.2. Synthesis of core shell nanoparticle CD-5A (Sphere) 180
SI 7.5.3. Characterisation 181
SI 7.5.3.1. XRD *181*
SI 7.5.3.2. TEM *181*
SI 7.5.3.3. SEM *181*
SI 7.5.3.4. Graph explanation (XRD, BET, and SEM) *182*
SI 7.5.3.5. Surface Charge- Zetapotential Measurements *183*
SI 7.5.3.6. Zeta Potential *183*
SI 7.5.3.7. X-ray Photoelectron Spectroscopy (XPS) *184*
SI 7.5.4 Protein Corona Preparation 184
SI 7.5.5. SDS Polyacrylamide Gel Electrophoresis (SDS PAGE) 185
SI 7.5.6. Liquid-Chromatography Mass-Spectrometry (LC-MS) Analysis. 186

Chapter 8. Conclusion.....193
8.1. Limitations and Future Work 197
Chapter 9. Reference.....199

I. List of Publications

The following is a list of published, accepted, or submitted manuscripts that are derived from the work performed in this thesis:

a. Manuscripts Published

1. **Visalakshan, R. M.**; Cavallaro, A.; Smith, L. E.; MacGregor-Ramiasa, M.; Hayball, J.; Vasilev, K., Downstream influences of oxazoline plasma polymerisation conditions on chemical and biological interactions. *Chemeca 2016: Chemical Engineering-Regeneration, Recovery and Reinvention* **2016**, 840.
2. **Visalakshan, R. M**.; MacGregor, M. N.; Cavallaro, A. A.; Sasidharan, S.; Bachhuka, A.; Mierczynska-Vasilev, A. M.; Hayball, J. D.; Vasilev, K., Creating Nano-engineered Biomaterials with Well-Defined Surface Descriptors. *ACS Applied Nano Materials* **2018,** *1* (6), 2796-2807.
3. **Visalakshan, R. M**.; Cavallaro, A. A.; MacGregor, M. N.; Lawrence, E. P.; Koynov, K.; Hayball, J. D.; Vasilev, K., Nanotopography-Induced Unfolding of Fibrinogen Modulates Leukocyte Binding and Activation. *Advanced Functional Materials* **2019**, 1807453.
4. **Visalakshan, R.M**.; MacGregor, M.N.; Sasidharan, S.; Ghazaryan, A.; Mierczynska-Vasilev, A. M; Morsbach, S.; Mailänder, V.; Landfester, k.; Hayball, J. D.; Vasilev, K., Biomaterial Surface Hydrophobicity-Mediated Serum Protein Adsorption and Immune Responses. *ACS Appl. Mater. Interfaces* **2019**,11,31, 27615-27623

b. Manuscripts Under Revision

1. Tailor-Engineered Modulation of Macrophages Differentiation by Geometric and Chemical Features in Nanoporous Substrates

2. Nanoparticle Shape Influence Protein Corona Formation

The following is a list of publications that are not related to the work performed in this PhD thesis but published during the PhD candidature:

1. MacGregor-Ramiasa, M.; Cavallaro, A.; **Visalakshan, R**.; Gonzalez, L.; Vasilev, K., Plasma deposited polyoxazoline coatings, a versatile new class of biomaterials. *Chemeca 2016: Chemical Engineering-Regeneration, Recovery and Reinvention* **2016**, 302.

2. Gonzalez Garcia, L. E.; MacGregor-Ramiasa, M.; **Visalakshan, R. M**.; Vasilev, K., Protein Interactions with Nanoengineered Polyoxazoline Surfaces Generated via Plasma Deposition. *Langmuir* **2017,** *33* (29), 7322-7331

3. Chen, Z.; Bachhuka, A.; Han, S.; Wei, F.; Lu, S.; **Visalakshan, R. M**.; Vasilev, K.; Xiao, Y., Tuning chemistry and topography of nanoengineered surfaces to manipulate immune response for bone regeneration applications. *ACS nano* **2017,** *11* (5), 4494-4506.

4. MacGregor, M.; Sinha, U.; **Visalakshan, R. M**.; Cavallaro, A.; Vasilev, K., Preserving the reactivity of coatings plasma deposited from oxazoline precursors− An in depth study. *Plasma Processes and Polymers* **2018**, e1800130.

5. Mierczynska-Vasilev, A.; Mierczynski, P.; Maniukiewicz, W.; **Visalakshan, R**. **M**.; Vasilev, K.; Smith, P. A., Magnetic separation technology: Functional group efficiency in the removal of haze-forming proteins from wines. *Food Chemistry* **2019,** *275*, 154-160.

6. Chen, Z.; **Visalakshan, R. M**.; Guo, J.; Wei, F.; Zhang, L.; Chen, L.; Lin, Z.; Vasilev, K.; Xiao, Y., Plasma Deposited Poly-Oxazoline Nanotextured Surfaces Dictate Osteoimmunomodulation Towards Ameliorative Osteogenesis. *Acta Biomaterialia 3368394* **2019**.(**Equal contributed first author**)

7. Hopp, I.; MacGregor, M. N.; Doherty, K.; **Visalakshan, R. M**.; Vasilev, K.; Williams, R. L.; Murray, P., Plasma polymer coatings to direct the differentiation of mouse kidney derived stem cells into podocyte-and proximal tubule-like cells. ACS Biomaterials Science & Engineering 2019

8. Goswami, N.; Bright, R.; **Visalakshan, R. M**.; Biswas, B.; Zilm, P.; Vasilev, K., Core-In-Cage Structure Regulated Properties of Ultra-Small Gold Nanoparticles. *Nanoscale Advances* **2019**.

9. García, L. E. G.; MacGregor, M. N.; **Visalakshan, R. M**.; Ninan, N.; Cavallaro, A. A.; Trinidad, A. D.; Zhao, Y.; Hayball, A. J. D.; Vasilev, K., Self-sterilizing antibacterial silver-loaded microneedles. *Chemical Communications* **2019,** *55* (2), 171-174.

c. Manuscripts Under Preparation and Revision

1. Jia Guo, **Visalakshan, R. M**, Peina Huang, Xuan Zhou, Fei Wei, Zhengmei Lin, Zetao Chen, Krasimir Vasilev, Yin Xiao, Manipulating the collaboration of immune and skeletal cells using poly-ethyl-oxazoline based nano-engineered topographies for improved osteogenesis.(**Equal contributed first author**)
2. Neethu Ninan, Blessy Joseph, **Visalakshan, R. M**, Richard Bright, Nandakumar Kalarikkal, Peter Zilm, Yves Grohens, Sabu Thomas, Krasimir Vasilev, Ornamenting plasma coated 3D printed scaffolds with multi-functional nanoparticles for skin rejuvenation
3. Blessy Joseph, Neethu Ninan, **Visalakshan, R. M**, Nandakumar Kalarikkal1, Peter Zilm, Yves Grohens, Krasimir Vasilev, Sabu Thomas, Surface engineered 3D printed scaffolds for skin regeneration
4. ArghaChakraborty, **Visalakshan, R. M,** Bryan cod,Krasimir Vasilev, Hans Griesser Tailoring biocompatibility of anti-infective biomaterial coatings by designing well-defined topography.
5. **Visalakshan, R. M**, Daniel Fernandes, Melanie N MacGregor, Arthur Ghazaryan, Agnieszka Mierczynska, Svenja Morsbach, Volker Mailänder , Katharina Landfester , John Hayball, and Krasimir Vasilev. The role of surface nanotopography in protein corona formation and immune response.

II. List of Conference Presentations and Awards

1. Downstream influences of oxazoline plasma polymerisation conditions on chemical and biological interactions. Chemeca 2016: Chemical Engineering-Regeneration, Recovery and Reinvention – 2016 Adelaide, Australia, **Rahul M Visalakshan,** A Cavallaro, LE Smith, M MacGregor-Ramiasa, K Vasilev. (**Poster presentation**)

2. Adelaide Immunology Retreat – 2016 Adelaide Australia, **Rahul M Visalakshan,** John Hayball, Krasimir Vasilev. (**Oral presentation**)

3. Surface engineered nanostructured biomaterials to control inflammation, 9th World Congress on Materials Science and Engineering – 2017 Rome, Italy, **Rahul M Visalakshan,** John Hayball, Krasimir Vasilev. (**Oral presentation**)

4. Biomaterial surface modification to control inflammation: Effect of nanotopography and surface chemistry on protein adsorption and cell response. (**Oral presentation**), ICMBB 2017: 19th international conference on molecular biotechnology and biomaterials – 2017 Amsterdam, Netherlands. **Rahul M. Visalakshan,** Alex Cavallaro, John Hayball, Krasimir Vasilev.

5. Role of Biomaterial Surface Nanotopography on Protein unfolding and Immune Response. (**Oral presentation**). International Conference on Emerging Advanced Nanomaterials - Newcastle from October 30th to November 2nd, 2018. **Rahul M. Visalakshan,** John Hayball, and Krasimir Vasilev

6. Surface Engineered Nanostructured Biomaterials to Control Inflammation. Australia-China Conference of Tissue Engineering and Regenerative Medicine (ACCTERM) November 2018 in Brisbane & Cairns, Queensland. **Rahul M. Visalakshan,** Alex Cavallaro, Melanie Macgregor, John Hayball, and Krasimir Vasilev (**Oral presentation**)

III. Awards

1. Received **John A Brodie Medal 2016** from The Chemical College Board of Engineers Australia for the best paper in the discipline of chemical engineering presented at the Chemeca Conference 2016.

2. **Best Presentation Award** at ICMBB 2017: 19th International Conference on Molecular Biotechnology and Biomaterials, Netherlands.

3. **Best Presentation Award** at Australia-China Conference of Tissue Engineering and Regenerative Medicine (ACCTERM) held in November 2018 in Brisbane & Cairns, Queensland.

IV. Grants

1. FII- National Conference Travel Fund ($1500) 2016

2. International Travel grant – Student mobility ($5000) 2017, University of South Australia.

3. Australian Synchrotron Travel fund ($570) 2018

4. Australian Nanotechnology Network Overseas Travel Fellowship ($3000) 2018

5. FII- National Conference Travel Fund ($1500) 2018

6. FII Research Student Competitive External or University-wide Grant Support ($3000) 2018

7. FII-International conference travel fund ($2500) 2019

V. Cover Images

1. Advanced Functional Materials Cover Image
2. Chemical Communication Cover Image
3. Plasma Processes and Polymers Cover Image

VI. Summary

Implants are ubiquitous to modern medical practice where they are used to enhance patient's health outcomes and further improve medical treatments. However, almost all medical implants lead to tissue injury and initiate host responses such as acute or chronic inflammation as well as detrimental foreign body reactions (FBR). Protein adhesion and arrival of inflammatory cells on biomaterial surfaces are the first two steps of FBR. To overcome the risks and challenges associated with biomaterial implantation and FBR, gaining a mechanistic understanding of protein: cell: biomaterial interface interactions is crucial.

Biomaterial surface nanotopography and chemical functionalities have been shown to play a critical role in modulating the host immune response. More specifically, the effect of surface characteristics are translated through the surface adsorbed protein layer to immune cells. However, limited studies have focused on identifying the type and amount of protein that adsorbs on modified biomaterial surfaces from clinically relevant protein solutions such as human serum. Also, little is known about the adsorption-induced unfolding of proteins and the subsequent immune responses. The aim of this thesis was to investigate serum protein adsorption patterns and protein structural changes upon adsorption to surfaces with tailored surface chemistry and well-defined nanotopography surfaces to finally establish the links between biomaterial surface properties and the ensuing immune cell reactions. Biomaterial surfaces chemical properties such as different chemistry, wettability, surface charge, and physical properties such as nanotopography size, nanoporous and synergetic effect of surface chemistry, and effect of nano shape were used to study the biological responses.

This work, we addressed the challenge faced by material scientists and engineers that is to develop facile and reliable methods for the preparation of nanotextured surfaces. Plasma polymer deposition was used to generate model biomaterial surfaces in a substrate independent manner. Firstly, the plasma deposition conditions of 2-methyloxazoline were optimized. It was clearly shown that the resultant plasma polymer could be tailored for maximum biocompatibility and this process could be used to generate surface nanotopography. These plasma polymerized methyl oxazoline (Me-PPOx) coatings facilitated covalent reaction with carboxylic acid functionalised gold nanoparticles (GNP). Nearly monodispersed carboxylic acid functionalised spherical GNP with three

different diameters of 16, 38, and 68 nm were synthesized and immobilized on Me-PPOx coated surfaces. Well-defined nanotopography with an equal number particle density of three different size GNP was developed by controlling the dilution of GNP solution and immobilization time of the particles. An additional 5 nm thin Me-PPOx coating was deposited over the surface-bound GNP to provide uniform outermost surface chemistry. Surface characterization techniques such as X-ray photoelectron spectroscopy (XPS) and time-of-flight secondary mass spectrometry(ToF-SIMS) were performed to confirm the uniform outermost surface chemistry. Transmission electron microscopy (TEM) and atomic force microscopy (AFM) were used for the morphological characterization.

These well-defined nanotopographic surfaces were used to study fibrinogen adsorption unfolding, cell attachment, and immune responses. This work, demonstrated for the first time that the amount and conformational state of surface adsorbed fibrinogen, a major constituent of physiological fluids (e.g. blood), plays an important role in driving inflammatory responses to biomaterial surface nanotopography. We provide evidence that surface nanotopography modulates the level of unfolding the adsorbed fibrinogen leading to exposure of normally hidden peptide sequences that activate the Mac-1 receptor of inflammatory cells (e.g. THP-1 monocytes). Using purposely designed and tailored surface nanotopography of the controlled scale we show distinct protein unfolding patterns that could upregulate or downregulate the expression of pro-inflammatory cytokines and cell attachment. The findings presented in this thesis shed light on the missing relationship between surface nanotopography, protein unfolding, and immune responses. This work also demonstrates the possibility to employ specifically tailored surface nanotopography to achieve desired immune responses.

Next, the role played by surface chemistry on adsorption of serum protein and subsequent immune responses was investigated. Plasma polymerization surface engineering methods were employed to generate a range of model substrates with controlled chemistry, wettability and surface charge. This study provides evidence that surface hydrophilicity regulates the type and amount of protein adsorption from human serum and plays an important role in driving inflammatory responses. This study unraveled the role of surface wettability in selective protein binding and immune response. Using purposely designed and tailored surface chemistry with a range of wettability we show distinct protein adsorption patterns which could upregulate or downregulate the expression of pro and anti-inflammatory cytokines

The synergistic effect of nanoporous structures with surface chemistry modification on modulating the immune response was studied. To investigate the combinational effect of nanotopography and surface chemistry, nanoporous surfaces of controlled pore size and lateral spacing with homogeneous outermost surface chemistry of amines, carboxyl, and hydrocarbon were fabricated. The results demonstrated the differential response of macrophage in cytokine expression. The production of pro-inflammatory cytokines decreased while the production of anti-inflammatory cytokines increased many fold on surfaces modified with a combination of -COOH coating and nanopores compared to nanoporous surfaces with other chemistries. This demonstrates that macrophage differentiation can be controlled by engineering the right combination of surface nanotopography and chemistry. This data provides the knowledge that could help in tuning the biomaterial surface properties to govern the foreign body response.

Finally, the role of nanoparticle shape in protein adsorption and the formation of protein corona from serum and plasma were investigated. Mesoporous silica nanoparticles of comparable size in one of the dimensions that were either rod or sphere-shaped were exposed to human serum and plasma to study the differential adsorption patterns. A significantly larger amount of protein attached from plasma and serum on the rod-like particles compared to the spheres. Interrogation of the protein corona revealed very small amounts of adsorbed abundant proteins such as albumin and fibrinogen. Shape dependent differences in the adsorption of immunoglobulins on both protein solutions and albumin proteins from serum were also formed. These results indicate that there could be a specialization of proteins used by the immune system to recognize and clear foreign objects simply based on the invading object's shape. These findings point to the need for further detailed studies focused on understanding the specific protein adsorption patterns on nanoparticles of different shapes and the conformational state of these proteins when they encounter objects of a certain geometry. A deep understanding of these phenomena can have a profound implication on how we design nanoparticles for medical therapies.

In conclusion, the central concept of this thesis was to demonstrate the ability of nanoengineered surfaces to control biological responses. This thesis also emphasizes the importance of protein interaction studies for designing biomaterial implants that offer better clinical outcomes.

VII. Declaration

This thesis presents work carried out by myself and does not incorporate without acknowledgment any material previously submitted for a degree or diploma in any university; to the best of my knowledge it does not contain any materials previously published or written by another person except where due reference is made in the text; and all substantive contributions by others to the work presented, including jointly authored publications, are clearly acknowledged.

Rahul M Visalakshan



Signature

27/05/2019
Date

VIII. Acknowledgments

First and foremost, I would like to express my gratitude to my primary supervisor ***Professor Krasimir Vasilev*** from the School of Engineering, for supporting me for the past four years. I appreciate all his contributions of time, ideas, and funding to make my Ph.D. experience productive and exciting. I am extremely thankful to Prof. Vasilev for his patience, guidance, flexibility, sincere care, and confidence in me during my research and for allowing me to grow as a biomaterial research scientist. He is very knowledgeable and skillful and provided me guidance and training not only being my research supervisor but also trained me in the gym. I am profoundly grateful to my co-supervisors ***Professor John Hayball*** from the School of Pharmacy and Medical Sciences, ***Dr. Melanie MacGregor*** and ***Dr. Alex Cavallaro*** from the Future Industries Institute for providing enormous support and guidance towards the completion of my thesis. I would like to acknowledge the ***Australian Government Research Training Program Scholarship*** for providing me the Ph.D. scholarship

I would like to express my special appreciation and thanks to ***Dr. Akash Bachhuka*** for training me in the material engineering and plasma science lab during my first year, especially with his great patience and consideration while he was extremely busy with his Ph.D. thesis submission. I would also like to thank all the team members in "intelligent materials and devices group" and all collaborators. ***Dr. Zetao Chen*** Sun Yat-Sen University China, ***Professor Yin Xiao*** Queensland University of Technology, ***Professor Katharina Landfester, Professor Volker Mailänder, Dr. Svenja Morsbach*** and ***Dr. Kaloian Koynov*** Max Planck Institute for Polymer Research, ***Dr. Agnieszka Mierczynska-Vasilev*** The Australian Wine Research Institute, ***Dr. Emma P. Lawrence*** University of South Australia Cancer Research Institute and ***Dr. Salini Sasidharan*** University of California, for being great colleagues which resulted serval quality research publications.

I also would like to acknowledge the funding body for this research, the ***Australian Research Council*** for DP15104212 and DP180101254, ***NHMRC*** for Fellowship APP1122825 and Project grant APP1032738, and the ***NIH*** grant EB-002027.

I would like to express my thanks to my friends in Adelaide**,** ***Ms. Nishtha Gaur, Ms. Laura García, Dr. Hanieh Safizadeh, Mr. Javed Naderi, Mr. Kola Ostrikov, Mr. Argha Chakraborty, Mr. Shankar Ganesh,*** and ***Dr. Krishna Shankar*** for providing

support and friendship through good and bad times. You guys made my life outside research colourful and joyful. Those nights out and movie nights will be missed and will be the memories to cherish for a lifetime.

I have been blessed with a very caring and supportive family. I thank my parents for their love, support, prayers, and encouragement throughout my life. I thank my sister Viji, parents-in-law, and brothers-in-law for their great support and care.

Finally, the pillar of my life, my wife, best friend, teacher, and soulmate, Salini. I found it difficult to express my gratitude to her because it is infinite. Halfway through my Ph.D., we went through some tough periods of missing each other since she had to move to the US for her Postdoc. Despite the busy stressful life, separation by the distance and time differences, she has been always there to take care and support me in my research and personal life. She has seen me through the happiest and toughest times of my entire Ph.D. process, and without her love, support, motivation, and inspiration, I would have lost. I love you and owe you this thesis!



Chapter 1. Introduction and Literature Review

1.1. Introduction

All implanted materials initiate a host response or foreign body reaction (FBR) upon insertion into a living organism.[1] The implantation and associated tissue injury trigger a succession of host reactions including blood-material interactions, provisional matrix formation, acute and chronic inflammation, development of granulation tissue as well as fibrous capsule growth.[2-8] The adsorption of host proteins occurring immediately after implantation and the accumulation of inflammatory cells on biomaterial surfaces are the first two key reactions that govern the whole immune response.[9]

In the last few decades, biomaterial research has been invested in engineering biomaterials with different surface chemistries and topographies in order to control protein adsorption and cellular behaviour such as adhesion, proliferation, and differentiation.[10-12] However, in-vitro studies often report contradictory, incomplete or unclear results and most of them failed to reproduce the results in–vivo.[13, 14] These discrepancies are mainly due to the fact that the majority of studies were conducted on a single or simple mixtures of protein prepared in a buffer solution which failed to account for competitive protein adsorption processes occurring in clinically relevant, yet complex biological medium such as human serum.[12] Another aspect that has too often been overlooked is the role played by the proteins conformational state once adsorbed to the biomaterial surface. Understanding what factors lead to protein unfolding is important because the state of the protein layer is an important cue in guiding immune cell adhesion and triggering an immune response. Therefore, a complete understanding of the effects of biomaterial surface properties on human serum adsorption, protein unfolding, and the subsequent immune response is essential for the development of a future generation of implantable devices with improved biocompatibility capable to enhance tissue regeneration.

Our current knowledge of the factors affecting materials biocompatibility is incomplete and does not support the systematic development of biocompatible implant surfaces with tailored immunomodulatory properties. According to Williamset.al 2009 “Biocompatibility is the ability of the material to perform with an appropriate host response in specific application”[15]. The size, shape, composition, surface characteristics such as wettability, topography, and chemistry of a biomaterial implant all

influence its overall biocompatibility. [10, 16] Therefore, the proposed research focuses on designing biocompatible biomaterials by engineering biomaterial surfaces with defined topography and controlled chemistry. The study will then investigate the effect of this defined nanotopographic profile and chemical signatures on serum proteins adsorption, protein unfolding, and immune cell responses.

1.1.1. Biomaterials

Biomaterials are widely used in modern medical practice to resolve a range of healthcare issues and enhance patients' quality of life. Biomaterials are primarily used for medical implant devices, tissue engineering scaffold's and drug delivery platforms.[17, 18] Each year millions of people undergo surgical procedures that involve implantation of medical devices, such as prosthetic implants, catheters, cardiovascular stents and pacemakers to replace, restore or enhance the function of damaged tissues or organs.[17] The global orthopedic implant market was valued at USD 4.3 billion in 2015 and is forecast to reach USD 6.2 billion by 2024.[19] The surge in lifestyle-related diseases such as cardiovascular disease also increases the demands for coronary stents, which have become a standard for an angioplasty procedure. Transparency market research estimated that the global biomaterials market value will reach USD 33.6 billion by 2019.[20] This rising need for implantable medical devices is leading to a significant increase in the demand for biocompatible biomaterials.

Biomaterials consist of a wide range of materials, with different function and structural features, Chosen for their bulk mechanical properties, such as flexibility and strength, modern biomaterials commonly consist of metals, ceramics, semiconductors, polymers as well as synthetic coatings.[21] Despite the large variety in the range of available biomaterials, they all share one common challenge. They are foreign to the body and therefore tend to induce adverse immune reactions as well as inflammation that may lead to fibrotic encapsulation and rejection of the implant.[18] Extensive research has been carried out over the last decades in the field of surface modification with the underlying aim to minimize the unwanted immune response and enhance the in-vivo performance.[22, 23]

1.1.2. Foreign Body Response to Biomaterial Implant

Biomaterial implantation is typically carried out through a surgical procedure. It causes injury to vascularised tissues or organs and results in blood and body fluids coming

in direct contact with the biomaterial surface. Implantation is followed by a series of physiological events including the inflammatory responses that determine the fate of the implant (Figure 1). [1, 8] As a response to injury, blood proteins adsorb on the biomaterial surface by the Vroman effect, the phenomena of rapid protein adsorption and desorption (Figure 1A).[24] Biomaterial surfaces are therefore covered with a layer of serum proteins before immune cells come in contact. [3, 9] At the initial stages immediately following implantation, blood-material interaction occurs and proteins, including fibrinogen, albumin, complement proteins, fibronectin, vitronectin, and globulins adsorb to the implant surface. [3, 25-27] The reaction of immune cells to the implant depends on the level, type and conformational changes of the adsorbed proteins and these are dictated by the surface properties of the biomaterial. [2, 28]

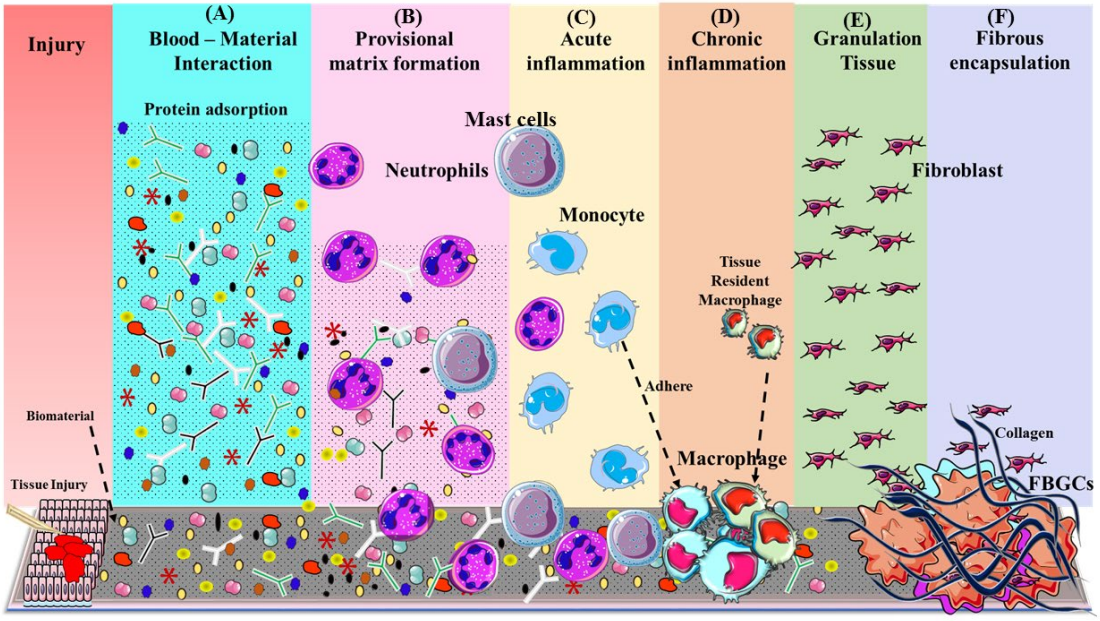

Figure 1: Foreign body response to biomaterial implantation. The FBR is a combination of protein adsorption, and acute and chronic phases of inflammation, which may lead to the granulation and fibrous encapsulation to form a foreign body giant cell formation and implant rejection.

The layer of surface adsorbed blood proteins mediates the formation of the provisional matrix (blood clot) consisting of cytokine, growth factors and chemokines which are capable of recruiting innate immune cells (Figure 1B). [2, 29] Depending on the type of biomaterial implanted and the extent of the injury, provisional matrix formation is followed by acute or chronic inflammation. [2, 3, 29] Acute inflammation is characterised by fibrinogen adsorption, histamine release, mast cell degranulation and the activation of neutrophils (Figure 1C).[30, 31] Degranulating mast cells release

interleukins - 4 and 13 which in turn control the level of foreign body reaction.[32, 33] Histamine associated phagocyte recruitment and their fibrinogen-assisted adhesion to the implant surface regulate the inflammatory response to the biomaterial.[2, 34, 35] Acute inflammation becomes chronic inflammation at the implant site upon the recruitment of other inflammatory cell types such as tissue-resident macrophages and undifferentiated monocytes (Figure 1D).[3] Macrophages and neutrophils try to phagocytose the damaged tissues and the biomaterial itself but this attempt fails due to the large size of the biomaterials.[15] In the next stage, acute and chronic inflammation causes the granulation of tissue and infiltration of fibroblast and matrix collagens which may lead to the formation of a fibrous capsule (Figure 1E). Subsequently, these macrophages fuse with each other to form foreign body giant cells (FBGC) on the implant surface and attract fibroblasts to produce matrix collagens (Figure 1F),[30] a type of chronic tissue inflammation to foreign bodies.[2, 5, 36, 37] This capsule physically separates the implanted biomaterial from the host tissue and can lead to implant failure. [2, 3, 37, 38]

1.1.3. Biomaterial Immune Responses

Over the last few decades research reports demonstrated that surface physical properties such as chemistry and nanotopography strongly affect cellular behaviour such as adhesion, proliferation, and differentiation.[39, 40] The majority of these published studies have used cells such as fibroblast and osteoblasts to investigate cellular responses and were therefore irrelevant for FBR studies,[41, 42] since innate immune cells such as neutrophils, monocytes, and macrophages are the first cells to arrive on the biomaterial surfaces after blood material interaction and protein adsorption.[42] The most recent research has since emphasized regulating the cellular response from macrophages and neutrophils to resolve biomaterial post-implantation inflammation and facilitate integration.[29, 43, 44].

1.1.4. Immune cell responses

Innate immune cells such as neutrophils and monocytes are the first line of defense that initiate the immune response to the foreign body.[22, 45] Similar to the human body response to microbes, a biomaterial as a foreign element also causes neutrophils and monocyte to secrete pro-inflammatory cytokines. These pro-inflammatory cytokines prompt the differentiation of monocytes into macrophages (monocyte-derived macrophages (MDM)) the chief scavenger cell type. Also more tissue-resident

macrophages will be recruited to the implantation site in response to chemoattractants such as chemokines and cytokines.[29, 46] The activated macrophages can switch polarization states to pro-inflammatory M1 and anti-inflammatory M2 in response to their microenvironment.[29] The M1 macrophages and neutrophils secrete pro-inflammatory cytokines IL-1β, IL-6, TNF-α, and IL-8. Even though the initial inflammatory response may be beneficial, the prolonged presence of M1 will lead to a severe FBR and result in chronic inflammation and the failure of the biomaterial integration.[47] In contrast, M2 macrophage secretes anti-inflammatory cytokines such as IL- 10 and IL-1ra and consistently express scavenger and mannose receptors (CD206) and arginase.[48, 49] These anti-inflammatory cytokines play a major role in the suppression of inflammatory response and tissue remodeling by inducing the production of transforming growth factor-b (TGF-b).[50] Sustained by the presence of anti-inflammatory cytokines and growth factors, the tissue remodeling response will prevent fibrous tissue formation and improve biomaterial integration allowing it to perform its intended function.[29, 51]

1.1.5. Biomaterial - Protein-Cell Interactions

One promising approach to avoid the inflammatory reaction resulting from biomaterial implantation is to control the initial protein adsorption by tailoring the implants physio-chemical surface properties.

1.1.5.1. Protein-Surface Interactions

Blood serum proteins are the first to be exposed to the implant surface well before immune cells. Immediately after the implantation, a layer of blood serum protein forms on the surface.[12, 52] The type, amount and conformational state of the adsorbed proteins significantly influences and mediates the subsequent biomaterial-cell interaction and foreign body reaction which can cause deleterious health effects. [2, 4, 29, 45] A large body of research over the years has taken approaches to develop protein resistant engineered surfaces to resolve this ubiquitous problem. Several works have demonstrated the ability of advanced stealth organic adlayers such as oligo- and polyethylene glycol (OEG and PEG) to minimize the protein fouling to an ultra-low (a few ng cm^2) level.[12, 14] However, most of these experiments were conducted using single protein types. Typically, model proteins such as albumin or fibrinogen are selected based on their physicochemical features (e.g. isoelectric point, molecular weight) to test surface absorptivity and understand the modified surfaces role in biological processes.[14, 52]

For instance, fibrinogen, a large plasma glycoprotein plays a major role in the coagulation cascade and is often used to investigate subsequent platelet adhesion.[53] Most studies of protein adsorption to surfaces were conducted in biologically irrelevant buffered solutions of single or multiple proteins in phosphate buffer with different concentrations. Unfortunately, not many studies have been conducted with biologically relevant proteinaceous media such as blood serum or plasma. Even the works reporting great success in the preparation of antifouling coatings capable of preventing protein fouling were mostly conducted with model proteins in buffer solution and therefore failed to account for the competitive adsorption process in clinically relevant complex protein such as serum or plasma.[12, 14] Thus, there is a need to investigate the protein adsorption and subsequent immune response of newly developed surface coatings in serum and plasma to meet the practical challenges.

1.1.5.2. Protein Conformational Changes

As mentioned above the adsorbed serum proteins cover the implant surface with different types of proteins mostly albumin, fibrinogen, IgG, and fibronectin as shown in (Figure 2A). [54-58] Recent studies have proven that upon adsorption to the surfaces, the protein may alter their conformational state and unfold to expose cryptic epitopes which are normally hidden in the folded state [35, 59-63]. Such surface-mediated conformational change has been observed using sodium dodecyl sulfate (SDS) elution, [64, 65] 'scanning force' microscopy, [66, 67] and scanning angle reflectometry.[68, 69] Studies have shown that unwanted reactions such as foreign body reactions, coagulation, and inflammation are due to the conformational changes of the adsorbed protein (Figure 2B). [9, 61] Proteins adsorbed on modified biomaterial surfaces may influence the protein unfolding and expose the hidden cryptic epitopes, which act as an epitope for the immune cells to attach and lead to the activation of immune response by the production of pro-inflammatory cytokines (Figure 2C).[70, 71]

Among plasma proteins, fibrinogen has been recognized as a key mediator of inflammatory responses as well as platelet activation, blood coagulation, and leukocyte binding.[27, 72] Interestingly, it has been recently shown that nanoparticles (NPs) in the

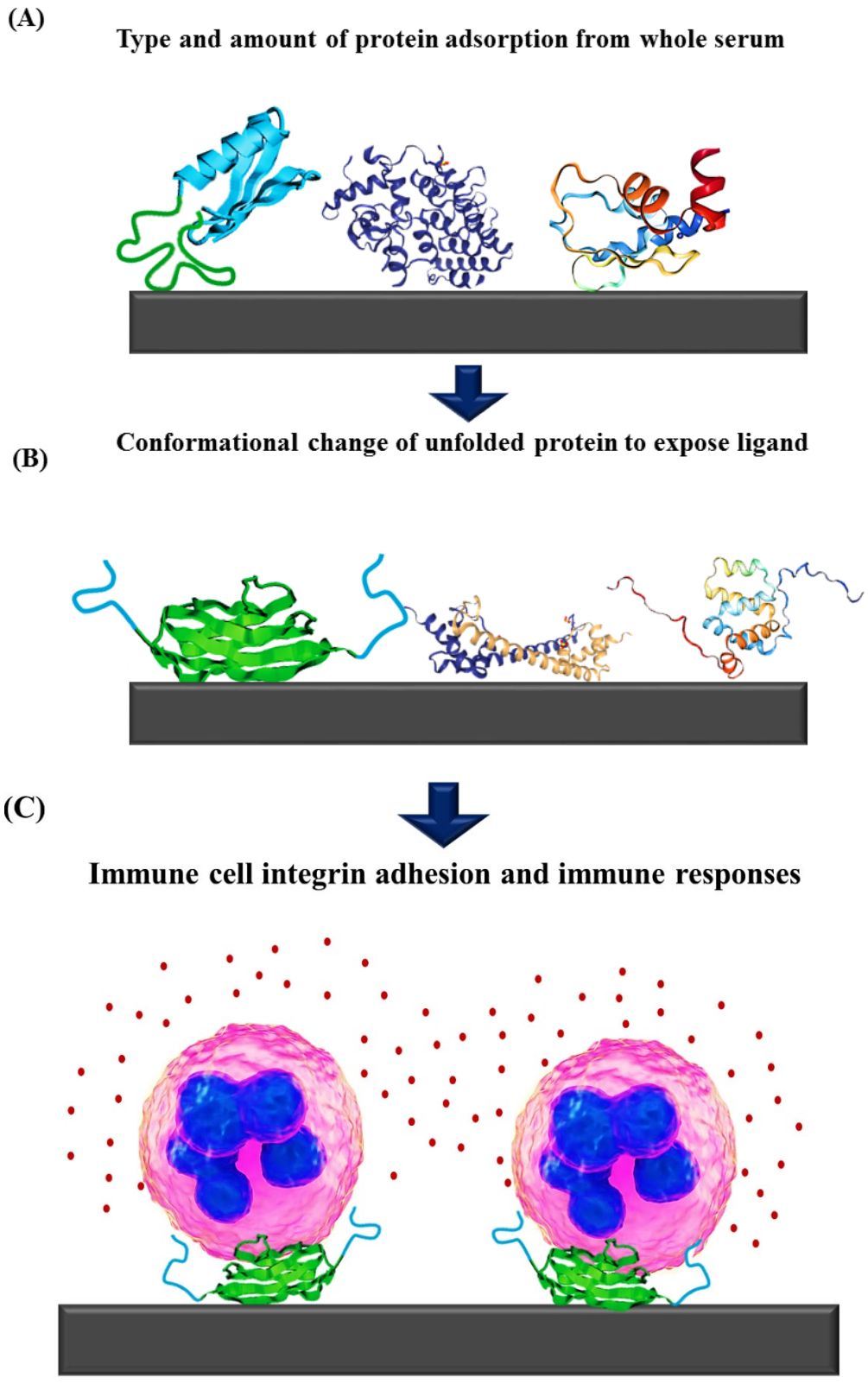

Figure 2: Schematic representation of biomaterial- protein-cell interaction.

solution can induce the unfolding of fibrinogen thus promoting inflammation.[70] More specifically, it has been shown that the denaturation of fibrinogen exposes P1 (γ190–202), P2 (γ377–395), short sequences on the D domain, which are potential inflammatory

epitopes. [73, 74] The 13 amino acid P1 sequence is hidden in normal or soluble fibrinogen. The adsorption and the conformational change of fibrinogen cause the exposure of P1and P2 epitopes.[35, 75, 76] The interaction of integrin Mac-1 (CD11b /CD18) with P1 (γ190–202), and P2 (γ377–395) induces phagocyte accumulation and thus adsorbed fibrinogen becomes pro-inflammatory.[35, 62, 74] Immediate adsorption and the conformational changes of predominant serum protein fibrinogen on implant surfaces may lead to inflammation.[9, 74] However, there is no record yet about the conformational behavior of fibrinogen on nanostructured surfaces and whether surface-mediated unfolding could also be responsible for the resultant immune responses.

Even though the literature shows that biomaterial physiochemical surface properties have a significant effect on the adsorbed protein-binding strength, orientation, conformational change as well as type and amount of the bound proteins, the subsequent responses from the immune cells is still not clear. [35, 76-79] Roach.et.al investigated the effect of surface properties on the extent of secondary protein structure alteration using grazing angle infrared (GA-FTIR) analysis on hydrophobic and hydrophilic surfaces with fibrinogen and albumin. A greater extent of structural deformation was observed on hydrophobic surfaces for both proteins.[80] Another study conducted by Clarke.et.al demonstrated the surface chemical property dependent conformational changes of fibrinogen.[81] In summary not only the type and amount of protein adsorption, the orientation and unfolding of adsorbed protein also influence the immune cell attachment and subsequent immune response of a biomaterial surface.[82] Therefore, it is important to study the unfolding of proteins upon adsorption to biomaterial surface modified with various surface chemistries and nanotopographical features.

1.1.5.3. Protein-Cell Interaction

Recently, surface topography and chemistry have been studied intensively in the context of neutrophil and macrophage modulation and polarization state. Studies have shown that the biomaterial surfaces physiochemical properties such as size, shape, charge and wettability influence the immune response from macrophage and neutrophils.[10, 44, 83, 84] Most of these published studies have relevance only when cells are cultured in-vitro, because immediately after implantation blood material interaction occurs and proteins cover the pristine biomaterial surfaces, therefore, the immune cells are likely to never see the implanted biomaterial surfaces.[13] Hence, the type, amount and

conformational state of the adsorbed protein are expected to be the major factors that dictate the immune response. Recent studies have also demonstrated that adsorption may cause conformational change in the protein structure and result in the exposure of ligands that can differentially bind and activate integrins. This may, in turn, result in immune cells producing inflammatory cytokines and chemokines through integrin-ligand interactions.[22, 29, 70] Integrin's are membrane receptors that are present on the surfaces of leukocytes and neutrophils. Macrophage differentiation antigen-1 (Mac-1) and lymphocyte function-associated antigen-1 (LFA-1) are β2 integrins made of α and β subunits.[85, 86] These integrins bind to the corresponding ligands on denatured proteins and leads to immune activation.[70, 87]

In summary, for the design of a future generation of biomaterials with better biocompatibility, it is necessary to study the protein adsorption from clinically relevant biological solution such as total human serum or plasma to incorporate the competitive protein adsorption patterns.[12, 14] Furthermore, future studies should also investigate the role of protein conformational changes on different physiochemical properties to understand the initiation of immune response via ligand-integrin interaction and protein unfolding.

1.1.6. Surface Properties

As the success of biomedical implantation and its fate is guided by the biological interactions occurring at its surfaces, extensive research has been carried out over the last decades on surface modification approaches to control the immune response. Studies have reported that the biomaterial surface nanotopography and chemical functionalities play a critical role in modulating the host immune response.[2, 88-90]

1.1.6.1. Chemical Modification

Surface chemical modification has been generally applied to generate different functional groups which in turn provide different surface wettability and surface charge (Figure 3). While all these parameters are known to affect the biological responses, the current state of knowledge is incomplete and does not allow for the predictive design of failure-proof implants.

A large variety of strategies have been developed to modify biomaterial surfaces with functional groups, in particular with carboxyl (−COOH), hydroxyl (−OH), amino (-

NH2), and methyl (−CH3) groups as they are also the principal functional groups present on biomolecules.[10, 52, 91] Among the chemical modifications used to generate biocompatible materials, poly (ethylene glycol) (PEG) remains the gold standard, while new alternatives such as poly oxazolines (POX), amphiphilic and polyzwitterions have also been explored as a strategy to create antifouling surfaces.[14] Tremendous effort has been devoted over many years in creating antifouling surface chemistries surfaces to inhibit protein adsorption and thereby avoid unwanted immune responses and FBR.[14] However, suppressing protein adsorption altogether is not necessarily the best way to control the immune response.[71, 92] In fact, some type of proteins are beneficial and known to promote implant integration.[56, 93] It is, therefore, necessary to gain a deeper understanding of the mechanism by which surface chemistry direct specific protein adsorption and their denaturation.[71]

One of the important features affecting protein's adsorption on a biomaterial that is directly linked to surface chemistry is the surface charge.[52] The surface charge influences the rate of protein adsorption, the amount, type, structural, and conformational changes of adsorbed proteins by influencing the electrostatic interaction between the proteins and the biomaterial surfaces.[94] In a physiological medium such as blood, serum, or plasma the surface charge for the solid biomaterial is generally negative due to the electrostatic double-layer present around the solid surface. Whereas, the surface charge for the protein molecules present in these physiological mediums is complex due to uneven charge distribution, the presence of differently charged surface domains, and the difference in isoelectric point for various protein molecules.[94-96] For instance, the isoelectric point for Alpha-1-acid glycoprotein 1 is 4.74 while that of Ig gamma-1 chain C region is 8.18. This means that the Alpha-1-acid glycoprotein and the Ig gamma-1 chain C regions are negatively and positively charged, respectively, at the physiological pH of 7.4. The variety in protein surface charge observed under physiological conditions limits our capacity to gain a mechanistic understanding of the influence a biomaterial surface charge has on protein adsorption. Most often, biomaterial surfaces used in research studies (glass, silica, and gold) are negatively charged under physiological conditions while most of the serum proteins (e.g., albumin, fibrinogen, and immunoglobulin) are also negatively charged.[94, 97] However, zwitterionic biomaterial surfaces that contain sites of opposite charge, such as Ca2+ and OH−, have been also developed.[98] Even though most proteins may have an overall negative charge, they all contain both

negatively or positively charged functional groups (e.g., amino, carboxyl, carbonyl).[99] Therefore, electrostatic interactions between the biomaterial and protein surfaces can either enhance or suppress protein adsorption depending on the solid surface composition and the type and direction of proteins in the vicinity of the surface.[97, 100, 101] Furthermore, the surface charge of a solid biomaterial surface also impacts the conformation and orientation of adsorbed proteins, which can subsequently affect the protein's biological functions and immune response. [11, 97] For all these reasons, there is no consensus on the effect of surface charge may have on the formation of proteins add-layers from complex body fluids.

Another surface property related to surface chemistry is wettability. It is widely observed that cell adhesion and subsequent immune responses are generally greater on hydrophilic surfaces.[102-104] On the other hand, many polymers commonly used for the preparation of biomaterials are hydrophobic in their native state and require surface modification or wetting procedures before cell studies.[105] Similar to the surface charge, the influence of wettability on protein adsorption is complex, due to the presence of both hydrophobic and hydrophilic domains in protein molecules.[99] Generally, proteins adsorb onto hydrophobic solid surfaces to a greater extent and more strongly than onto hydrophilic surface.[11, 97] However, adsorption of proteins such as glycoprotein is inhibited onto hydrophobic surfaces due to the presence of vast number hydrophilic domains on the protein's surface.[11, 97] In contrast, serum proteins such as vitronectin have been found to have a strong affinity towards hydrophilic surfaces.[102] The hydrophilicity of solid biomaterial surfaces varies depending on surface composition and topography.[11] The hydrophobicity of surfaces may also influence the bioactivity of adsorbed proteins by adversely affecting their conformational changes.[80] Overall, there is little doubt that cell responses can be modulated by tailoring the wettability of solid biomaterial surfaces. However, the influence of hydrophobicity on biomaterial-protein interactions has not been systematically investigated before. This is because surface wettability is a complex function of both chemistry and topography, as detailed below. In order to understand the role of surface wettability on protein adsorption, it is therefore necessary to control both chemistry and topography independently.

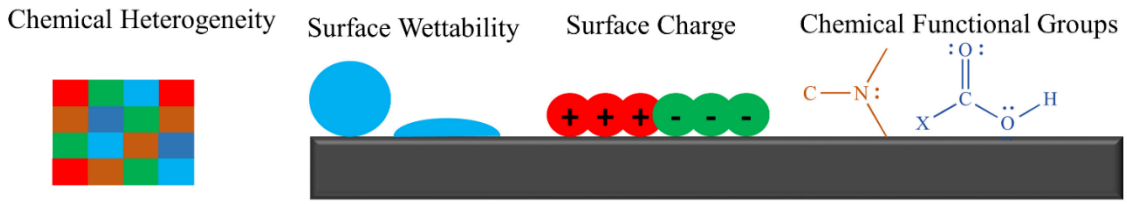

Figure 3: Illustration of surface chemical modification to generate a surface with different properties such as wettability, charge and different functional groups.

For all the reasons described above, it is clear that the role played by surface chemistry on directing the nature of the protein add-layer is intricate. The picture is further complicated by technical constraints limiting the ability to produce model surfaces with a wide range of well-controlled surface chemistries. Most recent studies have reported chemical modification techniques such as self-assembled monolayer (SAM), chemical graft modification, layer-by-layer (LBL) and physical adsorption modification.[9] However, each technique has its benefits and drawbacks as summarized below.

Chemical graft methods modify surfaces by chemically immobilizing compounds onto the surface via covalent binding which provides long-term stability. However, the toxic monomer residues left in the grafted surfaces and the need for high graft densities limit the practical application of this approach [9]. Physical adsorption methods modify surfaces by dip coating to form a thin film coating. , The major drawback, in this case, is the poor long term stability [9]. Self- assembled monolayers (SAM) modify the surface by activating the bulk material surface and subsequently grafting polymers onto the activated surface [106]. SAM provides well-ordered functionalities onto the surface and can achieve good control over functional group patterns and densities.[107] This method is, however, limited to only gold or silver coated surfaces as it relies on thiol reactions.[9] Other methods such as layer-by-layer deposition (LBL) needs an atomic layer deposition (ALD) face other limitations. The former is only applicable to charged surfaces,[108] while the latter is not versatile in that it can only achieve a limited range of surface chemistries. In short, the requirement of the special substrate, residues of organic solvents and poor choices of different chemistry are the major drawbacks of the commonly used surface modification techniques.

Another prevailing concern is the transferability of these surface functionalisation approaches to clinically relevant platforms or devices. Most *in-vitro* investigations have been conducted on a limited range of model surfaces such as silicon, glass, and gold .

However, these are not materials of choice for implants because they do not have the required bulk properties. For optimum strength and flexibility implants generally consist of metals such as titanium, steel, ceramic and semiconductors. Thus, there is a need for developing surface modification techniques applicable to real implant materials.

1.1.6.2. Plasma Polymerization

Plasma-assisted surface functionalization can be used to overcome the common technical limitations mentioned above. Plasma polymer deposited surface functionalization, modifies the surface with a thin film coating in nanometer range, using radio frequency power to excite gases into the energetic state.[109, 110] Plasma consists of highly energetic molecules, molecular fragments, ions, radicals, and free electrons. This plasma can be deposited on solid surfaces such as metal, plastic or any other material that comes in contact with them, and it changes the material's surface properties.[110] Therefore, this technique is a substrate independent method and can be used to create a thin polymer like film on any model surfaces.[111] A range of volatile organic precursors can be used to create polymeric film coating, resulting ina variety of functional groups on surfaces at low or atmospheric pressure[112]. Furthermore, this surface modification technique is a one-step dry procedure, and require very minimal amount of organic precursors, and does not produce liquid organic waste. Therefore, this technique is environmentally friendly and very cost-effective.[112, 113] As mentioned before, this technique offers the capacity to deposit same surface chemistry at a given condition on any type of substrate material. This substrate independence is possible because, after the initial deposition of a few angstroms on the material, the film growth becomes substrate independent.[111] This special feature makes the plasma polymer coating technique, the most favourable choice in biomedical applications, compared to the commonly used surface modification techniques such as layer-by-layer (L-b-L) and self-assembled monolayers (SAMs).[108] These techniques require highly specific substrate properties such as intrinsic chemistry of the base material, and charged surfaces, which hinders the opportunities for real-world applications.[114]

Plasma polymer deposition not only provides different chemical functionality, to study and modulate the complex biological responses, such as protein binding, and immune responses[115] but this technique also helps to precisely control the wettability, surface charge, and stiffness of the surfaces. These physiochemical properties are also

known to regulate the biological responses.[93, 114] Additionally, this technique can be used to generatenovel cell guidance surfaces and to underpin new bio-sensing platforms.[110, 116] Capacitively coupled parallel plate plasma chamber was used with an array of organic precursors including allylamine, octadiene, aldehyde, ethanol, acrylic acid, and perfluorooctane to modify surfaces for various applications.[110] These coatings demonstrated distinctive chemical functions, namely, amines, hydroxyls, carboxylic acids, ketones, etc.[117] The above mentioned plasma polymers have been widely used to investigate the systematic effect of surface chemistry on many biological processes such as bio-functionality of surface-adsorbed proteins, [118] the differentiation of embryonic,[119] kidney,[120] dental pulp,[121] and human adipose-derived stem cells [93]as well as the deposition of collagen by primary human dermal fibroblasts.[122]

In addition, the reactivity of the added chemical groups can be used to create surfaces with the specific binding capacity to selected ligands or proteins to develop diagnostic tools.[118, 123, 124] Similarly, fine-tuned chemical functionality facilitated by plasma polymers can be used to adsorb gold and silver nanoparticles to generate model nanotopography surface, with controlled nanofeatures size and density to study various biological responses.[125] A uniform and gradient nanotopography can be generated, using electrostatic binding of gold or silver nanoparticles coated with mercaptosuccinic acid to allylamine plasma polymers, or covalent binding to oxazoline-based coatings.[126] Additionally, the plasma polymerization provides the capacity to preserve the surface nanotopography, by depositing a thin layer of plasma polymer on top of the surface to control the outermost surface chemistry.[127] This approach would provide an opportunity to understand the influence of surface nanotopography and chemistry on inflammatory responses,[117, 127] which is vital for the utilization of plasma polymers in implantable devices.[42] The availability of a wide range of polymers allows the creation of intrinsic surface chemistry via thin film formation with a wettability ranging from 200 to 1200 contact angle on smooth surfaces.[110] Furthermore, plasma polymer based surface coating has also found application in preventing bacterial adhesion and biofilm formation to minimize the risk of infection. [128, 129] Plasma polymerisation technique will be used to create model surfaces in this proposed study.

1.1.6.3. Nano-Structural Modification

Another common strategy used to control biomaterial biocompatibility is to create nanotextured surfaces to control the cellular responses through physical cues.[10, 13, 117, 130] In the last few years a significant number of research papers have reported promising results for the potential use of surface nanotexturing in many biomedical fields such as cell transplantation,[131] controlling cancer cell function,[132, 133] tissue engineering,[134] gene transfection,[135, 136] skin regeneration,[137, 138] neural tissue engineering,[139, 140] stem cell differentiation,[141] bone regeneration,[44, 142] preventing infection and bacterial adhesion,[143, 144] nano-biosensors,[145] and, broadly, biomedical devices. Nano rough surfaces are widely used for the above mentioned biomedical applications, due to their ability to control protein adsorption and cell functions such as cell differentiation,[146] migration,[147, 148] attachment, and proliferation.[13, 22, 149]

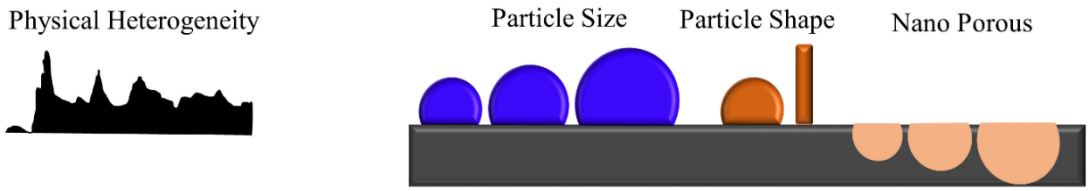

Figure 4: Illustration of physical properties that generate nanoroughness, nano-features with different size, shape, and porosity.

Various techniques have been developed in the last few years to create surfaces with nanosized surface features to incorporate different size, shape, pillars groves and pores as demonstrated in Figure 4. Most of the commonly used approaches to produce nanotopography are self-assembly, etching, blasting, lithography, anodization, UV irradiation, electron spinning polymer de-mixing, and glancing angle deposition.[10, 13, 22] However, despite a growing interest in the topic of biomolecules and cellular response to nanotopography, the exact role of nanostructures size shape and spacing on biological response is still not fully understood.[23, 127, 150, 151]There are many reasons why understanding the role of nanoroughness on protein−surface interaction remains a challenge. This is in part due to the fact that, for the effect of nanotopography to be singled out, other variables (surface chemistry, size, and shape of nanotopography) must be kept constant. To date, most fabrication methods used to impart nanoroughness to a substrate

inherently change its surface chemistry or failed to have a well-defined surface nanotopography.[152] Often different research laboratories have their own or preferred techniques for generation of nanoroughness, and therefore, a comparison of published reports can be difficult, and findings may also appear contradictory. For example, protein adsorption on various nanotopography has been investigated with conflicting results. Lord et al reported less fibrinogen adsorption on 21 nm colloidal silica compared to the smooth control. [153] They also found that nano rough silica surface with an RMS of 10 nm had the same adsorption as the planer surface while 15 nm RMS roughness significantly reduce fibrinogen adsorption. [53] Dolatshahi et al reported that fibrinogen and albumin adsorption on platinum surfaces increases as the surface roughness and size of nano features increases compared to the smooth surface. [154, 155]

Nanotpographic surfaces have shown the immunomodulatory effect on *in-vitro* studies and have been explored to develop a strategy to attenuate foreign body reaction.[156, 157] However, different type of nanotopography with different scale, shape and magnitude may have a diverse effect on the immune response.[10, 127] For example, Smith et al. demonstrated titania nanotube arrays with ∼170 nm in diameter reduced inflammatory response compared to the unmodified titania surface.[158] In a similar manner, Chamberlain et al and Lu et al also reported titanium nanotube with 70 nm and 80 nm also showed weakest immune responses respectively, compared to the smooth controls.[159, 160] On contrary Mohuiddin et al. demonstrated 100 and 200 nm nanostructured materials triggered immune responses.[161] These studies produced some insight into the influence of surface properties on foreign body reaction and tissue integration. However, due to the different types of topography, the outcomes are difficult to compare.Thus, there is a need to generate a model surface with well-defined, controlled nanotopography through creating surfaces with an equal number of nanoparticles, which change only in size along with uniform outermost chemistry in a substrate independent manner.

The current study utilizes plasma polymerisation and gold nanoparticle immobilization strategy to develop surfaces with controlled nanotopography.[44] Since plasma polymerisation is a substrate independent technique surface modification can be easily transferable to relevant implant surfaces.[117] Gold nanoparticle (GNP) with three different sizes will be used to generate nanotopography with a range of heights. A 5-10

nm thin overcoating will be applied on the top of immobilized GNP to avoid the mixed chemistry.[162] This additional overcoating will preserve the nanotopography and provide uniform outermost surface chemistry.[121] Plasma polymerized methyl oxazoline (Me-PPOX) coatings will be used to generate a model surface with well-defined nanotopography features. Me-PPOX is a stable coating that facilitates covalent attachment of carboxylic acid functionalized GNP, this will benefit in generating a surface with an equal number of particles that only change in the size. [115, 163]

1.2. Research Gap

The nanotopography and chemical functionality of a biomaterial surface have been shown to play a critical role in modulating the host immune response.[13, 164] However, the mechanism by which interactions between biomaterials, proteins and cell membranes trigger cellular immune response is still poorly understood, with several unanswered questions. Even though an increasing number of studies have been conducted using different surface chemical functionalities and topographical modifications on implant surfaces to investigate protein adsorption, cellular and tissue response.[164] These studies produced little insight into the influence of surface properties on foreign body reaction and tissue integration.

Firstly, even though advancing nanofabrication technology is enabling the creation of nanotpographic surfaces with more control on physiochemical properties.[10] It is still a challenge to generate substrate independent, inexpensive method to develop well-defined nanotpography surface which can be easily transferred to the industry or other laboratories.It is important to createwell-defined nanotopography surfaces with equal number of particle density of varying size along with homogenised surface chemistry to study the influence of nanotpography size on protein and cellular responses.

Second, while extensive research is focused on identifying the type and amount of protein adsorbed around nanoparticles through a competitive protein adsorption process from total human serum to form protein corona.[165] Very limited studies are focused on competitive protein adsorption on macroscopic biomaterial surfaces, and most of them fail to represent the selective protein adsorption occurring *in vivo* as they use a random mixture of selected protein solutions with varying protein concentration.[14, 166]

However, very few studies used the whole blood serum proteins to study platelet adhesion and hemocompatibility of biomaterials.[167]While the amount and type of adsorbed proteins play a key role in the subsequent immune cells response, [43] little is known about the influence of surface chemistry and its properties such as wettability, surface charge, and chemical functionality on selective protein adsorption (the type and concentration of individual proteins) from a complex clinically relevant protein solution such as total human serum. Still, further research is warranted since the type and amount of different protein adsorption and its influence on the subsequent immune responses is not known.

Third, while the conformational changes of adsorbed proteins play a key role in the subsequent immune cell response, [43] little is known about conformational change and bioactivity of proteins bound to surfaces with nanoscale topography.

Fourth, the nanotopography features like nanoporous structures are known to modulate the immune responses from macrophages.[168, 169] Surface chemistries such as amine, carboxyl, and hydrocarbon rich chemistries have shown to influence the implant biocompatibility and immune response as these chemistries also found in biological environment.[91] However, little is known about the cooperative interplay between nanoporous surface and these surface chemistries on modulating the immune responses. Fifth, nanoparticle with different shapes also known to influence the immune response and differently shaped particles are widely investigated for drug delivery applications. However, the effect of shape in protein adsorption from different biological media such as serum and plasma are not studied.

1.3. Hypothesis and Aims

1.3.1. Hypothesis

The hypothesis underlying this research is that surface engineered biomaterials with a well-defined nanotopography and controlled chemistry can be used to modulate the inflammatory response and foreign body reactions.

1.3.2. Aims

1.3.2.1 Material Aspect

1. Develop a substrate-independent technique to study the impact of chemical modification such as different chemical functional groups, wettability, and surface charges
2. Create well-defined nanotpographic structures with different size
3. Nanoporous (combinational effect of nanotopography and surface chemistry)
4. Nanoparticle shape (sphere and rode)

1.3.2.2. Biological Response

1. Study whole serum or plasma protein adsorption (type and amount)
2. Protein unfolding upon adsorption to the biomaterial surface
3. Immune cell responses (immune cell attachment, pro, and anti-inflammatory response)

1.4. Research Outcome as Research Manuscripts (structure of the thesis)

The thesis chapters are organized as research papers as follows. The introduction and literature background about the chapters along with materials and methods are contained in relevant research papers.

1. **Downstream influences of oxazoline plasma polymerization conditions on chemical and biological interactions:** Focused on optimizing the promising substrate independent plasma deposited polyoxazolines and confirmed their biocompatible nature and defined the conditions under which they can be used to generate surface nanotopography.

2. **Creating nano-engineered biomaterials with well-defined surface descriptors:** Used polyoxazoline (optimized in paper 1) to develop a biomaterial surface with a defined nanotopography and controlled outermost surface chemistry by employing plasma polymerization, nanotechnology, and surface engineering techniques.

3. **Nanotopography-Induced Unfolding of Fibrinogen Modulates Leukocyte Binding and Activation:** The model nano rough substrates created in Paper 2

were then used to investigate the role of surface nanotopography in fibrinogen adsorption and unfolding on integrin - cellular adhesion, and secretion of pro-inflammatory cytokines. This work reveals the role of protein binding and unfolding caused by surface nanotopography on cell adhesion, immune cell activation, and cytokine expression. (***Featured as the cover story on Advanced Functional Materials***).

4. **Hydrophobicity Mediated Serum Protein Adsorption Regulates Inflammatory Consequences to Biomaterial Surfaces:** Investigated the role played by surface chemistry on adsorption of serum protein and subsequent immune responses. Employed plasma polymerization surface engineering methods to generate a range of model substrates with controlled chemistry. The role of surface wettability in selective protein binding and an immune response is unravelled.

5. **Tailor-engineered modulation of macrophages differentiation by geometric and chemical features in nanoporous substrates:** Investigated the synergistic effect of nanoporous structures with surface chemistry modification on modulating the immune response.

6. **Nanoparticle shape influence protein corona formation:** This study reported the effect of shape in the formation of different protein corona from serum and plasma.

Chapter 2. Downstream Influences of Oxazoline Plasma Polymerisation Conditions on Chemical and Biological Interactions

Chemeca 2016: Chemical Engineering - Regeneration, Recovery and Reinvention
Imprint: Melbourne, Vic.; Engineers Australia; 2016
Extent: 1127 p.
ISBN: 9781922107831
Publication Type: Conference Paper
Subjects: Engineering; Chemical engineering



Downstream influences of oxazoline plasma polymerisation conditions on chemical and biological interactions

Rahul M. Visalakshan, Alex Cavallaro, Louise E. Smith, M. MacGregor-Ramiasa, John Hayball and Krasimir Vasilev

Chemeca, 2016

(Manuscript published as a Chemeca 2016 conference Proceedings)



Statement of Contribution of Co-Authors for Thesis by Published Paper

Author	Contribution
Rahul M Visalakshan	• Experimental design • Conducted experiments • Data analysis • Wrote the manuscript
Alex A Cavallaro	• Technical guidance • Aided data analysis • Assisted in reviewing the manuscript
Louise E. Smith	• Technical guidance in cell culture • Assisted in reviewing the manuscript
Melanie N MacGregor	• Assisted in reviewing the manuscript
John D Hayball	• Technical guidance • Involved in the conception and design of the project

	• Assisted in reviewing the manuscript
Krasimir Vasilev	• Technical guidance • Involved in the conception and design of the project • Assisted in reviewing the manuscript

Principal Supervisor Confirmation

I have sighted email or other correspondence from all Co-authors confirming their certifying authorship.

Krasimir Vasilev K. Vasilev **26/05/2019**

Name Signature Date

Citation:

Visalakshan, R.M., Cavallaro, A., Smith, L.E., MacGregor-Ramiasa, M., Hayball, J. and Vasilev, K., 2016. Downstream influences of oxazoline plasma polymerisation conditions on chemical and biological interactions. Chemeca 2016: Chemical Engineering-Regeneration, Recovery and Reinvention, p.840.

2.1. Abstract

The use of plasma polymerised films to fabricate highly functional surface coatings is a well-established process. Plasma polymerisation offers many advantages over conventional polymerisation techniques such as fast processing speeds, industrial scalability and the elimination of catalysts and solvents. The large breadth of potential plasma polymerizable monomers makes the prospect of generating coatings with various functionalities virtually boundless. In terms of applications towards biomaterial modification however, with each new polymer precursor, the roles of plasma deposition parameters and their effects on polymer functionality and cytotoxicity needs to be investigated. Herein we examine the crucial role that deposition pressure plays in the physical stability and potential biochemical reactivity of nano-thin plasma polymerised oxazoline (PPOx) coatings. Firstly, ellipsometry was used to determine the stability of PPOx films in aqueous solvents in terms of thickness loss. As expected, it was revealed that PPOx film stability is inversely proportional to deposition pressure. Secondly, the chemical reactivity of PPOx with acid functionalised gold nanoparticles (GNP) was examined. The complex role of deposition pressures on GNP binding and aggregation was elucidated. Next, the biological interactions of these surfaces were studied using human dermal fibroblasts. Metabolic activity of the cells revealed biocompatibility of various PPOx films. Further to this, the differences in cell proliferation on PPOx films for varying plasma polymerization deposition pressure were studied. This study reveals the critical role of deposition pressures of PPOx to create a stable coating, its effect on film chemical reactivity and how it influences the biocompatibility of the deposited films.

Keywords: biocompatibility, nanoparticle binding, plasma polymerisation, polyoxazoline, polymer stability.

2.2. Introduction

Surface modification of implantable medical devices is a promising technique to ensure biocompatibility of the surfaces and control foreign body reactions [9, 170, 171]. Biomaterial surface modifications such as surface chemistry and nanotopography play a critical role in modulating host immune responses [151, 171]. In vitro studies have suggested that surface topography and surface chemistry are translated through an

adsorbed protein layer into the immune cells and control immune responses [13]. Various methods have been developed to create surface coatings with specific chemistry [9, 172]. One of the most promising methods is plasma polymerisation [173].

Plasma polymerisation has gained interest due to its special attributes such as being solvent-free, substrate independent and a simple one-step process [174]. Polyoxazoline polymers are evolving new polymers for biomaterials known for their antifouling properties and excellent biocompatibility [175-177]. However, their application in the biomedical field seems to be hindered by the complex polymerisation techniques required to produce these polymers. Recently, Vasilev and co-workers developed the first plasma polymerised oxazoline-based films [163]. The capability of these plasma deposited polyoxazolines (PPOx) to bind proteins and modulate biofilm adhesion was demonstrated [115, 178]. It was also shown that plasma polymerised polyoxazoline enables covalent reactions with carboxylic acid functionalised nanoparticles and biomolecules [163], which demonstrates the vast potential of PPOx for numerous biomedical applications ranging from implantable devices to cell therapies and sensors. In addition, this type of coatings can have excellent antifouling properties as reported in reference [178].

In pioneering studies into PPOx, coating thickness loss was sometime observed after exposure to aqueous solutions [163]. Although this property may, to some extent, play a beneficial role in the antifouling nature of PPOx, it is important to understand the mechanism leading to the loss of polymeric material. Therefore, in this paper, we investigate the role of plasma polymer deposition parameters to not only shed light on what constitutes a stable coating but also determine the chemical and biological implications of the released of any loosely bound polymer fragments. To achieve this objective, we first built on our current understanding of how plasma polymerisation parameters influence PPOx stability. Next, we used a chemical and biological model to determine the impact of any released fragments. In this work 16 nm gold nanoparticles (GNP) were used to asses any potential impact of surface stability on the subsequent functionalization of PPOx. Biological interactions were studied using Human Dermal Fibroblast (HDF) in vitro. A metabolic reduction assay and cell counts were performed to study the biocompatibility and proliferation of cells on PPOx. We show the remarkable role pressure plays in not only determining the stability of the plasma polymer but how different PPOx interact in model chemical and biological environments.

2.3. Experimental

2.3.1. Materials

2-Methyl-2-oxazoline (Aldrich), hydrogen tetrachloroaurate (ProSciTech), trisodium citrate (BHD Chemicals), and 2-mercaptosuccinic acid (Aldrich), were used without further purification.13 mm glass coverslip and silicon wafers (ProSciTech) were used as substrates for PPOx film deposition after cleaning.

2.3.2. Methods

Plasma polymerisation

Plasma deposition was performed in a custom built coupled bell-chamber with a 13.56 MHz plasma generator [109, 111].13 mm glass coverslips and silicon wafers were used as sample substrates. These were cleaned with acetone and ethanol and dried under nitrogen flow before use. To remove any remaining organic materials the cleaned glass coverslips were air plasma cleaned at a working pressure of 0.11 mbar at 50 W for 5 minutes. The chamber was brought onto a base pressure of 0.02 mbar before introducing the oxazoline precursor (2-Methyl-2-oxazoline) using a needle valve to control the working pressure within the chamber. PPOx nano-thin films are deposited at a high working pressure of 1.1 mbar and a low working pressure of 0.08 mbar. A 20 or 50 W continuous wave 13.56 MHz radio frequency was used to ignite the plasma.

Gold nanoparticle synthesis

Gold nanoparticles (GNP) were synthesised by citrate reduction method of tetrachloro auric acid ($HAuCl_4$), as described previously [179]. Briefly, 50 µL of $HAuCl_4$ with 50 mL of MilliQ water was brought to a rolling boil in a reflux system under continuous stirring. Once boiling, 1v% of trisodium citrate (TSC) solution were added from 1 mL, 0.5 mL to 0.3 mL to get three different sized nanoparticles with a diameter of 16, 38 and 68 nm, respectively [180]. Samples were left to cool under continuous stirring and mercapto succinic acid (MSA) was added for surface modification of gold nanoparticles with –COOH groups [181].

Thickness measurement

Silicon wafers were used as substrates for plasma polymer film thickness measurements. An A J.A Woolam Co. Variable Angle Spectroscopic Ellipsometer (VASE) imaging ellipsometer with WVASE32 software was used to measure thickness.

To study the stability of the PPOx, silicon wafers were soaked in ultrapure water for 4 hours, then blow dried with nitrogen. Changes in total film thickness before and after washing were used as an indication of stability.

Immobilization of gold nanoparticles

Glass coverslips with PPOx deposited at different powers and flow rates were immersed with 1 mL of GNP solution in a 24 well plate. 16 nm GNP were immobilised for 1 hour and 38 nm and 68 nm GNP for 6 hours. After immobilisation, surfaces were rinsed three times with MilliQ water to remove any unbound nanoparticles and dried under a nitrogen gas flow.

Atomic Force Microscopy (AFM) imaging

Atomic force microscopy (AFM) studies were carried out using an NT-MDT NTEGRA SPM AFM in non-contact mode. NT-MDT, NSG03 Au coated silicon nitride tips was used on the reflective side at a resonance frequency of 65 – 100 kHz. Images were taken at an amplitude oscillation of 10 nm at a scan rate of 0.5 Hz. Nano topographical images of 5 x 5 μm size were taken to study the nanoparticle distribution on the surface.

Cell culture

Primary derived Human dermal fibroblast (HDF) were harvested and grown as described previously [182]. All patients gave informed consent for skin to be used for research through a protocol approved by the Ethical Committee at the Queen Elizabeth Hospital and the University of South Australia Human Ethics Committee. HDF cultures were maintained in Fibroblast Culture Medium (FCM) consisting of Dulbecco's modified Eagle medium (DMEM; Gibco, Life Technologies, Australia) supplemented with 10% v/v foetal bovine serum (FBS; Ausgenex, Australia), 100 $IU.mL^{-1}$ penicillin and 100 $mg.mL^{-1}$ streptomycin (Gibco, Life Technologies, Australia). Cells were maintained in an incubator at 37 ^{o}C with 95% humidity and 5% CO_2. The medium were changed every 3 days until the cells reached 80% confluency. Fibroblast cells of passage number between 4 and 7 were used for all experiments.

PPOx coated 13 mm glass coverslips were placed into a 24 well plate and treated with UV for 7 to 10 minutes to sterilise the samples. Each well was seeded with 1×10^4 cells in fresh media. Cells were left for three days to adhere and grow, and the cell

viability was measured with a metabolic reduction assay. Adhered cells were washed with PBS and 500 µL of 10 % (v/v) resazurin (110 mg.mL^{-1} stock solution) in FCM was added to each well and incubated for 2 hours. 200 µL of the reduced solution was collected in a 96 well plate and florescence intensity was measured at an excitation wavelength of 544 nm and emission wavelength of 590 nm [183].

To study the cell proliferation on PPOx films fibroblast cells were initially seeded at 1×10^4 cells per well. Cells were fixed after 24 hours and 72 hours using 10% formaldehyde and stained with DAPI. Nuclei counts were performed using fluorescent microscopy, with a minimum of 5 images per sample taken and data presented as the average of total cells per field of view per sample. All experiments were conducted with three technical repeats and three biological repeats.

2.4. Results and Discussion

2.4.1. Thickness changes as a function of plasma polymerisation parameters

The film thickness changes with the change in plasma polymerisation time, working pressure and RF power. To investigate the effect of deposition time on PPOx, the methyl-oxazoline precursor was ignited with a RF power of 50 W at working pressure of 0.08 mbar for set times. Ellipsometric measurements of thickness changes with respect to time is shown in Figure 1. As expected, the PPOx layer thickness increases with increasing deposition time. In this case between 30 seconds to 5 minutes of deposition shows a steady increase of thickness in a linear fashion from 5 nm to 24 nm. Here we demonstrated the increasing film thickness with increasing polymerisation time.

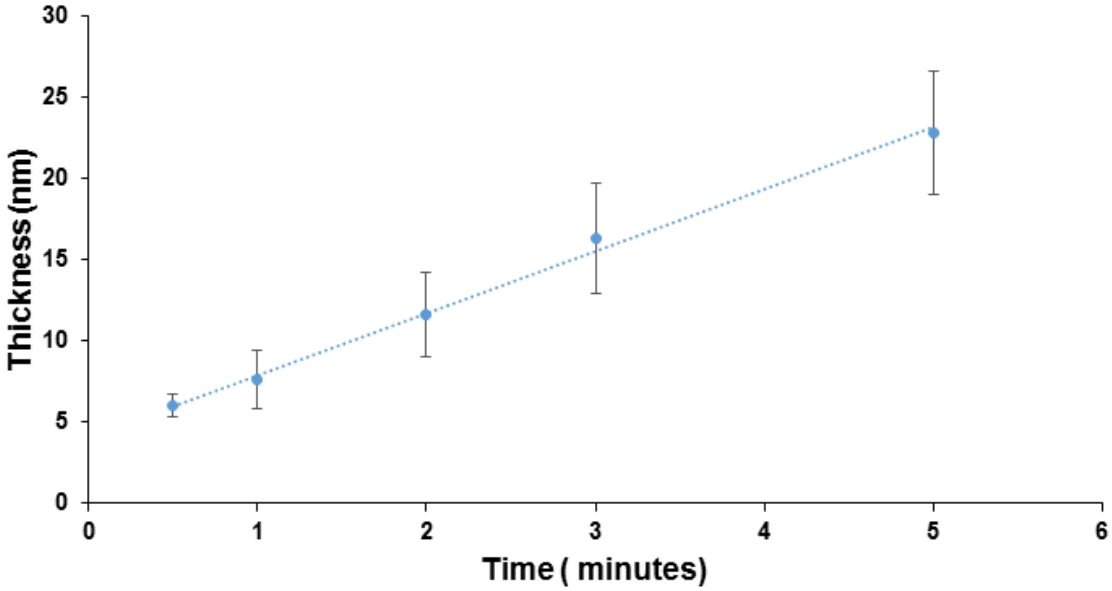

Figure 1: PPOX film thickness measured by ellipsometry for a range of polymerisation time points. Error bars are the standard deviation of three separate thickness measurements.

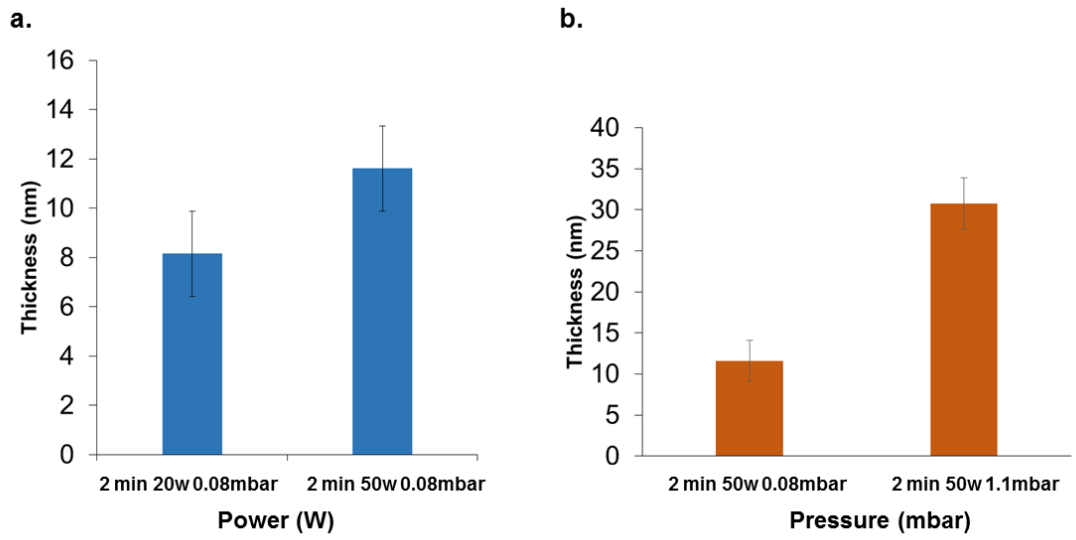

Figure 2: (a) Thickness measurement of PPOX films with low and high RF power. (b) Thickness of PPOX films with high and low working pressure.

Next the effects of changing deposition power and working pressure were interrogated. Figure 2 shows the effect of increasing deposition power and pressure on PPOx film thickness. As shown in Figure 2a, PPOx deposited at 0.08 mbar for 2 minutes has an increase of thickness from 8 nm to 11 nm when deposited at 20 and 50 W respectively. In this scenario it is assumed that the increase in power allows a greater

fraction of organic precursor to react within the chamber. As the total number of collisions within the plasma field increase there is more monomer fragments colliding with and depositing on the surface. In other words, at high power, less monomer is pumped out of the chamber without contributing to the film growth. However, with more power being conferred to the plasma, it is expected that less functionality of the original precursor would be retained in the final film due to the increased fragmentation of the original precursor[184].

Another method employed to increase polymer thickness is the use of different working pressures. Here adjusting the precursor flow rates directly influences how much monomer is available for the deposition. To evaluate the influence of deposition working pressure on thickness, PPOx was deposited at 0.08 mbar and 1.1 mbar for 2 minutes using the RF set at 50 W. In this case thickness increased by almost three folds from 11 nm to 30 nm for the 0.08 mbar and 1.1 mbar samples, respectively. In both aforementioned cases, beyond a simple increase in the net layer thickness, it is also expected that the end resultant chemistry would be extremely different due to the increased availability of total amount of precursor within the chamber which increases the overall net functionality of the surface[185].

2.4.2. Stability of coatings

The stability of PPOx coatings was studied in terms of retention of total layer thickness after interacting with an aqueous environment. As shown in Figure 3, PPOx films deposited at 50 W for 2 and 5 minutes at 0.08 mbar maintained the thickness after water treatment. Alternatively, those deposited at 1.1 mbar exhibited some loss in film thickness of 5 nm and 9 nm respectively for samples deposited for 2 and 5 minutes. Physically loose bound monomer fragments are rapidly eluted by water treatment on films deposited at higher pressures. As mentioned previously, in cases of high working pressures the plasma chamber is filled with more monomer. After the ignition of RF power, it is likely that a few reactive species left within the chamber physically get deposited on to the substrate, without undergoing any crosslinking. Any loosely bound monomer fragments may then leach into water and cause the loss of film thickness observed. When deposited at lower working pressures all the monomer can be highly fragmented and these more reactive species become bound to the substrate by secure cross-linkages. The higher degree of crosslinking within the PPOx films deposited at low

pressure, i.e. 0.08 mbar is evidenced by their high stability, regardless of the original film thickness.

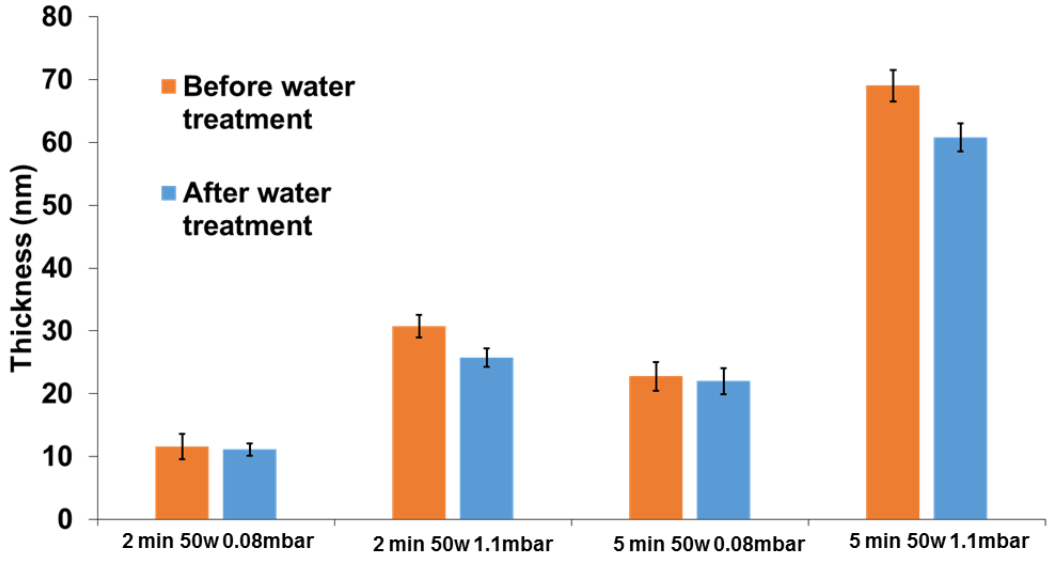

Figure 3: PPOX film thickness before and after water treatment measured by ellipsometry for range of PPOX films with low and high pressure at two time points.

2.4.3. Gold nanoparticle binding reaction of PPOX films

Carboxylic group functionalised GNP of 16, 38 and 68 nm diameters were synthesized and used to study the chemical reactions with PPOx films deposited at high and low power and pressure. To investigate the role of working pressure and power on chemical reactions, deposition times of PPOx films were kept constant as 2 minutes.

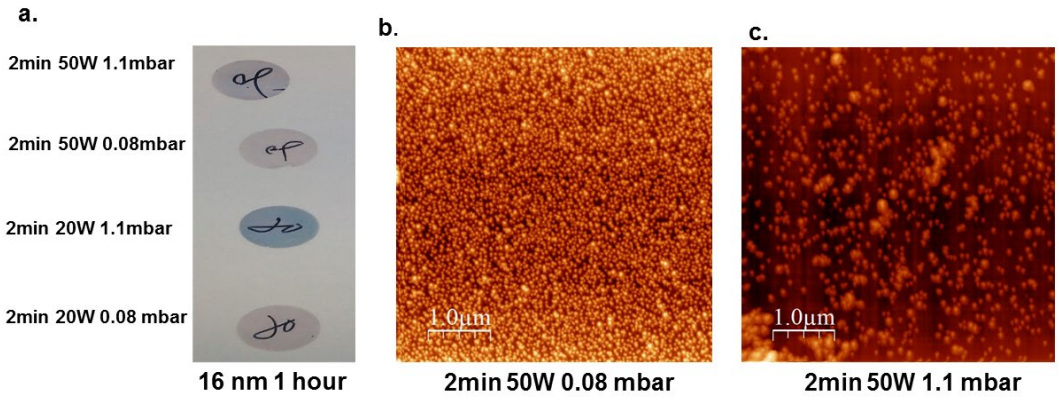

Figure 4: (a) Photograph of PPOX films of high and low, pressure and power on 13 mm glass coverslips reaction with 16 nm GNP. (b) AFM image of 16 nm GNP binding on low pressure PPOX film. (c) AFM image of 16 nm GNP aggregation on high pressure PPOX film.

The capacity of PPOx to bind GNP was previously studied [163]. Here the chemical bonds between the PPOx surfaces and COOH-GNP were challenged with strong detergents, high ionic strength and extreme pH solutions and proved the irreversible nature of the binding of GNP to PPOx [163]. 16 nm gold nanoparticles emit light at a wavelength of 520 to 550 nm due to their specific plasmon resonance characteristics, therefore, surfaces with GNP bound appear pink in colour. As shown on Figure 4a. 16 nm GNP bound to PPOx films appear pink on films deposited at 0.08 mbar and blue\purple on films deposited at 1.1 mbar.

AFM images of high- and low-pressure films reacted with the -COOH functionalised GNP was used to reveal the cause of this colour change. As it shown in Figure 4b. PPOx films deposed at 0.08 mbar bound to the GNP strongly with a homogeneous distribution correlating to what is expected for the bright pink colour on the glass coverslips. It is clearly evident form Figure 2c that GNP aggregate on the substrate surface when PPOx was deposited at higher pressures.

These aggregated GNP appear as dark blue\purple depending on the level of aggregation. From the stability studies we observed the loss of thickness due to the removal of loosely bound less crosslinked monomer species from PPOx deposited at higher pressures. Using nanoparticles of known surface functionalisation, it is clear that the less crosslinked monomer species from high pressure polymer films directly caused the aggregation of nanoparticles adhering to the surfaces.

This study shows the important role of working pressure in the stability of PPOx coatings and their reactivity with GNPs. PPOx has been proposed as a new platform for the covalent binding of biomolecules [115]. When attempting to functionalise PPOx, the potential effects brought on by low stability must be analysed further. For PPOx use as a biomaterial it is particularly important to have a stable coating, and strong chemical bonding with proteins. So far, the effects of the chemical fragments being released from unstable PPOx films on living organism are not known. To investigate this an *in- vitro* model of cytotoxicity was used.

2.4.4. Biocompatibility and cell proliferation

To investigate the biocompatibility of PPOx, HDF were grown on films deposited at different pressures with a set RF power of 50 W and deposition time of 2 minutes. To

study the role of working pressure of PPOx deposition on biological interaction was first determined by a cytotoxicity study. HDF were grown on PPOx films for three days and the cytotoxicity was tested with the resazurin viability assay. This assay measures the changes in fluorescent intensity of the reduced resorufin product which is directly related to the metabolic activity of fibroblast cells. Results are plotted in Figure 5a.

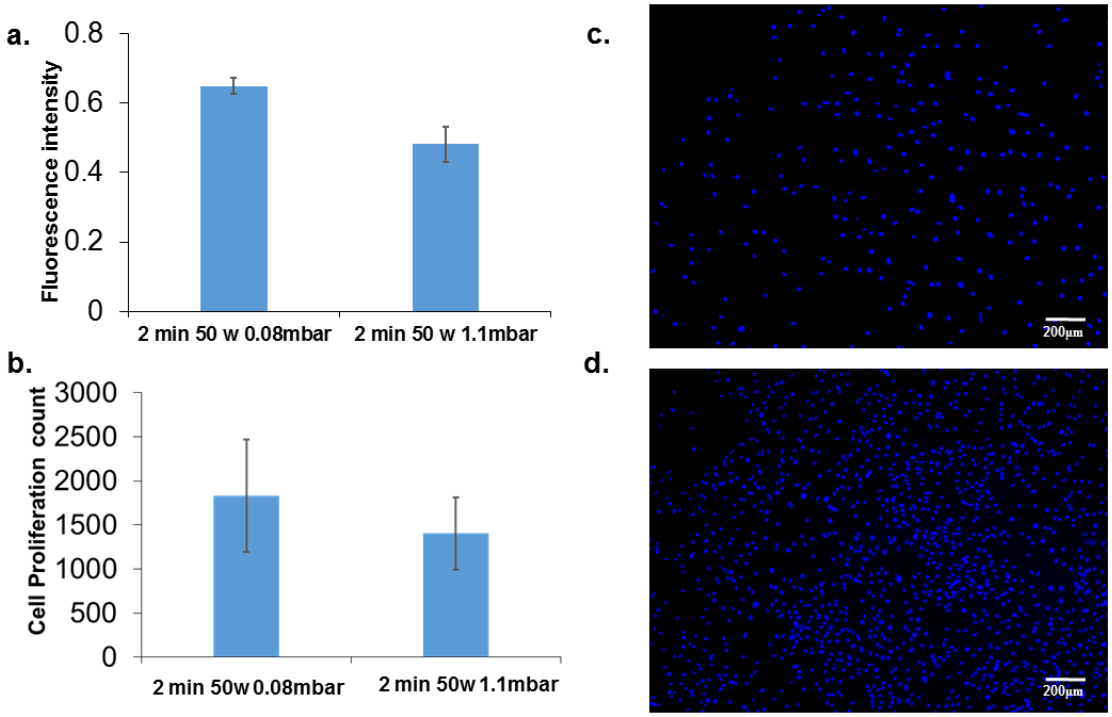

Figure 5: (a) Fibroblast metabolic activity resazurin assay and (b) proliferation on high and low pressure PPOX films. Fluorescent microscope images (scale bar = 200 µm) of DAPI nucleus stained fibroblast on PPOX films after (c) 24 hours and (d) 72 hours. Data expressed as mean ± SD of n=3 samples.

The results show that the viability of HDF on the different PPOx films is not statistically significant. Even though the trend shows that cells are comparatively less viable on PPOx films deposited at 1.1 mbar than on 0.08 mbar PPOx films. On these films deposited at high pressure some loosely bound reactive species get removed into the media as we had observed in the aqueous stability assay. This loss of chemical fragments may make the film less favourable to cell adhesion and growth. To investigate this further the proliferation of HDF within this time period was quantified.

For cell proliferation studies HDF were grown on PPOx films as before. Cells were fixed and quantified after 24 and 72 hours. The difference in cell number count from 72 hours to 24 hours is plotted as cell proliferation on Figure 5b. There is no statistically

significant difference of cell proliferation between both pressured films. However, the cell proliferation results show the same trend as the resazurin viability assay. In general, HDF proliferate more on low pressure films than high pressure films. Further investigation of this trend is currently being conducted to see if further increases in deposition pressure can influence cell adhesion and proliferation. This will be evaluated in terms of both surface stability and effects of released fragment interaction with cells.

2.5. Conclusion

The plasma deposition of oxazolines provides a versatile way to tune surface chemistry for a number of proposed biological functionalities. The critical effect of plasma deposition pressure on polymerisation of oxazoline films on the film stability, chemical and biological interactions has been studied. There is a critical distinction between surfaces deposited at 0.08 mbar and 1.1 mbar, where the PPOx becomes more stable. In the current work, this transition was clearly evident by the loss of layer robustness in aqueous environments when deposited at the higher working pressure. As observed when depositing plasma at higher deposition pressures, films may leach loosely bound chemical species and fragments. Using nanoparticles of known surface functionalisation, it was made evident that the less crosslinked monomer species from high pressure polymer films directly caused the aggregation of nanoparticles adhering to the surfaces. Although, there was no statistically significant changes in the biocompatibility of the different PPOx coatings made, there seems to be a trend towards less cell adhesion and proliferation on less stable surfaces. However, we require additional investigation as to the exact mechanism in which less stable PPOx films change cell interactions. We intend to further fine-tune the oxazoline plasma processes to manufacture stable nano-thin coatings with tailorable chemical and biological reactions.

2.6. Acknowledgements

The authors would like to thank Professor Michael Roberts at the School of Pharmacy, University of South Australia for help with the sourcing and collection of the skin.

2.7. Presenting Author Biography

Rahul M Visalakshan is pursuing his PhD in Biomaterial Engineering and Nanomedicine from School of engineering University of South Australia. He won

Australian Postgraduate Award scholarship to pursue his PhD. Rahul is a graduate from University of East London, UK where he received master's in biotechnology and Management. He completed his bachelor's in biotechnology from Mahatma Gandhi University, India.

After graduating Rahul joined CSIRO as a research trainee to study colloidal and microbial transport through saturated porous media. He also volunteered for university of Adelaide as a research assistant to gain more research experience in molecular biology and immunology.

2.8. Copy Right Permission

FW: Chemeca 2016 conference paper reuse permission for thesis
1 message

From: Conferences [mailto:Conferences@icheme.org]
Sent: Tuesday, 16 April 2019 5:18 PM
To: Madathiparambil Visalakshan, Rahul - madry008 <rahul.madathiparambil_visalakshan@mymail.unisa.edu.au>
Subject: RE: Chemeca 2016 conference paper reuse permission for thesis

Hi Rahul,

This is fine to allow. With full reference to the original source of publication as you have indicated below.

Kind regards,

Natalie Graser
Marketing & Events Executive
Institution of Chemical Engineers (IChemE)
+61 (0)3 9642 4494
ngraser@icheme.org
www.icheme.org

From: Madathiparambil Visalakshan, Rahul - madry008 <rahul.madathiparambil_visalakshan@mymail.unisa.edu.au>
Sent: Wednesday, 10 April 2019 9:51 AM
To: Conferences <Conferences@icheme.org>
Subject: Chemeca 2016 conference paper reuse permission for thesis

Hi,

I am Rahul M Visalakshan a PhD candidate from the University of South Australia, Australia. I have published my peer reviewed conference paper 'Downstream influences of oxazoline plasma polymerisation conditions on chemical and biological

interactions'' Paper no. 3405675, In: Chemeca 2016: Chemical Engineering - Regeneration, Recovery and Reinvention. Melbourne, Vic.: Engineers Australia, 2016: 840-848. Document Type: Conference Paper ISBN: 9781922107831. I would like to include this manuscript as a chapter in my thesis which is due to submit on 15th April 2019. Therefore, I would like to seek permission from you to add this manuscript as a chapter in my thesis. I will be citing the articles as needed. It would be great if you could please grant me the permission.

Thank you,

Rahul M Visalakshan

The contents of this email are confidential and may be privileged. It is intended for the addressee(s) only. If you are not the intended recipient of this email, any use of its content is prohibited. Please notify us immediately by reply email and then delete the email from your system

Any views expressed in this message are those of the individual sender, unless specifically declared to be a position statement of IChemE.

Although all reasonable precautions have been taken to ensure no viruses are present, IChemE cannot accept responsibility for any loss or damage arising directly or indirectly from this email or its contents.

IChemE is a registered charity in England & Wales (214379), and a charity registered in Scotland (SC 039661).

Chapter 3. Creating Nano-Engineered Biomaterials with Well-Defined Surface Descriptors



ACS Appl. Nano Mater.2018162796-2807
https://doi.org/10.1021/acsanm.8b00458

Creating Nano-Engineered Biomaterials with Well-Defined Surface Descriptors

Rahul M. Visalakshan, Melanie N. MacGregor, Alex A. Cavallaro, Salini Sasidharan, Akash Bachhuka, Agnieszka M. Mierczynska-Vasilev, John D. Hayball, and Krasimir Vasilev

ACS Applied Nano Materials. 1 (2018) 2796-807.

(Manuscript published in ACS Applied Nano Materials)



Statement of Contribution of Co-Authors for Thesis by Published Paper

Author	Contribution
Rahul M Visalakshan	• Experimental design • Conducted experiments • Data analysis • Wrote the manuscript
Melanie N MacGregor	• Aided data analysis • Assisted in reviewing the manuscript
Alex A Cavallaro	• Technical guidance with Tof-sims • Aided data analysis • Assisted in reviewing the manuscript
Salini Sasidharan	• Aided data analysis • Assisted in reviewing the manuscript
Akash Bachhuka	• Technical guidance in plasma polymerization and gold nanoparticle synthesis
Agnieszka M. Mierczynska-Vasilev	• Technical guidance • Assisted in reviewing the manuscript

John D Hayball	• Technical guidance • Involved in the conception and design of the project • Assisted in reviewing the manuscript
Krasimir Vasilev	• Technical guidance • Involved in the conception and design of the project • Assisted in reviewing the manuscript

Principal Supervisor Confirmation

I have sighted email or other correspondence from all Co-authors confirming their certifying authorship.

Krasimir Vasilev K. Vasilev **26/05/2019**

Name Signature Date

Citation:

Visalakshan, R.M., MacGregor, M.N., Cavallaro, A.A., Sasidharan, S., Bachhuka, A., Mierczynska-Vasilev, A.M., Hayball, J.D. and Vasilev, K., 2018. Creating Nano-Engineered Biomaterials with Well-Defined Surface Descriptors. ACS Applied Nano Materials, 1(6), pp.2796-2807.

3.1. Table of Contents (TOC) Graphic

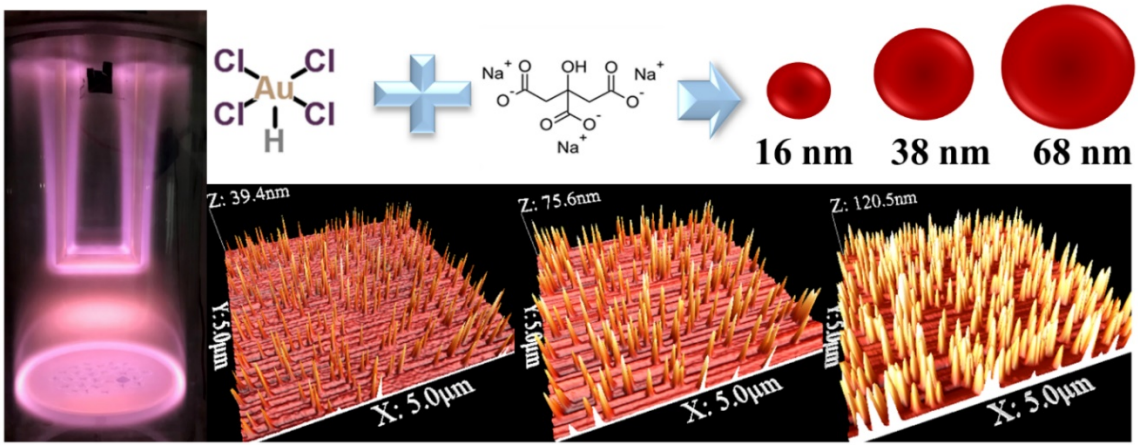

3.2. Abstract

The importance of nanostructured surfaces in a range of technological and biological processes is well documented within literature, yet often ill-understood. Simple and reliable methods for the preparation of nanotextured surfaces are required to advance both fundamental understandings of nanoscale phenomena and our capacity to design nano-engineered materials for specific applications. Nano-engineered surfaces are, for instance, needed to shed light on the effect of nanostructures size and density on immune cells cytokine production. In applied bioengineering, nanostructured artificial surfaces could be specifically tailored to enhance the osteo-integration of implants. This study presents a versatile, plasma polymer enabled method for the generation of surfaces with well-defined nanotopography and tailored outermost surface chemistry. This was achieved by finely controlling the covalent bonding of gold nanoparticles of desired size to plasma deposited polymethyloxazoline interlayer deposited on the material substrate. An additional 5 nm thin polymer was deposited over the nanostructures providing a uniformly tailored outermost surface chemistry whilst preserving the topography. This rapid, versatile, substrate independent, and scalable strategy for the preparation of well-defined nanotopography surface has promising prospects in many fields relying on surface engineering, including food and membrane technologies, biomaterial and environmental engineering, sensing, marine sciences and even pollution control.

Keywords: well-defined nano topography; polymethyloxazoline; homogeneous chemistry; plasma polymerization; biomaterial; nanoscale roughness.

3.3. Introduction

Biological events happening on and in the vicinity of biomaterials are governed by the material surface properties.[151, 186] While the impact of microtopography and surface chemistry on cellular response has been well studied, little is known about the exact role played by surfaces with nano-sized features.[93, 187, 188] Although cells are several microns in size, cellular function is underpinned by interactions between nanotopographical features of the growth substrates and nano-sized serum proteins, and cell surface receptors.[90, 118, 127, 179, 189, 190] In fact, it is well established that protein adsorption [152, 191, 192] and cell functions such as cell differentiation [146],

migration[147, 148], attachment, and proliferation [149, 162, 193] are altered by nanoscale interactions at the biomaterial/media interface.[13, 39, 44, 194-196] This is why significant effort has been devoted to creating sophisticated nanotextured surfaces for cell transplantation [131], controlling cancer cell function [132, 133, 197], tissue engineering [134], gene transfection [135, 136], skin regeneration [137, 138], neural tissue engineering [139, 140], stem cell differentiation [141, 198, 199], bone regeneration [44, 142], prevent infection and bacterial adhesion [143, 144, 200], nano-biosensors [145], and biomedical devices.[194, 201]

However, the specific impact of nanostructured surface descriptors (size and spacing) on biological responses is not yet fully understood, primarily because technologies able to generate well-defined nanotopography on biocompatible surfaces are scarce. Lithography, etching, blasting, electron spinning, UV irradiation, polymer de-mixing, glancing angle deposition, anodization, and self-assembly are the most commonly used approaches [39, 202] used to impart surface nanotopography and all bear significant practical limitations. They either are substrate dependent (specificity to a class of material), generate inconsistent topographic features, provide limited options for outermost surface chemistry or/and have prohibitive costs.[13] Yet, chemically tailored surfaces featuring controlled number of nanostructures of different sizes are required to reveal the individual and synergistic effect of targeted nanotopography descriptors such as root-mean-square (RMS) roughness, maximum height of roughness, or interparticle distance on biological processes. It is worth noting that, beyond their relevance to biological systems, well defined nano-engineered substrates are also needed to advance our understanding and exploitation of many nanoscale processes occurring in other technological fields. Careful nanostructuring can, for instance, be used to impart remarkable wetting and/or optical properties to materials [203], improve sensor sensitivity [204, 205], and even enhance the performance of electrodes used for energy conversion and storage.[206]

Herein, we report on a highly reproducible, easy and rapid way to create well-defined nanostructured surfaces where the size, density, and outermost chemistry of the nanotopograhy are tailored and finely controlled. In this strategy, gold nanoparticles (GNPs) functionalized with the carboxylic acid group are irreversibly bound to a plasma deposited methyl oxazoline (Me-PPOx) thin films.[163, 207-209] The covalent binding

of the nanoparticles to the surface is a major advance to our earlier strategy where nanoparticles were only electrostatically attached to the plasma polymer interlayer.[125, 151, 210] Covalent binding ensures significantly stronger bond providing firm grounds that the nanoparticles do not separate from the surface in complex or harsh media, such as biological fluids. Furthermore, the strategy described in this paper as illustrated in Figure 1 allowed us to create a surface having equal nanoparticle number density but different size which was unachievable by the electrostatic method of binding. Plasma polymerization is a substrate independent technique that is used to generate nano-thin polymer coating on any type of material without changing its bulk properties.[211] The plasma-assisted approach has the unique advantage to allow for well-defined substrates with nanostructures of three different sizes but equal number densities to be generated by tailoring the pH of the suspension, the nanoparticle concentration and the immobilization time. Furthermore, we demonstrate that it is possible to present homogenized outermost surface chemistry using a very thin layer of overcoating with a range of surface functionalities while preserving the nanotopography.

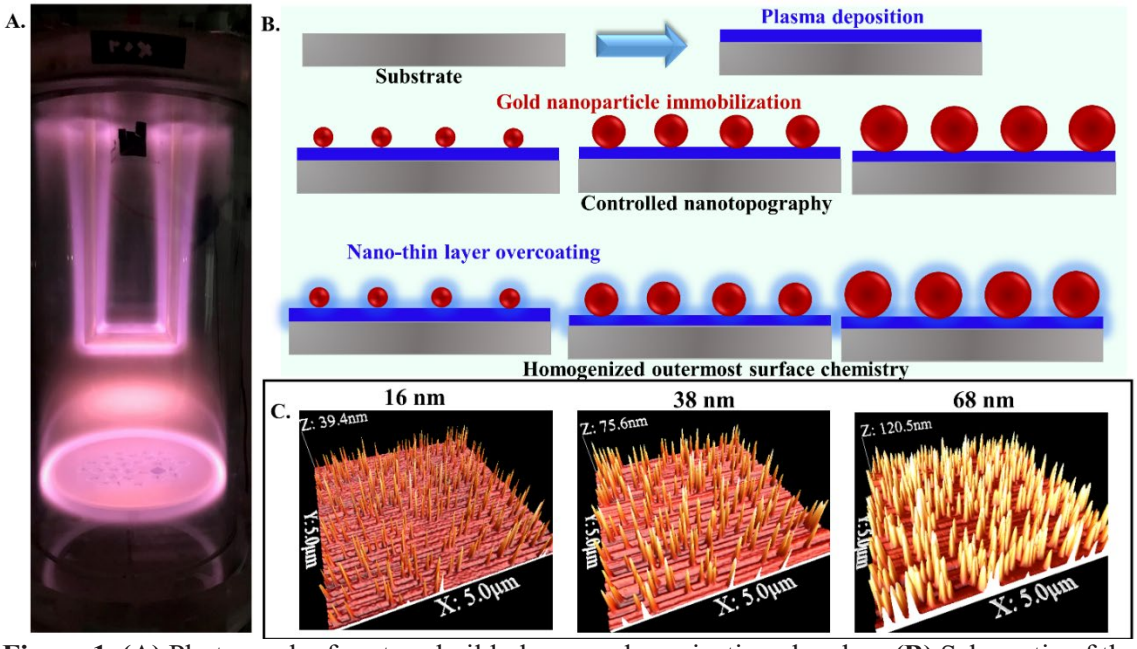

Figure 1. (A) Photograph of custom-build plasma polymerization chamber. **(B)** Schematic of the preparation of well-defined nanotopography (16, 38, and 68 nm) surface with uniform (5 nm) outermost surface chemistry. **(C)** AFM 3D image of well-defined nanotopography surfaces.

3.4. Materials and Methods

3.4.1. Materials

Glass coverslips (13 mm) and silicon wafers (ProSciTech, Australia) are used as substrates for plasma polymerization. 2-Methyl-2-oxazoline (Sigma-Aldrich, Australia) was used as a precursor for plasma polymerization. Gold (III) chloride trihydrate, trisodium citrate, mercapto succinic acid (Sigma-Aldrich, Australia) and sodium hydroxide (Chem-supply) were used for the GNP synthesis.

3.4.1.1. Surface Preparation

A custom build plasma reactor chamber with 13.56 MHz plasma generator was used for plasma polymer deposition.[109] Substrates were subsequently cleaned with acetone and ethanol for 10 min and dried with nitrogen flow. Cleaned substrates were loaded on to the plasma reactor and chamber brought to vacuum. Before polymer deposition, air plasma at 1.1×10^{-1} mbar pressure with 50 W radiofrequency power for 5 min was carried out to remove unwanted organic materials from the sample. The methyl oxazoline precursor was introduced into the chamber set at the base pressure of 2×10^{-2} mbar. The plasma was ignited for 2 min at 8×10^{-2} mbar pressure with 50 W radio frequency power to generate 20 nm thick plasma deposition. A 5 nm thick overcoating with Me-PPOx was added at 50 W power and 8×10^{-2} mbar pressure for 25 sec.

3.4.1.2. Gold Nanoparticle Synthesis

GNPs were synthesized by citrate reduction method of tetrachloro auric acid (HAuCl4). Colloidal gold in aqueous solution was produced by the reduction of tetrachloro auric acid (HAuCl4) with trisodium citrate (Na3Ct) in a controlled reflux system.[180] 0.01% of HAuCl4 was dissolved into a continuously stirred solution and left to boil, before adding the reducing agent Na_3Ct, and continued boiling for further 20 min. Three different sized nanoparticles (NP) with a diameter of 16, 38, and 68 nm was synthesized by controlling the amount of 1% trisodium chloride solution from 1, 0.5, and 0.3 mL, respectively.[125] Mercaptosuccinic acid (MSA) was used as a capping agent along with sodium hydroxide for the surface modification to provide stability to the colloidal GNPs.[181]

3.4.1.3 Immobilization of GNPs

Immobilization of GNPs was conducted by immersing the plasma polymerized Me-PPOx surfaces in GNPs solution for the various amount of time ranging from 10 min to 24 h. A surface with an equal number of particles that changes only in sizes was created by adsorbing 16, 38, and 68 nm diameter GNPs at various solution pH, dilution, and immobilization time. After immobilization, the loosely bound GNP were removed by rinsing the surface with MilliQ water for 3 times and drying under nitrogen gas.

3.4.1.4. Surface Characterization

X-ray Photo Spectroscopy (XPS)

XPS analysis was applied to determine the surface elemental composition of Me-PPOx surface and quantification of GNP binding. Spec SAGE XPS spectrometer with Al Kα radiation operated at 10 kV and 20 mA was used to record the XPS spectra. Survey spectrum were recorded from 0–1000 eV at 100 eV pass energy with 0.5 eV resolution. CasaXPS software was used for the data analysing and C1s carbon peak at 285 eV was kept as a reference for the elemental composition analysing.

Thickness Measurement

Plasma polymer film thickness was measured by Ellipsometry. A J.A. Woolam Co. variable angle spectroscopic ellipsometer (VASE) and data analysed using WVASE32 software. Three silicon wafers from separate plasma depositions were used for thickness measurements.

Transmission Electron Microscopy (TEM)

GNPs size and shape distribution were characterized using Transmission Electron Microscope (JEOL–2100F, Japan). Samples for TEM were prepared by drying a droplet of the GNP suspension on a carbon coated copper grid (ProSciTech, Australia).

Atomic Force Microscopy (AFM)

GNP binding and surface nanotopography were visualized using an NT-MDT NTEGRA SPM Atomic Force Microscope. AFM measurements were performed in a non-contact mode using gold-coated silicon nitride tip (NT-MDT, NSG03) with 65–100 kHz resonance frequencies. 5 μm × 5 μm images were taken with 10 nm amplitude oscillation at 0.5 Hz scan rate.

Surface Charge Analysis

The zeta potential of the GNPs under experimental solution chemistries was measured using ZetasizerNano (Malvern Instruments, U.K.). The pH of the GNP solution was adjusted using 1 M sodium hydroxide (NaOH), and 0.1 M hydrochloric acid (HCl). The 68 nm GNPs were measured at pH=4-7 and 16 and 38 nm GNPs were measured at pH=5.5. The surface charge of the the Me-PPOx coated solid surface in 10 mM KCl solution was measured using Anton Paar SurPASS Electrokinetic Analyzer (Anton Paar, Austria) with adjustable gap cell height. Measurements were begun with pH value of 8, adjusted by 0.1 M sodium hydroxide (NaOH), and gradually dropped the pH to 3 using a dosing pump to automatically add calculated amounts of 0.1 M hydrochloric acid (HCl). Four data points were collected at every 0.5 pH increment and the average value was calculated.

Time-of-Flight Secondary Mass Spectrometry (ToF-SIMS)

All Time-of-flight secondary ion mass spectrometry (ToF-SIMS) measurements were performed with a PHI TRIFT V nanoTOF (PHI Electronics, USA) equipped with a 30 kV Au+ liquid metal ion gun (LMIG). Any surface charge effects were compensated by dual charge neutralization comprising of a 25 eV electron flood gun and 10 eV Ar^+ ions. Spectra were acquired using a "bunched" Au^+ instrument setting to optimize mass resolution and raw data were collected in positive SIMS mode at a number of locations using a 100 × 100 μm raster area, with 1 min acquisitions. Data were analysed using WincadenceN software (PHI Electronics, USA) and processed with the aid of a principal component analysis (PCA) using NESAC/BIO Toolbox (NESAC/BIO, University of Washington, USA).

3.5. Result and Discussion

3.5.1. GNPs Deposition on the Model Surface

GNPs with low polydispersity of three different diameters (16, 38, and 68 nm) were synthesized in water by reduction of hydrogen tetrachloroaurate with trisodium citrate.[180, 212] Mercaptosuccinic acid (MSA) was used to functionalize the surface of the GNPs, according to existing procedures described by Zhu. et al.[181] In this step, a strong and stable Au-S bond is formed between the GNP and the MSA. As a result, the undefined ionic species present on the GNP surface after citrate reduction are replaced by a carboxylic acid monolayer. This type of functionalization also fosters the colloidal

stability of the GNP solution as the MSA dissociable carboxylic groups promote the electrostatic repulsion between individual GNPs. MSA-modified nanoparticles also exhibit an increased stability against pH changes (4–7) compared to unmodified ones, due to the differences in the thickness of the electrical double layer.[181] Citrate ions protonate below pH 4.7 which displaces the equilibrium of the coordination bond and leads to citrate desorption. On the contrary, the carboxylic groups of the MSA-functionalized GNP remain covalently bound to the gold through the Au-S bonds at all pH (4-7), as reported by Zhu. et al. by proving the stability of MSA modified particles against pH changes [181]. Figure 2A shows the Transmission Electron Microscopy (TEM) images of monodispersed MSA functionalized GNPs size distribution in the range of 16, 38, and 68 nm after surface modification.

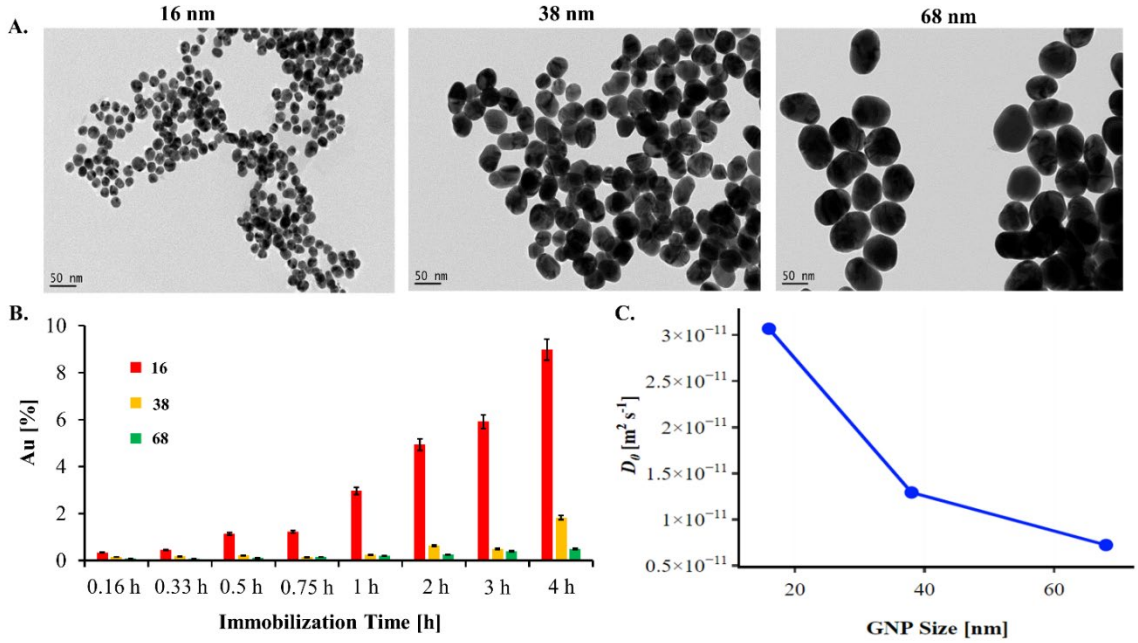

Figure 2. (A) TEM images of surface modified 16, 38, and 68 nm GNPs. **(B)** The atomic concentration of different size GNPs adsorbed to the Me-PPOx surface as a function of immobilization time from X-ray photoelectron spectroscopy (XPS). **(C)** Diffusion coefficient (D_0) for 16, 38, and 68 nm GNPs in the liquid phase at room temperature, calculated from Eq.1.

The COOH-functionalized GNPs were then immobilized on plasma deposited Me-PPOx thin films. Plasma deposited Me-PPOx was chosen for its unique chemical functionality and reactivity which makes it an excellent candidate for biomaterial surface coatings.[115, 178] In particular, previous work demonstrated that the retention of intact oxazoline rings on the surface of the Me-PPOx film facilitates the irreversible bonding of COOH-bearing ligand through the formation of amide bonds.[163] Briefly, the Me-PPOx

GNP binding was challenged with SDS (1V %) detergent, 5 M NaCl, and pH 10 solution for an hour and washed with MilliQ water. XPS analysis after washing treatment confirmed the strong binding of Me-PPOx with GNP.[163] This remarkable property is employed to securely bind the GNPs to the substrates.

3.5.2 Role of Diffusion and Interaction Energy on the GNPs Binding to the Surface

With the aim to create an equal density of GNPs on the surface, we first studied the binding process as a function of immobilization time. The 16, 38, and 68 nm particles were incubated with the surface for periods between 10 min and 4 hours at pH 5.5. Figure 2B the concentration of surface bound (as the percentage of gold atomic concentration) GNPs of different sized on the Me-PPOx coated surface as a function of time. The result shows that the binding of 16 nm GNP significantly increased with time. Whereas, both 38 nm and 68 nm GNPs showed a very slow rate of binding despite increasing the interaction time. The attachment of a colloid (GNPs in this case) to the solid surface is determined by (1) the initial transfer of GNPs from the bulk solution to the solid surface which is governed by diffusion and (2) the subsequent particle-surface interaction, directed by interaction energy forces.

The diffusion coefficient (D_0) for the 16, 38, and 68 nm GNPs was calculated using Stokes-Einstein equation as follows.[213]

$$D_0 = \frac{\bar{R}T}{N_A}\frac{1}{6\pi\eta r_p} \quad [1]$$

where, $\bar{R}$ [$ML^{-2}T^{-2}K^{-1}C^{-1}$; where M denotes the unit of mass, L denotes the unit of length, T denotes the unit of time, K denotes the unit of absolute temperature, C denotes the unit of molar concentration] is the gas constant; T [K] is the temperature, N_A [C^{-1}] is the Avogadro constant, η [$ML^{-1}T^{-1}$] is the fluid viscosity, and r_p [L] is the radius of the spherical particle. Figure 2C shows the calculated diffusion coefficient for all three GNPs under the experimental conditions. The value of D_0 for 16 nm (3.1×10^{-11} m^2 s^{-1}) and 38 nm (1.3×10^{-11} m^2 s^{-1}) is an order of magnitude higher than the 68 nm (7.2×10^{-12} m^2 s^{-1}). Therefore, the small 16 nm GNPs diffuse to the surface much faster than the 38 and 68 nm GNPs, as depicted in Figure 3A.

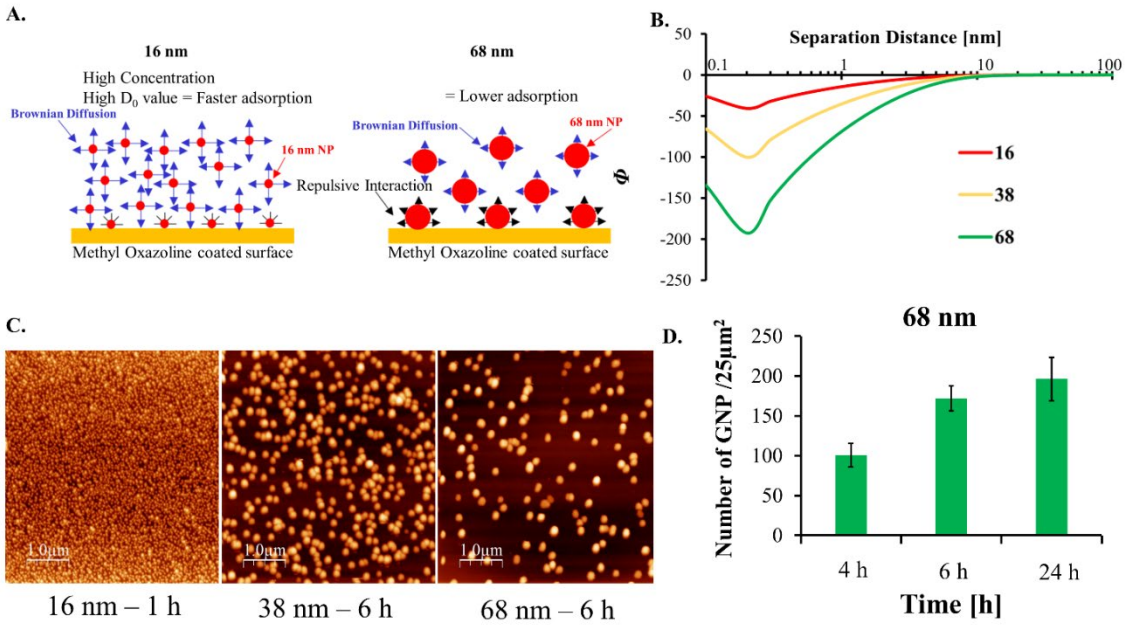

Figure 3. (A) Schematic of the binding process for 16 and 68 nm under the experimental condition. **(B)** The dimensionless interaction energy (Φ) profile for the GNPs at pH 5.5 under the experimental conditions. **(C)** Atomic Force Microscopy (AFM) images of 16 nm GNPs binding after 1 h, and 38 and 68 nm GNPs after 6 h. **(D)** The number of 68 nm GNPs adsorbed on Me-PPOx surface at different time points (4, 6, and 24 h). All the experiments were conducted at pH=5.5.

Moreover, since the same amount of gold was used for the preparation of all three NP sizes, the total number of 16 and 38 nm GNPs present in the NPs solution was approximately 4.2 and 1.8 times higher than the 68 nm NPs, respectively. According to the Fick's first law, which established that the diffusion flux (velocity) is a function of the concentration gradient, colloidal particles are expected to diffuse from high concentration regions to lower concentration regions of the dispersed phase, and faster for greater concentration gradient.[214] Therefore, the flux of the GNPs across the concentration gradient used in this study from the bulk of the suspension to surface, where initially the particle concentration in null is expected to be in the order of 16>38> 68 nm.

Beyond diffusive effect, binding of the colloid (GNP) to a solid surface is controlled by the total interaction energy present at the solid-water interface (SWI). The zeta potential value from Table 1 shows that the Me-PPOx coated surface was positively charged (+16 mV) while all the three NPs were negatively charged under the experimental conditions (pH=5.5). The total interaction energy between a negatively charged GNP and a positively charged solid surface was calculated using Extended Derjaguin-Landau-Verwey-Overbeek (XDLVO) theory [61-64] as follows:

$$\Phi = \Phi_{vdW} + \Phi_{EDL} + \Phi_{BR} \quad [2]$$

where Φ (ML^2T^{-2}, where M is the unit of mass, L is the unit of length, and T is the unit of the time) is the total interaction energy, Φ_{vdW} (ML^2T^{-2}) is the van der Waals interaction, Φ_{EDL} (ML^2T^{-2}) is the electrostatic double layer interaction, and Φ_{BR} (ML^2T^{-2}) is the interaction due to Born repulsion. The value of Φ_{vdW} was determined from the expression of Greogory.[215] The value of Φ_{EDL} was calculated using the Hogg-Healy-Fuerstenau expression [216] with zeta potentials (Table 1) in place of surface potentials. The value of Φ_{BR} was calculated using the approach of Ruckenstein and Prieve by setting the collision diameter at 0.21 nm to achieve a primary minimum depth at 0.157 nm.[217, 218] The interaction between the GNP and the solid surface was mainly controlled by the energy barrier to attachment in the primary minimum ($\Delta\Phi_a$), the depth of the primary energy minimum (Φ_{1min}); and the energy barrier to detachment ($\Delta\Phi_d$); the value of $\Delta\Phi_a=\Phi_{max}-\Phi_{2min}$ and the value of $\Delta\Phi_d=\Phi_{max}-\Phi_{1min}$, where Φ_{max} is the height of the energy barrier and Φ_{2min} is the depth of the secondary minimum.[219]

Table 1. The measured zeta potential value for COOH-functionalized GNPs and Methyl Oxazoline coated glass surface at various experimental pH.

Material	**Size**	**pH**	**Zeta Potential**
	[nm]	[-]	[mV]
NP	16	5.5	-31.1
	38	5.5	-32.5
	68	5.5	-35.4
	68	4	-32.4
		5	-34.1
		6	-36.5
		7	-38.3
Surface	NA	4	+26
		5	+16
		6	-8
		7	-12

Figure 3B shows the dimensionless (divided by the product of the Boltzmann constant and absolute temperature) interaction energy (Φ) profiles for the GNPs at pH 5.5 (other parameters including ionic strength = 10 mM and Hamaker constant = 1×10^{-20} J at 20°C were used). For all the three NPs, the height of the $\Delta\Phi_a$ was negligible (<0.009) while Φ_{1min} was very deep (16 nm = -40.67, 38 nm = -100.04, and 68 nm = -192).

Therefore, the conditions were highly favourable for attachment. At the initial stages of the experiment, the presence of a very high electrostatic attractive force between the positively charged surface and negatively charged GNPs enhances the binding of GNPs. However, as the number of the negatively charged GNPs adsorbed to the surface increases with time, the electrostatic attraction and the number of favourable sites available for attachment decreases. When the negatively charged GNP approaches the surface, it may experience the electrostatic repulsion from an already deposited negatively charged GNP which is located in the zone of influence and this might lead to blocking over time.[220] Therefore, the rate of attachment of GNPs decreases with the reduction in the number of available favourable sites over time.

However, due to their high concentration and D_0 values, the 16 nm NPs are finding favorable binding sites faster than the 38 and 68 nm NPs which require more time to diffuse and eventually establish a Φ_{1min} attachment on the surface (Figure 3A). In a first attempt to counterbalance the diffusion-interaction energy-effects, the 38 and 68 nm NPs were left to interact with the surface for longer time than the 16 nm particle, namely for six and one hours, respectively. AFM was used to visualize and quantify the number of adsorbed GNPs (Figure 3C). This initial experiment shows that six hours was not sufficient to reach a maximum number density of 68 nm GNPs. Therefore, longer incubation time (24 hours) were investigated. Analysis of the AFM images showed that the number of 68 nm GNPs bound to the surface (Figure 3D) reached only 200 GNPS per scan area (25 μm^2) after 24 h incubation.

3.5.3. Effect of pH

The effect of pH on GNPs binding to the Me-PPOx surface was investigated with the aim to increase the binding of 68 NPs. Figure 4A shows the AFM image of MSA-modified 68 nm GNPs bound to the Me-PPOx coated surfaces as a function of solution pH after 5 hours of incubation. The concentration of GNPs on the surface increased with decreasing pH and the maximum binding occurred at pH 4.

The MSA modified GNP have carboxylic acid groups on their surface which has pKa_1 3.30 and pKa_2 4.94.[221] Therefore, at pH 3, where all negative charges vanish, the GNPs lose colloidal stability and agglomerate on the surface (Figure S1). As the pH of the solution increases from 3 to 7 (pH >> pKa), the negative charge c ($-COO^-$) of the GNP increases thus increasing both the thickness of the electrical double layer and the

GNP stability.[222] The Me-PPOx surface, on the other hand, has a high positive charge at pH=4 which reduces as the pH goes up to eventually become negatively charged above pH =6 (Table 1). The presence of a thin electrical double layer for the GNPs (i.e. less negative charge ~-32 mV) and high positive charge (+26 mV) of Me-PPOx surface, therefore, explain the maximum binding observed at between pH 4 and 5, where conditions were most favourable for attachment.

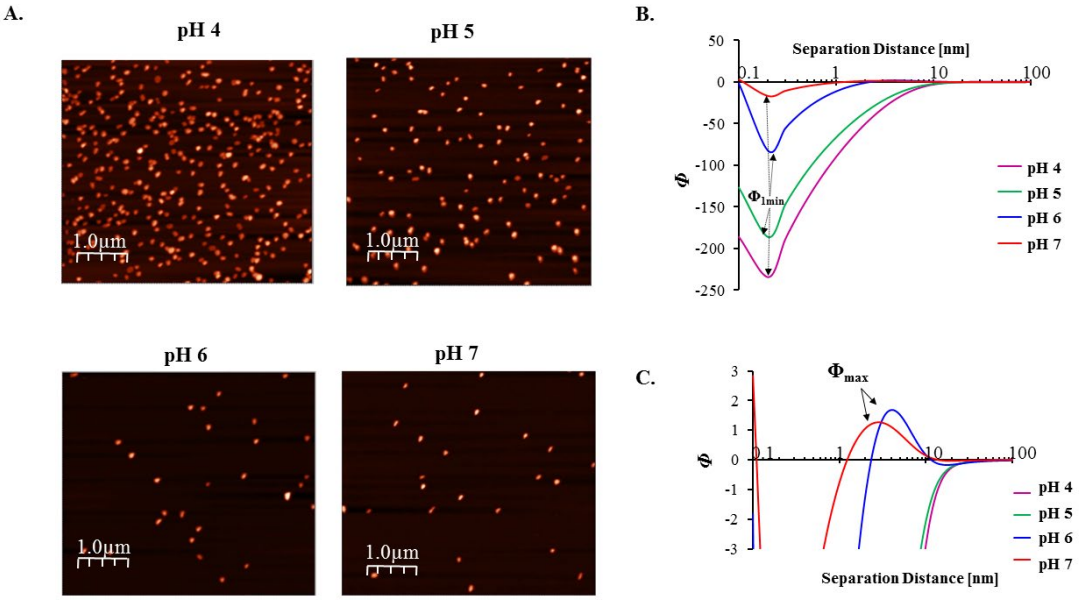

Figure 4. **(A)** AFM images of 68 nm GNP attached to the Me-PPOx surface after 5 hours with different pH. **(B)** The dimensionless XDLVO interaction energy (Φ) profile for COOH-functionalized 68 nm GNPs at pH=4, 5, 6, and 7. The depth of the primary minimum to attachment (Φ_{1min}) is highlighted with the arrows. **(C)** The inset plot with a smaller y-axis shows the height of the energy barrier to attachment (Φ_{max}) for pH=6 and 7 and the Φ_{1min} for pH=4 and 5 at a separation distance of 10 nm.

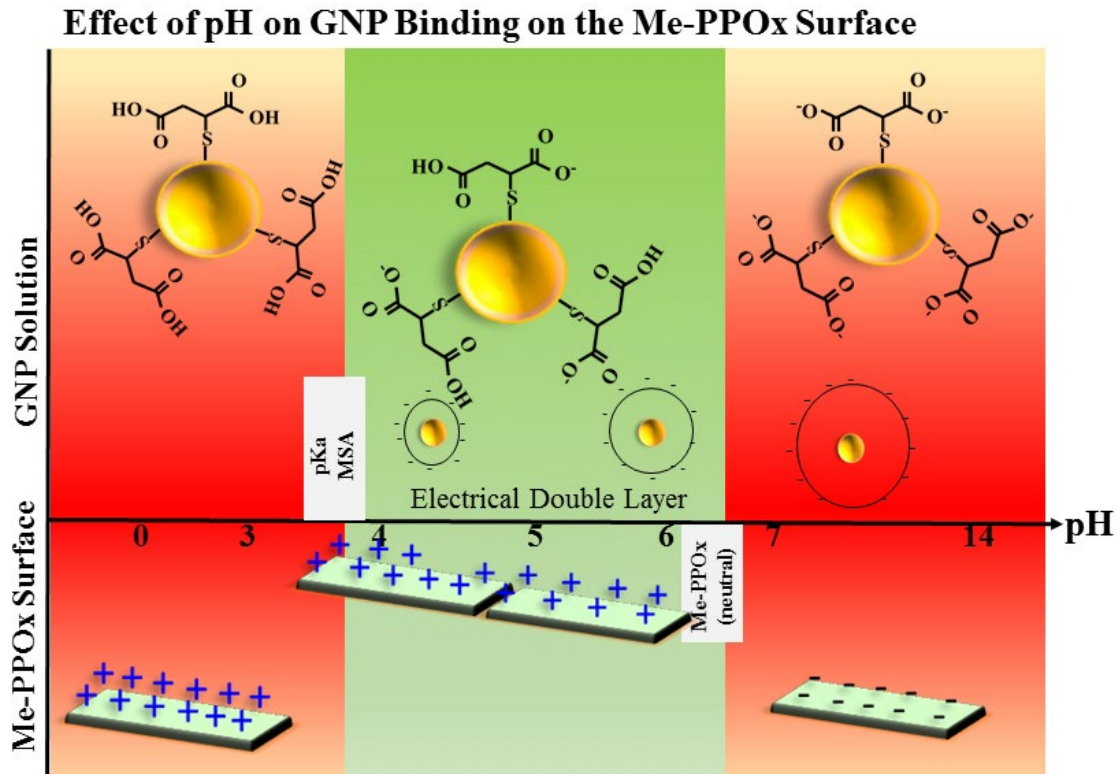

Figure 5. Schematic representation of GNP binding on Me-PPOx surface with different pH conditions.

Further increases in pH lead to a change of polarity in the Me-PPOx surface (+26 to -12 mV) and an increase in electrical double layer thickness (highly negatively charged) of the NPs therefore, leading to reduction in binding. Figure 4C shows the calculated XDLVO interaction energy profile for the 68 nm at pH=4, 5, 6, and 7. The result shows the presence of a shallow energy barrier to attachment of 1.7 and 1.3 at pH=6 and 7, respectively. While there is no energy barrier to attachment and a very deep primary minimum is present from a large separation distance (10 nm) at pH=4 and 5. Therefore, at pH >6 the electrostatic repulsion increases which hinder binding of GNPs to the surface. Thus, our result demonstrated that the most favorable condition for the attachment of 68 nm GNPs to the Me-PPOx surface is between pH=4 and 5. Therefore, in addition, the presence of a deep primary minimum at pH=4 (-234.19) and pH 5 (-186.77) indicate that the GNPs are strongly bound to the Me-PPOx surface. The deposition of GNPs in a deep primary minimum will lead to the irreversible attachment of the GNPs by the formation of a covalent binding between the intact oxazoline rings on the Me-PPOx film and the COOH- functional group on the GNPs through the formation of amide bonds.[163] Overall, the increase in the depth of primary minimum coupled with

the elimination of electrostatic repulsive force at the low pH (4–5) increased the GNPs attachment to the surface (Figure 5).

3.5.4. Well-defined Nanotopography with Equal Nanoparticle Density

The 68 nm GNP attachment has been increased to 300 GNPs per 25 μm^2 scan area after incubation for 5 hours at pH=4. A range of shorter incubation times was tested with the aim to generate a surface with an equal number (300 GNPs per 25 μm^2 scan area) of 16 and 38 nm GNP. The targeted number of 38 nm GNPs was obtained after 1 h 20 min incubation (Figure S2).

A very higher number (>>300) of 16 nm GNPs were attached to the substrates in a very short time. Therefore, in order to achieve a modified surface with an identical number of particles (300 GNPs per 25 μm^2 scan area), the 16 nm GNP suspension was diluted 10 times in MilliQ water. The surface concentration of GNP reached the targeted 300 GNPs per 25 μm^2 scan area density within 1 h 10 min incubation (Figure S3). In this manner, nanostructured surfaces with an equal number of nanoparticles of 16, 38, and 68 nm diameters were created.

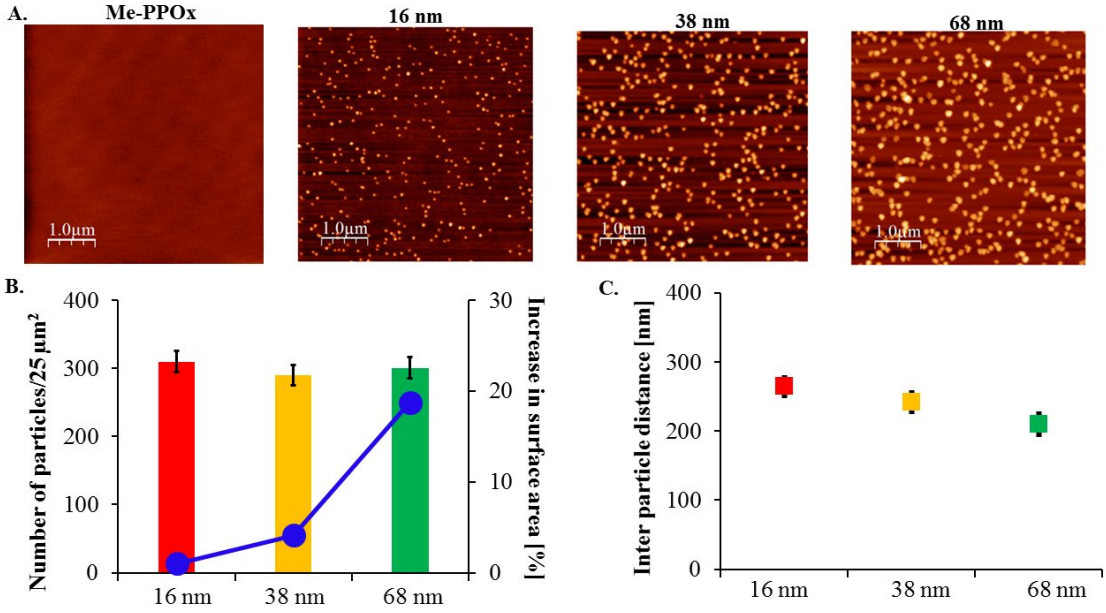

Figure 6. **(A)** A 2D representation of well-defined nanotopography surface with an equal number of 16, 38, and 68 nm GNPs with Me-PPOx overcoating. **(B)** The number of particle binding and percentage increase of surface area compared to the smooth surface. **(C)** Interparticle distance, all calculated from the AFM image of three different nanoparticle sizes.

The GNP was evenly distributed as a monolayer without any clustering and most importantly the surface density was controlled and identical for all 3 NP sizes. Although the GNP surface organization is a random distribution, the distribution is uniform across the whole sample and, therefore, the surface density is well defined. Figure 6A shows the 2D images of the nano-engineered surface decorated with an equal number of particles. Since the three substrates had the same number of surface-bound GNPs, the available surface area increased with the size of the GNP, according to $100n\pi R^2$. Compared to the smooth surface, the surface area increased by 1, 4, and 18%, respectively, for 16, 38, and 68 nm surfaces. Similarly, the average interparticle distance is dependent on the GNP size. The 16 and 38 nm surface had an average interparticle distance of 264 ± 9 and 241 ± 10 nm, respectively, with a difference of only 23 nm. But 68 nm had a comparatively smaller interparticle distance of 210 ± 11 nm, which is 54 nm less than the 16 nm particle bound surface. The reduction of interparticle distance is expected to be due to the difference in nanoparticle diameters.

3.5.5. Creating Uniform Surface Chemistry While Preserving Nanotopography

To generate uniform outermost surface chemistry, a 5 nm thin layer of Me-PPOx was deposited on top of the model substrates with surface-bound nanoparticles. This additional thin layer has the purpose to preserve the nanotopography while tailoring the surface chemistry and also plasma polymerised oxazoline coating with a high power of 50 W has shown to be stable at physiological conditions at 37 ˚C [207, 209]. Table 2 shows the corresponding route mean square roughness (RMS) before and after overcoating. The difference in RMS values before and after overcoating was non-significant. These well-defined nano rough surfaces are a very good model platform to study the specific role of RMS roughness changes from 0.5, 2, and 8 nm. Figure 7 shows the 2 × 2 μm scans and corresponding profile traces for 16, 38, and 68 nm nanotopography surfaces before and after Me-PPOx overcoating. This AFM z-scale analysis confirmed that the nanotopography was preserved after the Me-PPOx overcoating.

Table 2. Root Mean Square (RMS) roughness of modified surfaces before and after overcoating with Me-PPOx to create a homogenized surface chemistry.

RMS Roughness	Me-PPOx	16 nm	38 nm	68 nm
Before Over coating	0.6 ± 0.03	2.7 ± 0.3	8.6 ± 1.0	16.9 ± 0.5
After Over coating	-	2.6 ± 0.2	9.1 ± 0.8	16.8 ± 0.3

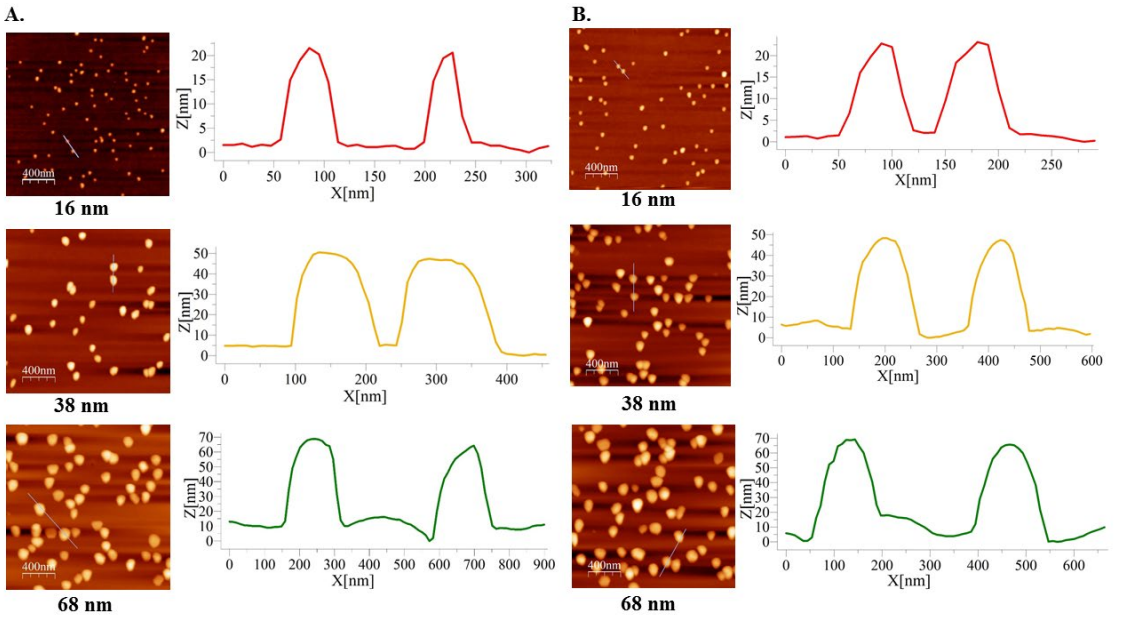

Figure 7. AFM z-scales of 16, 38, and 68 nm nanotopography surfaces (A) before and (B) after overcoating.

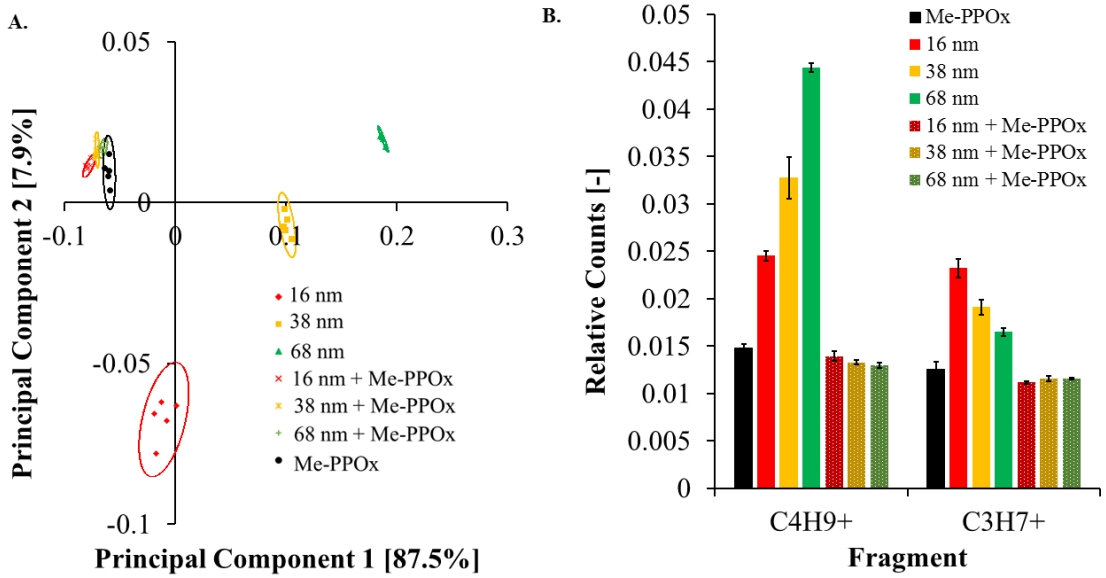

Figure 8. **(A)** Principle component analysis of Me-PPOx over coated surfaces by ToF-SIMS. **(B)** Relative counts of C4H9+ and C3H7+ fragments from +SIMS.

To confirm the uniformity of the overcoating, the outermost chemistry of the surfaces were characterized via ToF-SIMS. This technique is particularly suitable for this purpose since it samples only the first 1–3 nm from the surface. The principle component analysis was used to assess the differences in +SIMS spectra. PC1 (87.5%) was plotted against PC2 (7.9%) revealing discrete discrimination between the Me-PPOx and the surfaces with bare 16, 38, and 68 nm particles (no overcoating) (Figure 8A). The PC1 loadings plot reveled largest differences were caused by changes of C4H9+ (approx. 57 m/z) fragments from the surface (Figure S4). Further analysis of the spectra shows this difference was caused by an increase of secondary C4H9+ fragments ionizing from the surface. The relative counts of C4H9+ fragments are shown in Figure 8B. This fragment is presumably from the organic components encapsulating the GNPs. It is understandable that masking the GNPs with the overcoating will cover these organic components. Upon the addition of the overcoating, the outermost chemistry returns towards the Me-PPOx only state. This is indicated by the highly clustered nature of the PCA of the overcoated samples when compared to the Me-PPOx and the decrease in C4H9+. Interestingly, the PCA revealed that the greatest differences between the bare 16, 38, and 68 nm particles were caused by changes in CxHy+ groups such as C3H7+. As ToF-SIMS is highly dependent on the outermost chemistry of the surface, these changes are most likely due to the differences in total surface coverage of the GNP. As the larger particles cover a greater area of the total surface, the fragmentation patterns from the surfaces would be different, with the most predominant differences being between the 16 and 68 nm surfaces.

Fragmentation during ToF-SIMS is highly dependent on the matrix of the surface being analysed. This makes ToF-SIMS highly sensitive to any small changes in surface chemistry. In this study, the addition of the Me-PPOx overcoating returned the surface chemistry back to the chemistry expected from the planar Me-PPOx. We can, therefore, conclude that Me-PPOx overcoating on top of the nanotopography is uniform and provide homogenized surface chemistry to the well-defined nanotopography surfaces.

Recent studies have proven that geometrical physical cues at the nanoscale affect protein and cellular responses [13, 186, 223] to surfaces. In fact, it is a key parameter in communication between artificial interphase and biological systems.[224] However, published studies where interactions of biological cells and proteins are investigated often

present contradictory results.[53, 152, 154, 189, 194] For example, Dolatshahi et al. reported the protein adsorption studies on nano rough surfaces with glancing angle deposition that shows an increase in fibrinogen adsorption with the increase in surface nano feature size (6, 16, 29, and 39 nm).[154] Whereas, Lord et al. reported a significant decrease in fibrinogen adsorption on silica surfaces with nano feature size of 21 nm, whereas no significant difference in adsorption was observed on 14 nm size surface compared to the planner silica surface.[53]

Studies on cell adhesion and proliferation on nano rough surfaces also reported conflicting results. Adhesion and proliferation of human endothelial cells on nano-scale colloidal silica surfaces (21 nm) were significantly reduced compared with control silica surfaces.[153] Gerecht et al. also reported reduced adhesion of human embryonic stem cells on surfaces with 600 nm nano rough features.[225] Whereas, Rebollar et al. reported an increased proliferation of human embryonic kidney cells on surfaces with 200–430 nm nano rough features.[226] This conflicting reports on protein and cell response can be attributed to the inconsistent nanotopography features used in these studies in terms of size and shape of nanotopography features and surface chemical composition. Carefully tailored nanotopography could be used as biomimetic cell modulating cues to effectively control the biological responses [10, 44], but only if both their physical and chemical properties can be controlled effectively. The model surfaces we report here have the unique features such as controlled and well-defined nanotopography, high reproducibility, and uniform outermost surface chemistry that can be tailored at nanoscale in desired manner. These model surfaces will help to understand the real effect of nanotopography size on biological responses. This will facilitate the development of next-generation immunomodulatory biomaterials with nanoscale surface structures to integrate and control the host response. Other fields that could benefit from the model surfaces developed in this work encompass all those relying on the unique optical, electrical, mechanical and above all interfacial properties of nanostructured materials

3.6. Conclusion

In summary, we present a novel approach to prepare well-defined nanotopography by the covalent assembly of GNPs on Me-PPOx surfaces. The nanoparticle surface coverage was found to depend on the pH of the nanoparticle solution, concentrations of nanoparticles in suspension, and reaction time. Well-defined nanotopography were

created by depositing three different size GNPs (16, 38, and 68 nm) with equal number of particle densities on plasma polymer deposited methyl oxazoline surfaces. It is shown that the maximum binding of 68 nm bigger nanoparticle is attained by changing the pH of solution. Equal number density of 16 and 38 nm particle is accomplished by tuning the immobilization time and nanoparticle solution concentration. The additional 5 nm thin overcoating provided homogenized outermost surface chemistry and also preserved the nanotopography. These novel materials provide a unique platform for studies requiring surfaces with controlled densities of different size nanoparticles. These surfaces would be particularly useful for studying protein and cell interactions since an equal number of nanoscale features that varies only in size and a tunable outermost surface chemistry can be derived. The developed platform does not require expensive lithography equipment and can be adopted by the many laboratories working towards understanding and using biological interfaces.

Author Information

Krasimir Vasilev*

School of Engineering, Future Industries Institute,

University of South Australia, Mawson Lakes,

South Australia 5095, Australia

Email: krasimir.vasilev@unisa.edu.au

Tel.: +618-30-25697

Notes

The authors declare no competing financial interest.

3.7. Acknowledgments

The authors are grateful for the scientific and technical assistance of the South Australian node of the Australian Microscopy & Microanalysis Research Facility. The authors thank Dan Graham, Ph.D., for developing the NESAC/BIO Toolbox used in this study and NIH grant EB-002027 for supporting the toolbox development. KV thanks ARC for

DP15104212 and DP180101254, NHMRC for Fellowship APP1122825 and Project grant APP1032738, and the Alexander von Humboldt Foundation for Fellowship for Experienced Researchers.

3.8. Associated Content

Supplementary data for this article (Figures S1(An AFM image of the aggregated GNP (68 nm) at pH3 on Me-PPOx surface.), S2 (AFM images of 38 nm GNP adsorption on the Me-PPOx surface at different immobilization times 10, 20, 30, 60, and 80 min), S3 (AFM images of 16 nm GNPs adsorption on Me-PPOx surface after 10, 20, 30, 45, and 70 min with different GNPs concentrations), S3 (PC1 and PC2 loadings plots showing relative weightings of positive mass spectra ion fragments used in principle component analysis) can be found online.

SI 3.9. Supporting Information

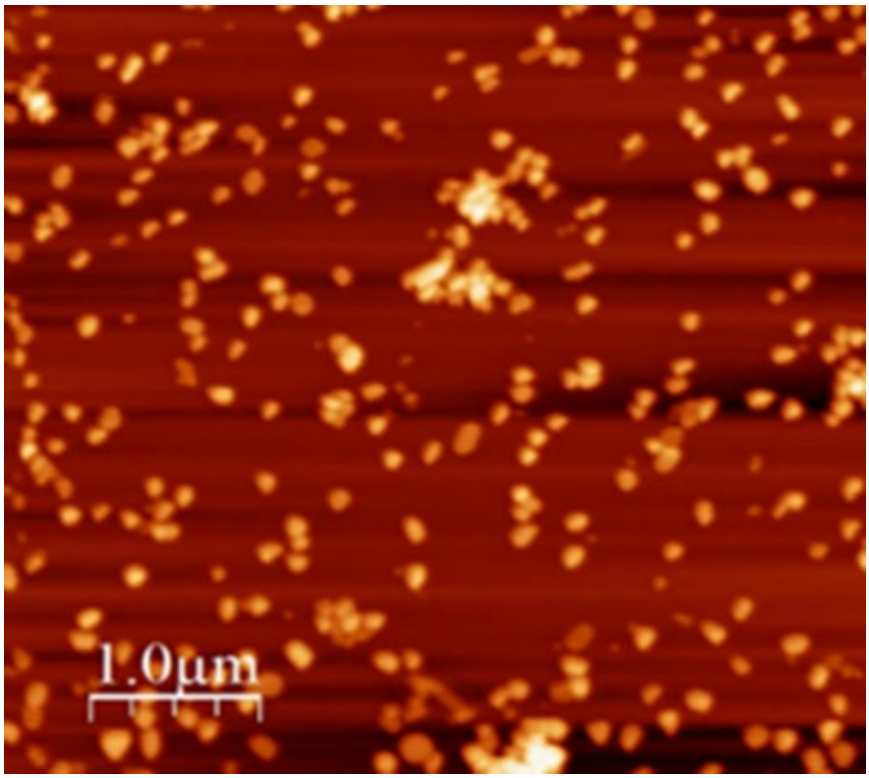

Figure S1: An AFM image of the aggregated Gold nanoparticle (GNP- 68 nm). At pH3 GNP loss colloidal stability and aggregate on Me-PPox surfaces.

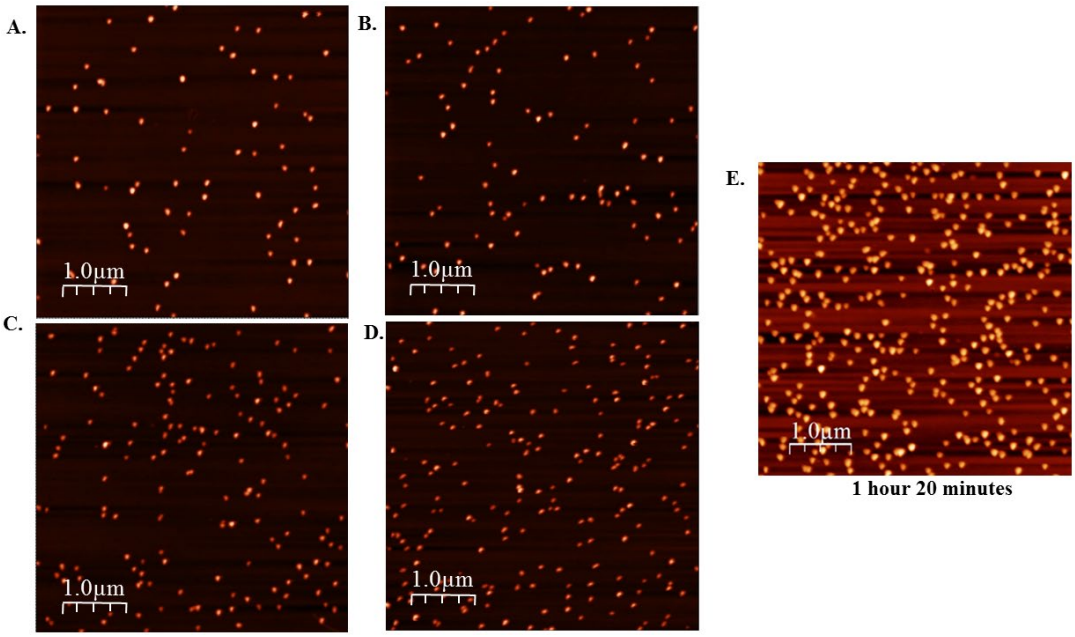

Figure S2. AFM images of 38 nm GNP adsorption on the Me-PPOx surface at different immobilization time points of (A) 10 min, (B) 20 min, (C) 30 min, (D) 60 min and (E) 80 min. As immobilization time increases GNP adsorption increased and reached the required adsorption after 80 min of immobilization.

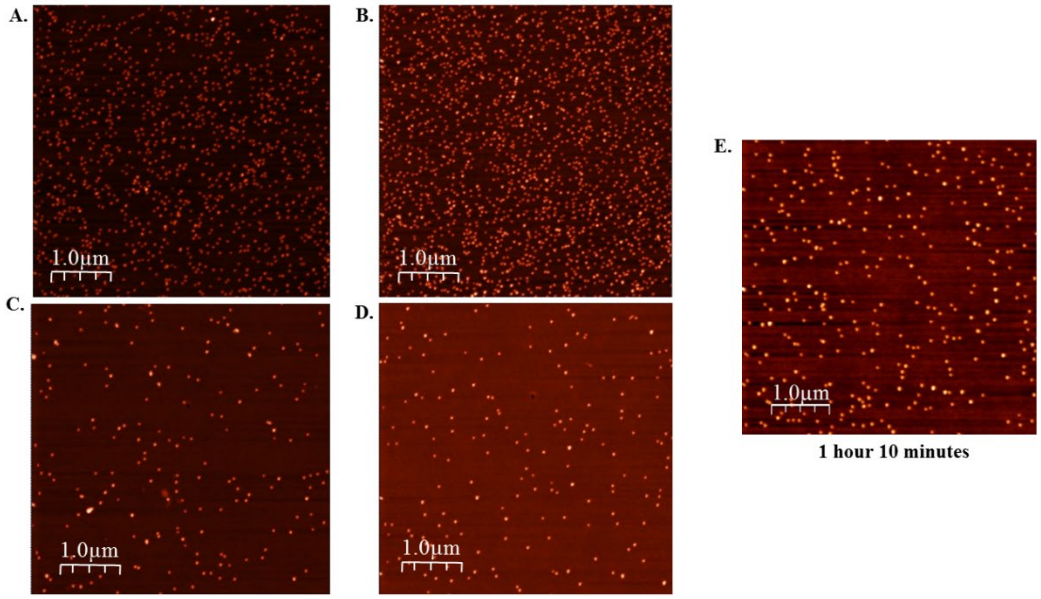

Figure S3. AFM images of 16 nm GNPs adsorption on Me-PPOx surface after (A) 10 and (B) 20 minutes immobilization. (C) 30 minutes and (D) 45 minutes immobilization with 10 time diluted 16 nm GNP. (E) Required number of GNP attached after 70 minutes immobilization with 10 time diluted 16 nm GNP.

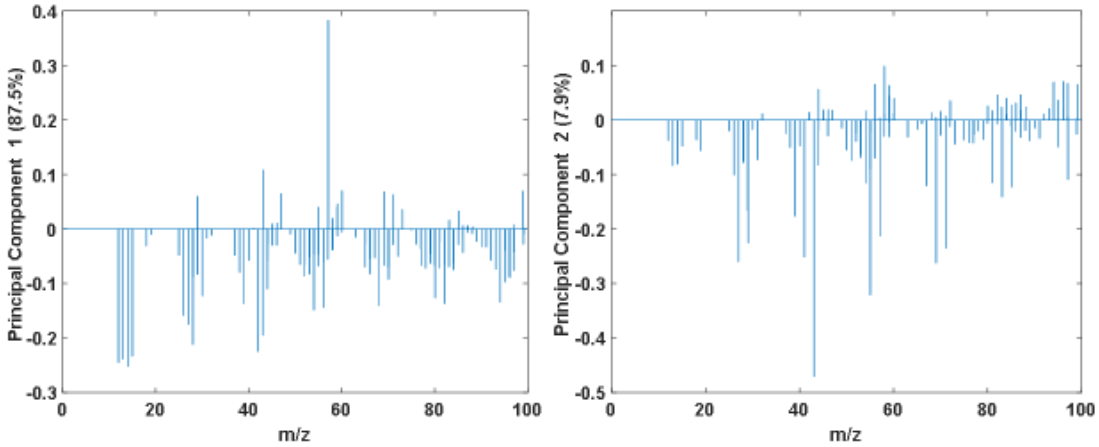

Figure S4. PC1 and PC2 loadings plots showing relative weightings of positive mass spectra ion fragments used in principle component analysis.

SI 3.10. Copy Right Permission

eic@anm.acs.org

4/9/2019 7:49 AM

To: Madathiparambil Visalakshan, Rahul - madry008 Cc: eic@ami.acs.org

Dear Dr. Visalakshan,

Thank you for your message. Prof. Lee grants his approval for your use of the paper in your thesis. Please properly cite the materials and obtain permissions where needed.

Regards,

Aimee Greene
Coordinating Editor, ACS Applied Nano Materials
email: eic@anm.acs.org
TEL: 919-259-3046

-----Original Message-----
From: "Madathiparambil Visalakshan, Rahul - madry008"
<rahul.madathiparambil_visalakshan@mymail.unisa.edu.au>
Sent: Monday, April 8, 2019 3:08am
To: "eic@ami.acs.org" <eic@ami.acs.org>
Subject: Reuse permission for Thesis

Dear Dr. Schanze,
I am Rahul M Visalakshan a PhD candidate from the University of South Australia, Australia. I have published my manuscript ‘’Creating Nano-engineered Biomaterials with Well-Defined Surface Descriptors’’, **DOI:** 10.1021/acsanm.8b00458 in ACS Applied Nanomaterials. I would like to include this manuscript as a chapter in my thesis which is due to submit on 15th April 2019. Therefore, I would like to seek permission from you to add this manuscript as a chapter in my thesis. I will be adhering to the ACS

copyright policy and will be citing the articles as needed. It would be great if you could please grant me the permission.

Thank you,

Rahul M Visalakshan

Chapter 4. Nanotopography-Induced Unfolding of Fibrinogen Modulates Leukocyte Binding and Activation

Wiley Online Library

ADVANCED FUNCTIONAL MATERIALS

https://doi.org/10.1002/adfm.201970088

Nanotopography-Induced Unfolding of Fibrinogen Modulates Leukocyte Binding and Activation

Rahul M Visalakshan, Alex A Cavallaro, Melanie N MacGregor, Emma P Lawrence, Kaloian Koynov, John D Hayball, and Krasimir Vasilev.

Advanced Functional Materials (2019) 1807453.

(Manuscript Published in Advanced Functional Materials)



Statement of Contribution of Co-Authors for Thesis by Published Paper

Author	Contribution
Rahul M Visalakshan	• Experimental design • Conducted experiments • Data analysis • Wrote the manuscript
Alex A Cavallaro	• Technical guidance • Aided data analysis • Assisted in reviewing the manuscript
Melanie N MacGregor	• Aided data analysis • Assisted in reviewing the manuscript
Emma P Lawrence	• Technical guidance for Circular Dichroism Spectroscopy • Aided data analysis
Kaloian Koynov	• Technical guidance for FRAP experiments • Assisted in reviewing the manuscript
John D Hayball	• Technical guidance • Involved in the conception and design of the project • Assisted in reviewing the manuscript
Krasimir Vasilev	• Technical guidance

	• Involved in the conception and design of the project • Assisted in reviewing the manuscript

Principal Supervisor Confirmation

I have sighted email or other correspondence from all Co-authors confirming their certifying authorship.

Krasimir Vasilev 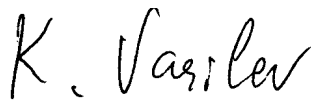 **26/05/2019**

Name Signature Date

Citation:

Visalakshan, R.M., Cavallaro, A.A., MacGregor, M.N., Lawrence, E.P., Koynov, K., Hayball, J.D. and Vasilev, K., 2019. Nanotopography-Induced Unfolding of Fibrinogen Modulates Leukocyte Binding and Activation. Advanced Functional Materials, p.1807453.

4.1. TOC

Nanotopography-induced unfolding of fibrinogen modulates leukocyte binding and activation

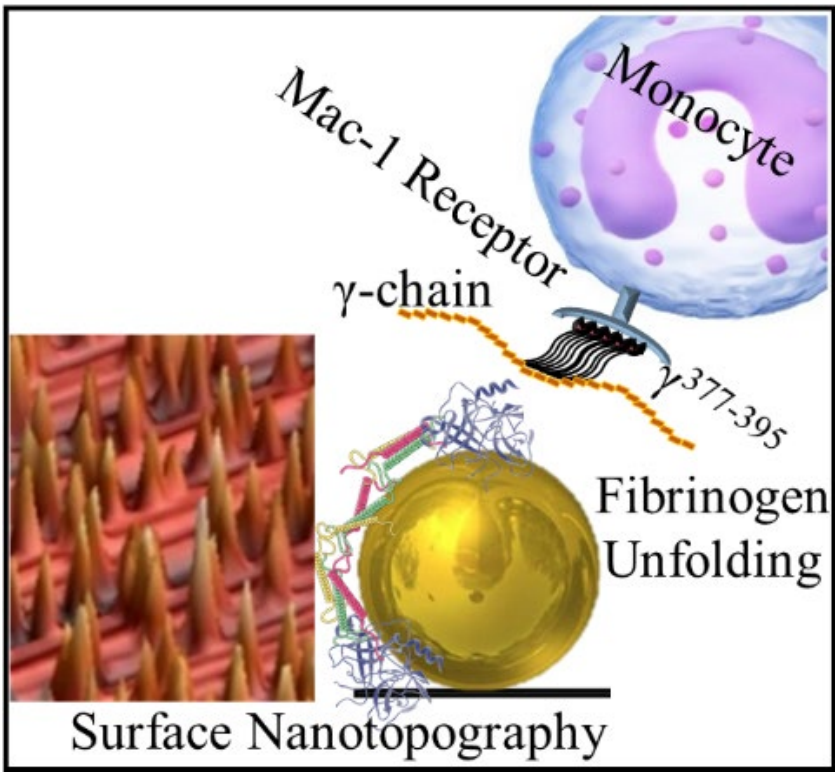

This study provides the missing link between surface nanotopography, protein unfolding, and immune responses. Precisely engineered surfaces demonstrate nanotopography size dependent fibrinogen unfolding and exposure of hidden peptide sequences, which activate the Mac-1 receptor of inflammatory cells. Nanofeatures of around 38 nm lead to minimal protein unfolding and reduced expression of pro-inflammatory cytokines.

4.2. Abstract

Surface nanotopography has been recognized as an important regulator of cellular responses including those of immune cells, the latter being of particular importance for implantable materials since these can determine biomaterial fate. In this paper, evidence is provided that the scale of surface nanotopography modulates the conformation of attached serum proteins which in turn controls immune cell adhesion and activation. Model surfaces of tailored nanotopography of heights of 16 nm, 38 nm, and 68 nm are created by covalent immobilization of gold nanoparticles to an oxazoline rich plasma polymer film. This strategy not only produces surfaces of tailored nanofeature density but allows control of the outermost surface chemistry. Circular Dichroism Spectroscopy and Mac-1 positive THP-1 monocytes studies demonstrate distinct protein unfolding patterns which upregulate or downregulate the expression of pro-inflammatory cytokines and cells attachment. The findings presented in this paper shed light on the missing relationship between surface nanotopography, protein unfolding and the immune response. On another hand, this work demonstrates the possibility to use specifically tailored surface nanotopography scales to modulate and achieve desired immune responses.

Keywords: biomaterial surface nanotopography, protein adsorption, fibrinogen unfolding, cell attachment, immune response

4.3. Introduction

Medical devices are central to modern regenerative medicine where they are used for enhancing, replacing, and restoring organs or bodily functions. However, the performance of biomedical devices is often compromised by unfavorable host immune responses to foreign biomaterials. [1, 2] The pathogenesis of biomaterial-mediated immune response, [3, 4] is an effect dictated by the type of proteins spontaneously adsorbing to the biomaterial surface prior to immune cells accumulation. [5,6] Besides, the amount of adsorbed proteins and their conformational changes depend on the biomaterial surface properties. [3, 7-9] It is therefore essential to understand the role of surface chemistry and topography in regulating protein adsorption, orientation and structural changes and how these biophysical processes affect the subsequent immune responses. [8,10-13] Amongst plasma

proteins, fibrinogen has been recognized as a key mediator of inflammatory responses as well as platelet activation, blood coagulation and leukocyte binding. [14,15] Interestingly, it has been recently shown that nanoparticles in solution can induce the unfolding of fibrinogen thus promoting inflammation [16]. However, there is no record yet about the conformational behavior of fibrinogen on nanostructured surfaces and whether surface-mediated unfolding could also be responsible for the resultant immune responses.

Despite a growing interest in studying cellular responses and protein adsorption to different nanorough substrates, [7,17,18,19] a mechanistic understanding of the actual role of nanostructures on surface - protein - cellular interactions is still missing and published data often appear contradictory. For instance, conflicting reports show that fibrinogen adsorption and cellular adhesion may be either encouraged or discouraged by surface nanotopography. [20-24] Such discrepancies arise because many studies concerned with the role of surface nanotopography have until now lacked consistency in terms of nanofeature size, shape, and surface chemical composition. Cell studies have been conducted with a variety of nontopographical features such as tubes, rods, pillars, particles or random surface roughness produced by etching, resulting in a significant degree of polydispersity of height and lateral spacing and importantly, outermost surface chemistry that was not tailored but rather resultant from the fabrication process. [25] To reveal the role of surface nanotopography on protein and cellular response, it is vital to single out the effect of nanotopography, while other variables (surface chemistry, nanofeature size, and shape) are carefully tailored.

Compared to smooth surfaces, nanostructured materials possess a high surface to volume ratio which enhances non-specific protein adsorption. Upon adsorption, proteins may undergo conformational changes and thus expose otherwise hidden sequences toward subsequent interaction with cells which can lead to unpredicted immune responses. [26] This was evidenced by Minchin *et al*. for nanoparticles in suspension. They found that fibrinogen bound to polyacrylic acid-coated gold nanoparticles (NP) unfolds and reveal an active site in the C- terminus of the γ chain which specifically interacts with Mac-1 receptors (CD11b/CD18 or αMβ2) and results in the activation of the NF-kβ pathway to produce cytokines from monocytes. [16] Whether similar protein unfolding phenomena occur when nanoparticles are bound to a solid surface is unknown. Significant effort has been carried out to determine the immune response of cells to various

nanorough surfaces, [19,27-29] but little is known about the role of adsorbed proteins on these nanoscale processes. How proteins adsorb and unfold in response to nanotopography, and how this affects immune responses is still an open question that must be answered to gain predictable control over host responses to implanted biomaterials.

In this study, we examined how surface nanotopography, and its scale, can affect the unfolding of fibrinogen protein and affect the Macrophage-1 antigen (Mac-1 receptor) cell binding to modulate leukocyte immune responses. To derive a mechanistic picture of these nanoscale interactions we engineered model surfaces having controlled nanotopography height of 16, 38, and 68 nm and tailored the outermost surface chemistry to be uniform and identical for all samples. We further interrogated the role of unfolded proteins and adhesion molecules in how immune cells interact with these nanoengineered substrates using the THP-1 monocyte/macrophage cell line.

4.4. Results and Discussion

4.4.1. Model Surface with Well-Defined Nanotopography and Surface Chemistry

In order to understand the role of nanotopography, it is important to create substrates where nanostructures size and surface density are well-defined, and the outermost surface chemistry is identical for all samples. To achieve this goal, we used a combination of plasma-assisted nanoengineering techniques which have been well documented as a utility in surface modification of biomaterials. [25,30,31] Substrates were first coated with 20 nm thick plasma polymerized methyl oxazoline films (Meox). These coatings were chosen for their biocompatibility, [32,33] and their low-fouling properties, [34] but most importantly for their reactivity towards carboxylic-acid functions. Meox polymer coatings are known to facilitate the covalent binding of ligand with a carboxylic acid functional group, including gold NPs and biomolecules. [35] To produce a well-defined nanotopography with a controlled surface density of bound NPs, Meox modified surfaces were incubated in a suspension of monodispersed COOH-functionalized gold nanoparticles with diameters of 16, 38, and 68 nm (TEM image **Figure S1**). This approach results in the irreversible binding of nanoparticles to Meox surfaces. [35] The incubation time and NPs concentration was adjusted for the three different NPs sizes in order to achieve a controlled number density of NPs assembled on to the surface. [36] In a final step, a 5 nm thin overcoating of Meox chemistry was deposited on top of the surface-

bound NPs to provide an outermost surface of uniform chemical composition for the following biological studies. Without this final step, the resultant surface would have had mixed chemistry consisting of both the negatively charged carboxylic acid group from NPs and the underlying Meox chemistry.

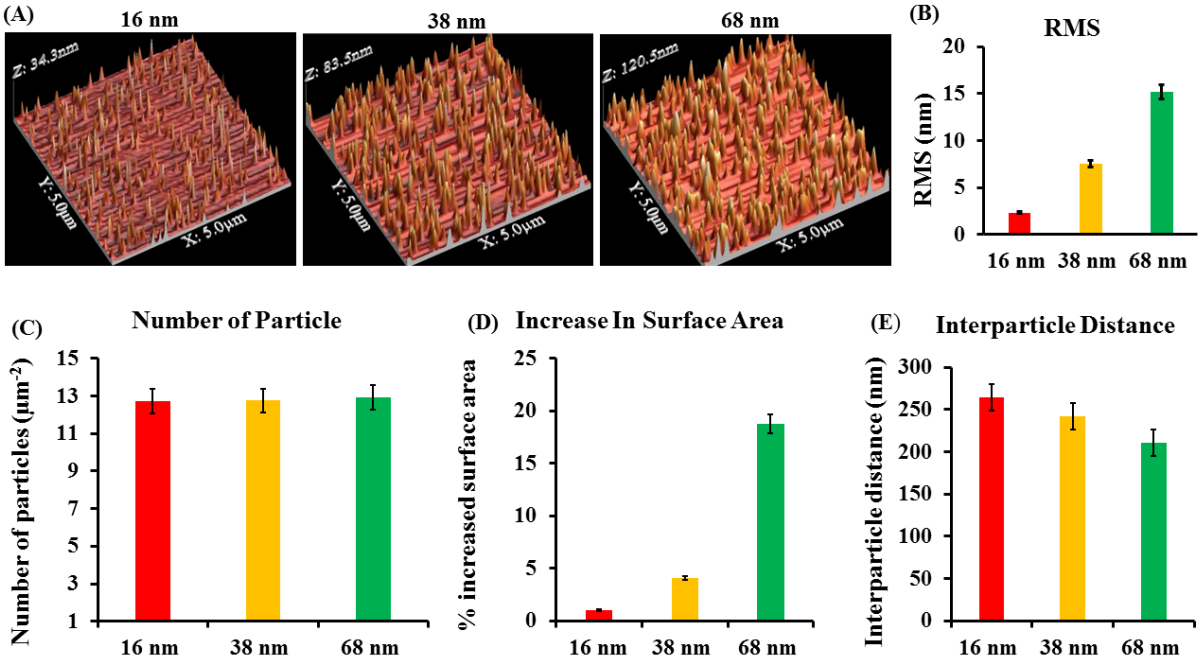

Figure 1. (A) 3D representation of AFM images of gold nanoparticles of 16 nm, 38 nm, and 68 nm immobilized on Meox showing the modified surface nanotopography in 3D format and overcoated with 5 nm thin plasma polymer film. **(B)** RMS values, **(C)** number of particles on different surfaces, **(D)** increase in surface area with NPs size, and **(E)** interparticle distance extracted from the AFM images.

Atomic force microscopy (AFM) was used to characterize the substrate nanotopography. The 3-dimensional AFM images in **Figure 1A** demonstrate that the nanotopography was well preserved after the deposition of a 5 nm thin overcoating and that the number of surface-bound particles were identical for all three NP sizes, namely 12±2 per µm, **Figure 1C**. As a result, all surfaces had a comparable average inter-particle distance in the range of 210 to 260 nm (**Figure 1E**). As expected, the overall surface area increased significantly with increasing nanoparticle diameter (**Figure 1D**). The root mean square (RMS) roughness extracted from AFM measurements was the highest (15 nm) for the nanotopography produced using 68 nm nanoparticles and gradually reduced to 7 nm and 2 nm for 38 nm and 16 nm nanoparticles, respectively (**Figure 1B**). From earlier studies, we knew that plasma polymer coatings thicker than 5 nm are continuous and pinhole free warranting a uniform outermost surface chemistry. [19, 37] This was confirmed

for the present case of Meox films, using XPS and ToF-SIMS principle component analysis.

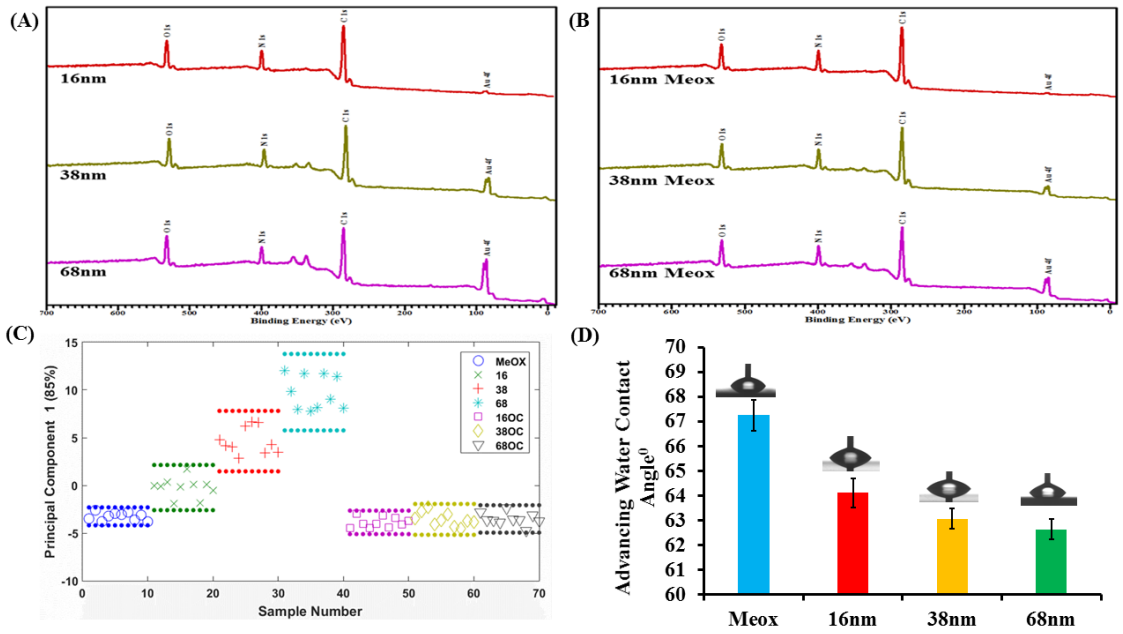

Figure 2. (A) XPS spectra of nanotopography modified surfaces before and **(B)** after methyl oxazoline overcoating. **(C)** Principle component analysis of surfaces from ToF-SIMS before and after Meox overcoating. **(D)** Advancing water contact angle of surface nanotopography with Meox overcoating.

The elemental composition of the nanostructured surfaces before and after overcoating was analyzed by XPS (**Figure 2A and B**). The atomic concentration of carbon, nitrogen, and oxygen measured by XPS were comparable for all nanoengineered surfaces with Meox overcoating, which is evidence that the outermost surface chemistry was homogeneous. The detection of a small amount of gold on these surfaces confirmed that the Meox overcoating was thinner than the 10 nm sampling depth of XPS. The chemistry of the outermost (~ 1-3 nm) layer of the surfaces was probed via ToF-SIMS to confirm the pinhole-free nature of the overcoating. The principle component analysis of +SIMS spectra PC1 (85%) highlighted the differences between nanostructured surfaces with and without Meox overcoating and confirmed a uniform outermost surface chemistry (**Figure 2C**).

Modifying the surface nanotopography led to changes in wettability. **Figure 2D** shows the static advancing water contact angle of nanotopography modified surfaces after Meox overcoating. The addition of nanotopography increased the hydrophilicity of the

surfaces as expected for a pure Wenzel state. Compared to the smooth Meox surface, as the size of the nanotopography increases, the hydrophilicity also increased.

4.4.2 Fibrinogen Adsorption on Surfaces with and Without Nanotopography

The adsorption of fibrinogen on the nanoengineered surfaces was examined using Micro–BCA, QCM-D (Quartz crystal microbalance with dissipation) and FRAP (Fluorescent recovery after photo bleaching) methods (**Figure 3**). FRAP and Micro–BCA measurements were performed directly on surfaces after one hour incubation in 1 mg mL^{-1} fluorescently labeled fibrinogen and rinse with PBS to remove the unbound proteins. FRAP results confirmed strong adsorption of fibrinogen to the Meox (**Figure S2**) and Meox coated nanorough surfaces. The FRAP images and cross-section intensity profiles on **Figure 3A** clearly show that after one hour recovery, both bleached and unbleached parts of the images only slightly increase in intensity. This increase is a result of the continuing adsorption of labeled proteins from solution to both bleached and unbleached interfaces and not from lateral diffusion of the adsorbed proteins, nor from an adsorption-desorption equilibrium, as in the latter cases, a decrease of the intensity difference between the bleached and unbleached parts would have been observed over time. After rinsing the samples and replacing the protein solution with PBS buffer, no further change of intensity in both bleached and unbleached parts occurred. This further confirms that the increase in fluorescence intensity observed in the bleached sections was related to further adsorption of proteins from the solution and not from lateral diffusion or adsorption-desorption events. We can, therefore, conclude that the protein attached strongly on all three nanorough surfaces and that they were not mobile and did not desorb at least at the studied time scale of one hour. These results are in good agreement with our previous work which also demonstrated the irreversible adsorption of proteins on Meox surfaces. [25,32,35]

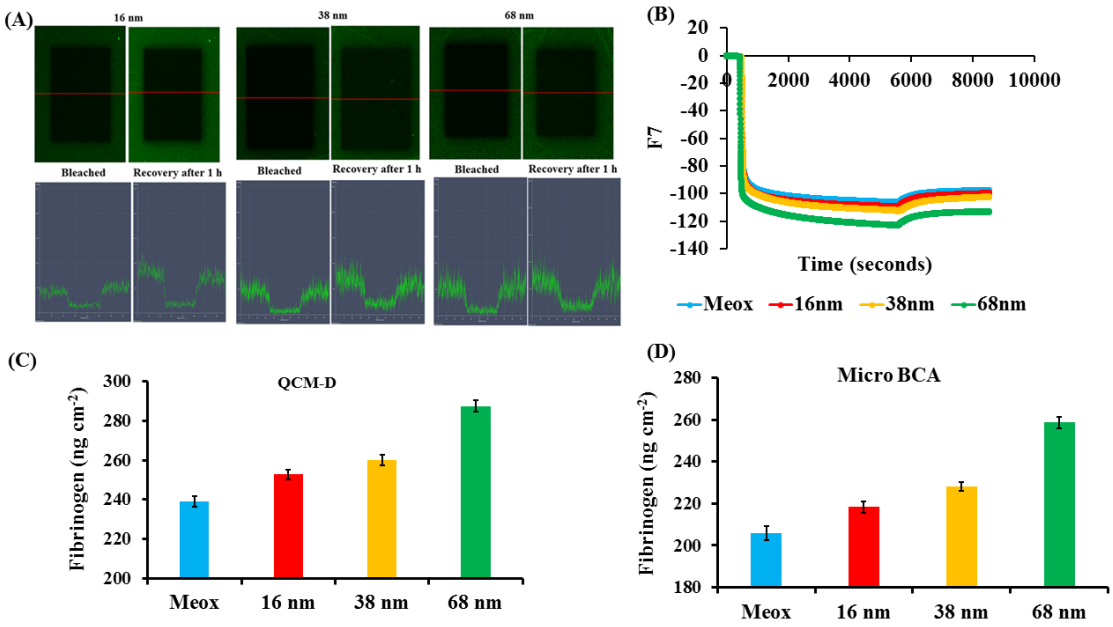

Figure 3. (A) Confocal Fluorescence Microscopy images of nanorough surfaces with adsorbed fluorescent fibrinogen immediately after bleaching and after 1 h of recovery (top), and corresponding cross section intensity profile of FRAP images showing the recovery (bottom). **(B)** QCM-D spectra showing frequency change (Δ f) as a function of time of fibrinogen adsorption on smooth and nanotopography modified surfaces. **(C)** QCM-D and **(D)** Micro-BCA results of fibrinogen adsorbed on smooth and nanotopography modified surfaces.

The amount of surface adsorbed protein was studied by QCM–D and Micro-BCA. For QCM–D measurements, surfaces were initially equilibrated in PBS before introducing 1 mg mL^{-1} fibrinogen solution. The substrates were then incubated with fibrinogen solution in static conditions until a stable frequency was reached, then rinsed with PBS. The data (**Figure 3C**) shows that increasing the size of nanotopography leads to attachment of larger amounts of protein. An identical trend was determined by Micro-BCA (**Figure 3D**). Slightly greater fibrinogen adsorption of about 30 ng cm^{-2} for all samples was measured via QCM- D. This is due to the nature of the technique, which also includes in the measurement the mass of water molecules associated with the proteins. [38,39]

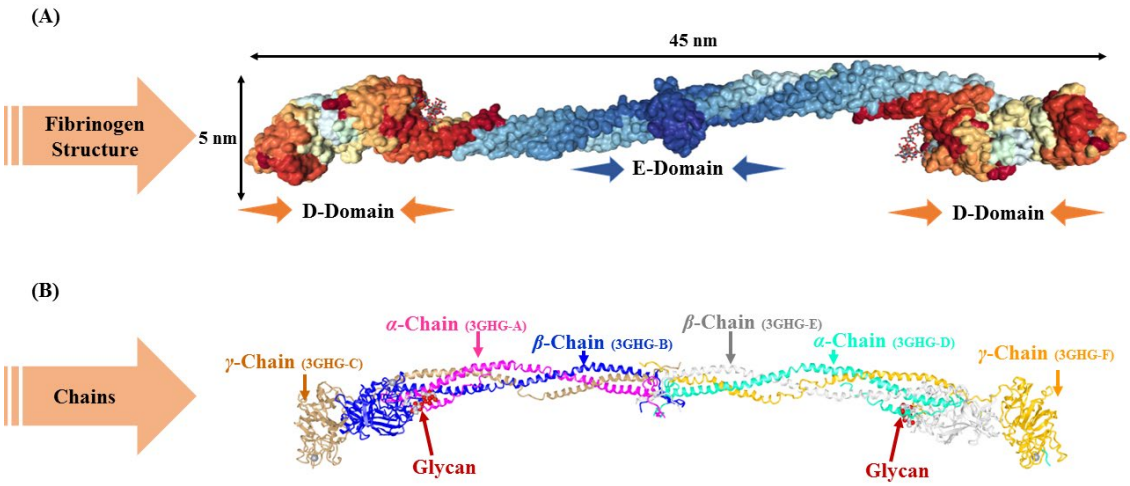

Figure 4. (A) The structure of the human fibrinogen protein obtained from Protein Data Base (PDB ID: 3GHG) (B) The crystal structure of the fibrinogen obtained from the NCBI database that shows the constituting chains and domains.

Fibrinogen consists of three protein chains, namely α, β and γ, organized as a dimer with three domains, two outer D domains and one central E domain (**Figure 4A and B**). [40] In physiological conditions the D and E domains are negatively charged. Meox surfaces are also negatively charged at pH 7.4 (**Figure S3**) therefore, an electrostatic repulsion is expected during the interaction. However, the alpha-C chain is positively charged at physiological pH. [41] Therefore, a localized attractive electrostatic force from the alpha C-chain present on both side of the fibrinogen (which is a free moving end), can draw the protein to the surface and lead to attachment. Both Micro-BCA and QCM measurements showed that fibrinogen adsorption increased significantly with increasing surface nanotopography compared to smooth Meox surfaces. In fact, compared to smooth surfaces, the surface area of the nanoengineered substrate rose by 1%, 4%, and 18% for the 16, 38, and 68 nm surfaces respectively, whereas the percentage of increased fibrinogen adsorption was 6%, 10%, and 21% (**Figure S4**). In other words, the increase in protein adsorption was greater than the corresponding increase in surface area.

Fibrinogen has a rod-like structure of 45 nm in length and 5 nm in width, [16] which may adsorb either parallel to the surface or perpendicular to it, in what we refer to as "side-on" and "end-on" orientations. Based on theoretical calculations, a full monolayer of "side-on" adsorbed fibrinogen adsorption corresponds to 140 ng cm^{-2}, [38,42] which is less than what was measured on any of the surfaces investigated here, including smooth

surfaces (**Figure 3C and D**). On the other hand, the theoretical maximum of fibrinogen adsorption for end-on orientation is 1050 ng cm^{-2}, which is well above the amount measured here. [38] It is therefore likely that on our surfaces a mixture of "side-on" and "end-on" adsorption occurs. However, the surface nano-curvature appear to play a role in dictating the preferred orientation. Since the shape of nanotopography is spherical, the nano-curvature can be calculated as $1/r^2$. Therefore, the curvatures are (16 nm) 0.016 nm^{-2}; (38 nm) 0.0028 nm^{-2}; and (68 nm) 0.00087 nm^{-2}. According to our results, fibrinogen adsorption shows an inverse relationship with the curvature of the surface nanotopography surfaces. Similar fibrinogen adsorption behavior has been observed for hydrophilic and hydrophobic silica beads in solution. [39] This trend was also reported for laminin adsorption on nanostructured surfaces, [43] and albumin adsorption to nanotubes. [44]

4.4.3 Effect of Surface Nanotopography on the Conformation of Adsorbed Fibrinogen

Protein adhesion and conformational changes taking place at the biointerface between an artificial material and the body play a major role in determining the implant biocompatibility .[45] As it binds to surfaces, fibrinogen can unfold and expose amino acid sequences which are usually buried in the folded state. The hidden amino acid sequences 377-395 of the γ chain at the C-terminus of the D domain (Figure 4B), which are exposed upon fibrinogen unfolding, are responsible for the recruitment of leukocytes by acting as a Mac-1 integrin receptor. [46] The effect of surface nanotopography on the unfolding of adsorbed fibrinogen and the associated exposure of the hidden sequences was investigated using far-ultraviolet Circular Dichroism Spectroscopy (CD) and ELISA.

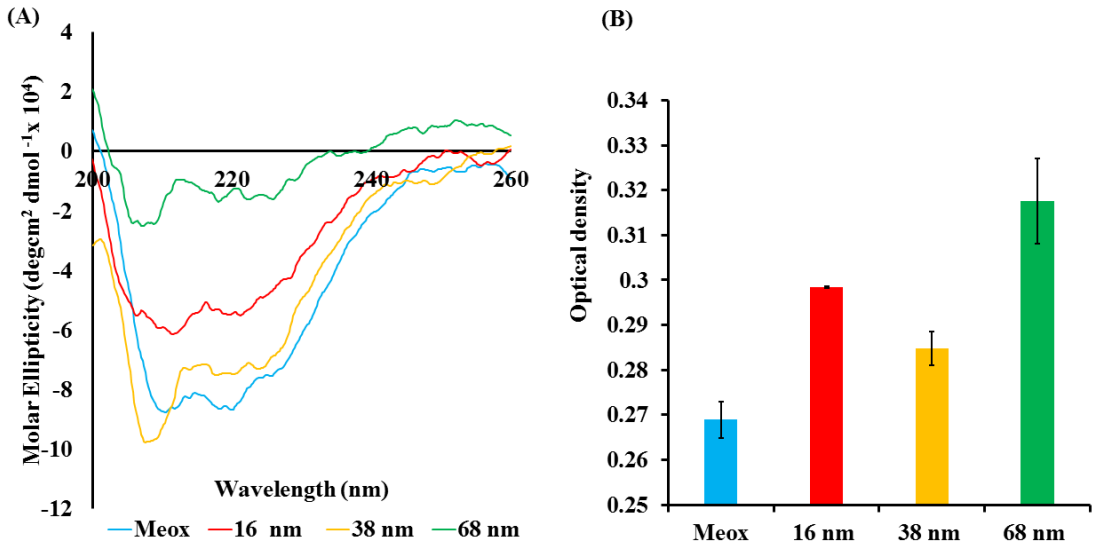

Figure. 5 (A) Circular Dichroism spectra and **(B)** ELISA of recombinant protein fragment corresponding to a region within amino acids 1 and 405 of fibrinogen γ chain of human fibrinogen adsorbed on smooth and nanotopography modified surfaces.

The secondary structure of the fibrinogen adsorbed on smooth Meox surface and those having 16, 38, and 68 nm scale nanotopography was measured by CD and is presented in **Figure 5A**. The α helical structure of fibrinogen in PBS solution is presented in Supplementary **Figure S5**. The spectra of adsorbed fibrinogen on smooth and nanorough surfaces show significant changes in α helicity in the 200–240 nm range of the spectra of adsorbed fibrinogen on smooth and nanorough surfaces indicating that fibrinogen goes through prominent adsorption-induced conformational changes compared to the native fibrinogen solution in PBS. The loss of fibrinogen secondary structure is evidenced in Figure 5A by the progressive increase in molar ellipticity at wavelength of 208 nm and 222 nm. Meox smooth surface and those having surface nanotopography scale of 38 nm appear to cause less unfolding compared to 16 nm and 68 nm surfaces. Fibrinogen may well adsorb differently on the surfaces with 38 nm particles because this topography size is comparable to the size of the protein itself which is 45 nm along its long axis. As the surface nanotopography size increased to 68 nm, fibrinogen underwent a greater degree of adsorption-induced conformational change.

ELISA tests were used to determine whether the nanotopography-induced unfolding leads to the exposure of immune-active sequences. The recombinant protein fragments corresponding to a region within amino acids 1 and 405 (P02679) of the γ chain of fibrinogen were targeted using ELISA. The results showed that smooth surfaces and

those having 38 nm nanofeature size showed comparatively less antibody binding compared to samples with 16 and 68 nm roughness scale (**Figure 5B**). This indicates greater exposure of integrin receptor sequences on the later surfaces due to greater fibrinogen unfolding. In contrast, fibrinogen secondary structure was better preserved on smooth and 38 nm surfaces. ELISA results were in agreement with CD results and showed that the surface nanotopography did alter the fibrinogen unfolding and exposure of integrin receptor sequence. Together with the CD data, these results indicate that the adsorption mechanism of fibrinogen is different on 38 nm topography, namely causing less protein unfolding compared to both smaller (16 nm) and larger (68 nm) surface nanostructures.

4.4.4 Fibrinogen Unfolding and Mac-1 Receptor Binding

Monocytes and macrophages are important mediators of inflammatory and foreign body responses to implanted biomaterials. These cells have the capacity to traffic through systemic circulation and adhere to the surface of an implanted material, [47] and bind to unfolded proteins adsorbed onto the surface of the foreign bodies through cell surface receptors such as Macrophage-1 antigen or Mac-1. [48]

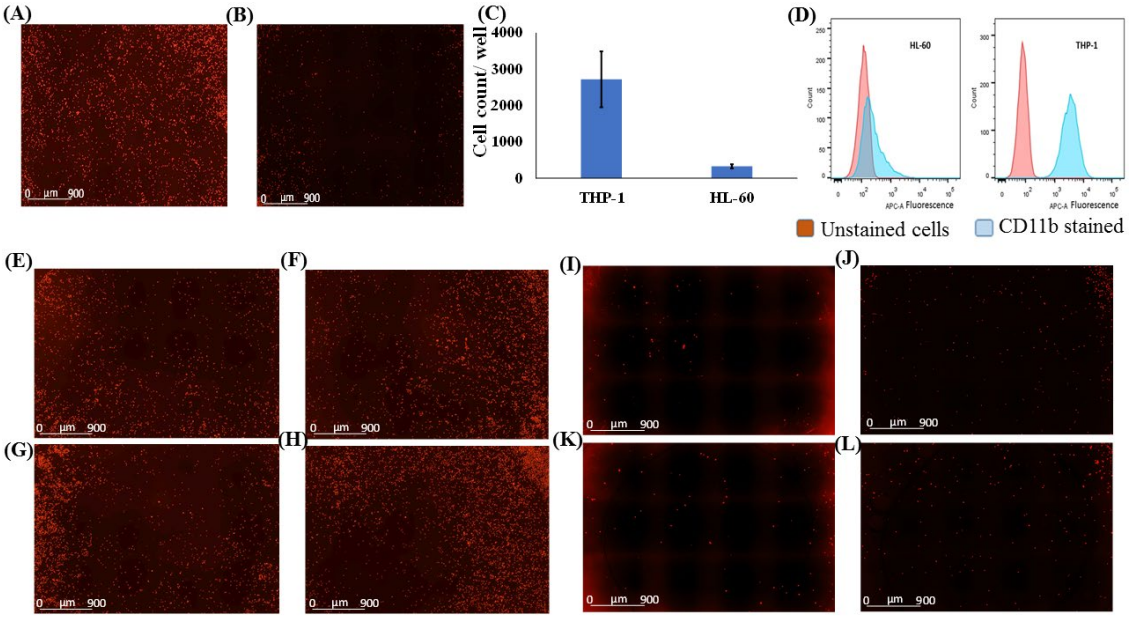

Figure 6. Images of fluorescently labelled **(A)** THP-1 cells and **(B)** HL-60 cells binding to tissue culture plate coated with fibrinogen and **(C)** number of cells attached; **(D)** THP-1 cells are Mac-1 positive cells and HL-60 cells are Mac-1 negative cells as shown by flow cytometry following labeling with CD11b antibody; Images of THP-1 cells attachment to Meox **(E)**, 16 nm **(F)**, 38 nm **(G),** and 68 nm **(H)** surfaces with bound fibrinogen ; Images of THP-1 cell attachment to Meox **(I)**, 16 nm **(J)**, 38 nm **(K),** and 68 nm **(L)** without fibrinogen on.

To test the hypothesis that conformational changes of fibrinogen on nanorough surface modulate immune response, we used Mac-1 positive (THP-1) and Mac-1 negative (HL-60) cells. Flow cytometry studies with CD11b antibody, presented in **Figure 6D**, confirmed that the THP-1 cells were truly Mac-1 positive and the HL-60 cells were Mac-1 negative. A control test using tissue culture plates coated with fibrinogen was first carried out. After 30 min of incubation and PBS washing, only THP-1 cells were found attached to the fibrinogen-coated surfaces (**Figure 6A, B, and C**). This experiment was repeated with the smooth and nanotopography modified Meox coated model surfaces with and without adsorbed fibrinogen (**Figure 6E to L**). Surface attached THP-1 cells were found only on the surfaces having adsorbed fibrinogen (**Figure 6E to H**) while almost no cells were bound to surface without fibrinogen (**Figure 6I to L**). These findings provide evidence that upon adsorption to the surface at least some of the bound fibrinogen was in an unfolded configuration that results in exposure of normally hidden sequences, which act as epitopes for Mac-1 integrin binding. These findings agree with published studies reporting unfolding of fibrinogen and activation of the Mac-1 receptor. [16,46] Fibrinogen is the third most abundant protein in human plasma, normally present in concentrations ranging from 1.5 to 3.5 g L^{-1}. [49] When fibrinogen binds to a surface, it experiences some degree of unfolding which results in the exposure of amino acid sequences normally hidden in its unfolded state. [50] This unfolded epitope acts as a receptor for macrophage integrin's Mac-1 receptor to bind. Activation of Mac-1 receptor, in turn, activate the NF-kB signaling pathway, resulting in the release of inflammatory cytokines, [16] which is investigated as a function of surface nanotopography scale in the next section.

4.4.5 Nanotopography-Induced Unfolding of Fibrinogen Modulates THP-1 Leukocyte Binding and Activation

Pro-inflammatory cytokines are signaling molecules released from immune cells to promote inflammation. Mac-1 receptor activation leads to an increase in the NF kβ signaling pathway and results in the secretion of pro-inflammatory cytokines including IL-8 and TNF-α. [51] TNF-α is one of the key regulators of the immune response and is responsible for the positive regulation of NF kβ pathway. To test how the fibrinogen bound to nanotopography modified surfaces could influence the secretion of cytokines through differences in cell attachment, THP-1 cells were cultured with and without fibrinogen. To eliminate any interference of Fetal Bovine Serum, serum-free media was

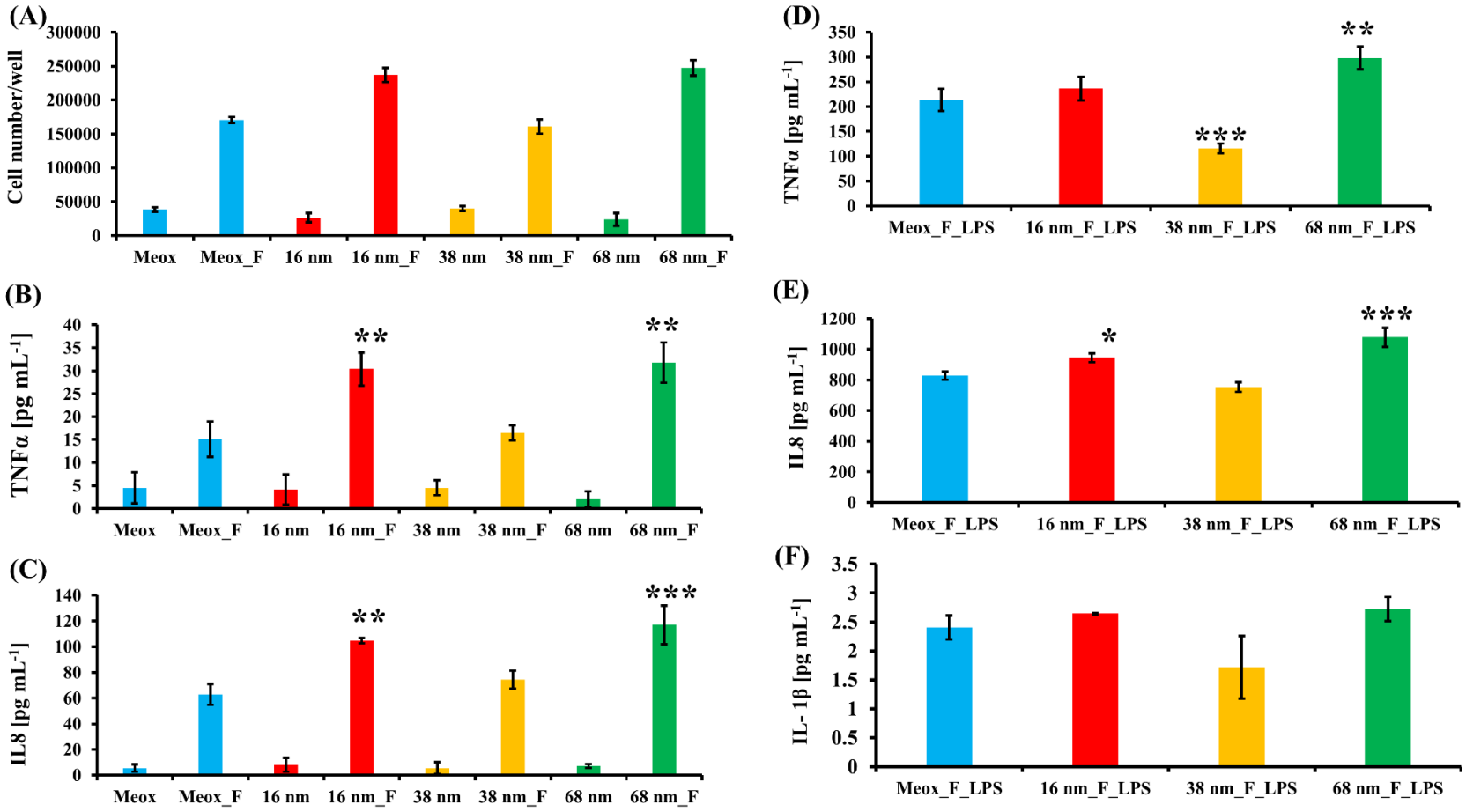

Figure 7. (A) Number of THP-1 cells attached to smooth and nanotopography modified surfaces with and without fibrinogen; Cytokine production **(B)** TNF-α, **(C)** IL-8 from surfaces with and without fibrinogen. Cytokine **(D)** TNF-α **(E)** IL- 8 and **(F)** IL-1β production from THP-1 monocytes stimulated with 1μg mL^{-1} LPS on surface nanotopography with bound fibrinogen. Results are mean+ standard error of the mean, n=3. Asterisk indicates P<0.05 compared to smooth Meox control.

used to carry out these assays. After 2 hours of incubation, the culture supernatants were collected, and the amount of inflammatory cytokines was measured using commercially available human ELISA kit. Cells were then washed with PBS and re-suspended in trypsin buffer. The total numbers of cells were estimated using a hemocytometer.

As shown in **Figure 7A**, the number of attached Mac-1 positive THP-1 cells was governed by the presence of fibrinogen as well as the degree of fibrinogen unfolding. The cell attachment results indicated a strong correlation with fibrinogen unfolding data presented in **Figure 5**, namely a greater number of cells attached to nanotopography scales on 16 nm and 68 nm compared to surfaces that were smooth or had 38 nm high nanoscale features. It is important to recall that the absolute fibrinogen adsorption was proportional to the increase in nanotopography size and surface area (**Figure 3**). However, the cell attachment data showed no such correlation which suggests that small differences in the amount of adsorbed fibrinogen caused by the increased surface area due to added nanotopography does not significantly influence cell attachment.

Surfaces with pre-coated fibrinogen dramatically increased the production of IL-8 and TNF-α (**Figure 7B and C**) on smooth and nanotopography modified surfaces. Expression of both pro-inflammatory cytokines was stimulated on surfaces having nanotopography scale of 16 nm and 68 nm. This increase was greater than 2-fold in the case of TNF-α when compared to smooth Meox surfaces and samples with 38 nm nanotopography (**Figure 7B**). Stimulation with lipopolysaccharide (LPS) naturally increased the overall level of IL-8 and TNF-α expression, however, the observed influence of nanotopography was preserved (**Figure 7D and E**). We should note that TNF-α expression upon stimulation with LPS on 38 nm nanotopography was significantly lower than on smooth surface. We also measured the expression of IL-1β pro-inflammatory cytokine (**Figure 7F**). This cytokine was expressed only upon stimulation with LPS. As with TNF-α, reduced expression was observed when nanotopography scale was 38 nm whereas greatest expression was measured with samples having the highest surface roughness. This data demonstrate that the level of fibrinogen unfolding is significant modulator of pro-inflammatory cytokines expression. Importantly, the nanotopography scale can not only increase but also decrease the release of inflammatory factors by immune cells, phenomenon that can be related to the degree of protein unfolding.

Published studies have so far shown that surface properties such as surface nanotopography and chemistry are some of the important parameters influencing immune cellular reactions. [2, 7, 18] It is also well documented that changes in cellular responses are associated with the concentration and conformation of serum proteins on the surface. [7,8,11,52] However, a detailed understanding of how the scale of surface nanotopography affect conformational changes in serum proteins and the link to inflammatory responses has been missing. In our study, we provide some of these missing links. To achieve this, we created model surfaces where nanofeature size was tailored to 16 nm, 38 nm, and 68 nm using covalently immobilized gold nanoparticles, while spacing between nanofeatures and outermost surface chemistry was tuned identical for all substrates. All stages of the immune response were independently evaluated, beginning from the amount of adsorbed protein, the degree of protein unfolding, integrin-mediated cell adhesion and the levels of cytokine production from THP-1 cells. Interestingly, fibrinogen adsorption increased with increasing the size of surface nanofeatures, but the degree of unfolding did not follow the same trend. Instead, more unfolding was evidenced for 16 and 68 nm nanofeatures compared to smooth surfaces and those with 38 nm protrusions. Cascading from this difference in protein unfolding, both cell attachment and cytokine expression differed markedly between smooth and 38 nm nanoscale surfaces on one hand, and surfaces having 16 nm and 68 nm nanotopography on the other hand, the latter causing increased inflammatory response.

This effect can be explained by the nature of the physicochemical interaction between the spherical nanoparticles and proteins. We first considered purely geometric factors to explain the different behavior observed in terms of “side-on”, “end-on” adsorption orientation. The amount of fibrinogen absorbing to the smooth surfaces indicates that most proteins adsorbed “side on”, with only 7.2% adsorbing with an end-on orientation (discussed above). Increasing the scale of surface nanoroughness has the dual effect of increasing the actual surface area, as well as promoting “end-on” orientation around the spherical nanofeatures, an effect that is strongly size-dependent. Indeed, because the fibrinogen molecule itself is 45 nm long, greater side-on adsorption is expected on the surface with nanoprotusion of comparable size i.e. those having 38 nm nanofeatures. As a result of this parallel orientation to the nanoparticle surface, (schematized in **Figure 8**) strong interactions between both D-domain of the fibrinogen and the surface becomes possible. The presence of strong adhesive force hinders the

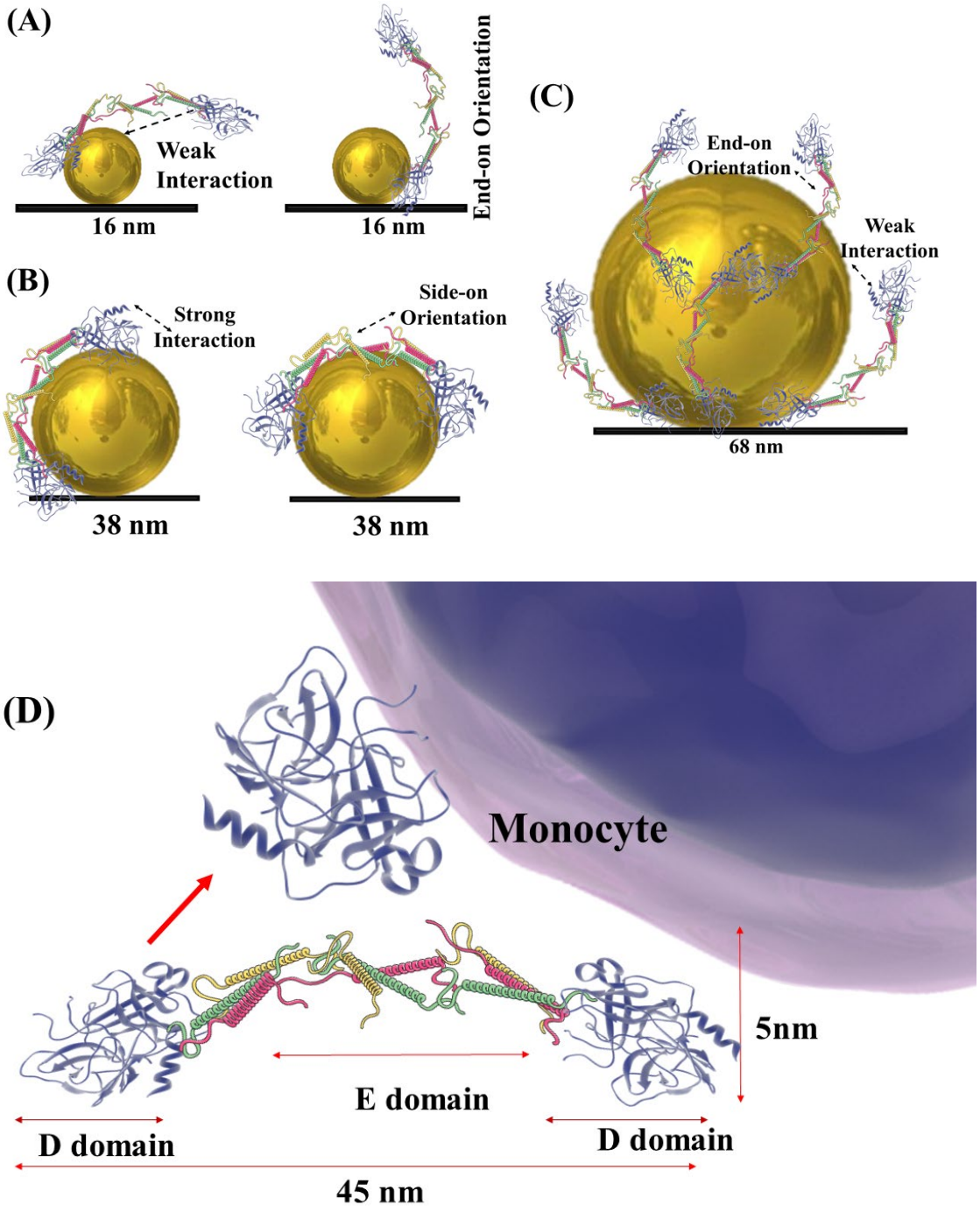

Figure 8. Schematic representing visually and to scale, the adsorption orientation and interaction between fibrinogen molecules and the different size nanotopography surfaces **(A)** on 16 nm surfaces: weak interaction of fibrinogen via end-on and side-on attachment, **(B)** on 38 nm surfaces: strong interaction of fibrinogen via side-on orientation, and **(C)** weak interaction of fibrinogen on 68 nm surface via end-on orientation. **(D)** Pictorial representation of unfolded sequence of fibrinogen (C–terminus of the γ chain on D domain) interaction with Mac-1 receptor of immune cells.

unfolding of the D-domain and therefore reduce the exposure of Mac 1 binding sequences and subsequently the immune response. Minchin *et al*. also observed a similar effect for fibrinogen in solution for particles larger than 20 nm in diameter. [16] In contrast, due to

the difference in curvature, a major fraction of the fibrinogen adsorbing to the 16 and 68 nm surfaces is likely to have a week interaction with at least one of the end D-domain, depicted in **Figure 8**. This can lead to unfolding of the fibrinogen D-domain and presenting of immune response triggering sequences.

Electrostatic considerations further add to the effect of nanotopography size. The presence of the positively charged alpha-C chain will indeed enhance the electrostatic attractions between the fibrinogen and the surface (Meox is negatively charged at physiological pH). [36] With the spiral chain between two D-domains being 17 nm long, even side-on orientation of the fibrinogen onto a 16 nm nanosphere would lead to the alignment of D-domain to the upper hemisphere of the 16 nm feature (**Figure 8A**). In this configuration, the unfolded fibrinogen sequence can be easily detected by the immune cells. Similarly, because the fibrinogen molecule is 1.5 times smaller than the 68 nm nanoparticles, any side-on orientation will still lead to the exposure of one D-domain to the upper hemisphere of the 68 nm nanoparticles (**Figure 8C**). Here again, the unfolded sequence may become easily accessible for immune cells to initiate stronger immune response. In contrast, the 38 nm nanoparticle is only 1.18 times smaller than the fibrinogen molecule. Therefore, any side-on orientation will lead to the alignment of D-domain to intersect between the sphere and the planar surface. We assume that the presence of unfolded D-domain sequences at these intersects will be much more difficult to access by the immune cells. In fact, on the 38 nm nanoparticles, because of the small difference in curvature compared to the 45 nm size of the fibrinogen, strong interactions are also expected for end-on fibrinogen standing against 38 nm nanospheres (**Figure 8B**).

4.5. Conclusion

In summary, our study demonstrates that surface nanotopography strongly affects the unfolding of fibrinogen molecules. This leads to presenting of peptide sequences such as these activating the Mac-1 receptor and subsequent modulation of immune responses. The fibrinogen adsorption to nanotopography in the size ranges of 16 nm, 38 nm, and 68 nm has revealed a distinctive pattern of nanotopography induced fibrinogen unfolding, cell adhesion, and cytokine expression compared to flat surface controls. Notably, nanofeatures size of 68 nm increased Mac 1 positive THP-1 cells binding and pro-inflammatory cytokines expression. The opposite was seen for 38 nm nanofeatures where these cells binding, and pro-inflammatory cytokines expression was reduced. These

findings are important not only because they shed light of the missing link between surface nanotopography, protein unfolding, and immune responses but also because they demonstrate that carefully tailored surface nanotopography can be an effective mean to direct inflammatory response and potentially the foreign body responses to implanted biomaterials.

4.6. Experimental Section

4.6.1. Plasma Polymerization

The model surface was prepared using plasma polymerization technique. A custom-built reactor with 13.56 MHz plasma generator was used. Plasma polymerization is a substrate independent single step method to create pinhole free nanometre thick coatings on any substrates. Methyl Oxazoline was used as a precursor in this study. Substrates were cleaned with acetone and ethanol followed by air plasma cleaning for 5 min at a pressure of 0.1 mbar. A 20 nm thick coating was created by 2 min plasma polymerization of methyl oxazoline at 0.08 mbar pressure, as previously described. [53]

4.6.2. Gold Nanoparticle Synthesize

Gold nanoparticles (NPs) were synthesized by citrate reduction of hydrogen tetrachloroaurate (HAuCl4). HAuCl4 in Milli-Q water was boiled in a reflux loop system under constant stirring. Once boiled, the gold solution was reduced by the addition of 1% trisodium citrate of 1, 0.5, and 0.3 mL to get three different sizes of NP with a diameter of 16, 38, and 68 nm, respectively, which changed the colour of the solution to wine red. This resulting solution was heated for a further 20 min under vigorous stirring and allowed to cool at room temperature. The surface of the gold (NPs) was modified by the addition of 2-mercaptosuccinic acid which provides carboxylic acid (-COOH) surface functional groups.

4.6.3. Immobilization of Gold NPs and Overcoating

Model surfaces decorated with an equal number of surface-bound NPs were prepared with 3 different NPs size by controlling the suspension dilution and the immobilization time onto plasma polymerized methyl oxazoline surfaces (Meox), as previously reported. [36] The experimental pH was kept at pH=4. The 16 nm NPs were diluted to 1:10 with Milli-Q water and immobilized for 1 hour. The 38 and 68 nm NPs were immobilized for 1.5 and 5 hours respectively. Following immobilization, surfaces were washed with Milli-

Q water to remove the unbound NPs and dried under nitrogen flow. The gold NPs bound to the Meox surface created a well-defined nanorough surface with an equal number of particles that differ only in size. The NP bound surfaces were overcoated with a thin layer of Meox (5-10 nm) by adding Meox plasma for 25 sec at 0.08 mbar pressure. This overcoating provides a homogenized chemistry on the surface.

4.6.4. Atomic Force Microscopy (AFM)

An NT-MDT NTEGRA SPM AFM was used to characterize the nanotopography and surface roughness of the samples. AFM was operated in a non-contact mode with Au-coated silicon nitride tips on the reflective side at resonance frequencies between 65 and 100 kHz. Images were taken at an amplitude oscillation of 10 nm and a scan rate of 0.5 Hz. Three images per sample with a scale of 5 × 5 μm were taken and the number of particles were analyzed using Image J software.

4.6.5. X-ray Photoelectron Spectroscopy (XPS)

XPS analysis was performed to characterize the chemical composition of the polymer coating and the atomic concentration of Au NP bound to the polymer surface. Silicon And GErmanium (SAGE) XPS spectrometer was used with monochromatic Mg radiation source operated at 10 kV and 20 mA. The chemical composition of sample surface was analyzed from survey spectra recorded over a 0−1000 eV range with pass energy of 100 eV at a resolution of 0.5 eV. Curve fitting and processing of spectra were performed using Casa XPS software and all binding energies (BE) were referenced to the neutral carbon C1s peak at 285.0 eV.

4.6.6. ToF-SIMS

All ToF-SIMS experiments were performed using a PHI TRIFT V nanoTOF instrument (Physical Electronics Inc., Chanhassen, MN, USA) equipped with a pulsed liquid metal Au+ primary ion gun (LMIG), operating at 30 kV energy. Dual charge neutralization was provided by an electron flood gun (10 eV electrons) and 10 eV Ar+ ions. Experiments were performed under a vacuum of 5×10^{-6} Pa or less. +SIMS spectra were collected from areas of 100 × 100 μm, with an acquisition time of 1 min. Sample spectra and images were processed and interrogated using WincadenceN software V1.18.1 (Physical Electronics Inc., Chanhassen, MN, USA) and PCA performed using NESAC/BIO Toolbox (http://mvsa.nb.uw.edu).

4.6.7. Micro BCA

Protein adsorption onto the surface with nanotopography was analyzed using Micro BCA protein assay kit (Thermo Fisher Scientific, Life Technologies Australia.). A 12 well plate with a surface area of 4 cm^2 was used as a substrate to create surfaces with nanotopography to study the protein adsorption. [54,55] Human Fibrinogen (Sigma-Aldrich), 1 mg mL^{-1} in phosphate buffer saline (PBS), was pipetted onto the surface and incubated for 1 hour at room temperature. After washing three times with PBS to remove the unbound proteins, the micro BCA reaction mixture (250 µL) was placed onto the surface and incubated for 2 hour at 37 °C. The samples were removed from the incubator and transferred to a 96 well plate (200 µL/well, 3 replicates). The absorbance of the colored solution was measured at 562 nm using a spectrophotometer. [56] The amount of protein adsorption was calculated from the standard curve.

4.6.8. Quartz Crystal Microbalance with Dissipation (QCM-D)

Quartz crystal microbalance with dissipation monitoring (QCM-D) was used to study the fibrinogen adsorption on the Meox–coated nanotextured surfaces. QCM-D measurements were performed using a Q-Sense E4 instrument (Q-Sense, Sweden). It was used to assess the real time interaction of fibrinogen with the nanoengineered surfaces created on gold QCM sensors. All 4 sensors were initially equilibrated in PBS. The fluid flow was set to 0.1 mL min^{-1} using a variable-speed peristaltic pump (ISM935, IDEX Health and Science, Germany). After equilibrating the sensors with PBS, fibrinogen 1 mg mL^{-1} concentrated solution was injected and left under static condition for adsorption. After 1.5-hour incubation, the system reached equilibrium and the surfaces were flushed with PBS for another 1 hour to obtain a stable frequency shift. Fluorescence recovery after photobleaching (FRAP): Confocal Laser Scanning Microscopy, images were recorded on a commercial confocal laser scanning microscope LSM880 (Carl Zeiss, Jena, Germany) using a C-Apochromat 40x/1.2 W water immersion objective. The Alexa Fluor®488-labeled human fibrinogen was excited with the 488 nm line of an Argon laser and the fluorescence emitted in the wavelength range 500-553 nm was detected by a spectral detection unit (Quasar, Carl Zeiss). The nanostructured samples with Meox overcoating (16, 38, and 68 nm surfaces were prepared on a glass slide, with diameter of 25 mm and thickness of 0.15 mm) were mounted in an AttofluorTM Cell Chamber (Thermo Fisher Scientific) and covered by 0.5 mL of 1 mg mL^{-1} fibrinogen solution made in PBS buffer. After 10 min incubation, the image plane of the microscope was adjusted on the liquid-

solid interface and a square region of the surface was continuously scanned at high excitation laser intensity in order to photobleach the adsorbed proteins. After that, the laser intensity was decreased to prevent further bleaching and images of the large area of the surface were recorded after 1 hour.

4.6.9. Circular Dichroism Spectroscopy (CD)

The conformational change of the protein bound to the surface nanotopography was measured using a Jasco Model *J-815* spectropolarimeter (ATA Scientific). For CD measurement, a 40 × 9.5 × 1 mm quartz slide with the model surface nanotopography was used as a substrate. Fibrinogen solution with 1 mg mL^{-1} concentration was added to the surface and incubated for 1 hour at ambient temperature. Far-UV CD were acquired in the range 200 to 260 nm with a resolution of 0.2 nm, the bandwidth of 1 nm, and a scanning speed of 50 nm min^{-1}. Eight accumulations were recorded and each spectrum was corrected for background signal by the subtraction of the same sample before protein binding. The sample temperature was kept constant at room temperature by a cell holder incorporating a Peltier device and the sample compartment was continuously flushed with N_2 gas. For the CD measurement of fibrinogen in the solution, 1 mg mL^{-1} fibrinogen dissolved in the PBS was used and a baseline correction was made with PBS solution.

The raw data in millidegrees was converted to molar ellipticity (deg cm^2 $dmol^{-1}$) using the following equation [57-59]

$$(\boldsymbol{\theta}) = \frac{(\boldsymbol{\theta} \times \boldsymbol{M_0})}{(\mathbf{10{,}000} \times \boldsymbol{Q_{ads}})} \quad (1)$$

where, θ is the ellipticity in mdeg, M_0 is the mean residue molecular weight of 118 g mol^{-1} and Q_{ads} [g cm^{-2}] is the concentration of the adsorbed protein on the surface.

4.6.10. Probing unfolding with antibody ELISA

The conformational changes and unfolding of fibrinogen on model nanotopography surface was probed using recombinant protein fragment corresponding to a region within amino acids 1 and 405 (P02679) of fibrinogen gamma. Model nanotopography surface was created on 96 well plate and 1 mg mL^{-1} (100 µL) of fibrinogen added to the surface and incubated for 1 hour. After washing with PBS to remove the unbound proteins, the fibrinogen bound surface was blocked with 2% BSA. Fibrinogen unfolding and exposure of particular sequence responsible for leukocyte binding was detected using the rabbit

primary polyclonal antibody PA5-21968, followed by anti-rabbit HRP secondary antibody. The samples were washed with PBS T (0.05% Tween) in each step. Chromogen and stop solution added afterward and absorbance was measured at 450 nm.

4.6.11. In vitro Cell Culture

THP-1 human monocytic cell line and human myeloblastic/promyelocytic leukemia cell line HL-60 cell lines were maintained in Roswell Park Memorial Institute (RPMI) 1460 media with 10% fetal bovine serum and 1% penicillin- streptomycin at 37% C and 5% CO_2 humidified air. All experiments were performed using exponentially growing cell cultures at cell densities between 1×10^5 and 1×10^6 viable cells mL^{-1}.

4.6.12. Selective Binding and Mac-1 Receptors Expression

THP-1 cells and HL-60 cells were stained with a fluorescent dye Cell Tracker Red CMTPX Dye (Life Technologies, Australia) were incubated on fibrinogen pre-coated 96 well plates for 30 min at 37 °C. Cells were then washed three times with PBS to remove unbound cells and images were taken with a fluorescent microscope.

Mac-1 receptor expression on THP-1 and HL-60 cell lines were studied using flow cytometry. Receptor expression was assessed by flow cytometry after labeling cells with the anti-CD11b antibody (APC anti-human CD11b antibody-Bio Legend).

4.6.13. Immune responses

The immune response to surface nanotopography with and without fibrinogen adsorbed and the role of fibrinogen unfolding on immune cells cytokine expression were examined. Model surfaces with nanotopography were prepared on 24 well tissue culture plates and incubated with 1 mg mL^{-1} fibrinogen for an hour and washed with PBS to remove the unbound proteins. THP-1 cells with a seeding density of 2×10^5 cells mL^{-1} were seeded onto the surfaces with and without fibrinogen. Serum free media were used for the assays subsequently one set of assay were carried with LPS activation, cells were stimulated with LPS (1 μg mL^{-1}). After 2 hours of incubation conditioned media was collected, centrifuged, and the supernatant was stored in -80 °C for further analysis. Cytokine secretion of IL-8, TNF-α, and IL-1β were quantified using human ELISA kits (Bio-legend) according to manufacturer's protocols. Statistical significance was calculated using GraphPad Prism software with One-way ANNOVA analysis. Results are

represented as mean+ standard error of the mean, n=3. Asterisk indicates P<0.05 compared to smooth Meox control.

4.7. Supporting Information

Supporting Information is available from the Wiley Online Library or from the author.

4.8. Acknowledgments

The authors acknowledge the facilities of the Australian Microscopy and Microanalysis Research Facility at the South Australian Regional Facility (SARF), University of South Australia, a facility that is funded by the University, and State and Federal Governments. KV thanks ARC for DP15104212 and DP180101254, NHMRC for Fellowship APP1122825 and Project grant APP1032738, and the Alexander von Humboldt Foundation for Fellowship for Experienced Researchers.

4.9. Conflict of Interest

The authors declare no conflict of interest

SI 4.10. Supporting Information

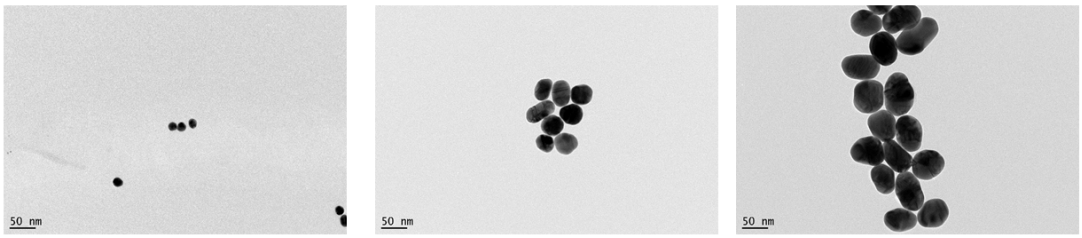

Figure S1. TEM image of MSA modified gold nanoparticles

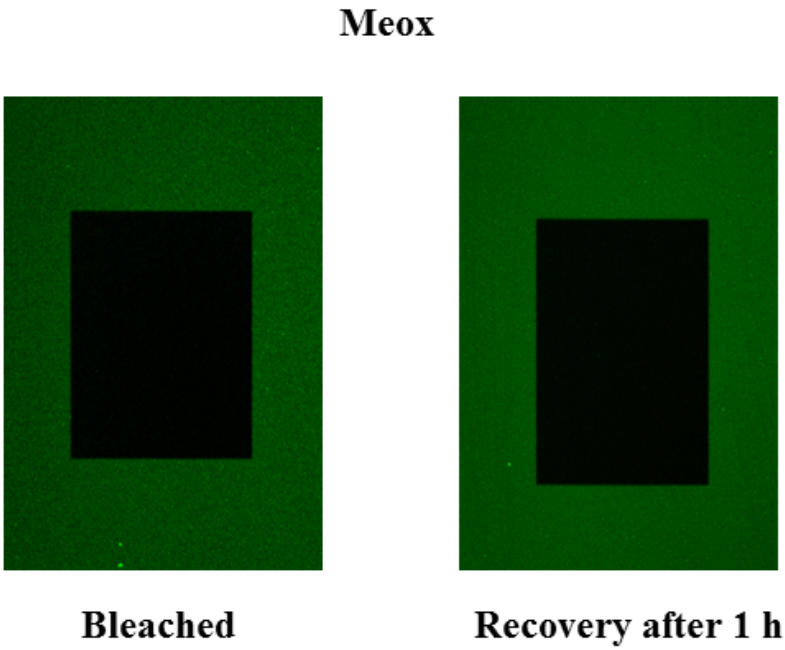

Figure S2. Confocal fluorescence microscopy FRAP images of Meox surfaces with adsorbed fluorescent fibrinogen immediately after bleached (left) and after 1 h of recovery (right).

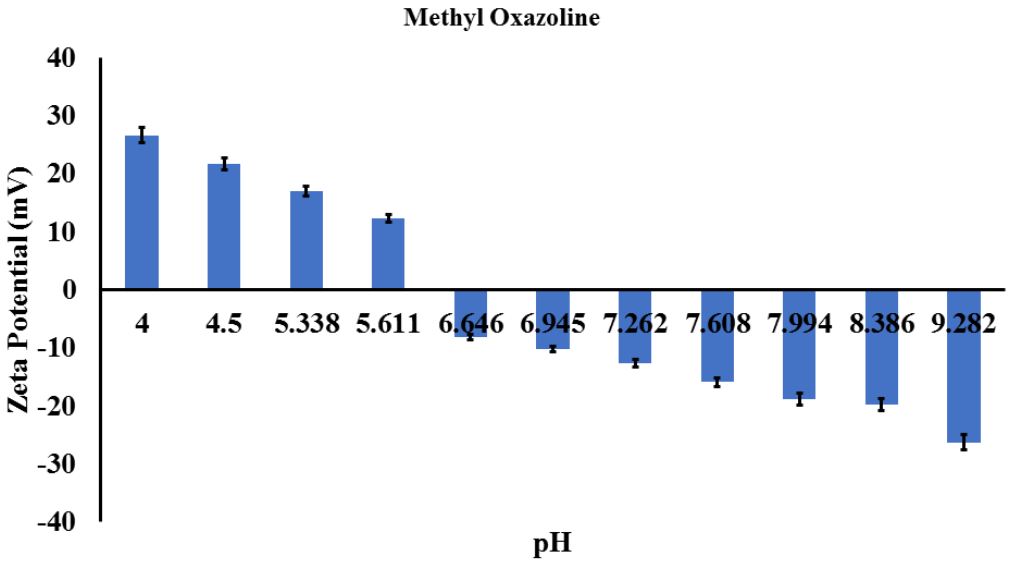

Figure S3. Meox surface zeta potential

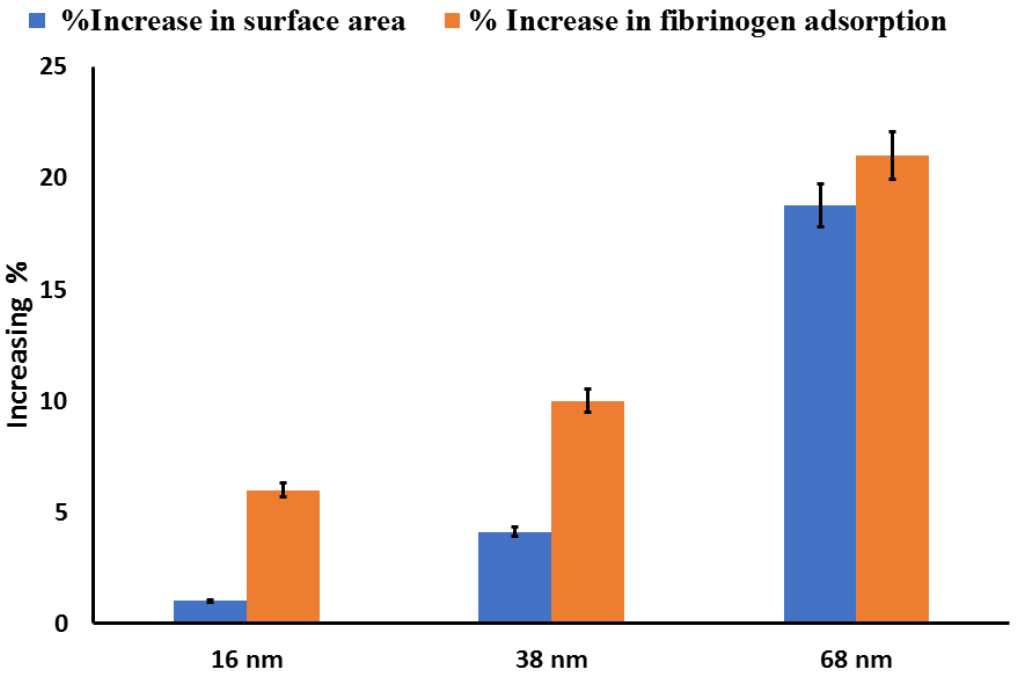

Figure S4. Comparison of increase in surface area and increase in fibrinogen adsorption compared to smooth surfaces

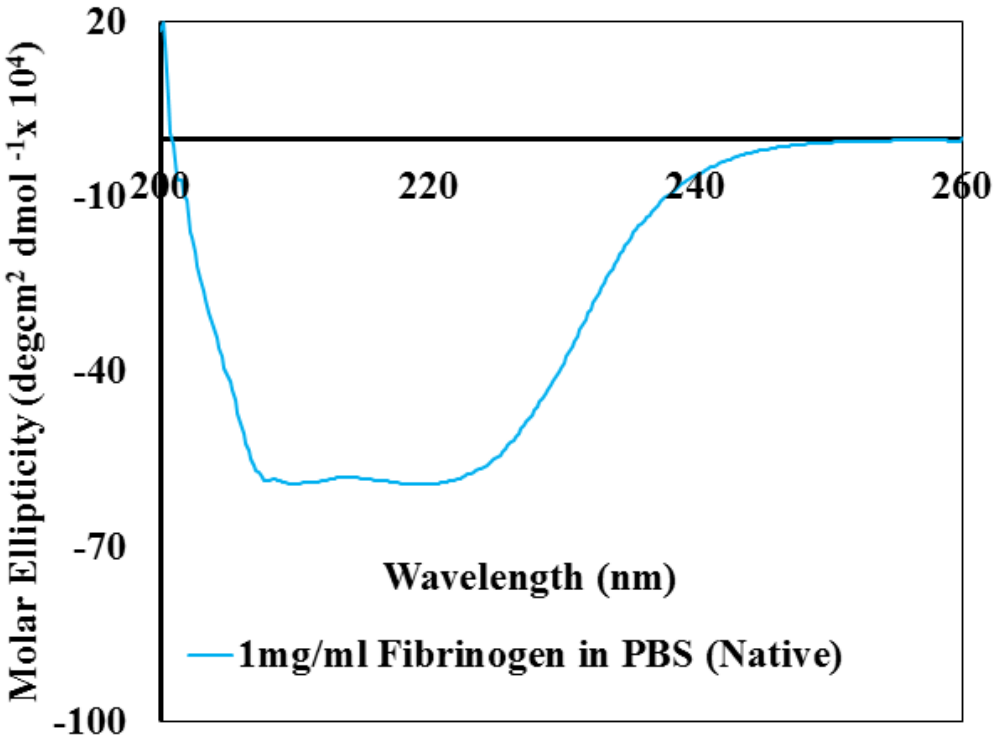

Figure S5. Control CD for fibrinogen in PBS solution

SI 4.11. Copy Right Permission

From: Rights DE

To: Madathiparambil Visalakshan, Rahul - madry008

Cc: Rights DE; AFM

Subject: WG: Permission to Reproduce Article in Thesis adfm.201807453

Date: Monday, 8 April 2019 7:42:31 PM

Dear Rahul M Visalakshan,

We hereby grant permission for the requested use expected that due credit is given to the original source. If material appears within our work with credit to another source, authorisation from that source must be obtained.

Credit must include the following components:

- Journals: Author(s) Name(s): Title of the Article. Name of the Journal. Publication year. Volume.Page(s). Copyright Wiley-VCH Verlag GmbH & Co. KGaA. Reproduced with permission.

If you also wish to publish your thesis in electronic format, you may use the article according to the Copyright transfer agreement:

3. Final Published Version.

Wiley-VCH hereby licenses back to the Contributor the following rights with respect to the final published version of the Contribution: a. […]

b. Re-use in other publications. The right to re-use the final Contribution or parts thereof for any publication authored or edited by the Contributor (excluding journal articles) where such re-used material constitutes less than half of the total material in such publication. In such case, any modifications should be accurately noted. [This applies to each article, not the three articles in total].

Kind regards

Heike Weller

Rights Manager

Rights & Licenses

Wiley-VCH Verlag GmbH & Co. KGaA

Boschstraße 12

69469 Weinheim

Germany

www.wiley-vch.de

T +(49) 6201 606-585

F +(49) 6201 606-332

rightsDE@wiley.com

From: Madathiparambil Visalakshan, Rahul - madry008

<rahul.madathiparambil_visalakshan@mymail.unisa.edu.au>

Sent: Monday, April 8, 2019 09:09

To: AFM

Subject: Reuse permission for Thesis

Dear Dr. Ritterbusch,

I am Rahul M Visalakshan a PhD candidate from the University of South Australia, Australia. I have published my manuscript 'Nanotopography-Induced Unfolding of Fibrinogen Modulates Leukocyte Binding and Activation' in Advanced Functional Materials, https://doi.org/10.1002/adfm.201807453. I would like to include this manuscript as a chapter in my thesis which is due to submit on 15th April 2019. Therefore, I would like to seek permission from you to add this manuscript as a chapter in my thesis. I will be adhering to the Wiley Publishers copyright policy and will be citing the articles as needed.

It would be great if you could please grant me the permission.

Thank you,

Rahul M Visalakshan

SI 4.12. Cover Image Published in the Journal

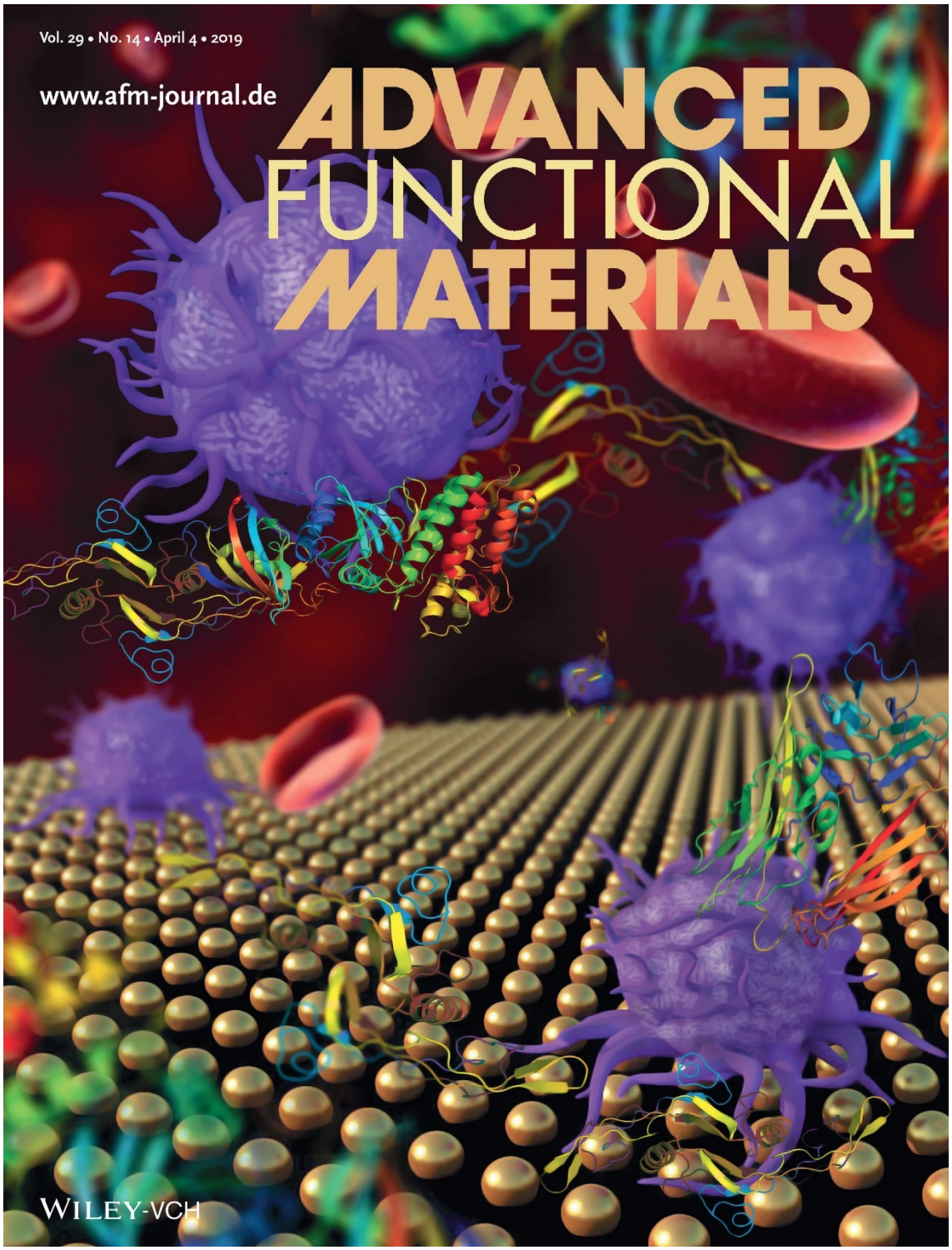

Chapter 5. Hydrophobicity Mediated Serum Protein Adsorption Regulates Inflammatory Consequences to Biomaterial Surfaces





https://pubs.acs.org/doi/10.1021/acsami.9b09900

Biomaterial Surface Hydrophobicity-Mediated Serum Protein Adsorption and Immune Responses

Rahul M Visalakshan, Melanie N. MacGregor, Salini Sasidharan, Artur Ghazaryan, Agnieszka M. Mierczynska-Vasilev, Svenja Morsbach, Volker Mailänder, Katharina Landfester, John D. Hayball, and Krasimir Vasilev.

ACS Appl. Mater. Interfaces 2019,11,31,27615-27623

(Manuscript Published in ACS Applied Materials & Interfaces)



Statement of Contribution of Co-Authors for Thesis by Published Paper

Author	Contribution
Rahul M Visalakshan	• Experimental design • Conducted experiments • Data analysis • Wrote the manuscript
Melanie N. MacGregor Salini Sasidharan	• Aided data analysis • Assisted in reviewing the manuscript
Artur Ghazaryan	• Technical guidance for LCMS • Aided data analysis of LCMS
Agnieszka M. Mierczynska-Vasilev	• Technical guidance for zetapotential measurement • Aided data analysis of Zetapotential
Svenja Morsbach Volker Mailänder Katharina Landfester John D. Hayball and Krasimir Vasilev	• Technical guidance • Involved in the conception and design of the project • Assisted in reviewing the manuscript

Principal Supervisor Confirmation

I have sighted email or other correspondence from all Co-authors confirming their certifying authorship.

Krasimir Vasilev	K. Vasilev	**22/10/2019**
Name	Signature	Date

Citation:

Visalakshan, R.M., MacGregor, M.N. Salini Sasidharan, Artur Ghazaryan,Agnieszka M. Mierczynska-Vasilev, Svenja Morsbach, Volker Mailänder, Katharina Landfester, John D. Hayball, and Krasimir Vasilev., 2019. Biomaterial Surface Hydrophobicity-Mediated Serum Protein Adsorption and Immune Responses. ACS Appl. Mater. Interfaces 2019,11,31, 27615-27623

5.1. Abstract

The nature of the protein corona forming on biomaterial surfaces can affect the performance of implanted devices. This study investigated the role of surface chemistry and wettability on human serum-derived protein corona formation on biomaterial surfaces, and the subsequent effects on cellular innate immune response. Plasma polymerization, a substrate independent technique, was employed to create nano-thin coatings with four specific chemical functionalities, and a spectrum of surface charges and wettability. The amount and type of protein adsorbed was strongly influenced by surface wettability but did not show any dependence on surface charge. An enhanced adsorption of the dysopsonin albumin was observed on hydrophilic surfaces while high opsonin IgG2 adsorption was seen on hydrophobic ones. This in turn led to distinct immune response from macrophages; hydrophilic surfaces drove greater expression of anti-inflammatory cytokines by macrophages, whilst surface hydrophobicity caused increased production of pro-inflammatory signalling molecules. These findings map out a unique relationship between surface hydrophobicity, protein corona formation and subsequent cellular innate immune responses; the potential outcomes of these studies may be employed to tailor biomaterial surface modifications, to modulate serum protein adsorption and to achieve desirable innate immune response to implanted biomaterials and devices.

Keywords: biomaterial; plasma polymerization; serum protein; protein corona; immune response

5.2. Introduction

The success of biomedical device implantation and its pathophysiology is dictated by the biological interactions at its surface.[42, 44, 117, 227] This is because, immediately after implantation, a biomaterial comes in contact with blood, and serum proteins adsorb to surfaces, giving it a new biological identity almost instantly.[102, 228] It is this protein

layer and its composition that innate immune cells including macrophages, neutrophils, and monocytes detect, rather than the pristine biomaterial surface.[102] Therefore, the protein layer formed on a biomaterial surface has paramount importance in determining the fate of the associated hypothetical implant. This layer of adsorbed proteins, also referred to as protein corona when they adsorb around nanoparticles, consists of a hard and soft layer.[229] The 'hard corona' results from the irreversible adsorption of proteins while the dynamic exchange of proteins between biomaterial surface and the surrounding tissues and vasculature is termed 'soft corona'.[102, 230, 231] Previously we have reported on the role of hydrophilicity in reducing innate immune reactions with polyphosphoester-coated nanocarriers, by encouraging selective adsorption of dysopsonin proteins in the corona.[232] Whilst extensive research is focused on understanding the protein corona formed around various nanoparticles, the nature of the protein corona and the surface parameters influencing its formation on the macroscopic surfaces of implantable biomedical devices remains an open question. Thus, to be able to design immunomodulatory biomaterial surface capable of controlling protein adsorption to modulate immune responses, it is essential to understand the molecular mechanisms driving protein adsorption from human serum and how they dictate behaviour of innate immune cells, including key contributors, macrophages.

In this study, we addressed the role of surface chemistry and wettability in regulating the type and amount of adsorbed protein, with the aim of interrogating how these biophysical processes affect cellular innate immune responses, specifically macrophage responses. To create model surfaces with a desirable range of chemical and wetting properties, we employed plasma polymerization.[233] This technique was chosen for surface modification because it provides a range of attractive features; it facilitates the deposition of polymer-like coatings that have a broad range of 'tunable' chemical and physical properties in a single step, and is a solvent-free process.[44] The coating thickness is readily controllable, and can be as little as just few nanometers thin.[108] Most importantly, plasma-derived coatings can be deposited on practically any type of substrate material. The latter is attractive since any particular surface property can be directly transferred to actual functional products, including medical devices.[111] In contrast, other methods for surface preparation such as self-assembled monolayers (SAM) and layer-by-layer (LBL), are limited to specific types of substrate materials and cannot be readily transferred to current medical devices.[108, 111, 172, 183] This creates

a significant disconnection between the results obtained using model substrates in the laboratory and these from *in vivo* studies where surface properties need to be transferred on only selected types of materials.[108, 234, 235] Another reason for the discrepancy often observed between *in vitro* and *in vivo* studies is that, in the laboratory, most protein adsorption studies are conducted either using a single protein or simple mixtures of selected proteins such as albumin, fibrinogen, and immunoglobulin.[70, 118, 152, 236] These studies typically fail to account for the dynamic processes and competing protein adsorption events occurring *in vivo.*[234, 237] As a result, the outcomes of studies involving clinically-relevant bodily fluids often appear contradictory to what is seen in single protein adsorption studies. For instance, a study conducted on polymer brushes surfaces demonstrated negligible protein adsorption from a single fibrinogen buffer solution. However, when incubated with undiluted plasma the surface shows an enrichment in singular and diverse protein adsorption.[238] Vitronectin adsorption studies also showed altered adsorption behaviour when adsorbed from plasma, with considerable enrichment on to various polymers surface as compared with its single protein solution.[239, 240] The disconnection discussed above, points to the need for employing protein adsorption studies in biological solutions that have greater relevance.

In this work, we provide an in-depth investigation of the protein corona formed from complete human serum on a range of model biomaterial surfaces with tailored chemical composition and wettability. Human serum is a complex protein solution that exhibits multifaceted and dynamic adsorption patterns compared to model simple protein solutions.[241] Thus, unlike adsorption studies from reconstituted single or mixed protein suspensions, this approach provides a practically-relevant insight on the nature of the protein layer that could form on the surface of an implanted material. Furthermore, we attempted to derive a link between the adsorbed protein corona and inflammatory responses by measuring the production of pro- and anti-inflammatory cytokine signalling molecules from macrophages. Macrophages are the sentinels of the body and can direct a cascade of events that can decide the fate of an implanted material, from effective tissue regeneration and successful integration to foreign body giant cell formation and rejection.[23, 29] The response of these cells is known to be modulated by material surface chemistry and the amount of adsorbed serum proteins, their conformation and even their physical orientation [1, 42, 117, 242, 243]

In order to shed light on the host immune response as a whole to different implant surface chemistry,[102] we investigated the protein adsorption pattern from whole human serum and correlated the findings with *in-vitro* studies of macrophages immune response. To achieve the goal of this study we used plasma polymerization (Figure 1A) to generate four model surfaces having tailored chemical functionality and wettability. Schematically these surfaces are depicted in Figure 1B and were based on the following precursors: allylamine (AA) (NH_3, hydrophilic), acrylic acid (AC) (COOH, hydrophilic), methyl oxazoline (MEOX) (C_4H_7NO, hydrophilic) and octadiene (OD) (CH_3, hydrophobic). The surface chemical composition of the coatings was characterized by X-ray photoelectron spectroscopy (XPS) and is shown in Figure 1C. The survey spectra of coatings deposited from acrylic acid (AC) and octadiene (OD) contain 72.1 and 92.5 At% carbon (C1s) and 27.8 and 7.4 At% oxygen (O1s), respectively (Table 1). Whereas, the spectra for Allylamine (AA) and methyl oxazoline (MEOX) plasma polymer feature an additional nitrogen peak (N1s) of 15 At% (Table 1), which is consistent with the precursor's chemical composition and previously published studies.[122, 208, 244]

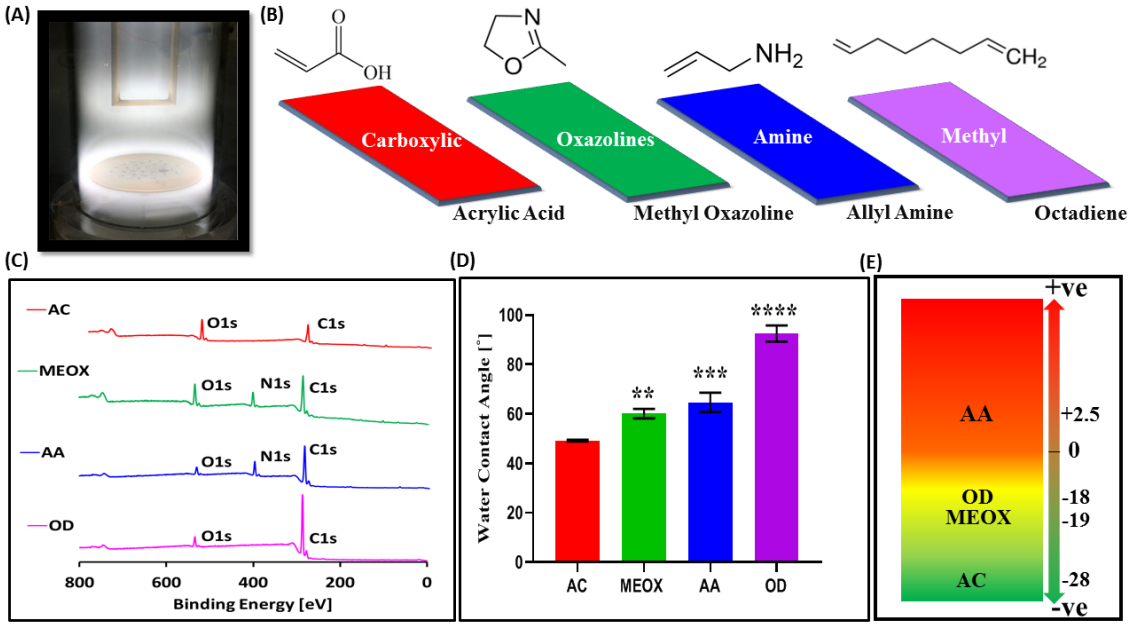

Figure 1. (A) Photograph of the custom-build plasma polymerization chamber used to generate model nanothin coatings with controlled chemistry from selected precursor and their respective predominant surface functional groups (B). (C) XPS survey spectra of the plasma polymer coated surfaces. (D) Water contact angle of the modified surfaces, data are shown as means ± standard deviation and the * represents significant difference compared to AC ($P < 0.05$) using one-way ANOVA followed by Dunnett's multiple comparisons test. (E) Surface charge of modified surfaces.

Wettability measurements shows that the static water contact angle on the plasma deposited coatings ranged between 49˚ and 92˚ (Figure 1D). AC coating had the most hydrophilic surface with a contact angle of 49˚. MEOX and AA modified surfaces displayed similar hydrophilicity with a water contact angle of 58˚ and 67˚, respectively. OD surface was the most hydrophobic surface with a water contact angle of 92˚. These wettability behaviours are consistent with previously published reports for comparable plasma polymer coatings.[122, 163] Plasma polymer surface modification also provided a range of surface charges at physiological pH = 7.4 (Figure 1E). AA surfaces were positively charged (+2.5 mV), MEOX and OD coatings had slightly negative charge -18 mV and -19 mV, respectively, whereas the AC coatings had the highest negative charge of -28 mV.[245, 246] Thus, for the following protein corona formation and immune response studies we had model surfaces covering a range of chemistry, wettability and surface charge parameters which are all known to affect biological responses.

Table 1. Atomic concentration of chemical elements on plasma polymer modified surfaces. All XPS data contains a standard error of 5%.

Surface	C1s	O1s	N1s	C/O	N/C
	[At%]	[At%]	[At%]		
AC	72.1	27.8	-[a]	2.6	-[a]
MEOX	71.1	13.8	15	5.1	0.21
AA	77	8	15	9.6	0.19
OD	92.5	7.4	-[a]	12.5	-[a]

[a] Not present

The model surfaces were incubated in human serum for 1 h and the unbound proteins or/and soft corona were removed by several rinsing steps. The remaining hard corona, constituted of proteins strongly bound to the surface, was then further interrogated. First, the serum proteins in the hard corona were removed by treating the surface with SDS-Tris HCl buffer at 95 °C and quantified with a colorimetric protein assay as previously described [247].

More than 100 proteins were identified in the hard protein corona formed on the four different surface chemistries using liquid chromatography–mass spectrometry (LC-MS) (Table S1). The proteins present in the protein corona were grouped according to

their functions and shown in Figure 2B. The total amount of the serum proteins adsorbed on the AA and MEOX surface was lower compared to the AC and OD surfaces. OD surfaces had the highest amount of serum protein adsorbed (7.05 ± 0.9 μg cm^{-2}), 2.07 μg cm^{-2} of which was immunoglobulins. AC surface showed the second highest amount of protein (6.74 ± 0.8 μg cm^{-2}), main component being albumin at 3.06 μg cm^{-2}. AA (5.07 ± 0.2 μg cm^{-2}) and MEOX (5.14±0.8 μg cm^{-2}) modified surfaces had the least serum protein adsorption, which consisted of high amounts of lipoproteins of 3.06 μg cm^{-2} and 2.73 μg cm^{-2}, respectively. The type of protein bound to the different surface chemistries differed significantly with no straightforward link between the protein isoelectric point and the surface charge.

Figure 2C shows the heat map of the most abundant proteins in the protein corona formed on the modified surfaces. Hydrophilic AC surface demonstrated higher affinity to albumin, which constituted 45% of the total protein corona. MEOX showed high affinity to clusterin and apolipoprotein B-100, which contributed to 24% and 16% of the total serum protein corona, respectively. AA surfaces had Ig gamma-2 chain C region (IgG2) (17%), clusterin (16%), and apolipoprotein B100 (16%) as the most prominent proteins. Interestingly these proteins have also been found on poly(ethylene glycol) coated surfaces of nanoparticles.[248] Whereas, hydrophobic OD surfaces had high affinity to immunoglobulins IgG2 (26%). Interestingly, surface charge did not offer any clear correlation to the type of protein adsorbed. For instance, albumin, which is negatively charged at physiological pH of 7.4 and has an isoelectric point (pI) of 5.86,[249] bound in large amount to the AC surface which also have a net negative charge in these conditions. If protein adsorption was purely driven by electrostatic interaction, one would expect the negatively charged proteins to preferentially bind to positively charged surface and vice versa. However, the data shows that this is not the case as noted previously for nanoparticles.[250] Neutral IgG2 (pI = 7.4) and negatively charged apolipoprotein B-100 (pI = 6.58) and clusterin (pI = 5.84) appear to adsorb strongly to the different surfaces with no particular concern for their net charge.[249]

In contrast, surfaces with similar functionalities and comparable wettability, namely MEOX and AA having nitrogen-containing chemical groups, both attracted more apolipoprotein B-100 and clusterin, and in comparable amounts. OD and AC had opposite patterns of serum protein adsorption which points to a strong effect of surface wettability on the type and amount of protein attracted. Adsorption of IgG increased from 5% to 26%

as the surface become more hydrophobic i.e. AC and OD having water contact angles of 49˚ and 92˚, respectively. Whereas, the adsorption of albumin increased from 7% to 45% as the surface become more hydrophilic (from OD to AC). Together, these results seem to indicate that the selectivity of serum protein adsorption is a surface wettability (i.e. hydrophobic or hydrophilic) dependent phenomenon.

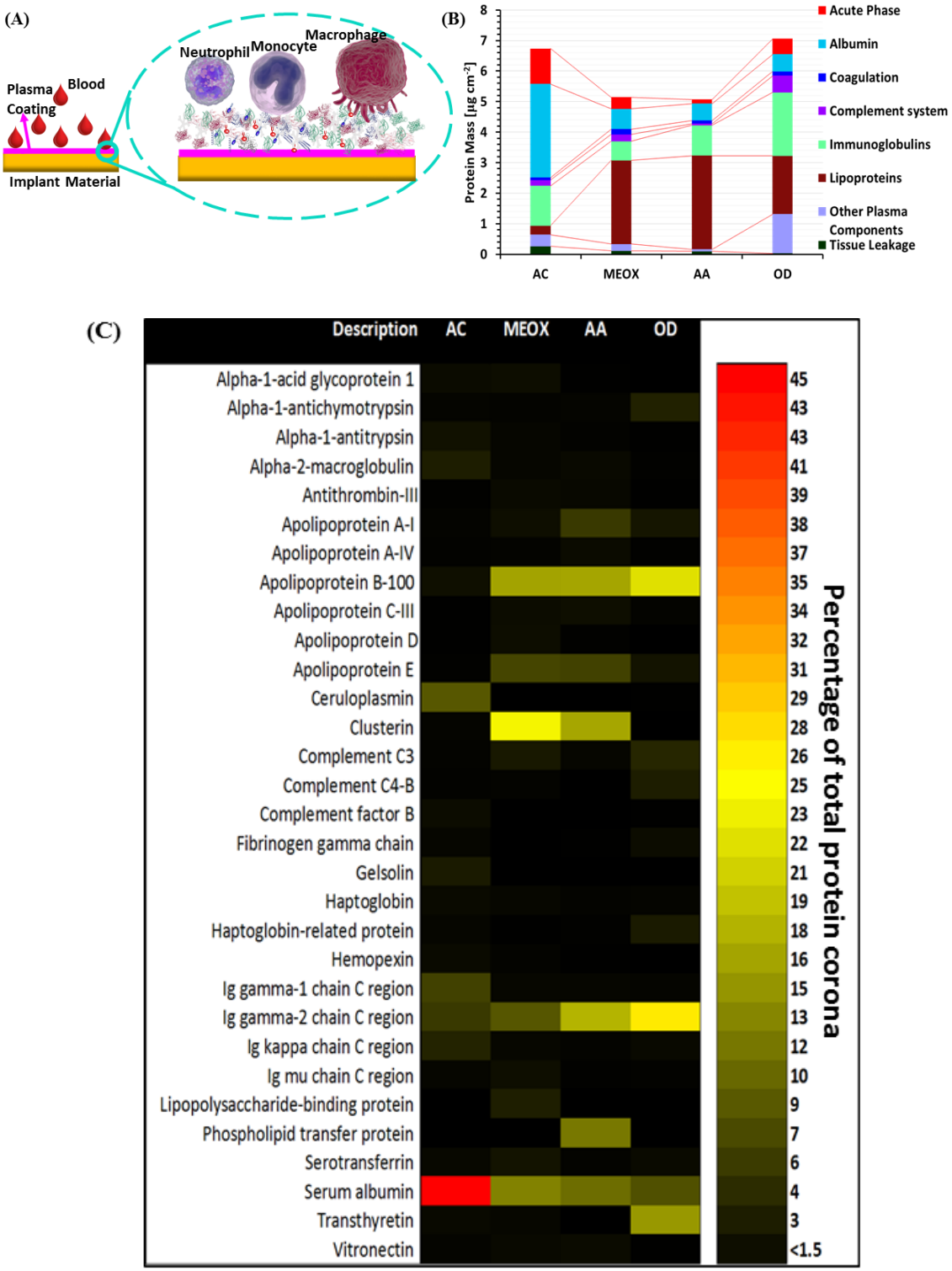

Figure 2. (A) Schematic illustration of the fate of a biomaterial post implantation. Blood-material interaction leads to the adsorption of serum protein to the pristine biomaterial surfaces, which then attracts the subsequent immunological response. **(B)** Quantification of protein adsorption to the modified surfaces along with classification of identified proteins according to their function. **(C)** Heat map of the most abundant proteins in the protein corona of the modified surfaces determined by liquid chromatography–mass spectrometry. Only those proteins that constitute more than 1% of the protein corona on each of the surfaces are shown in the heat map.

Previous reports involving model protein solutions have investigated the role of surface hydrophobicity on the type and amount of protein adsorbed. In single protein adsorption studies, it has been previously reported that the adsorption of human serum albumin (HSA) or bovine serum albumin (BSA) was enhanced on both hydrophilic[237, 251] or hydrophobic surfaces[252] and that no significant difference existed between hydrophobic and hydrophilic surfaces.[253-255] While this may seem contradictory, in their native conformation, the external and internal surfaces of proteins are comprised of hydrophobic and hydrophilic regions as well as charged and uncharged domains, which can make adsorption energetically favourable on both hydrophobic and hydrophilic substrates.[255] Similarly, the orientation of adsorbing albumin molecule determines the functional group (non-polar CH_3 group or polar -COOH) exposed to the solid surface and thus its affinity with hydrophobic or hydrophilic surfaces.[251] These aspects become particularly intricate in real body fluids because proteins arrangements and orientations are different in single and in mixed protein solutions.[237] Similarly, IgG also showed varying adsorption behaviour with respect to surface wettability when experiments were conducted as a single protein solution or in combination of multiple proteins.[237, 256] Our results uniquely reveal preferential protein adsorption pattern on hydrophilic and hydrophobic surfaces from human serum. Testing protein corona in human serum is a scenario practically relevant for subsequent correlation with both *in vitro* and *in vivo* tests as it accounts for competing adsorption-desorption event that occur in cell culture medium or blood. In the following, immune cells were grown in foetal bovine serum, which has a composition comparable to that of human serum in an attempt to evaluate the inflammatory responses arising as a consequence of the protein corona formed on surfaces of different chemical and wetting properties.

Human THP-1 cells were differentiated with phorbol 12-myristate 13-acetate (PMA) to become macrophages and were cultured on the plasma polymer coated surfaces overnight with serum containing media.[257, 258] Macrophages are model cells used to study immune responses because they can undergo measurable functional changes in response to matrix clues which can be correlated with *in vivo* results[29]. Depending on the stimuli in the residing environment these cells can be polarized from the resting M0 phenotype to the pro-inflammatory M1 or anti-inflammatory M2 subsets. M1 macrophages typically produce pro-inflammatory cytokines (e.g., TNF, IL-1β, IL-6, and IP-10) which promote strong immune responses.[259, 260] Conversely, M2 macrophages

antagonize the inflammation by enhancing the production of anti-inflammatory cytokines and other substances involved in repairing function, such as arginase, TGF-β, IL-10 and mannose receptors. M2 are present in the advanced stages of the healing process and participate in resolution of inflammation, tissue repair and angiogenesis. [259]

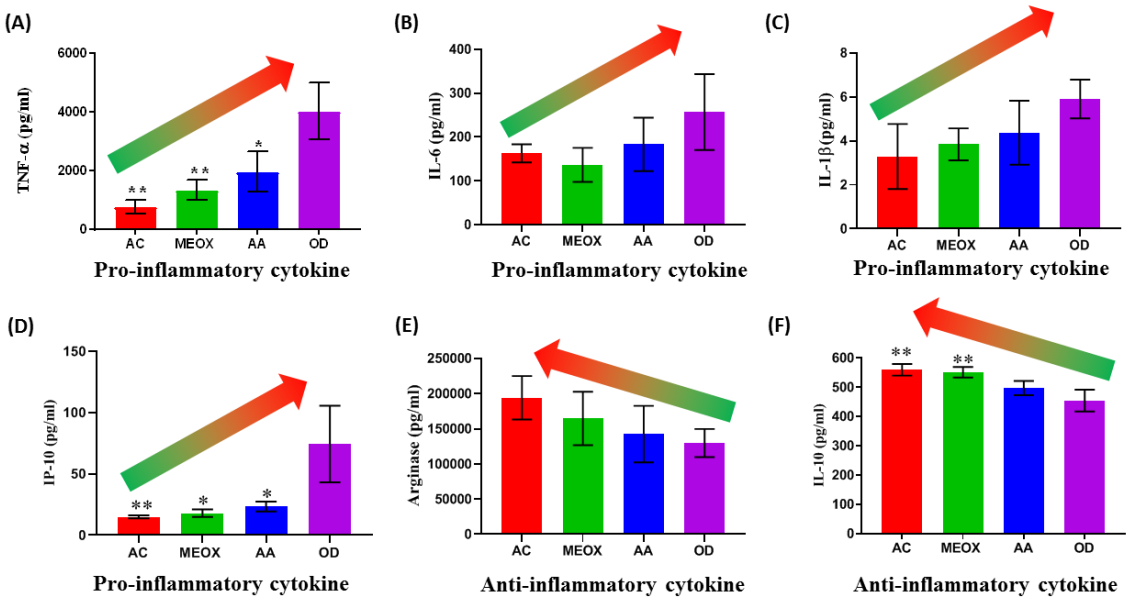

Figure 3. Cytokine expression of macrophages cultures on plasma polymer coated surfaces having different surface chemistries. Production of pro inflammatory cytokines TNF-α (A) IL-6 (B) IL-1β (C) IP-10 (D) and anti-inflammatory cytokine arginase (E), and IL-10 (F) as quantified by multiplex ELISA. *Significant difference compared to OD ($P < 0.05$) one-way ANOVA analysis.

Figure 3 shows the effect of plasma polymer derived model surface chemistry on cytokine production by lipopolysaccharide (LPS) activated macrophages obtained from ELISA. Hydrophobic OD surfaces caused an increase in pro-inflammatory cytokine production while hydrophilic AC surfaces resulted in the expression of least pro-inflammatory cytokines, specifically, significantly lower amounts of TNF-α and IP-10. Compared to OD surfaces, the macrophages also produced lower amounts of pro-inflammatory cytokines on the AA and MEOX surfaces. In perfect contrast, the production of anti-inflammatory cytokines arginase and IL-10 was higher on the hydrophilic AC surfaces, and the least on the hydrophobic OD surfaces. These results collectively highlight a remarkable trend between immune responses and surface wettability and chemical functionalities. The surface hydrophobicity appears to first dictate the type and amount of protein adsorbing to the surface which in turn modulates the following immune response, as summarized in scheme 1. To gain further insight on

the connection between protein adsorption and immune response, in the following we consider the specific function of each protein adsorbing to the different modified surfaces.

In the field of immune response proteomics, some proteins and biomolecules have been identified as opsonins or dysopsonins based on their tendency to promote or decelerate/inhibit phagocytosis, respectively. [261] Human serum albumin is a dysopsonin that can substantially inhibit phagocytosis even when combined with a strong opsonin such as α2GP or IgG. [236] In contrast, opsonins, like IgG, signal for innate immunity and inflammation by recognition through Fc receptors to antigen-presenting cells (e.g. macrophages) and activate immune response or phagocytosis. [236, 262]

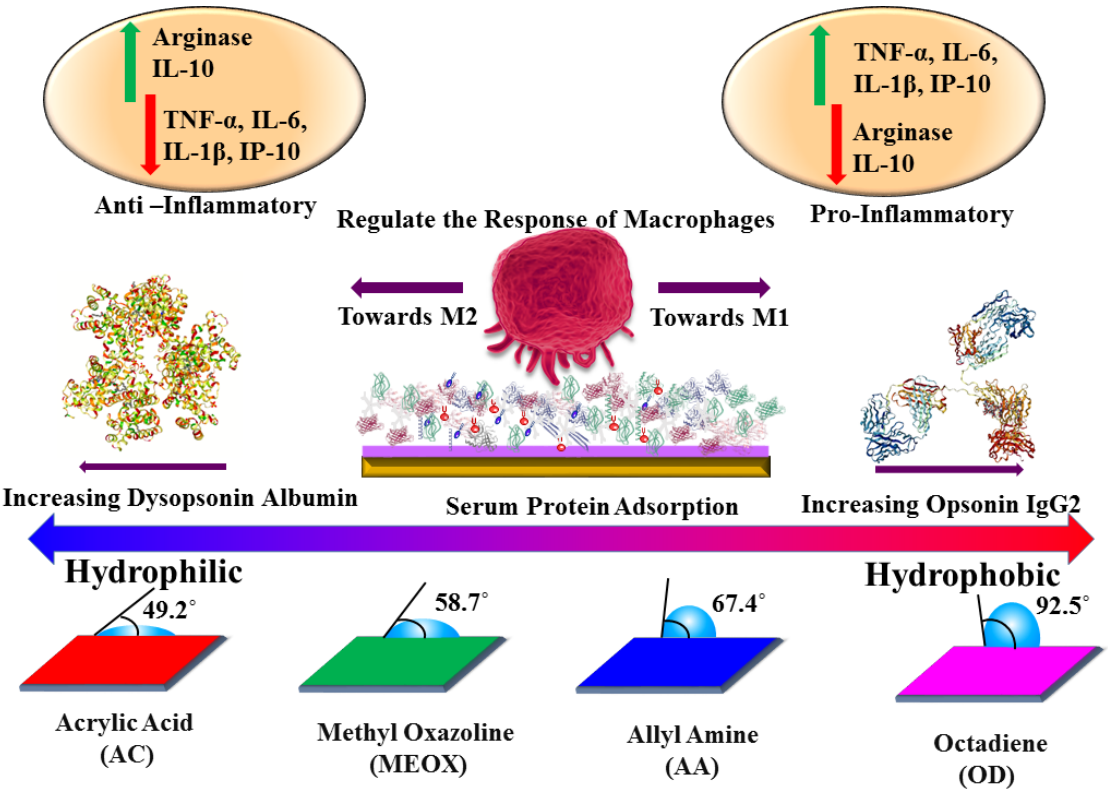

Scheme 1. A schematic illustration of the influence of surface wettability on serum protein adsorption to modified surfaces and the immune responses determined in culture of macrophages. The bottom panel shows plasma polymer coated model biomaterial surfaces with varying wettability. The middle panel illustrates how hydrophobicity determines the amount and relative abundance of serum proteins adsorbed to the modified surfaces after exposure to serum. As the surface become hydrophilic, dysopsonin albumin adsorption increases while the opsonin IgG2 chain c region adsorption increases on hydrophobic surfaces. The top panel illustrate the macrophage immune response towards M2 anti-inflammatory and M1 pro-inflammatory on hydrophilic and hydrophobic surfaces, respectively.

The protein corona study presented here showed that hydrophilic AC surfaces having -COOH functional groups displayed the highest affinity to albumin. Whereas,

hydrophobic OD surfaces rich in -CH_3 functional groups displayed highest affinity to IgG2. We then demonstrated that the AC modified surface, which attracted more serum dysopsonin albumin, initiated the M2 pathway by upregulating the production of anti-inflammatory cytokine and down regulating the pro-inflammatory cytokines (Scheme 1, left). In contrast, the OD modified surface having high amounts of opsonin IgG2 adsorbed appears to have initiated the M1 macrophage as evidenced by an increase in the production of pro-inflammatory cytokines and a reduction in the production of anti-inflammatory cytokines (Scheme 1, right).

These results are in good agreement with published reports which indicate that nanoparticles bound with immunoglobulins (IgGs) played a critical role in activating immune responses, opsonization, and phagocytosis.[263, 264] A recent study from Simberg et al (2019) reported that IgGs can bind to foreign and self-antigens and can modulate complement activation through all three complement (classical, alternative, and lectin) pathways.[265] Therefore, the adsorption of IgG on hydrophobic (OD, AA, and MEOX) surfaces is likely to be responsible for the increase in pro inflammatory cytokines expression observed here. On the other hand, surfaces that bind albumin reduced immune response or phagocytosis.[236, 261, 266] Since, albumin adsorbed on surface does not trigger immune responses, albumin is used as a pre-adsorption strategy to reduce host response to foreign biomaterials.[267, 268] Therefore, adsorption of albumin on hydrophilic (AC) surfaces may be the reason for the reduction in pro-inflammatory cytokines determined in our work. Similarly, clusterin, an apolipoprotein that has a high affinity to nitrogen containing MEOX and AA surfaces, is also known for its stealth properties and documented to help avoid unwanted immune responses has also led to lower pro inflammatory cytokines expression on these surfaces. [248]

In summary, we demonstrated the role of surface chemistry and wettability in total human serum adsorption to form the hard corona and the following immune responses. Substrate independent plasma polymerization technique was utilized to create nano-thin model biomaterial coatings with different chemical functionalities (AC, MEOX, AA, and OD) that possess a range of wettability and surface charge properties. We identified the effect of hydrophobicity in the selectivity of serum protein adsorption; enhanced dysopsonin albumin and opsonin IgG2 adsorption was observed on hydrophilic and hydrophobic surface, respectively. This in turn led to an increase in anti-inflammatory cytokine expression on the hydrophilic surfaces while pro-inflammatory cytokine

production increased on hydrophobic surfaces. These results lead to fundamental insights that must be considered for future biomaterial design, to control the protein adsorption process to modulate innate immune responses and govern the fate of implantable biomedical devices.

5.3. Experimental Section

Detailed experimental methods can be found in the Supporting Information.

5.4. Supporting Information

Supporting Information is available from the Wiley Online Library or from the author.

5.5. Acknowledgements

K.V. thanks ARC for DP15104212 and DP180101254, NHMRC for Fellowship APP1122825 and Project grant APP1032738, and the Alexander von Humboldt Foundation for Fellowship for Experienced Researchers.

SI 5.6. Materials

SI 5.6.1. Materials for Plasma Polymerization

Acrylic acid, 2-methyl-2-oxazoline, allyalamine (AA), and 1, 7-octadiene (OD) and (Sigma-Aldrich, Australia) where used as received for surface preparation.

SI 5.6.2. Materials for Protein Corona Studies

Pooled normal human serum was purchased from Innovative Research, Inc (Michigan, USA) where used for protein corona studies.

SI 5.6.3. Materials for Immune Studies

Phorbol-12-myristate-13-acetate (PMA) for THP-1 macrophage differentiation were purchased from Sigma-Aldrich (Australia). Cytokine production where quantified using human ELISA kits and LEGENDplex from BioLegend (USA).

SI 5.7. Supporting Materials and Methods

SI. 5.7.1. Methods

SI 5.7.1.1. Surface Preparation

Plasma Polymerization

Surfaces with different chemical functionalities were coated on tissue culture plates using plasma polymer deposition in a custom build reactor with a 13.56 MHz plasma generator.[109] Plasma chamber reactor were brought to vacuum, once the chamber reaches a base pressure of 0.02 mbar a 5 minute air cleaning was carried out at 0.11 mbar pressure with 50 W. Plasma deposition of allylamine and acrylic acid was carried out at 0.13 mbar pressure for 2 minutes at 40 and 10 W respectively, octadiene was deposited for 10 minutes at 20 W power. Methyl oxazoline deposition was carried out at 0.08 mbar pressure for 2 minutes at 50 W power. Using these plasma conditions, we obtained stable polymer film coating with thickness in the range of 20 to 30 nm as per ellipsometry measurements.

SI 5.7.1.2. Surface Characterization

X-Ray Photoelectron Spectroscopy (XPS)

Surface chemical composition of plasma polymer deposited layer was analyzed using SPECS Silicon and Germanium (SAGE) XPS spectrometer. XPS spectra were recorded with monochromatic Mg radiation source operated at 10 kV and 20 mA. The chemical composition of plasma deposited surfaces was identified from survey spectra over a 0−1000 eV range with pass energy of 100 eV at a resolution of 0.5 eV. Casa XPS software were used for data processing and curve fitting in reference to the binding energy of neutral carbon C1s peak at 285.0 eV.

Water Contact Angle

Water contact angle was measured using sessile drop contact angle goniometer in a class 1000 cleanroom. Plasma polymer deposited silicon wafers were used as substrates for the wettability measurements. Using a 50 µL Hamilton microsyringe, a 5 µL Milli-Q water droplet was brought in contact with the surface and imaged for advancing contact angle. Captured image of the droplet was processed with SCA20 Data Physics software.

Zeta Potential Measurement

Plasma-coated silica particles were used as substrates to measure the surface charge. Zetapotential measurement was carried out using Zetasizer Nano ZS (Malvern, UK) and transformed into zeta potential using the Smoluchowsky equation (Müller, 1991) for recognition. Measurements were carried out with 10^{-3} M KCl.

Ellipsometry

Silicon wafers were used as substrates for plasma polymer film thickness measurements. An A J.A Woolam Co. Variable Angle Spectroscopic Ellipsometer (VASE) imaging ellipsometer with WVASE32 software was used to calculate thickness.

SI 5.7.1.3. Serum Protein Adsorption Studies

Protein Corona Formation and Quantification

Human pooled serum was purchased from Innovative research to study the protein corona formation. The serum samples were centrifuged for an hour at 20,000 g to remove the aggregated proteins. For serum protein adsorption studies, 500 µL of serum where added to the plasma polymer deposited wells and incubated for 1 hour at 37 °C with constant shaking. After 1 hour the serum was removed and the wells were washed three times using 1 mL of PBS with 5 min shaking to remove the loosely bound soft corona. To isolate the hard corona or strongly bound serum proteins 150 µL of SDS-trizHCl buffer (40 mg SDS + 125 µL Triz-HCl + MilliQ water up to a total of 2 mL) was added to the wells and incubated by shaking at 95 °C for 15 minutes.[247] The total protein concentration were determined using Pierce 660 nm protein assay according to the manufacturer's instructions.

SDS Polyacrylamide Gel Electrophoresis (SDS PAGE)

Gel electrophoresis were used for the visual representation of protein corona contents based on molecular weights. 16.25 µl of the protein sample, 6.25 µl of NuPAGE LDS Sample Buffer, and 2.5 µl NuPAGE of sample reducing agent were mixed together and applied onto a NuPAGE 10 % Bis-Tris Protein Gel (all Novex, Thermo Fisher Scientific). The electrophoresis was carried out in NuPAGE MES SDS Running Buffer at 150 V for 1.5 h and See Blue Plus2 Pre-Stained Standard (Invitrogen) was used as a molecular marker. The gel was stained using Pierce Silver Stain Kit (Novex, Thermo Fisher Scientific).

Liquid-Chromatography Mass-Spectrometry (LC-MS) Analysis

A nanoACQUITY UPLC system coupled with a SynaptG2-Si mass spectrometer (Waters Corporation) was used for performing quantitative analysis of protein samples. Tryptic peptides were separated on the nanoACQUITY system equipped with a C18 analytical reversed-phase column (1.7 μm, 75 μm × 150 mm, Waters Corporation) and a C18 nanoACQUITY Trap Column (5 μm, 180 μm × 20 mm, Waters Corporation).[248]

SI 5.7.1.4. Immune response studies

Human monocytes, cell line THP-1, were used in this study. RPMI 1640 (Sigma Aldrich) was used as growth medium for THP-1 cells along with 10 % fetal bovine serum (FBS, Thermo Scientific) and 1% (v/v) penicillin/streptomycin (Life Technologies). Cells were maintained in a humidified atmosphere containing 5% CO_2 at 37 °C. THP-1 cells were differentiated into macrophages dTHP-1 using PMA (phorbol-12-myristate 13-acetate) according to the protocol previously reported[269], briefly 100 ng/ml PMA was added to the media and incubated for 48 hours and another 24 hours with PMA free media. Differentiated dTHP-1 macrophages were seeded on plasma polymer deposited 24 well plate at a density of 1 x 10^5 cells/ml. After overnight growth, the medium was removed and cells were washed with PBS. Fresh medium was added to the wells along with LPS (1 μg/ml) to activate macrophages. After 6 hours of incubation conditioned media were collected and centrifuged to remove the cell debris. Supernatant were collected and analysed for pro and anti-inflammatory cytokines using LEGENDplex ELISA kits (BioLegend, San Diego, CA, USA) following the manufacturer's instructions.

SI 5.7.1.5 Statistical Analysis.

All statistical computations were performed using GraphPad Prism software, and the statistical significance was analyzed using one-way analysis of variance (ANOVA) followed by Dunnett's multiple comparisons test. All of the data are shown as means ± standard deviation, and the level of significance was set α ($P < 0.05$).

SI 5.8. Supporting Figures and Tables

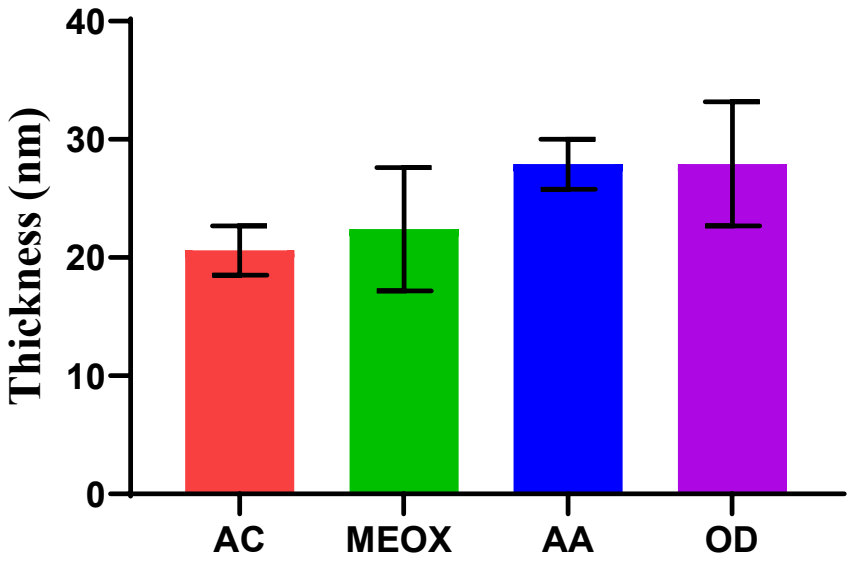

Figure S1. Ellipsometry Thickness measurement, plasma polymer deposited film thickness ranging from 20 to 30 nm.

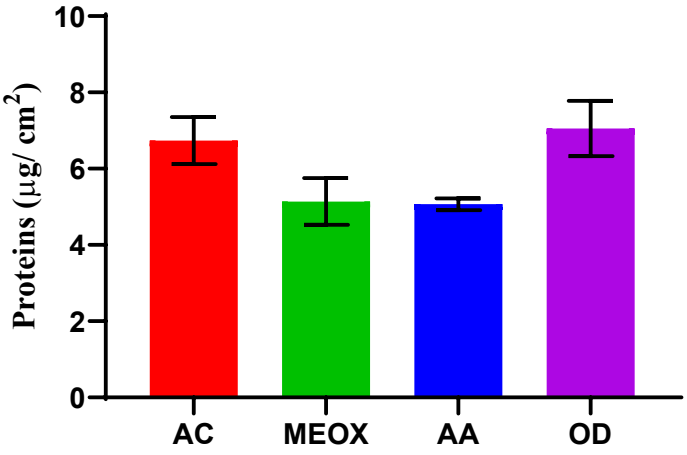

Figure S2. Total serum protein adsorption on the modified surfaces, quantified using pierce assay.

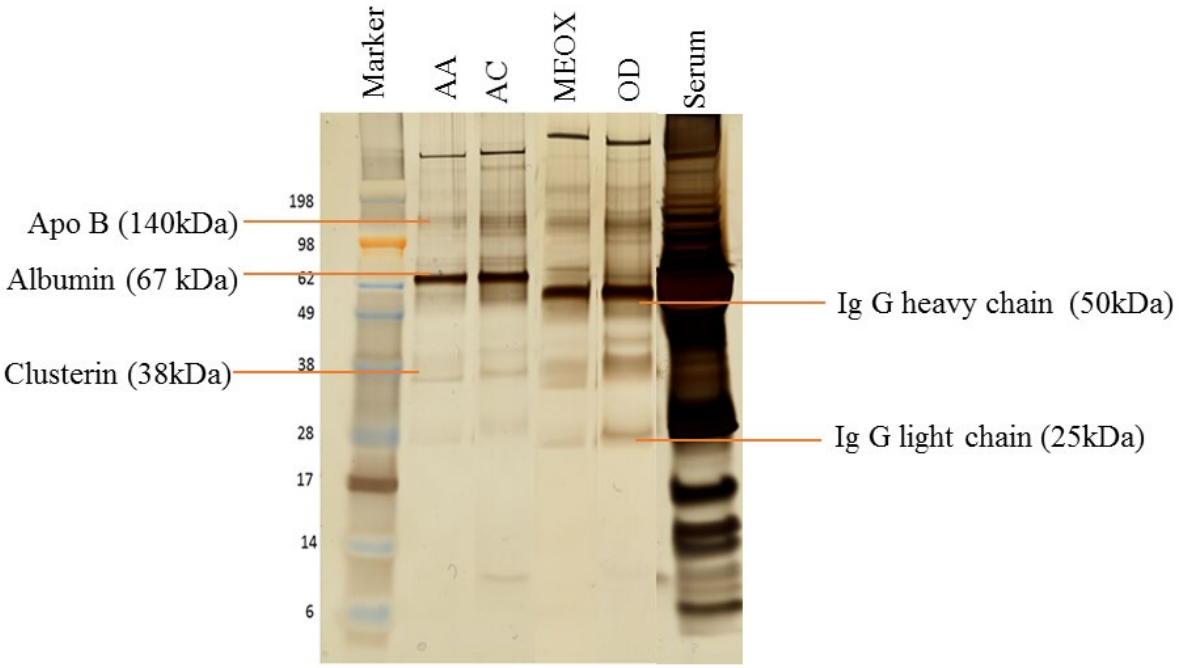

Figure S3. SDS PAGE gel electrophoresis, visual representation of the protein corona composition based on the molecular weights.

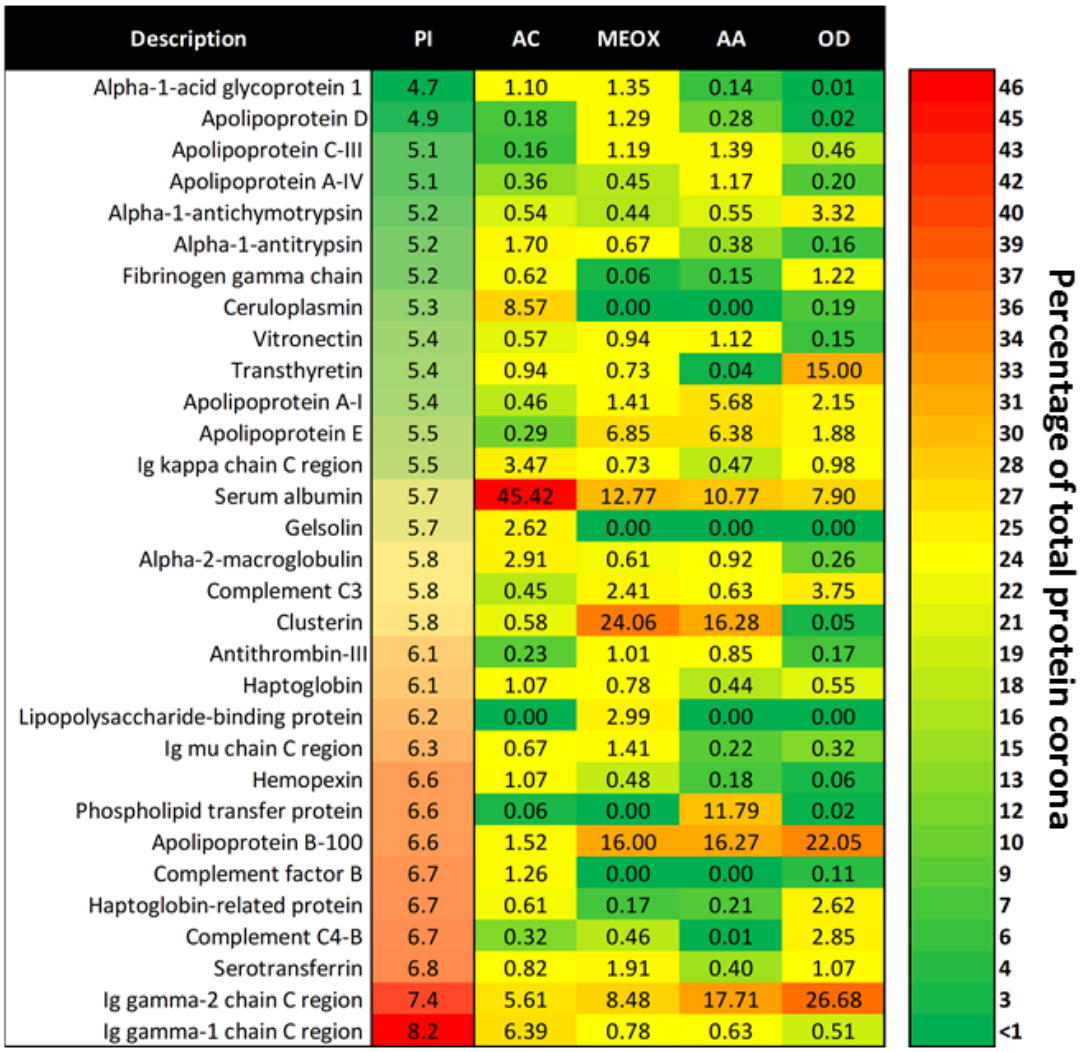

Figure S4. Heat map for major protein components of protein corona formed on the model surfaces sorted against increasing isoelectric point (pI). The isoelectric charge analysis shows no correlation to the protein corona on the surfaces.

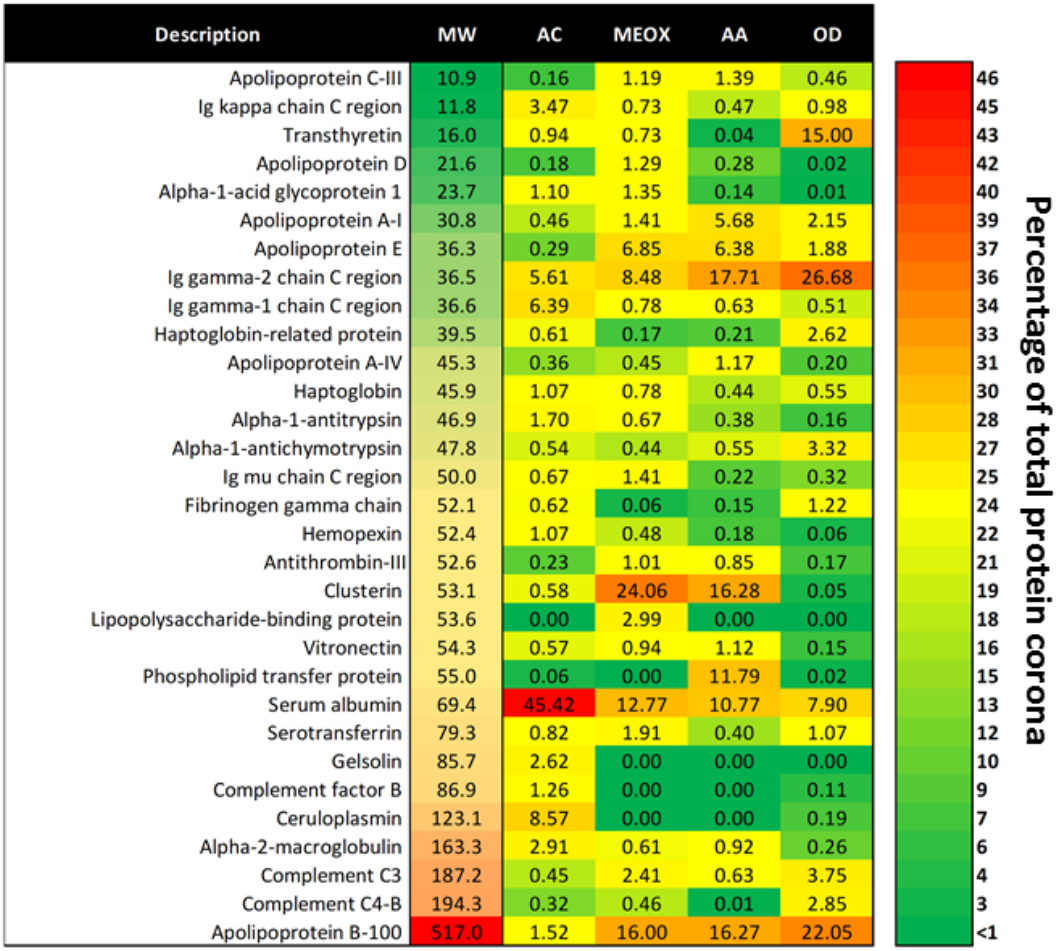

Figure S5. Heat map of major protein components of protein corona formed on the model surfaces sorted by increasing molecular weight (MW). The protein analysis based on the molecular weight shows no correlation to the protein corona on the surface.

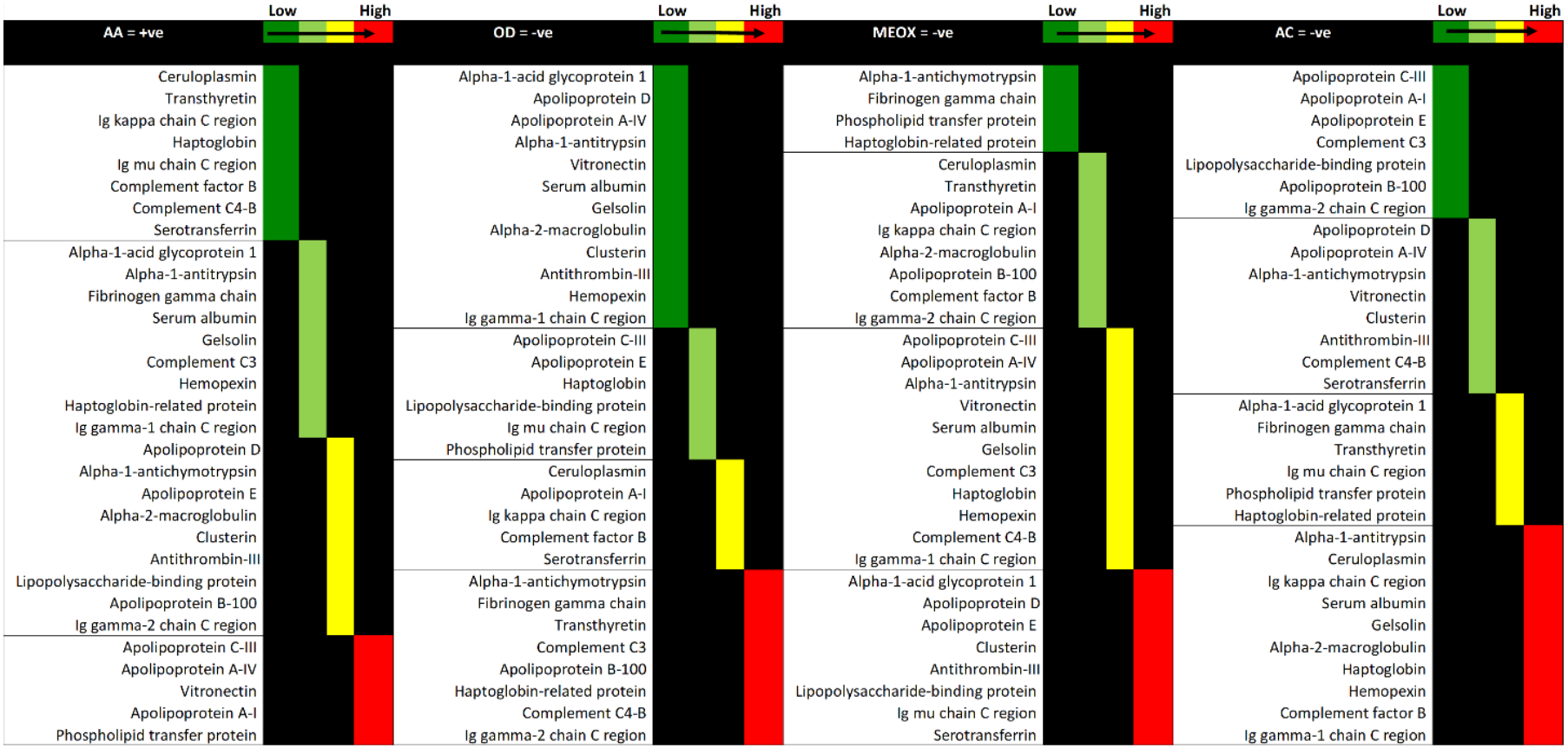

Fig. S6. The major protein components of protein corona adsorbed on the modified surfaces are grouped based on the lowest (green) to highest (red) adsorbed concentration ranking between all four surfaces. For e.g. Ceruloplasmin has lowest adsorbed concentration on AA surface (ranked as low, green) and highest adsorbed concentration on AC surface (ranked as high, red). The result shows that the positively charged AA surface's highest (red) adsorbed protein ranked group contains majority of apolipoproteins. Whereas, the negatively charged AC surface shows that it has comparatively low (green) adsorbed concentration for apolipoprotein groups. However, this observation did not correlate with any specific protein characterizations such as MW, pI, structure, surface functional groups, or wettability of these group of protein.

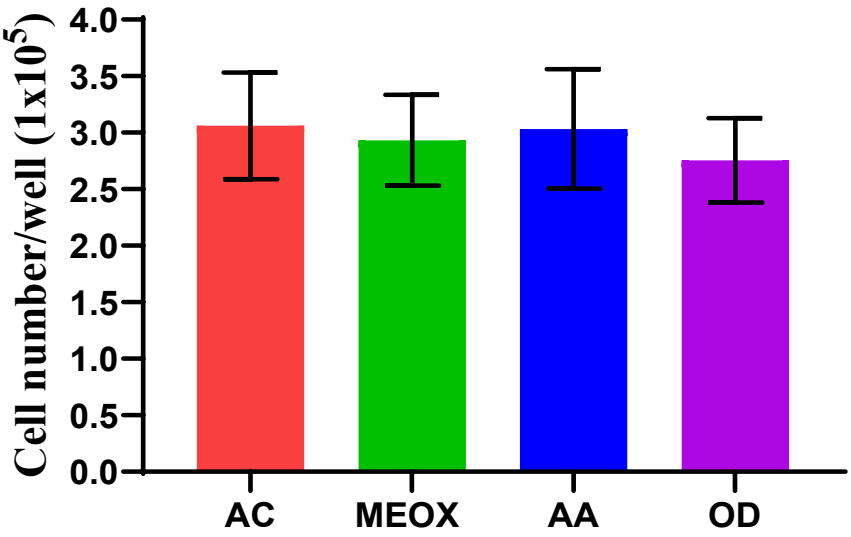

Figure S7. Macrophage cell count, number of cells quantified after collecting the conditioned media for quantification of cytokines. The cell number are comparable for all conditions investigated, this confirms that the difference in cytokine expression was in response to the surface chemistry and not simply a direct effect of cell numbers.

Table S1. List of all (111) corona proteins identified by LC-MS. Average normalized amount [molar percentage] of total protein, for each surface chemistry investigated and protein classification.

		Molar Percentage of Protein				
Description	**Annotation**	**Serum**	**AC**	**OD**	**AA**	**POX**
Alpha-1-acid glycoprotein 1	Acute Phase	1.119	1.119	0.009	0.140	1.366
Alpha-1-acid glycoprotein 2	Acute Phase	0.343	0.094	0	0.010	0.287
Alpha-1-antichymotrypsin	Acute Phase	0.363	0.537	3.325	0.553	0.444
Alpha-1-antitrypsin	Acute Phase	1.244	1.708	0.158	0.384	0.680
Alpha-2-macroglobulin	Acute Phase	0.895	2.918	0.260	0.933	0.612
Ceruloplasmin	Acute Phase	0.371	8.588	0.187	0	0
Fibronectin	Acute Phase	0.091	0.398	0.065	0	0
Haptoglobin	Acute Phase	2.373	1.069	0.554	0.449	0.790
Haptoglobin-related protein	Acute Phase	0.017	0.608	2.624	0.211	0.174
Lipopolysaccharide-binding protein	Acute Phase	0	0	0	0	3.025
Serum amyloid P-component	Acute Phase	0	0.181	0.005	0	0

Alpha-2-antiplasmin	Coagulation	0.041	0	0	0	0.018
Fibrinogen alpha chain	Coagulation	0	0	0	0.287	0.173
Fibrinogen beta chain	Coagulation	0	0	0	0.207	0.844
Fibrinogen gamma chain	Coagulation	0.000	0.623	1.223	0.147	0.057
Heparin cofactor 2	Coagulation	0	0	0	0.004	0.156
Histidine-rich glycoprotein	Coagulation	1.195	0	0	0	0
Kininogen-1	Coagulation	0.153	0.237	0.191	0.023	0.071
Plasminogen	Coagulation	0.237	0	0	0.112	0.202
Platelet factor 4	Coagulation	0	0	0	0.036	0.068
Prothrombin	Coagulation	0.103	0.070	0.463	0.425	0.838
Thrombospondin-3	Coagulation	0	0	0	0	0
Antithrombin-III	Coagulation	0	0.230	0.174	0.861	1.020
C4b-binding protein alpha chain	Complement System	0.439	0.250	0.415	0	0
Complement C1q subcomponent subunit C	Complement System	0.041	0.187	0.154	0.130	0.159
Complement C3	Complement System	0.810	0.456	3.756	0.637	2.432

Complement C4-A	Complement System	1.586	0.000	0.000	0.015	0.247
Complement C4-B	Complement System	1.092	0.321	2.851	0.008	0.461
Complement component C9	Complement System	0.053	0	0	0	0
Complement factor B	Complement System	0.139	1.262	0.106	0	0
Complement factor H	Complement System	0.171	0.211	0.401	0	0
Plasma protease C1 inhibitor	Complement System	0.225	0.086	0.013	0.008	0.074
Complement C5	Complement System	0	0.052	0.021	0.174	0.977
Ig alpha-1 chain C region	Immunoglobulins	4.204	0.226	0.488	0.184	0.145
Ig alpha-2 chain C region	Immunoglobulins	0.358	0	0	0.004	0.026
Ig delta chain C region	Immunoglobulins	0.032	0	0	0	0
Ig gamma-1 chain C region	Immunoglobulins	7.988	6.406	0.508	0.635	0.790
Ig gamma-2 chain C region	Immunoglobulins	2.144	5.621	26.729	17.866	8.570
Ig gamma-3 chain C region	Immunoglobulins	0.750	0.546	0.158	0.017	0.211
Ig gamma-4 chain C region	Immunoglobulins	1.024	0.308	0.007	0.012	0.047
Ig kappa chain C region	Immunoglobulins	9.168	3.473	0.980	0.470	0.741

Ig lambda-2 chain C regions	Immunoglobulins	5.033	0.998	0.149	0.066	0.063
Ig mu chain C region	Immunoglobulins	0.569	0.672	0.324	0.220	1.421
Ig mu heavy chain disease protein	Immunoglobulins	1.107	0.181	0.014	0.007	0.060
Immunoglobulin heavy variable 3-7	Immunoglobulins	0.072	0.060	0.001	0	0
Immunoglobulin heavy variable 3-9	Immunoglobulins	0.180	0.207	0.012	0	0
Immunoglobulin heavy variable 4-59	Immunoglobulins	0.044	0.111	0.018	0	0
Immunoglobulin J chain	Immunoglobulins	0.034	0	0	0	0
Immunoglobulin kappa variable 1-9	Immunoglobulins	0.074	0	0	0	0
Immunoglobulin kappa variable 1D-33	Immunoglobulins	0.139	0	0	0	0
Immunoglobulin kappa variable 1D-39	Immunoglobulins	0.086	0	0	0	0
Immunoglobulin kappa variable 2D-26	Immunoglobulins	0.013	0	0	0	0
Immunoglobulin kappa variable 3-11	Immunoglobulins	0.227	0	0	0	0.007
Immunoglobulin kappa variable 3-15	Immunoglobulins	0.116	0.132	0.006	0	0
Immunoglobulin kappa variable 3-20	Immunoglobulins	0.008	0.504	0.078	0	0
Immunoglobulin kappa variable 4-1	Immunoglobulins	0.236	0	0	0	0

Immunoglobulin lambda variable 1-47	Immunoglobulins	0.038	0	0	0	0
Immunoglobulin lambda variable 1-51	Immunoglobulins	0.036	0	0	0	0
Immunoglobulin lambda variable 3-1	Immunoglobulins	0.046	0	0	0	0
Immunoglobulin lambda variable 3-19	Immunoglobulins	0.066	0	0	0	0
Immunoglobulin lambda variable 3-25	Immunoglobulins	0.072	0	0	0	0
Immunoglobulin lambda-like polypeptide 5	Immunoglobulins	2.117	0	0	0.156	0.123
Apolipoprotein A-I	Lipoproteins	0.390	0.465	2.150	5.732	1.422
Apolipoprotein A-II	Lipoproteins	0.098	0.084	0.000	0.266	0.283
Apolipoprotein A-IV	Lipoproteins	0.419	0.359	0.201	1.179	0.457
Apolipoprotein B-100	Lipoproteins	0.348	1.520	22.089	16.407	16.165
Apolipoprotein C-I	Lipoproteins	0.026	0	0	0	0
Apolipoprotein C-II	Lipoproteins	0.014	0.061	0.053	0.273	0.498
Apolipoprotein C-III	Lipoproteins	0.023	0.160	0.466	1.399	1.206
Apolipoprotein E	Lipoproteins	0.046	0.287	1.888	6.430	6.920
Beta-2-glycoprotein 1	Lipoproteins	0.435	0.516	0.055	0.102	0.431

Clusterin	Lipoproteins	0.214	0.581	0.055	16.419	24.305
Phospholipid transfer protein	Lipoproteins	0	0.062	0.024	11.890	0
Serum paraoxonase/arylesterase 1	Lipoproteins	0	0.045	0.004	0.016	0.133
Apolipoprotein D	Lipoproteins	0	0.182	0.019	0.280	1.306
Apolipoprotein L1	Lipoproteins	0	0	0	0.007	0.020
Apolipoprotein M	Lipoproteins	0	0	0	0.152	0.088
Afamin	Other Plasma Components	0.144	0	0	0.022	0.013
Alpha-1B-glycoprotein	Other Plasma Components	0.351	0.075	0.015	0.070	0.081
Alpha-2-HS-glycoprotein	Other Plasma Components	0.856	0.195	0.007	0.233	0.683
Carboxypeptidase N subunit 2	Other Plasma Components	0.049	0	0	0	0
Hemoglobin subunit alpha	Other Plasma Components	0.155	0	0	0.018	0.093
Hemoglobin subunit beta	Other Plasma Components	0.348	0.175	0.163	0.136	0.051
Hemopexin	Other Plasma Components	1.514	1.073	0.061	0.179	0.490
Inter-alpha-trypsin inhibitor heavy chain H1	Other Plasma Components	0.831	0.415	0.088	0	0
Inter-alpha-trypsin inhibitor heavy chain H2	Other Plasma Components	0.123	0.683	1.062	0	0

Inter-alpha-trypsin inhibitor heavy chain H4	Other Plasma Components	0.128	0.383	0.064	0.013	0.053
Pigment epithelium-derived factor	Other Plasma Components	0.019	0	0	0	0
Pregnancy zone protein	Other Plasma Components	0.051	0.105	0	0	0
Protein AMBP	Other Plasma Components	0.098	0	0	0.006	0.012
Serotransferrin	Other Plasma Components	2.823	0.820	1.070	0.402	1.934
Transthyretin	Other Plasma Components	0.214	0.941	15.024	0.037	0.742
Vitamin D-binding protein	Other Plasma Components	0.810	0.027	0.006	0.045	0.035
Zinc-alpha-2-glycoprotein	Other Plasma Components	0.175	0.639	0.645	0.050	0.079
Cholesteryl ester transfer protein	Other Plasma Components	0	0.142	0.031	0.072	0
Actin, gamma-enteric smooth muscle	Tissue Leakage	0	0.117	0.104	0.000	0
Angiotensinogen	Tissue Leakage	0.263	0.163	0.044	0.609	0.577
CD5 antigen-like	Tissue Leakage	0.042	0.304	0	0	0
Gelsolin	Tissue Leakage	0.082	2.629	0	0	0
Glyceraldehyde-3-phosphate dehydrogenase	Tissue Leakage	0	0.060	0.122	0.175	0.090
N-acetylmuramoyl-L-alanine amidase	Tissue Leakage	0.051	0	0	0	0

POTE ankyrin domain family member F	Tissue Leakage	0	0	0	0	0.511
Vitronectin	Tissue Leakage	0.204	0.568	0.145	1.131	0.949
Zinc finger Ran-binding domain-containing protein 2	Tissue Leakage	0.306	0	0	0	0
Profilin-1	Tissue Leakage	0	0	0	0	0.090
Leucine-rich alpha-2-glycoprotein	Tissue Leakage	0.062	0	0	0	0
Metallo-beta-lactamase domain-containing protein 1	Tissue Leakage	0.231	0	0	0	0
Putative ATP-binding cassette sub-family A member 11	Tissue Leakage	0.306	0	0	0	0
Putative C-type lectin domain-containing protein LINC00083	Tissue Leakage	0.076	0	0	0	0
Tetraspanin-33	Tissue Leakage	0.028	0	0	0	0
Serum albumin	Albumin	38.561	45.526	7.918	10.860	12.902

SI 5.9. Copy Right Permission

Reproduced (or 'Reproduced in part') with permission from [Visalakshan, R.M., MacGregor, M.N., Sasidharan, S., Ghazaryan, A., Mierczynska-Vasilev, A.M., Morsbach, S., Mailänder, V., Landfester, K., Hayball, J.D. and Vasilev, K., 2019. Biomaterial Surface Hydrophobicity-Mediated Serum Protein Adsorption and Immune Responses. ACS applied materials & interfaces, 11(31), pp.27615-27623.] Copyright [2019] American Chemical Society **Copyright © 2019 American Chemical Society**

Chapter 6. Tailor-Engineered Modulation of Macrophages Differentiation by Geometric and Chemical Features in Nanoporous Substrates

6.1. TOC

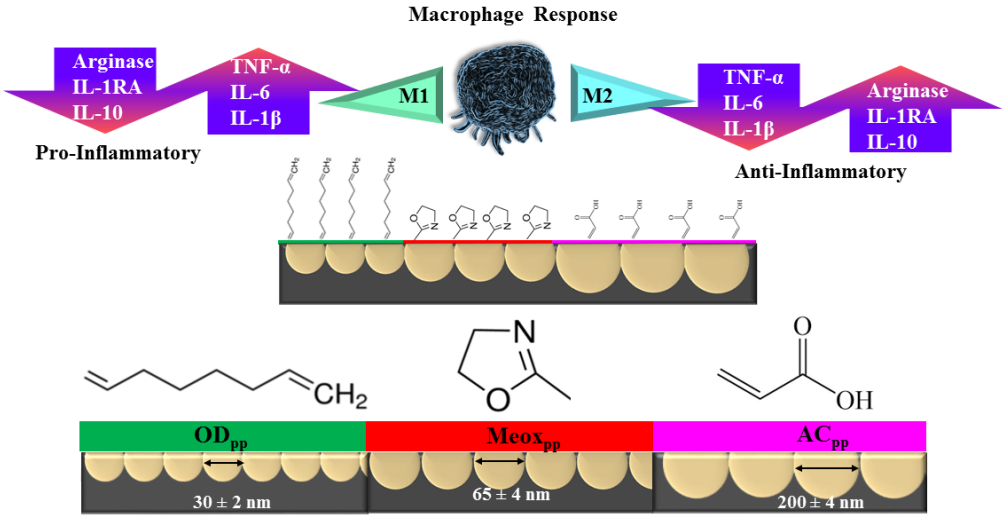
Macrophage Response
Arginase
IL-1RA
IL-10
Pro-Inflammatory
TNF-α
IL-6
IL-1β
M1
M2
TNF-α
IL-6
IL-1β
Anti-Inflammatory
Arginase
IL-1RA
IL-10
CH2
N
O
O
OH
ODpp
Meoxpp
ACpp
30 ± 2 nm
65 ± 4 nm
200 ± 4 nm

6.2. Abstract

The fate of tailor engineered biological implants relies on its capability to differentiate macrophages into M1 (inflammatory) and M2 (wound healing) phenotypes. The biophysical properties of the extra cellular matrix have been well known to affect macrophages behaviour. Mimicking these biophysical properties have led to the implementation of biomaterial implants with tailored engineered surface nanotopography and chemistry. However, none of the studies so far has analysed in depth the role played by combinational effect of nanotopography and surface chemistry. To address this gap, we have fabricated nanoporous surfaces of controlled pore size and lateral spacing with homogeneous outermost surface chemistry of amines (NH_2-), carboxyl (COOH-) and hydrocarbon (CH_3-).

We have shown that the concentration of pro-inflammatory cytokines decreased while the concentration of anti-inflammatory cytokines increased many fold on surfaces modified with combination of -COOH coating and nanopores compared to nanoporous surfaces with other chemistries. This demonstrates that macrophage differentiation can be controlled by engineering the right combination of surface nanotopography and chemistry. Our data provides pioneering knowledge that could help in tuning foreign body response and in turn govern the design of tailor engineered biomaterial implants to produce more prominent clinical outcomes.

Keywords: plasma polymerization, nanoporous substrates, surface chemistry, pro-inflammatory cytokines, anti-inflammatory cytokines, foreign body response, wound healing.

6.3. Introduction

Tailor-engineered biomaterial implants are gaining popularity, due to aging population and advances in personalized therapies. However, the biggest performance challenge that biomaterial implants face is the host immune response. Upon implantation, adsorption and desorption of different proteins occurs on the bio-synthetic interface in accordance with the Vromann effect[270, 271]. This governs the subsequent phenomena

underlying binding and activation of waves of innate immune effector cells (dendritic cells, mast cells, granulocytes, natural killer cells and macrophages)[272-276]. Then, these macrophages start fusing among themselves forming foreign body giant cells (FBGC) in an attempt to eliminate the foreign body (i.e. biomaterial implant). Macrophages have been known to be critical in the host immune response –both to implants and microorganisms– through their phagocytic activities. In the past few decades the role of macrophages in haemostasis, tissue repair and remodelling has been established[277]. Based on these different roles, macrophages are considered as 'plastic' cells and have been categorized into 'M1' and 'M2' phenotypes[90, 278-280]. M1-activated macrophages are key elements in inflammation and in 'cleaning the site' by expressing pro-inflammatory cytokines such as tumour necrosis factor (TNFα) and interleukin (IL6 and IL1β), while the M2-activated macrophages produce anti-inflammatory cytokines (arginase, IL10 and IL1ra) and are involved in wound healing and remodeling.

Recently, several studies have shown that macrophage adhesion, phagocytic activity, and cytokine production can be controlled by using different surface chemistry (synthetic and natural) and nanotopography (nanotubes, nanopits, nanofibers, nanodots, nanorods, nanogrooves and nanopores), [169, 281, 282] as they mimic the extra cellular matrix to regulate specific cell functions[283]. However, how these nanotopography and chemistry combined can affect the fate of macrophages remains unanswered. Herein, we hypothesize that the combination of both surface nanotopography and chemistry can be important regulators in macrophage differentiation.

In this article, we report nanoporous anodic alumina (NAA) produced by anodization of aluminium (industrially scalable, three-dimensional nanofabrication method based on electrochemical oxidation of aluminium) as an ideal nanotopography nanomaterial model to study bio-interface phenomena. NAA provides a nanoporous surface with hexagonally distributed nanopores, the geometric features of which can be precisely tuned by the fabrication conditions. NAA is recognised as a non-cytotoxic material and has been extensively used in orthopaedic and dental implants[284]. NAA surfaces have been engineered as active drug-releasing coatings in orthopaedic, dental and coronary implants and in immunoisolation.[285, 286] Pioneering osteogenesis studies demonstrated the biocompatibility of NAA, suggesting that its nanoporous structure is a key element in bone cell adhesion and osseointegration[287-289]. *In vitro*

immunoisolation studies performed onto NAA surfaces suggest that this nanoporous material does not generate significant complement activation, though *in vivo* transient inflammatory response was observed for unmodified and PEG-functionalized NAA surfaces upon implantation into the peritoneal cavity of rats[285]. However, reduction in granulation along with the existence of blood vessels in the tissue surrounding the NAA biological implant indicated that the inflammation was mainly due to the implantation procedure itself. These pioneering studies did not analyse in depth the role played by combinational effect of nanotopography and surface chemistry. To differentiate between the effect of nanotopography and chemistry a thin layer of polymer was deposited on the nanoporous surfaces using plasma deposition. A key benefit of plasma polymerization is that it is substrate independent and no pre-modification of the surface is required [290-293]. Another advantage is that it deposits uniform and homogeneous thin films in a single step coating procedure[294, 295]. Finally, macrophages were seeded on these nanotopography and chemically modified surfaces and a control in their differentiation was established by modulating pro-inflammatory and anti-inflammatory cytokines.

6.4. Materials and Methods

6.4.1. Materials

High purity (99.9997%) aluminium (Al) foils 0.32 mm thick were supplied by Goodfellow Cambridge Ltd. (UK). Oxalic acid ($H_2C_2O_4$), perchloric acid ($HClO_4$) and chromic acid (H_2CrO_4), were purchased from Sigma-Aldrich (Australia). Ethanol (C_2H_5OH, EtOH), sulfuric acid (H_2SO_4) and phosphoric acid (H_3PO_4) were supplied by ChemSupply (Australia). Aqueous solutions used in this study were prepared with ultrapure Milli-Q® water (18.2 mΩ·cm).

6.4.2. Fabrication of Nanoporous Materials

Prior to anodization, Al substrates were sonicated in EtOH and Milli-Q® water for 15 min each and dried under air stream. Then, Al substrates were electropolished in a mixture $HClO_4$ and EtOH 1:4 (*v*:*v*) electrolyte at 20 V and 5 ºC for 3 min, using an electrochemical reactor with a circular window of ~1 cm in diameter. Three types of nanoporous anodic alumina (NAA) substrates were fabricated by two-step anodization to tune the geometric features of nanopores [296-299]: i) NAA produced in sulfuric acid (NAA-Su), ii) NAA fabricated in oxalic acid (NAA-Ox), and iii) NAA anodized in phosphoric acid (NAA-Ph). The first anodization step was performed for 20 h in 0.3 M

sulfuric acid at 6 ºC for NAA-Su, 0.3 M oxalic acid at 6 ºC for NAA-Ox, and 0.1 M phosphoric acid for NAA-Ph at 1 ºC, with anodization voltages of 25, 40 and 195 V, respectively. The resulting NAA layers with disordered nanopores at the top surface were chemically removed by wet etching in 0.2 M H_2CrO_4 and 0.4 M H_3PO_4 at 70 ºC for 3 h. The second anodization step was performed using the same conditions than those used during the first step but for 2 h. Finally, to finely tune the nanopore size, the NAA films were pore-widened by wet chemical etching in H_3PO_4 5 *wt* % at 35 ºC for 8, 18 and 30 min for NAA-Su, NAA-Ox and NAA-Ph samples, respectively.

6.4.3. Plasma Polymerization

The surface chemistry of NAA substrates was modified by plasma polymerization in a custom-built reactor with a 13.56 MHz plasma generator.[26] Oxygen plasma was applied for 2 min at 50W to clean all nanoporous membranes. The vapors of methyl oxazoline, acrylic acid and octadiene were used to overcoat the top surface of NAA substrates with a ~5 nm thick polymer film. Thin films of methyl oxazoline, acrylic acid and octadiene were deposited using a power of 40, 10 and 20 W, respectively, while the deposition time was kept constant at 20 s for all three monomers.

6.4.4. Scanning Electron Microscopy

The structural features of the NAA substrates were established by field emission gun scanning electron microscopy (FEG-SEM FEI Quanta 450). FEG-SEM images were processed using ImageJ.

6.4.5. X-Ray Photoelectron Spectroscopy

XPS was used to determine the surface composition of the plasma polymers deposited onto the surface of the NAA substrates. All spectra were recorded using a Spec SAGE XPS spectrometer equipped with a monochromatic Mg radiation source operated at 10 kV and 20 mA. Atomic compositions of the polymers were identified from survey spectra recorded over a 0–1000eV with pass energy of 100 eV at a resolution of 0.5 eV. All binding energies (BE) were corrected relative to a neutral C1s carbon peak at 285.0 eV. Processing and curve fitting were performed using CasaXPS.

6.4.6. Cell Culture

Human monocyte cell line THP-1 were used for immune response studies. THP-1 cells were grown in RPMI 1640 (Sigma Aldrich) with 10 % fetal bovine serum (FBS,

Thermo Scientific) and 1% (*v*/*v*) penicillin/streptomycin (Life Technologies). Cells were maintained in an incubator humidified atmosphere containing 5% CO_2 at 37 °C, and growth media were changed every 3 days until the flask got 80% confluent.

6.4.7. Inflammatory response of macrophage

THP-1 cells were differentiated into macrophages (dTHP-1) using PMA (phorbol-12-myristate 13-acetate) according to the previously reported protocol.[257, 269] Briefly, cells were treated with media containing 100 ng ml^{-1} PMA for 48 h and further 24 h with PMA free media. Differentiated dTHP-1 macrophage cells were seeded on unmodified and modified NAA substrates at a density of 1 x 10^5 cells ml^{-1} and grown overnight for cell attachment. Once the cells were attached, the media was changed with fresh media containing 1 μg ml^{-1} LPS (lipopolysaccharide) to activate the macrophages. Cells were exposed with LPS for further 6 h and conditioned media were collected for quantification of cytokine production.[258] After collecting the media, macrophage cell counts were performed using trypsin and hemocytometer to quantify the number of cell that produced cytokines on each surface (**Figure S1&S2**). Pro- and anti-inflammatory cytokines [IL-12p70, TNF-α, IL-6, IL-1β, IL-12p40, IL-23, IFN-γ, IP-10, IL-4, IL-10, arginase, and TARC] were quantified using LEGENDplex human macrophage/microglia Panel (13-plex) and ELISA kits (BioLegend, San Diego, CA, USA) following the manufacturer's instructions.

6.4.8. Statistical Analysis

All statistics were performed using graph pad prism 6 software. All data was expressed as mean ± standard error mean (SEM). Statistical significance was determined using a 1-way ANOVA with Dunnett's multiple comparison test. All experiments were performed thrice in triplicates.

6.5. Results

6.5.1. Fabrication of uniformly overcoated NAA substrates

The geometric features of NAA (i.e. nanopore diameter – d_p; nanopore length – L_p; interpore distance – d_{int}; pore density r_p; **Figures 1a and b**) were established by FEG-SEM image analysis. **Figures 1c–e** compile a set of representative FEG-SEM images showing the cross-sectional and top views of NAA substrates fabricated by two-step anodization process.[296-299] **Figures 1c–e** show cross-sectional FEG-SEM images of

NAA substrates featuring straight cylindrical nanopores from top to bottom, which grow perpendicularly to the underlying aluminium substrate during anodization, with a closed oxide barrier layer at their bottom (**Figure 1a**). The average nanopore length of NAA-Su, NAA-Ox and NAA-Ph substrates under the fabrication conditions used in our study were L_p = 13.1 ± 0.5, 6.1 ± 0.4 and 7.5 ± 0.3 μm, respectively. The top surface of NAA substrates shows an array of nanopores of uniform size and distribution arranged in a self-organized hexagonal pattern (**Figures 1c–e**). The average nanopore diameter and interpore distance for NAA-Su, NAA-Ox and NAA-Ph substrates were d_p = 30 ± 2, 65 ± 4 and 200 ± 4 nm and d_{int} = 66 ± 3, 105 ± 5 and 449 ± 24 nm, respectively. The pore densities (i.e. number of nanopores per unit area) were $r_p = 2.65 \times 10^{11}$, 1.05×10^{11} and 5.73×10^{9} cm^{-2} for NAA-Su, NAA-Ox and NAA-Ph substrates, respectively.

In order to ensure a uniform outermost surface chemistry on the NAA substrates, an overcoating of ~5 nm thin layer of plasma polymer generated from vapor of either acrylic acid, methyl oxazoline and octadiene (ACpp, Meoxpp, ODpp) was deposited. These plasma polymer coatings were chosen because they represent chemical compositions of amino acids in proteins (i.e. COOH- (ACpp), NH_2- (Meoxpp) and CH_3- (ODpp).[11, 99] These coatings also represent different surface charges in aqueous medium at physiological pH = 7.4 as Meoxpp and ODpp coatings are slightly negative charged -18 mV and -19 mV, respectively, whereas the ACpp coatings had the highest negative charge of -28 mV.[244, 245] Respectively, the different chemistries result in different wetting characteristics, described by typical water contact angles of 35° for ACpp, 60° for Meoxpp and 85° for ODpp.[122, 242] The plasma polymer films, of only 5 nm in thickness, are continuous and pinhole-free, allowing us to preserve the nanotopography generated by the NAA substrates and thus study the combinational effect of nanotopography and surface chemistry. FEG-SEM images of NAA substrates after overcoating are shown in **Figure 2**. The images demonstrate that the pores are hexagonally arranged on the surface and that the overcoating used to tailor the outermost surface chemistry does not affect the surface morphology (i.e. nanopore diameter).

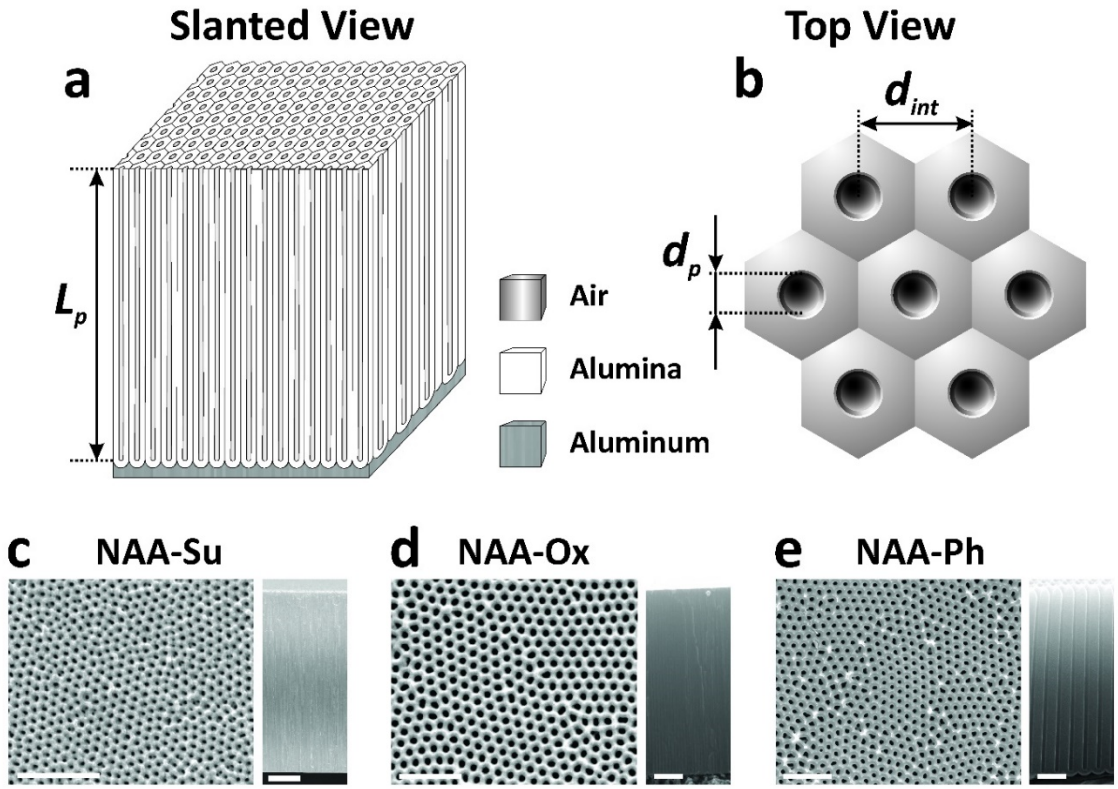

Figure 1: Structural features of NAA substrates produced by two-step anodization. a,b) Slanted and top view schematics of a NAA substrate with details of geometric features (i.e. nanopore diameter – d_p; nanopore length – L_p; interpore distance – d_{int}). c-e) Top (left) and cross-sectional (right) FEG-SEM images of NAA produced in sulfuric (scale bar (left) = 500 nm; scale bar (right) = 2 µm), oxalic acid (scale bar (left) = 500 nm; scale bar (right) = 1 µm), and phosphoric acid (scale bar (left) = 2.5 mm; scale bar (right) = 1 µm), respectively.

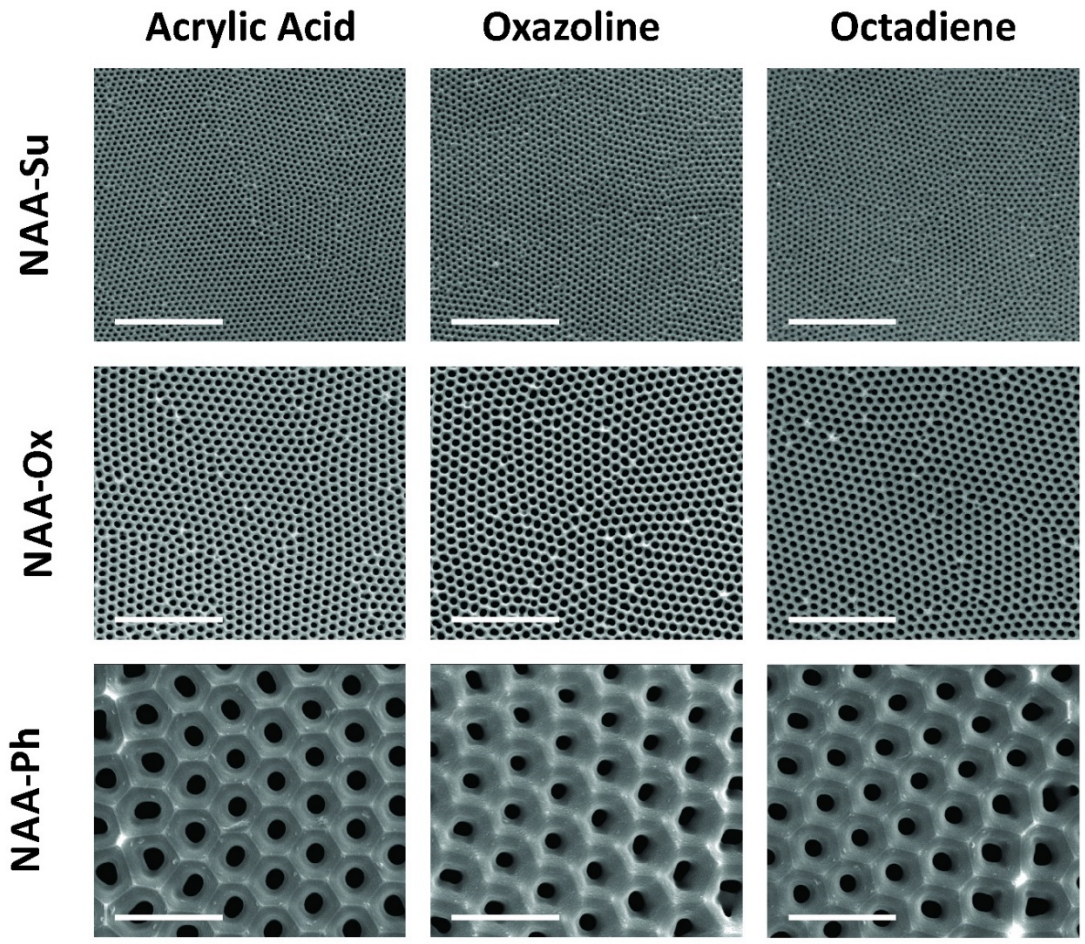

Figure 2: FEG-SEM image of nanoporous anodic alumina with three different pore sizes, NAA-Su, NAA-Ox and NAA-Ph (scale bars = 1 µm) overcoated with three different chemistries (acrylic acid, methyl oxazoline and octadiene).

The surface chemical composition of the coatings deposited by plasma polymerization on NAA substrates was characterized by XPS. The atomic percentage of aluminium (**Figure 3a**) shows that unmodified NAA substrates have 35% of aluminium. After deposition of a plasma polymer coating (Meoxpp, ODpp and ACpp), the atomic percentage of aluminium decreased by half, which indicates that the coatings were successfully deposited on the NAA substrates. Furthermore, the aluminium by carbon (Al/C) and oxygen by carbon (O/C) ratios decreased by one fourth in case of Meoxpp and ODpp coated planar and NAA substrates as compared to their uncoated counterparts (**Figures 3b and c**). This is due to the high concentration of carbon present in these monomers. Whilst Al/C ratio decreased by half and O/C ratio remained the same in ACpp overcoated NAA substrates compared to their uncoated analogues (**Figures 3b and c**). This is due to high concentration of oxygen present in the acrylic acid monomer. Moreover, alumina membrane has a top oxide layer which leads to high percentage of

O/C ratio in case of uncoated alumina surface. In **Figure 3d,** nitrogen by carbon (N/C) ratio is observed in case of Meoxpp and not in case of ODpp and ACpp coated planar and nanoporous surfaces. This is due to the presence of nitrogen in the Meox monomer while no nitrogen is present in case of OD and AC monomers.

6.5.2. Characterization of Surface Chemistry

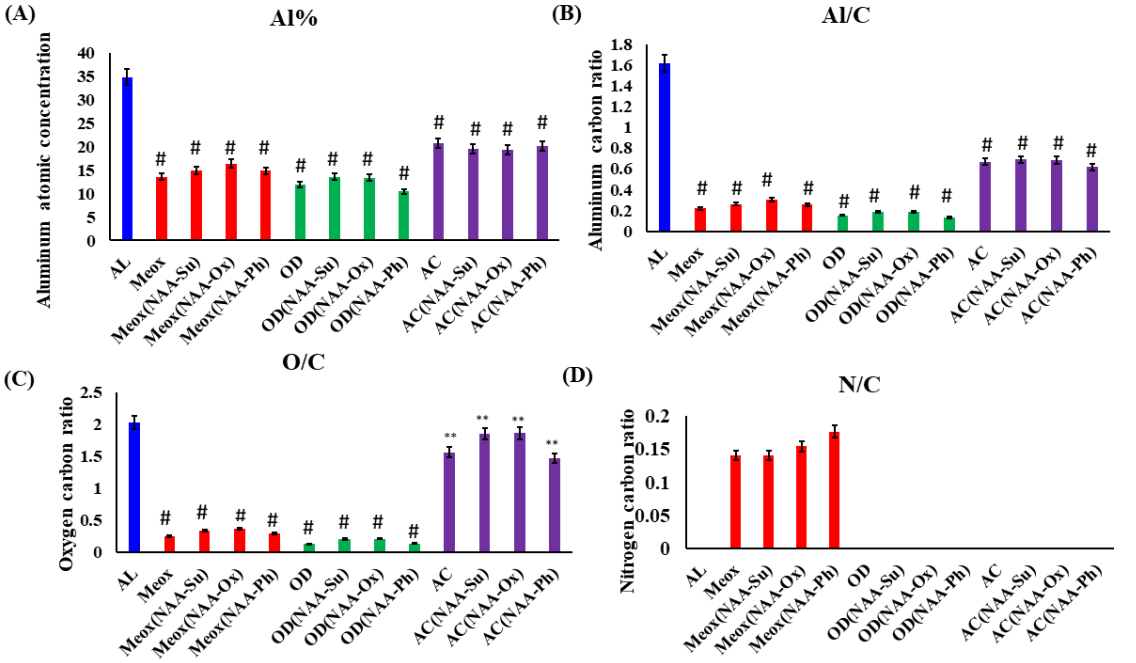

Figure 3: XPS results: (A) Percentage of atomic elemental concentration of aluminium, (B) aluminium carbon ratio, (C) oxygen carbon ratio and (D) nitrogen carbon ratio of NAA substrates modified by plasma polymerized surface coating with methyl oxazoline, octadiene and acrylic acid chemistries. Significant difference compared to AL (# = $p < 0.0001$, ** = $p < 0.0024$) using one-way ANOVA followed by the Dunnett's multiple comparisons test.

6.5.3. Inflammatory responses (pro-inflammatory and anti-inflammatory) on different chemistry and nanoporosity

Macrophages play a central role in the host response to biomaterial implants due to their capability to polarize into M1 (inflammatory) and M2 (wound healing) phenotypes, which further generate an array of pro-inflammatory and anti-inflammatory cytokines, respectively. Using *in vitro* cultured human monocyte cell line (THP-1), we assessed how surface chemistry and nanoporosity (individually and in combination) influence the functionality of THP-1 cells. This analysis was performed by quantifying inflammatory response upon activation. The results are presented in **Figures 4** and **5**.

An overall reduction in cytokine expression levels was observed upon addition of a combination of nanoporosity and chemistry compared to uncoated alumina membranes

(**Figure 4**). In the case of Meoxpp (** = p<0.01) and ACpp (* = p<0.05) coated surfaces, a significant reduction in the concentration of the cytokine tumour necrosis factor alpha (TNFα) was observed, while only a moderate reduction in concentration of interleukin-6 (IL-6) and interleukin-1β (IL-1β) was observed as compared to aluminium control surfaces (**Figures 4 A, D and G**). Upon addition of nanoporosity, a significant increase in the concentration of all three cytokines (TNFα, IL-6 and IL-1β) was observed on NAA-Su surfaces, while the cytokine concentration decreased significantly on surfaces with bigger pore size (i.e. NAA-Ox and NAA-Ph) (**Figures 4 B, E and H**).

The combination of nanoporosity and surface chemistry led to an overall significant decrease in the concentration of proinflammatory cytokines (TNFα, IL-6 and Il-1β) compared to the control aluminium surfaces (**Figures 4 C, F and I**). Though an overall decrease in cytokines level was observed, the chemistries in combination with large pore size showed a more prominent decrease in the cytokine concentration compared to chemistries on smaller pore sizes (i.e. NAA-Ox and NAA-Su).

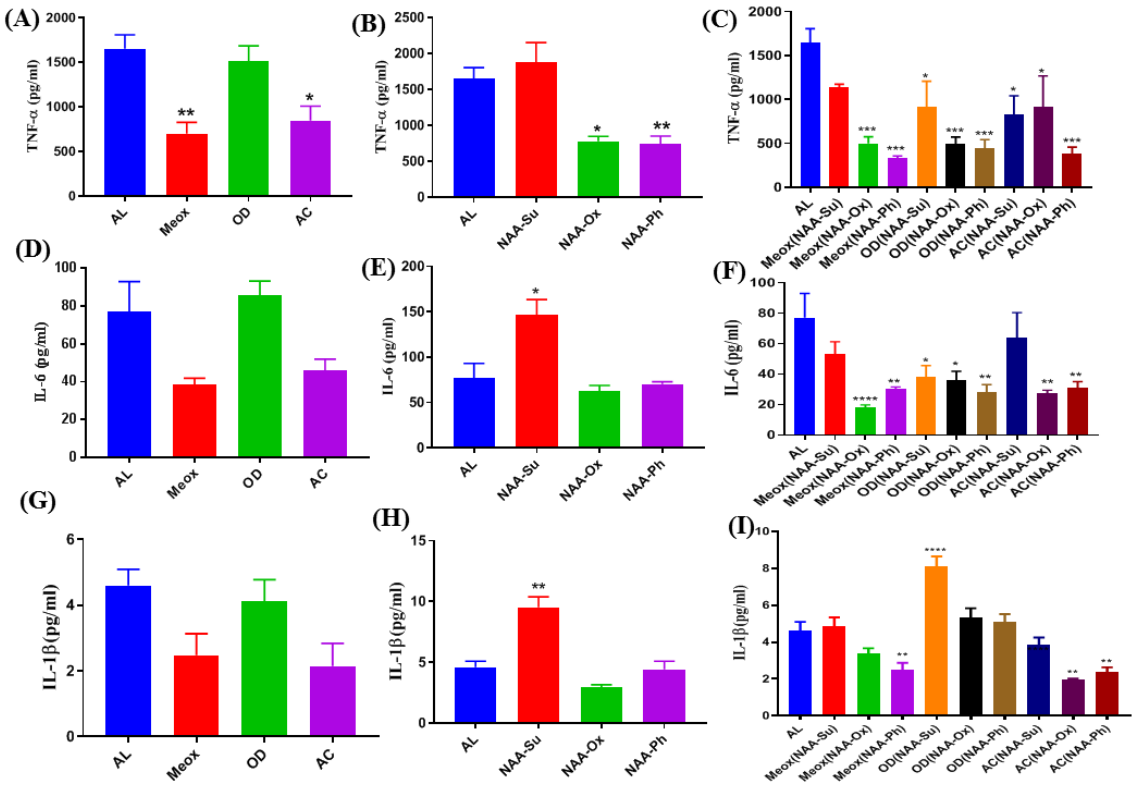

Figure 4: Pro-inflammatory response of macrophages stimulated by LPS (1 µg/mL) on nanoporous alumina surfaces with different pore size and surface chemistry. Release of pro-inflammatory cytokines (TNFα, IL-6, and IL-1β), as determined using Legendplex ELISAs. Cytokines TNFα, IL-6, and IL-1β from alumina modified with various surface chemistries methyl oxazoline, octadiene and acrylic acid (A, D &G)), alumina with different pore sizes NAA-Su,

NAA-Ox and NAA-Ph (B, E &H), cytokines from nanopores with different surface chemistries (C, F&I). * = $p<0.05$, ** = $p<0.01$ and *** = $p<0.001$

An overall increment in anti-inflammatory cytokine concentration upon combination of nanoporosity and chemistry for all surface chemical modifications was observed (**Figure 5**). Meoxpp and ACpp coated surfaces displayed a significant increase in the concentrations of the cytokines, interleukin 1 receptor antagonist (IL-1RA) and interleukin-10 (IL-10), and only a moderate increment in concentration of cytokine (arginase) as compared to aluminium control surfaces (**Figure 5 A, D and G**). Upon addition of nanoporosity, the concentration of IL-1ra increased significantly on surfaces with bigger nanopores (NAA-Ph) compared to their counterpart surfaces with smaller nanopores (NAA-Su and NAA-Ox), while an increase in the concentration of IL-10 was more significant on NAA-Ox surfaces compared to NAA-Su and NAA-Ph surfaces, and only a moderate increase in concentration of arginase as compared to aluminium control surfaces was observed (**Figures 5 B, E and H**).

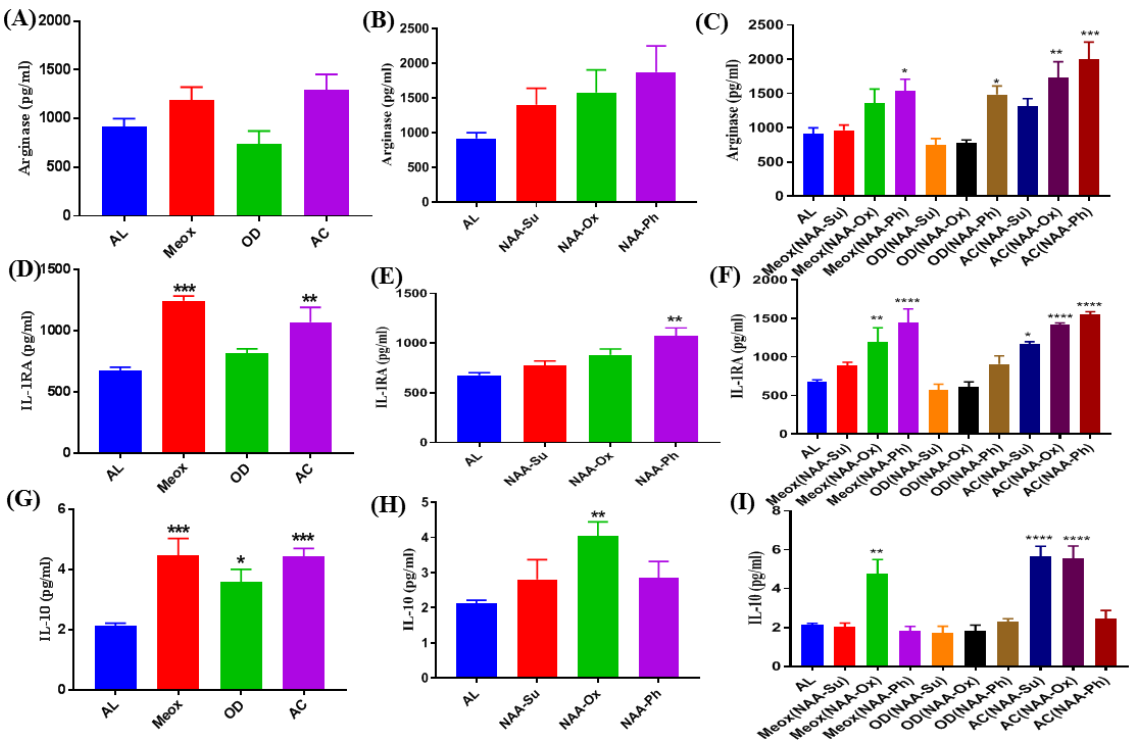

Figure 5: Anti-inflammatory response of macrophages stimulated by LPS (1µg/ml) on nanoporous alumina surfaces with different pore size and surface chemistry. Release of anti-inflammatory cytokines (Arginase, IL-1RA and IL-10), as determined using Legendplex ELISAs. Cytokines Arginase, IL-1RA and IL-10 from alumina modified with various surface chemistries

oxazoline, octadiene and acrylic acid (A, D &G)), alumina with different pore sizes NAA-Su, NAA-Ox and NAA-Ph (B, E &H), cytokines from nanopores with different surface chemistries(C, F&I). * = $p<0.05$, ** = $p<0.01$ and *** = $p<0.001$

To summarize, the combination of different nanoporosity with these chemistries led to an overall significant increase in the concentration of the anti-inflammatory cytokines (arginase, IL1ra and IL-10) compared to the control aluminium surfaces (**Figures 5 C, F and I**). Although, an overall increase in cytokines level was observed, the chemistries in combination with large pore size showed a more prominent increase in the cytokine concentration compared to chemistries on smaller pore size.

6.6. Discussion

Understanding the factors underlying modulation of innate immune responses to surface features has critical implications on the design and engineering of implantable biomaterials. This study reveals that a combination of surface nanoporosity with tailored surface chemistry can be readily used to modulate macrophage activation by modulating the secretion of pro-inflammatory and anti-inflammatory cytokines. NAA substrates were fabricated by two-step anodization to tune the geometric features of nanopores with precision[296-299]. A thin layer of Meoxpp, ODpp and ACpp (~5 nm) was deposited onto these nanoporous surfaces to generate desired uniform surface chemistries to further modulate macrophage responses. Using this approach, we were able to generate 15 independent types of surfaces with unique combinations of nanoporosity and chemistry. FEG-SEM and XPS analysis were used to establish the geometric features of the nanopores and chemical composition of the model substrata used in this investigation.

Our data demonstrates that the expression of pro-inflammatory cytokines decreased while anti-inflammatory cytokines increased on Meoxpp and ACpp coated surfaces, and the effect was boosted by combining these chemistries with increasing the size of nanoporosity (30<65<200 nm). This is consistent with previous studies showing that hydrophilic -COOH surfaces have reduced inflammatory responses and fibrotic encapsulation[300, 301]. Additionally, our previous studies demonstrated that the combination of nanotopography (nanoparticles) with the -COOH surfaces reduced the inflammatory response*[117]* and fibrotic capsule thickness*[179]* while increasing the expression of collagens[162]. Furthermore, the results presented in this chapter indicates that the expression of cytokines can be modulated to a greater extent by using nanoporous surfaces with same chemistry compared to gold nanoparticles nanotopography surfaces

with the same chemistry*[117]*. It is noteworthy that the cell numbers were same across all 15 substrates (**Figure S1**). Therefore, the decrease in pro-inflammatory signals or the increase in anti-inflammatory signals were not affected by number of adherent cells.
Furthermore the levels of TNFα decreased significantly on Meoxpp and ACpp coated surfaces as well as on nanoporous surfaces with greater nanoporosity compared to uncoated alumina membranes. The reductions in IL-6 and IL-1β concentrations were only observed upon combination of nanoporosity with surface chemistry. Additionally, IL-1ra and IL-10 increased significantly on Meoxpp and ACpp surfaces and remained unchanged on different nanoporous surfaces compared to uncoated alumina membranes. The concentration of arginase only increased when a combination of nanoporosity with chemistry was utilized. Interestingly, hydrophobic ODpp surfaces showed no change in inflammatory responses (pro and anti). Also, concentration of TNFα decreased while IL-1RA increased, but there was no change observed in the concentration of IL-6, IL-1β, Arginase and IL-10 on surfaces with higher nanoporosity (30<65<200 nm). However, ODpp and nanoporous surfaces with increasing nanopore size have been known to enhance inflammatory responses and fibrotic encapsulation around biomaterials [102, 169, 281, 301, 302]. Our data, on the contrary, have shown a significant reduction in the concentration of TNFα and IL-6, and an increment in the concentration of arginase, on combining ODpp with higher nanoporosity surfaces. This suggests that surface nanoporosity or surface chemistry cannot be used alone as a reproducible correlate of cell functionality. A possible explanation for nanoporosity mediated macrophage differentiation could be nanotopography induced orientation and conformational changes of adhered proteins,[102, 303] exposing unknown cell-surface receptors, causing unprecedented cellular behaviour.[242]

One of the biggest problems with medical devices is fibrosis or fibrous encapsulation.[304-307] To overcome these unwanted effects several strategies involving

addition of growth factors[308-311], surface chemical modifications[91, 122, 312, 313] or the addition of surface nanotopography[44, 121, 314, 315] have been explored. The data presented here suggest that synergetic effect of surface nanoporosity with surface chemistry can be used to control macrophage differentiation by modulating pro-inflammatory and anti-inflammatory cytokines. To the best of our knowledge, this is the first comprehensive study demonstrating that the interplay between surface nanoporosity and chemistry can be used to control macrophage differentiation. As pro-inflammatory cytokines decreased and anti-inflammatory cytokines increased on -COOH surfaces with high nanoporosity, these surfaces can be utilized to fabricate biomaterials that can tune immune responses to enhance implant healing and can be used to establish a base for the future rational design of biomaterial implants.

6.7. Conclusion

In this study, the role of surface nanoporosity and chemistry on pro-inflammatory and anti-inflammatory cytokines production by macrophages was evaluated. We have utilized three different sizes of nanoporous surfaces (30, 65 and 200 nm) to generate controlled surface nanotopography. To tailor the outermost surface chemistry, a ~5 nm plasma polymer film deposited from vapors of methyl oxazoline, 1, 7 octadiene and acrylic acid were employed. This model system enabled the evaluation of the interplay between surface nanotopography and chemistry. We have shown that the concentration of pro-inflammatory cytokines (TNFα, IL-6 and IL-1β) decreased significantly on nanoporous surfaces featuring large nanopores and having Meoxpp and ACpp surface coatings compared to surface with smaller pore sizes and chemistry. Furthermore, the concentration of anti-inflammatory cytokines (Arginase, IL-1RA and IL-10) increased significantly on large nanoporous surfaces with Meoxpp and ACpp coatings. Our data suggests that the macrophage differentiation can be controlled by selecting desired combinations of surface nanoporosity and chemistry. The knowledge obtained from this study provides cues that could aid in tuning foreign body response and will eventually facilitate the rational design of biomaterial implants.

6.8. Acknowledgment

KV thank to ARC grant ARC DP15104212, NHMRC for Fellowship APP1122825 and the Humboldt Foundation for the Humboldt Fellowship for Experienced Researchers.

SI 6.9. Supporting Information

SI 6.9.1. Macrophage Cell Count

Macrophage cell count, number of cells quantified after collecting the media, macrophage cell counts were performed using trypsin and hemocytometer to quantify the number of cells that produced cytokines on each surface. The cell number are comparable for all conditions investigated, this confirms that the difference in cytokine expression was in response to the surface chemistry and nanoporous structures and not simply a direct effect of cell numbers.

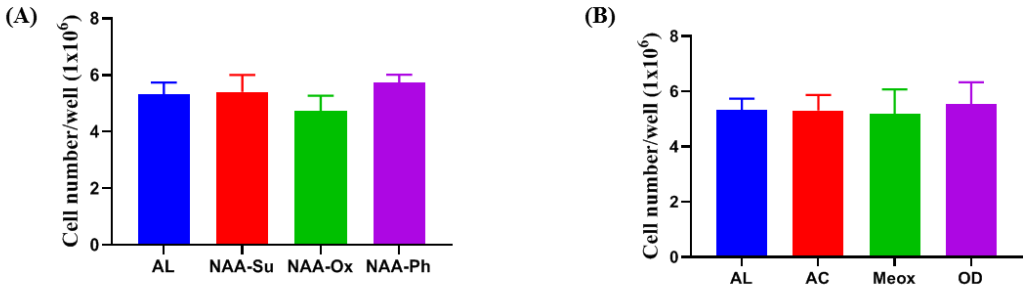

Figure S1. Macrophage cell count on (A) alumina with different pore sizes NAA-Su, NAA-Ox and (B) alumina modified with various surface chemistries acrylic acid, methyl oxazoline, and octadiene.

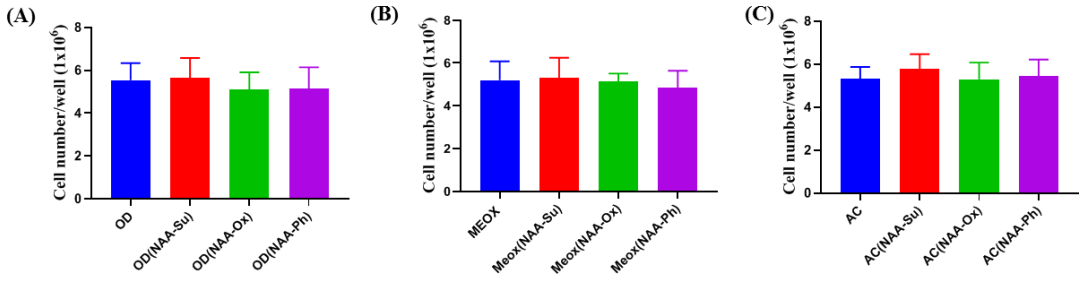

Figure S2. Macrophage cell count on (A) alumina with different pore sizes of NAA-Su, NAA-Ox and combination with octadiene (A) methyl oxazoline (B) and acrylic acid (C) surface chemistries.

Chapter 7. Nanoparticle Shape Influence on Protein Corona Formation

7.1. TOC

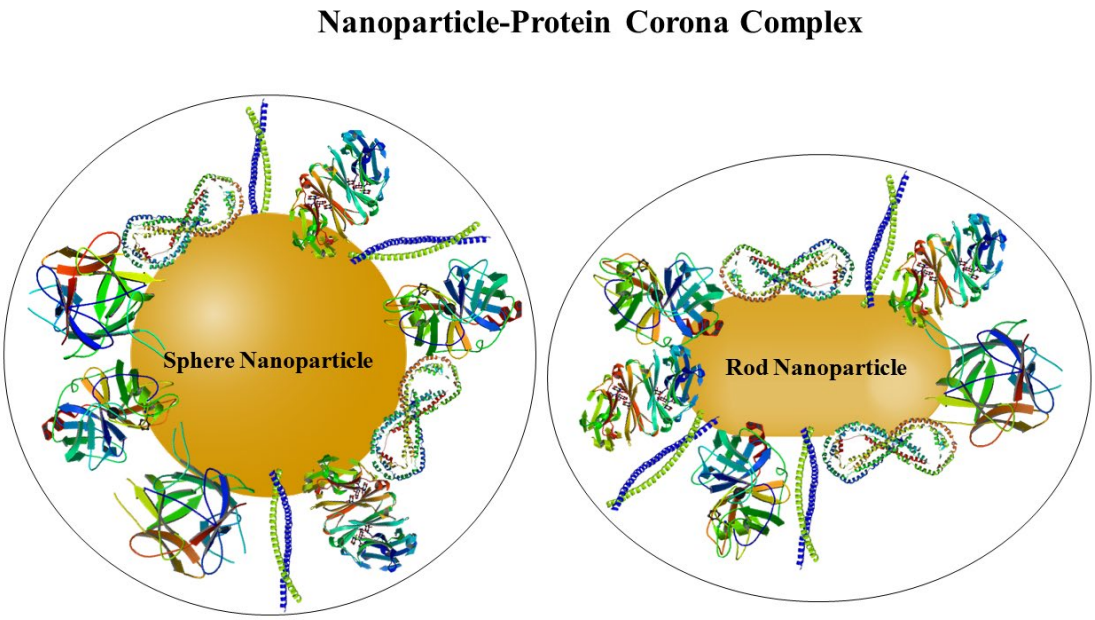

Upon exposure to blood, proteins adsorb onto the surface of nanoparticles and form a protein corona, which determines the particles biological faith. Here we report on how nanoparticles with identical surface chemistry but different shape result in different protein corona composition, both in serum and plasma.

7.2. Introduction

Nanoparticles (NPs) have become an integral part of many aspects of modern medicine, having utility in a wide range of areas such as drug delivery, medical imaging and diagnostics.[316, 317] In this context, mesoporous silica nanoparticles (MSNs) are particularly interesting for medical applications because of their biocompatibility, biodegradability, large surface to volume ratio and tuneable pore structures.[318-320] Thus, MSNs have shown great potential to be applied as drug and biomolecular carriers, targeted cancer therapies and theragnostic.[320]

However once administered, the NPs are exposed to the innate immune system which may neutralize them prior to reaching the target location.[321] This defence mechanism is part of the foreign body reaction, a process that begins with the indiscriminate attachment of proteins from the body fluids to the nanoparticle's surface. In order to create efficient therapies, it is important to understand how proteins interact with nanoparticles and the composition (and potential impact) of the protein corona that

subsequently forms. Recent research has demonstrated how the protein corona composition controls NPs' non-specific cellular uptake by immune cells[248, 250], its influence on inflammation[322] as well as oxidative stress.[323] Because of the importance of protein corona on the biological fate of a material placed in bodily fluids, extensive research has been carried out to understand the factors affecting its formation,[249, 324, 325] including the effects of particle size,[325] surface charge,[326] surface chemistry[327] and biological media composition.[328]

Recently, it has been demonstrated that the shape of the nanoparticles can also significantly impact their performance. Since changing the shape of NPs is similar to changing the size, both effectively changing the curvature of the nanoparticle comparable results are expected for different size. These include their circulation time in blood, cellular internalization, bio-distribution, endocytosis by immune cells and residence time within the cell.[329, 330] [331] As an example, non-spherical particles have been demonstrated to have longer circulation time, reduced phagocytosis by macrophages and less cellular uptake than their spherical counterparts. [332, 333],[334] It has been also reported that specific cells can be selectively targeted by controlling the shape of NPs.[335] Studies with Hela and Caco-1 cells have shown high efficiency in cellular uptake of rod shape particles.[336] Another study of MSNs shaped as spheres and tubes involving Chinese hamster ovary (CHO) and fibroblast cells illustrated how cellular uptake was morphology and cell line independent, however, the endocytosis rate was greater for sphere than rod shape particles.[337] Interestingly, recent haemolysis studies indicate that haemolytic activity in red blood cells (RBC) is also shape dependent and that cytotoxicity was reduced in the presence of serum proteins,[319] albeit using only a few selected proteins.

The examples provided above point to the need to understand the role of nanoparticle shape on protein corona formation because such knowledge will equip us with the tools to create the next generation of nanomaterials that intelligently interact with biological fluids.

7.3. Result and Discussion

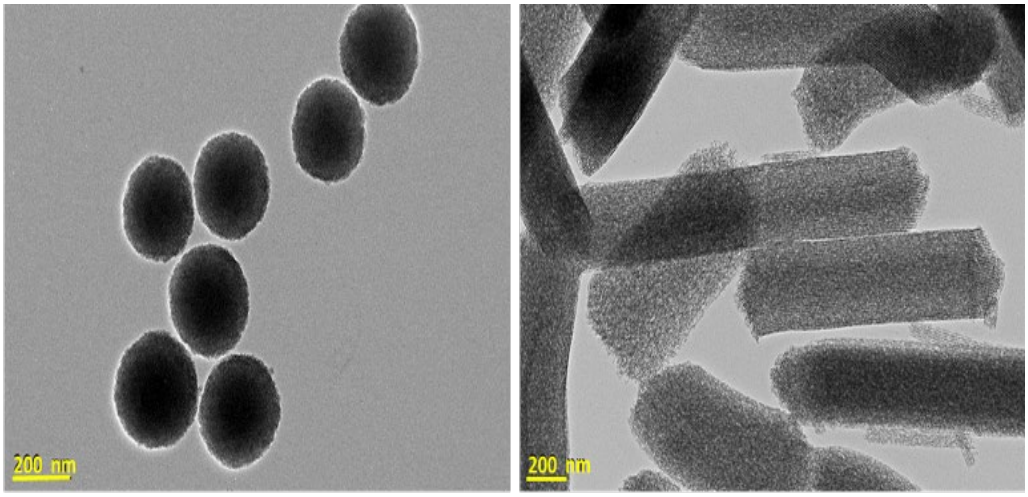

Figure 1: TEM images of sphere (CD-5) and rod (SAB-15) mesoporous silica nanoparticles.

To address this challenge, we prepared two chemically identical mesoporous silica nanoparticles of comparable size in one of the dimensions that were either rod or sphere shaped and exposed them to human serum and plasma. The two types of MSNs are shown in the TEM images in Figure 1. The rod shape MSNs (SBA-15) were prepared under static conditions using a soft templating approach in an acidic condition as previously reported.[338, 339] The core-shell spherical MSNs (CD-5) were specifically synthesised for this study. Both synthesis procedures are detailed in the supporting information.

The TEM images in Figure 1 and SEM in Figure S1 of the supporting information show that CD-5 had spherical morphology with particle diameters of 315±65 nm. The rode-like SBA-15 had nearly identical size in the *y*-dimension as CD-5 but average length (*x*-dimension) of 1100 nm. Further characterisation presented in the supporting information show that both particles have very similar average pore sizes between 10 nm and 11 nm and nearly identical pore volume of 0.97 $cm^3 g^{-1}$ and 1.06 $cm^3 g^{-1}$ for CD-5 and SBA-15, respectively.

The surface chemical composition of both nanoparticles obtained from XPS analysis is shown in Table 1. Within the experimental uncertainty of XPS, the atomic percentage of carbon, oxygen, and silicon in the outermost 10 nm of the surface is nearly identical for both types of nanoparticles. Finally, we analysed the surface charge of the nanoparticles, an important regulator of protein interaction with surfaces. Figure S3 of the supplementary information shows that CD-5 and SBA-15 have almost the same zeta

potential of -20 mV at pH 7. The comprehensive analysis of CD-5 and SBA-15 demonstrates that in our study we take forward two nanoparticles that have identical structure, chemical composition and zeta potential and only differ by their shape – one being spherical and the other rod shape, both having one dimension of comparable size.

Table 1: Atomic composition of the surface of the nanoparticles as determined via XPS. All XPS data contains a standard error of 5%.

	C%	O%	Si%
Sphere	7.3	51.2	41.4
Rod	6.6	50.9	42.3

To study the effect of NP shape on protein adsorption, we prepared the sphere and rod MSN suspension in MilliQ water and incubated with human serum and plasma for 1 hour with continuous agitation using a rotating shaker. To address the differences in rod and sphere shaped particle's surface area and ensure reproducibility, 0.05 m^2 of nanoparticle sample's surface area was exposed to 1 mL serum and plasma in three replicates. Afterwards, the samples were centrifuged and washed three times to remove and unbound proteins (for details see supporting information). Subsequently, the total protein adsorption was determined via a Pierce assay. The results presented in Figure 2 and Figure S4 show that significantly larger total amount of protein adsorbed on the rod-shaped particles compared to those having spherical shape. This trend was observed for both serum and plasma, 3-fold increase for plasma and 4-fold increase for serum. The result is in agreement with a published study by Gagner and co-workers who reported that selected proteins i.e. lysozyme and α-chymotrypsin attached in greater amounts on gold nanorods compared to gold nanospheres.[340]The rod-shaped NP possess two dimensions and average curvatures that is defined by the circumference of the rod, and then a relatively flat surface along the cylindrical/longitudinal axis of the rod NP. It might be possible that the longitudinal axis of the rods, where the curvature is only one dimensional, allows for greater protein packing density resulting to an overall larger protein amount that is adsorbed. For small proteins with dimensions less than the diameter of the rod-shaped NP's facets, this surface can be considered as a relatively flat surface. Therefore, an increased lateral interaction on the relatively 'flat' cylindrical surface may facilitate a higher packing density of proteins adsorbed on rod-shaped NPs when compared to spherical NPs.[340] Previous studies with spherical NPs of different size also displayed an inverse relationship with the protein adsorption and curvature.[242, 341] Similarly a high degree of curvature may prevent protein-protein interaction and interfere with the

efficient close packing on the NP surfaces.[342] Further studies at single protein level, which allow for revealing potential conformational changes of proteins on curvatures in one and two dimensions, are required to fully unravel the observed phenomenon.

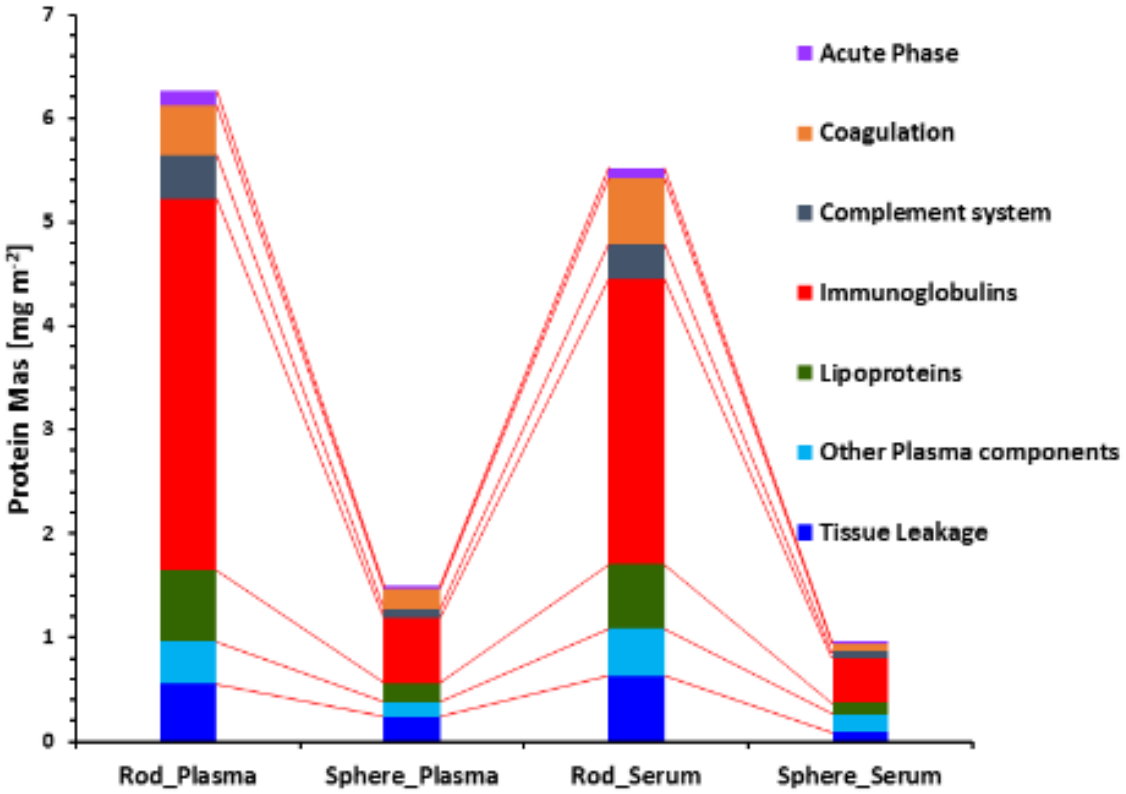

Figure 2: Quantification of human plasma and serum protein mass adsorbing to the mesoporous nanoparticles along with classification of protein corona components identified by quantitative LC-MS. Identified proteins were grouped according to their function in biological processes.

To bring insight in the composition of protein corona, we carried out analysis by sodium dodecyl sulphate polyacrylamide gel electrophoresis (SDS – PAGE) and label-free liquid chromatography mass spectrometry (LC-MS). The molecular weight distribution pattern of proteins and protein complexes, shown in the SDS – PAGE images presented in supplementary Figure S5, reveals that the corona is composed of a large number of different constituents. Overall, the type of proteins that adsorb does not appear to be significantly different for sphere and rod-shaped particles. LC-MS was employed to identify individual proteins forming the corona. We further grouped the constituents of the protein corona in terms of their functions into acute phase, coagulation, complement, lipoproteins, immunoglobulins, tissue leakage and others (Figure 2). The exact constituents of each group are shown in table S1 of the supporting information. Immunoglobulins were the most abundant protein in the corona from both serum and plasma for rod and sphere. Rod shape had the highest amount of immunoglobulin

compared to sphere with 57% (3.57 mg/m^2) on plasma and 50% (2.7 mg/m^2) on serum corona. Sphere particle adsorbed 42 % (0.62 mg/m^2) and 45% (0.43 mg/m^2) of immunoglobulins from plasma and sphere respectively. All the other group of proteins accounted for less than 20% protein with comparable percentage for both the shapes and protein solutions, with more quantities on rod.

Most abundant proteins found in the corona formed from plasma and serum on the surface of the nanoparticles are summarised in a heat map (figure 3).The heat map shows several interesting facts. Notably, all the corona contained very large quantities (30% or above) of Ig gamma-2 chain C region and significantly higher on rod shape (8 % more) for both serum and plasma corona. Other proteins found in greater amounts on the corona are Immunoglobulin heavy variable 3-66 with slightly higher on rod shape (10% from plasma 9% from serum) compared to sphere (7% from plasma 8% from serum). Figure 3 also shows large amounts of albumin adsorption on to sphere from serum compared to rod (12% vs 2%). However, when adsorption was carried out in plasma, the amount of albumin was less and identical for both the particles. The corona also appears to be rich in apolipoprotein B-100 with identical adsorption on both the particles.

Immunoglobulins attach in great quantities to the nanoparticles. The function of these proteins is to activate the immune defence system.[343, 344] The significantly greater amount of immunoglobulins binding to the rod-like particles suggests that nanoparticles with non-spherical shapes may triggers stronger immune responses. These results reveal a complex pattern of recognition of spherical and rod-shaped entities. Thus, it may be possible that specific sets of proteins specialise in clearing foreign objects dependent on their shapes. Since it is known that the protein corona formation strongly influence the retention, transport and phagocytosis of nanoparticles.[345] The enrichment of opsonin such as immunoglobulin may induce macrophage recognition and phagocytosis leads to the fastest removal from the body.[346, 347] These immunoglobulins triggered macrophage recognition also could lead to accumulation of nanoparticle in liver and spleen which may be useful for target delivery to these organs.[348-350]It is also important to note that the corona enriched with dysopsonin such as albumin could lead to an extended circulation time in the body.[345, 346]

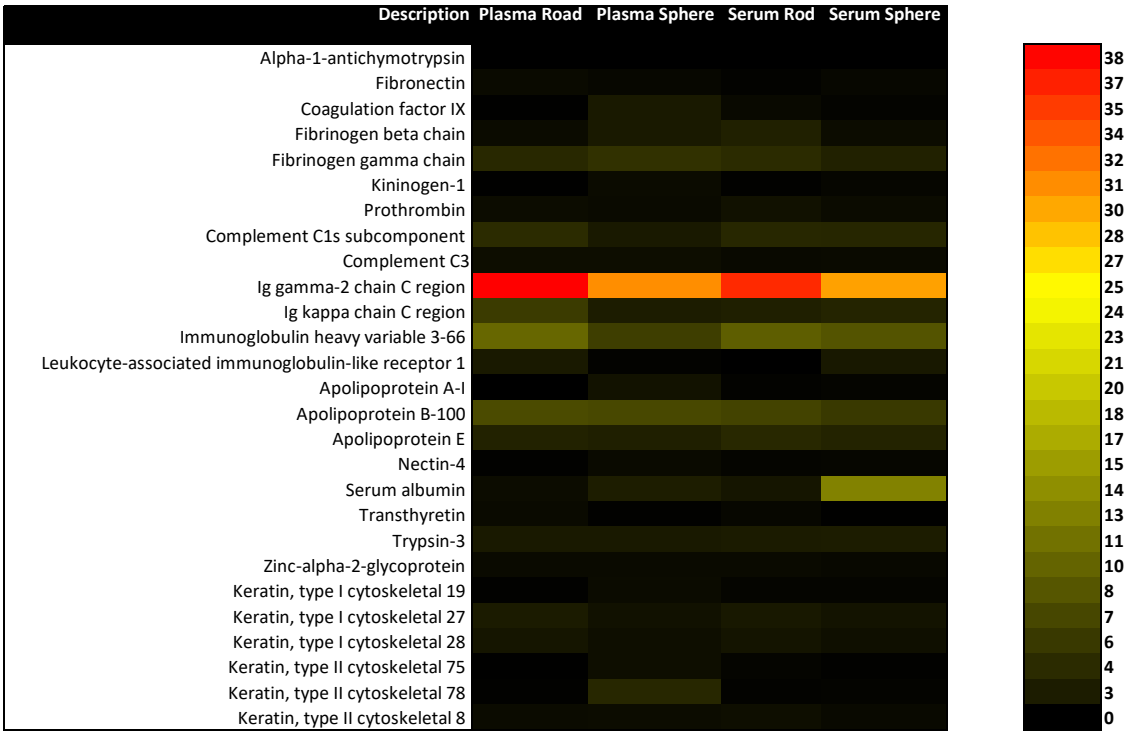

Figure 3: Heat map of most abundant proteins in the protein corona of the sphere and rod mesoporous nanoparticles with serum and plasma determined by proteomic mass spectrometry. Values were calculated from the molar masses of each protein identified by liquid chromatography–mass spectrometry. Only those proteins that constitute more than 1% of the protein corona on each of the surfaces are shown in the heat map.

Collectively, we present the first study of protein corona formation, from both serum and plasma, on spherical and rod-shaped nanoparticles. We prepared two types of silica nanoparticles which had identical chemistry, porosity, structure, surface potential and size in y-dimension, one being a sphere and the other a rod. We found significantly larger amount of protein attaching from plasma and serum on the rod-like particles compared to the spheres. Interrogation of the protein corona by LC-MS and SDS – PAGE revealed very small amounts of adsorbed abundant proteins such as albumin and fibrinogen. We also found shape dependent differences in the adsorption of immunoglobulins on both protein solutions and albumin proteins from serum. Our results indicate that there could be specialization of proteins used by the immune system to recognize and clear foreign objects simply based on invading objects shape. These findings point to the need of further detailed studies focused on understanding of the specific protein absorption patterns on nanoparticles of different shapes and the conformational state of these proteins when they encounter objects of certain geometry. Understanding of these phenomena can have profound implication of how we design nanoparticles for medical therapies.

7.4. Acknowledgement

K.V thanks ARC for DP15104212 and DP180101254, NHMRC for fellowship APP1122825 and project grant APP1032738, and the Alexander von Humboldt Foundation for Fellowship for Experienced Researchers.

SI 7.5. Supplementary Information

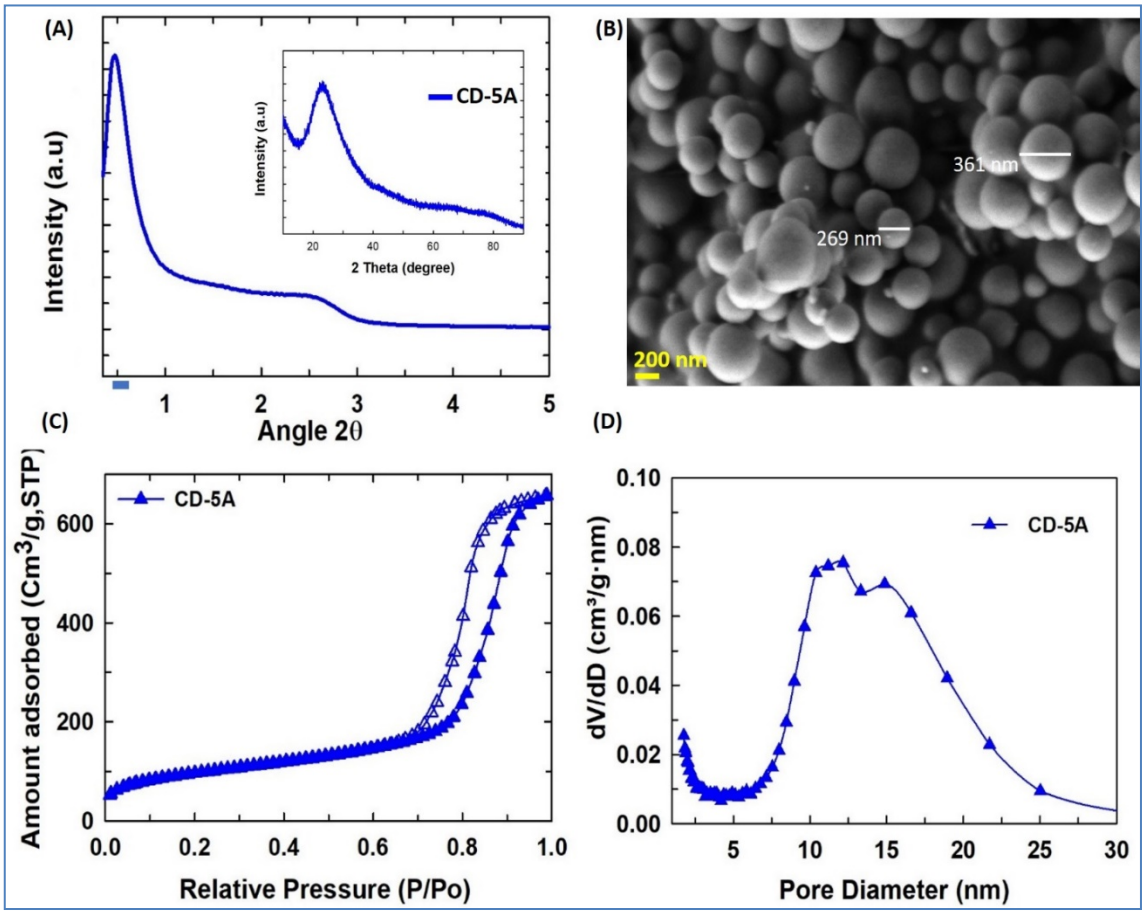

Figure S1: (A) Lower angle XRD pattern of Core shell nanoparticle, insert-shows higher angle XRD pattern. (B) SEM image (C) and (D) Nitrogen adsorption-desorption pattern with pore size distribution.

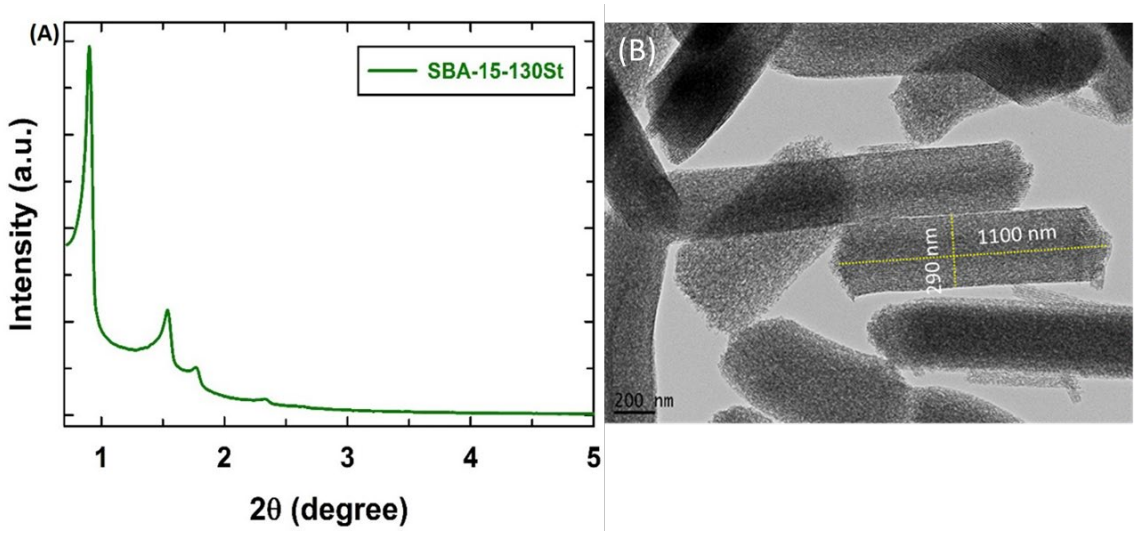

Figure S2: (A) Lower angle XRD pattern of SBA-15-130 synthesised at static condition. (B) HR-TEM image of SBA-15-130st particles.

SI 7.5.1. Synthesis of SBA-15-130st (rod)

The SBA-15, mesoporous silica material was prepared under static condition using the soft templating approach in an acidic condition.[338, 351] In a typical synthesis, 4 g of non-ionic surfactant Pluronic P-123, a triblock copolymer with the molecular formula $EO_{20}PO_{70}EO_{20}$ was added with 30 ml of double distilled water and stirred continuously for 3 h. Subsequently, 120 g of 2 M HCl was added and then the temperature was gradually increased to 40 ˚C and the sample was further stirred for 2 h. 9 g of tetraethyl orthosilicate (98% TEOS) was added dropwise and the mixture was stirred for 20 minutes. Stirring was discontinued afterwards and the sample was allowed to rest for the next 24 hours at the constant temperature of 40 ˚C. Finally, the milky solution obtained was transferred to a Teflon lined autoclave and kept under hydrothermal condition at 130 °C for the next 48 h. The resulting product was filtered with hot deionised water and washed three times with the same solution. The final precipitate obtained after thorough percolation was dried at 100 °C for 6 h and then calcined at 540 °C for 12 h for the removal of the leftover polymeric surfactant and any impurities present. The obtained samples were labelled SBA-15-130st where st denotes the static synthesis condition.

SI 7.5.2. Synthesis of core shell nanoparticle CD-5A (Sphere)

In a typical synthesis, 0.1 g of F127 Pluronic surfactant ($(EO)_{106}(PO)_{70}(EO)_{106}$) was weighed and dissolved in 20 ml of tetrahydrofuran (THF). Then, 0.2 g of hexadecyl trimethyl ammonium bromide (CTAB) were dissolved in 80 ml of deionized water and 3 ml of ammonia solution was slowly mixed with the above solution and stirred for 10

minutes at room temperature. Subsequently, 1g of tetraethyl orthosilicate (98% TEOS) was added dropwise and the stirring was continued for 24 h at room temperature. The milky solution obtained after 24 h was collected and allowed for ageing under hydrothermal condition at the temperature of 130 °C for another 24 h. The precipitate formed was then centrifuged at 8000 rpm for 10 minutes and the pellet was collected. Finally, the pellet was dried at 70 ˚C for 6 hours and allowed for calcination at 550 °C, and the final product was collected as a white powder.

SI 7.5.3. Characterisation

SI 7.5.3.1. XRD

The Powder X-ray diffraction measurement were recorded using Panalytical Empyrean XRD instrument. The measurement was collected using Cu K_α radiation from a sealed tube source operating at 40 kV and 40 mA with a scan rate of 0.01° /sec. Nitrogen adsorption and desorption isotherms were measured at −196 °C on a Micromeritics ASAP 2420 surface area and porosity analyser. The sample was degassed for 6 h at 250 °C under vacuum ($p < 1 \times 10^{-5}$ pa) in the degas port of the adsorption analyser. The specific surface area was calculated using the BET model. Pore size distribution was obtained using the BJH model from the adsorption branch of the isotherm.

SI 7.5.3.2. TEM

The structural morphology of SBA-15-130st and core shell nanoparticles were observed in transmission electron microscope (JEOL – 2100F, Japan). Samples for the transmission electron microscope were prepared by placing 10 µl of NPs solution in MilliQ (1 mg/mL) water on a carbon coated copper grid (ProSciTech, Australia). The grid was left to dry overnight at room temperature prior to TEM analysis.

SI 7.5.3.3. SEM

The structural morphology of core shell nanoparticles were observed using Carl ZEISS MERLIN SEM equipped with a field-emission gun operated at 2kV to scan the samples. The sample preparation for HR-SEM involved sprinkling of the powder sample on the carbon tab mounted on the SEM stub. The sample stubs were vacuum baked at 70 °C for 8 h before inserting the sample into the SEM measurement chamber.

SI 7.5.3.4. Graph explanation (XRD, BET, and SEM)

The structure of the prepared core shell nanoparticle (CD-5A) material was confirmed by powder X-ray diffraction analysis. Fig.1A shows a lower angle powder XRD pattern for core-shell mesoporous silica nanoparticles. The XRD pattern exhibits a major higher ordered peak at the 2θ of 0.5˚ and the second minor broader peak which is around the 2θ of 2.5 °C, confirming the ordered mesoporous structure in the sample. On the other hand, wide angle XRD pattern (Fig.1, insert) displays a peak ca 23 °, confirming that the material is amorphous in nature. HRSEM analysis revealed that the material exhibits spherical morphology with the particle size of approximately 260 to 360 nm in diameter. Moreover, the core and shell are identified from the TEM image. The material exhibits a type IV isotherm with a sharp capillary condensation step and a H1 hysteresis loop, which is typical of mesoporous materials with well-ordered cylindrical pores type with large pore diameter (Fig. 1C). The surface area of this material was found to be 351.3 $m^2\ g^{-1}$ with the pore diameter of 11.9 nm and pore volume being 0.97 $cm^3\ g^{-1}$ (Fig. 1D).

Fig.2 A shows a low angle powder XRD pattern for the SBA-15-130st which exhibits three well-ordered peaks that can be indexed as (100), (110) and (200) reflection planes on a two-dimensional hexagonal lattice with p6mm symmetry.[338, 351-353] The structure of the material is similar to that of pure SBA-15 which was prepared under dynamic hydrothermal synthesis. Likewise, the morphology of SBA-15-130st (rod) was found to have uniform rod-shaped structures with the particle size of 1100 nm in length and 290 nm in thickness as measured from the HR-TEM image. The shape of the particles is rectangular in nature with a surface area of 560.9544 $m^2\ g^{-1}$ and pore diameter 10.14 nm with a pore volume of 1.066718 $cm^3\ g^{-1}$.

SI 7.5.3.5. Surface Charge- Zetapotential Measurements

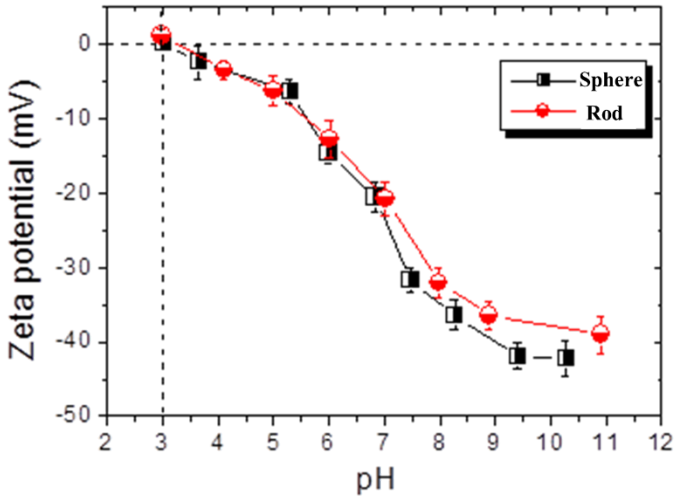

Figure S3: Zetapotential measurement of rod and sphere MSNs

SI 7.5.3.6. Zeta Potential

A Malvern Zetasizer Nano ZS (Malvern Instruments Ltd, Worcestershire, UK), equipped with a 633 nm He-Ne laser was used to measure zeta potential. Instrument control and data analysis were performed with Zetasizer software (version 7.10). For each measurement, the temperature was maintained at 25 °C, and the angle of detection was set at 90°. Measurement position, attenuator level and measurement duration were all set to be automatically optimized by the software. Electrophoretic mobility was measured using disposable folded capillary cells (Malvern Instruments Ltd, Worcestershire, UK) and zeta potential was derived from Henry's equation:

$$U_E = \frac{2\varepsilon\zeta f(k\alpha)}{3\eta}$$

where U_E is electrophoretic mobility; ε is dielectric constant; ζ is zeta potential; f (kα) is Henry's function and η is dispersant viscosity. Each sample was measured three times.

The zeta potential measurements of 0.05% by weight of silica suspensions in 10^{-3} M KCl were carried out as a function of pH in the pH range from 1 to 11. The pH of the silica suspensions was adjusted to the desired pH values using small quantities of HCl or KOH solutions.

SI 7.5.3.7. X-ray Photoelectron Spectroscopy (XPS)

XPS analysis was performed to characterize the surface chemical composition of the mesoporous nanoparticles. SPECS Silicon And GErmanium (SAGE) XPS spectrometer was used with monochromatic Mg radiation source operated at 10 kV and 20 mA. The chemical composition of sample surface was analysed from survey spectra recorded over a 0−1000 eV range with pass energy of 100 eV at a resolution of 0.5 eV. Curve fitting and processing of spectra were performed using Casa XPS software and all binding energies (BE) were referenced to the neutral carbon C1s peak at 285.0 eV.

SI 7.5.4 Protein Corona Preparation

Human blood plasma (Heparin anticoagulant) and serum was purchased from Innovative research.inc. to remove any aggregated proteins the samples were centrifuged for 1 h at 20,000 g before usage. Each nanoparticle solution prepared in MilliQ water was incubated with plasma and serum in three replicates. Using the surface area calculated from BET the nanoparticle surface concentration to the serum and plasma was kept contestant at 0.05 m^2 per 1 mL and incubated with 1 mL human plasma and serum for 1 h with constant agitation. The particles were separated from the supernatant by centrifugation at 20,000 g for 1 h. The particle pellet was resuspended in PBS and washed by three centrifugation steps at 20,000 g for 1 h and subsequent redispersion in PBS. Before the last washing step, the dispersion was transferred into a new tube. After the final wash, 150 µL of SDS-triz HCl buffer (40 mg SDS + 125 µL Triz-HCl + MilliQ water up to a total of 2 mL) was added and incubated by shaking at 95°C for 15 min. A final Centrifugation were performed for 1h 4 °C at 20,000 G to isolate the proteins. The total protein concentrations were determined using Pierce 660 nm protein Assay according to manufactures instruction.

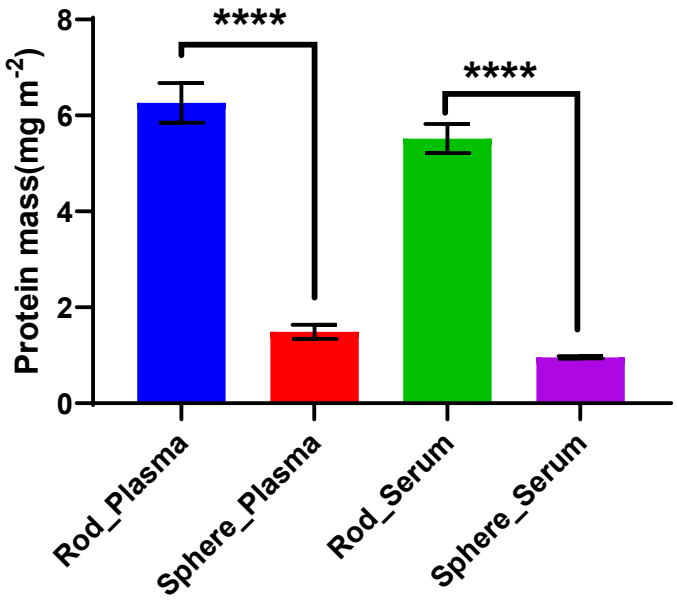

Figure S4: Serum and plasma protein adsorption on rod and sphere particles, quantified using pierce assay

SI 7.5.5. SDS Polyacrylamide Gel Electrophoresis (SDS PAGE)

For SDS PAGE 16.25 µl of the protein sample were mixed with 6.25 µl NuPAGE LDS Sample Buffer and 2.5 µl NuPAGE sample reducing agent and applied onto a NuPAGE 10 % Bis-Tris Protein Gel (all Novex, Thermo Fisher Scientific). The electrophoresis was carried out in NuPAGE MES SDS Running Buffer at 150 V for 1.5 h with SeeBlue Plus2 Pre-Stained Standard (Invitrogen) as a molecular marker. The gel was stained using Pierce Silver Stain Kit (Novex, Thermo Fisher Scientific).

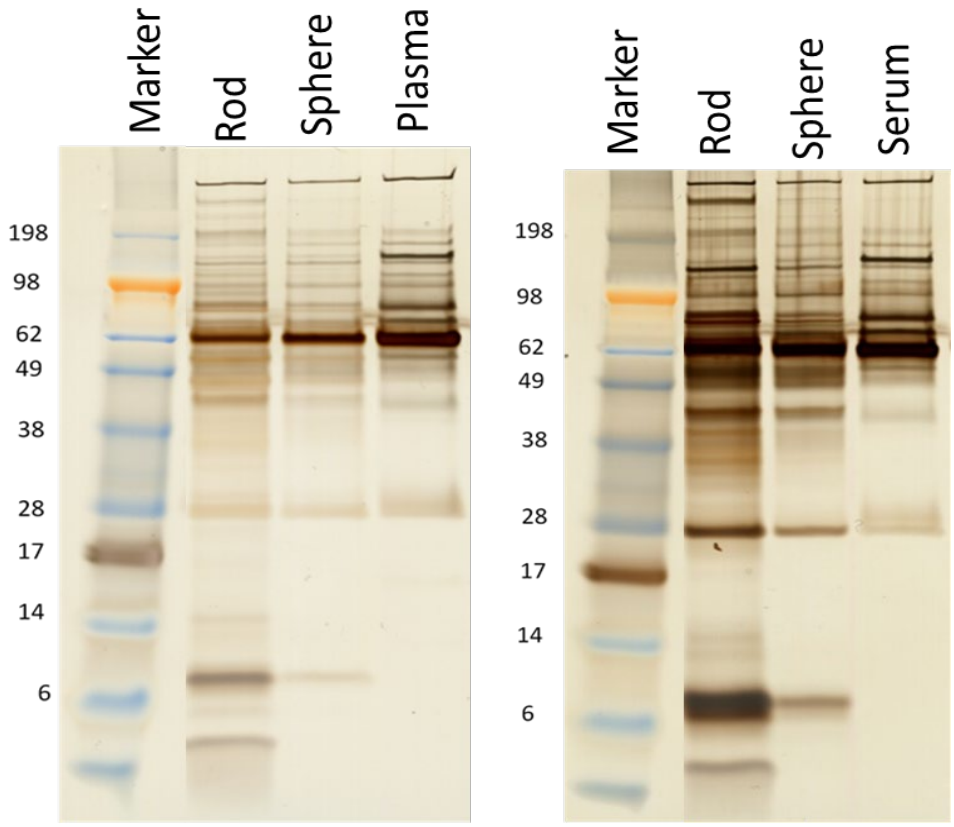

Figure S5: Gel electrophoresis: visual representation of protein corona contents based on molecular weights

SI 7.5.6. Liquid-Chromatography Mass-Spectrometry (LC-MS) Analysis.

Quantitative analysis of protein samples was performed using a nanoACQUITY UPLC system coupled with a SynaptG2-Si mass spectrometer (Waters Corporation). Tryptic peptides were separated on the nanoACQUITY system equipped with a C18 analytical reversed-phase column (1.7 µm, 75 µm x 150 mm, Waters Corporation) and a C18 nanoACQUITY Trap Column (5 µm, 180 µm x 20 mm, Waters Corporation).

Table S1. List of corona proteins identified by LC-MS. Average normalized amount [molar%] of total protein.

Description	Annotation	Serum	Plasma	Rod (S)	Sphere (S)	Rod (P)	Sphere (P)
Alpha-1-antitrypsin	Acute phase	1.244	1.232	0.698	0.990	0.956	0.511
Fibronectin	Acute phase	0.091	0.123	0.367	0.752	1.017	0.693
Haptoglobin	Acute phase	2.373	2.006	0.251	0.305	0.083	0.517
Haptoglobin-related protein	Acute phase	0.017	0.840	0.405	0.338	0.116	0.117
Antithrombin-III	Coagulation	0.000	0.299	0.328	0.495	0.031	0.139
Coagulation factor IX	Coagulation	0.000	0.000	0.895	0.468	0.169	2.501
Coagulation factor X	Coagulation	0.000	0.000	0.141	0.112	0.218	0.241
Fibrinogen alpha chain	Coagulation	0.000	0.267	0.071	0.040	0.476	0.329
Fibrinogen beta chain	Coagulation	0.000	0.670	3.195	1.217	1.172	2.512
Fibrinogen gamma chain	Coagulation	0.000	1.078	4.296	3.304	3.982	4.900
Heparin cofactor 2	Coagulation	0.000	0.000	0.145	0.095	0.007	0.061
Histidine-rich glycoprotein	Coagulation	1.195	0.178	0.144	0.166	0.182	0.109
Kininogen-1	Coagulation	0.000	1.028	0.276	0.660	0.098	1.167
Prothrombin	Coagulation	0.103	0.091	1.698	1.154	1.211	1.064
C4b-binding protein alpha chain	Complement System	0.439	0.276	0.038	0.043	0.012	0.189
Complement C1q subcomponent subunit A	Complement System	0.000	0.000	0.030	0.272	0.043	0.045
Complement C1q subcomponent subunit B	Complement System	0.000	0.000	0.033	0.031	0.042	0.044

Complement C1q subcomponent subunit C	Complement System	0.041	0.000	0.567	0.484	0.517	0.583
Complement C1r subcomponent	Complement System	0.000	0.000	0.002	0.006	0.003	0.005
Complement C1s subcomponent	Complement System	0.000	0.000	3.869	3.780	4.269	2.530
Complement C3	Complement System	0.810	0.241	0.977	1.012	1.281	1.311
Complement C4-A	Complement System	1.586	0.039	0.046	0.106	0.051	0.096
Complement C4-B	Complement System	1.092	0.021	0.037	0.085	0.041	0.077
Complement component C8 beta chain	Complement System	0.000	0.000	0.203	0.163	0.120	0.122
Complement component C8 gamma chain	Complement System	0.000	0.000	0.161	0.128	0.156	0.114
Complement factor H	Complement System	0.139	1.934	0.081	0.164	0.129	0.252
Complement factor H-related protein 1	Complement System	0.000	0.000	0.060	0.045	0.012	0.042
Plasma protease C1 inhibitor	Complement System	0.225	0.131	0.206	0.267	0.120	0.309
Complement component C9	Complement system	0.053	0.011	0.058	0.066	0.009	0.196
Ig alpha-1 chain C region	Immunoglobulins	4.204	1.594	0.057	0.014	0.009	0.077
Ig alpha-2 chain C region	Immunoglobulins	0.358	0.147	0.051	0.043	0.035	0.053
Ig gamma-1 chain C region	Immunoglobulins	7.988	4.648	0.668	0.324	0.153	0.511
Ig gamma-2 chain C region	Immunoglobulins	2.144	1.361	36.128	29.904	38.247	30.879
Ig gamma-3 chain C region	Immunoglobulins	0.750	0.401	0.039	0.059	0.012	0.110
Ig gamma-4 chain C region	Immunoglobulins	1.024	0.400	0.064	0.079	0.088	0.068
Ig kappa chain C region	Immunoglobulins	9.168	7.079	3.129	3.561	5.873	2.773
Ig lambda-2 chain C regions	Immunoglobulins	5.033	1.184	0.194	0.082	0.044	0.163

Ig mu chain C region	Immunoglobulins	0.569	0.497	0.043	0.080	0.011	0.112
Ig mu heavy chain disease protein	Immunoglobulins	1.107	0.393	0.059	0.109	0.017	0.340
Immunoglobulin heavy variable 3-66	Immunoglobulins	0.000	0.060	9.267	8.283	10.194	6.099
Leukocyte- associated Ig-like receptor 1	Immunoglobulins	0.000	0.000	0.004	2.368	2.463	0.376
Apolipoprotein A-I	Lipoproteins	0.390	0.641	0.368	0.573	0.093	1.851
Apolipoprotein A-II	Lipoproteins	0.098	0.250	0.034	0.097	0.055	0.060
Apolipoprotein B-100	Lipoproteins	0.348	0.362	6.603	5.614	7.364	7.126
Apolipoprotein C-I	Lipoproteins	0.026	0.000	0.096	0.020	0.052	0.130
Apolipoprotein E	Lipoproteins	0.046	0.065	4.016	3.508	3.374	3.113
Apolipoprotein(a)	Lipoproteins	0.000	0.176	0.000	0.000	0.000	0.000
Clusterin	Lipoproteins	0.214	0.646	0.145	0.980	0.013	0.294
Serum paraoxonase/arylesterase 1	Lipoproteins	0.000	0.063	0.016	0.046	0.005	0.029
Aldo-keto reductase family 1 member C1	Other plasma components	0.000	0.400	0.145	0.115	0.171	0.191
Alpha-1-antichymotrypsin	Other plasma components	0.363	0.940	0.071	0.055	0.018	0.047
Alpha-2-HS-glycoprotein	Other plasma components	0.856	0.425	0.029	0.104	0.010	0.037
Desmoglein-1	Other plasma components	0.000	0.025	0.649	0.438	0.204	0.983
Glyceraldehyde-3-phosphate dehydrogenase	Other plasma components	0.000	0.267	0.116	0.091	0.019	0.133
Hemoglobin subunit beta	Other plasma components	0.348	0.077	0.013	0.013	0.000	0.024
Inter-alpha-trypsin inhibitor heavy chain H2	Other plasma components	0.123	0.000	0.002	0.011	0.003	0.011
Inter-alpha-trypsin inhibitor heavy chain H4	Other plasma components	0.128	0.000	0.068	0.257	0.062	0.119

Keratinocyte proline-rich protein	Other plasma components	0.000	0.065	0.604	0.316	0.053	0.286
Nectin-4	Other plasma components	0.000	0.049	0.561	0.686	0.206	1.039
Protein S100-A9	Other plasma components	0.000	0.050	0.195	0.134	0.216	0.526
Serotransferrin	Other plasma components	2.823	2.034	0.108	0.060	0.003	0.107
Serum albumin	Other plasma components	38.561	30.113	2.125	12.806	1.246	2.910
Transthyretin	Other plasma components	0.000	0.406	0.716	0.109	1.045	0.232
Trypsin 3	Other plasma components	0.000	0.051	2.700	2.790	2.507	2.452
Zinc-alpha-2-glycoprotein	Other plasma components	0.175	1.012	1.060	0.818	1.019	1.021
CD5 antigen-like	Tissue Leakage	0.042	0.011	0.247	0.229	0.111	0.866
Dermcidin	Tissue Leakage	0.000	0.077	0.876	0.273	0.213	0.628
Gelsolin	Tissue Leakage	0.082	0.000	0.015	0.109	0.016	0.022
Keratin , type I cytoskeletal 27	Tissue Leakage	0.000	0.263	2.438	1.871	2.694	1.695
Keratin, type I cuticular Ha1	Tissue Leakage	0.000	0.073	0.683	0.768	0.764	0.662
Keratin, type I cuticular Ha2	Tissue Leakage	0.000	0.000	0.051	0.039	0.060	0.052
Keratin, type I cuticular Ha5	Tissue Leakage	0.000	0.425	0.071	0.060	0.018	0.067
Keratin, type I cytoskeletal 12	Tissue Leakage	0.000	0.057	0.002	0.001	0.000	0.028
Keratin, type I cytoskeletal 18	Tissue Leakage	0.000	0.385	0.043	0.024	0.040	0.058
Keratin, type I cytoskeletal 19	Tissue Leakage	0.000	0.016	0.520	0.524	0.249	1.124
Keratin, type I cytoskeletal 24	Tissue Leakage	0.000	0.059	0.126	0.127	0.171	0.115
Keratin, type I cytoskeletal 27	Tissue Leakage	0.000	0.082	2.438	1.871	2.694	1.695

Keratin, type I cytoskeletal 28	Tissue Leakage	0.000	0.035	1.983	1.560	2.115	1.416
Keratin, type II cuticular Hb4	Tissue Leakage	0.000	0.037	0.439	0.473	0.459	0.596
Keratin, type II cytoskeletal 7	Tissue Leakage	0.000	0.035	0.057	0.030	0.012	0.077
Keratin, type II cytoskeletal 74	Tissue Leakage	0.000	0.001	0.005	0.013	0.000	0.009
Keratin, type II cytoskeletal 75	Tissue Leakage	0.000	0.178	0.511	0.278	0.118	1.406
Keratin, type II cytoskeletal 78	Tissue Leakage	0.000	0.003	0.379	0.402	0.243	3.894
Keratin, type II cytoskeletal 79	Tissue Leakage	0.000	0.238	0.287	0.261	0.040	0.226
Keratin, type II cytoskeletal 8	Tissue Leakage	0.000	0.480	1.402	0.895	1.084	1.247
Neurofilament heavy polypeptide	Tissue Leakage	0.000	0.014	0.106	0.066	0.030	0.236
Prolactin-inducible protein	Tissue Leakage	0.000	0.023	0.202	0.045	0.045	0.168
Vitronectin	Tissue Leakage	0.000	0.371	0.136	0.655	0.109	0.348

Chapter 8. Conclusion

An in-depth understanding of the biomaterial surface interaction mechanism with proteins and cells is necessary for the successful designing of future biomaterial surfaces with improved biocompatibility. Within this thesis, the effects of different physiochemical surface properties on selective protein adsorption from the whole serum, and the role of surface nanotopography on the protein conformational change and the resulting cellular immune response were investigated in-vitro. From each of the studies conducted on different surface properties, the hypothesis that nano-engineered, and tailored chemistry surfaces modulate the inflammatory response by controlling the surface-protein-cell interactions has been demonstrated to be correct.

A plasma polymerization technique was employed to create substrate independent model biomaterial surfaces. Plasma deposited methyl oxazoline (Me-PPOx) coatings and gold nanoparticles of different diameters were used to create well defined nanotopography surfaces. The effect of plasma deposition pressure on polymerization of oxazoline films on the film stability, chemical and biological interactions was extensively studied in **chapter 2.** These optimized plasma polymerization conditions were then used to generate precise surface nanotopography. To create nano-engineered biomaterials with well-defined surface descriptors, three different sized nearly monodispersed gold nanoparticles (16, 38, and 68 nm) were synthesized and functionalized with carboxylic acid groups. As shown in **chapter 3** these GNPs were covalently immobilized on Me-PPOx coated surfaces to generate an equal number density population of the different sized particles. The nanoparticle surface coverage was found to depend on the pH of the nanoparticle solution, concentrations of nanoparticles in suspension, and reaction time. An additional 5 nm thin polymer was deposited over the bound nanoparticle to provide uniform outermost surface chemistry and preserving the topography. TEM images of the GNP demonstrated nearly monodispersed spherical structure, AFM imaging was used to confirm the nanotopography modification, further image analysis clearly showed the equal number particle density and increasing roughness with an increase in the GNP size. ToF-SIMS principle component analysis of GNP bound to Me-PPOx surfaces before and after overcoating confirmed the pinhole-free coating and the uniform outermost chemistry of the surfaces.

The well-defined nanotopography surfaces created in **chapter 3** were then used to investigate the role of surface nanotopography in fibrinogen adsorption and unfolding

on integrin - cellular adhesion, and secretion of pro-inflammatory cytokines. Fibrinogen adsorption studies were conducted using QCM-D (Quartz crystal microbalance with dissipation), FRAP (fluorescent recovery after photobleaching) and calorimetric micro-BCA methods. The unfolding of adsorbed fibrinogen was investigated using circular dichroism spectroscopy and ELISA of recombinant protein fragment corresponding to amino acids on the unfolded regions. This study demonstrated the distinct protein unfolding patterns with nanotopography surfaces that upregulate or downregulate the expression of proinflammatory cytokines and Mac-1 positive THP-1 monocytes cells attachment. Nano features size of 68 nm increased immune cell binding and proinflammatory cytokine expression. The opposite was seen for 38 nm nanofeatures where the cell binding and proinflammatory cytokines expression was reduced. These findings are important not only because they shed the light on the missing link between surface nanotopography, protein unfolding, and immune responses but also because they demonstrate that carefully tailored surface nanotopography can be an effective means to direct inflammatory response and potentially the foreign body responses to implanted biomaterials.

In **chapter 5** the effect of different surface chemistry on selective adsorption of proteins from human serum and subsequent immune responses was investigated. Plasma polymerization surface engineering methods were employed to generate a range of model substrates with controlled chemistry. A range of different surface chemistry was created using the precursors of allylamine (AA) (NH3, hydrophilic), acrylic acid (AC) (COOH, hydrophilic), methyl oxazoline (MEOX) (C4H7NO, hydrophilic) and octadiene (OD) (CH3, hydrophobic). The surface chemical composition of the coatings was characterized by (XPS) and the wettability was analysed using a static water contact angle. The protein adsorption studies using liquid chromatography-mass spectrometry (LC-MS) and colorimetric protein assay, demonstrated the effect of hydrophobicity in the selectivity of serum protein adsorption. Enhanced dysopsonin albumin and opsonin IgG2 adsorption were observed on hydrophilic and hydrophobic surfaces, respectively. This, in turn, led to an increase in anti-inflammatory cytokine expression on the hydrophilic surfaces while pro-inflammatory cytokine production increased on hydrophobic surfaces. These results lead to fundamental insights that must be considered for future biomaterial design, to control the protein adsorption process to modulate innate immune responses and govern the fate of implantable biomedical devices.

Furthermore, the synergistic effect of nanoporous structures with surface chemistry modification on modulating the immune response was investigated in **chapter 6**. To study the role played by the combinational effect of nanoporous and surface chemistry, nanoporous surfaces of controlled pore size (30, 65 and 200 nm) and lateral spacing were created from nanoporous anodic alumina (NAA). Plasma polymerization techniques were then used to provide homogeneous outermost surface chemistry of amines, carboxyl, and hydrocarbon. Nano-structural modification was confirmed by SEM and the chemical modification was confirmed by employing XPS. The interplay between surface nanotopography and chemistry on the immune response from macrophages were then analysed using ELISA. The concentration of pro-inflammatory cytokines (TNFα, IL-6, and IL-1β) decreased significantly on nanoporous surfaces featuring large nanopores and having Meoxpp and ACpp surface coatings compared to surface with smaller pore sizes and chemistry. Furthermore, the concentration of anti-inflammatory cytokines (Arginase, IL-1RA, and IL-10) increased significantly on large nanoporous surfaces with Meoxpp and ACpp coatings. This study demonstrates that macrophage differentiation can be controlled by modulating pro-inflammatory and anti-inflammatory cytokines, by selecting desired combinations of surface nanoporosity and chemistry. The knowledge obtained from this study provides cues that could aid in tuning foreign body response and will eventually facilitate the rational design of biomaterial implants.

Finally, the effect of nanoparticle shape in protein adsorption to form different protein corona from human serum and plasma was studied. Two types of mesoporous silica nanoparticles which had identical chemistry, porosity, structure, surface potential and size in y-dimension, one being a sphere and the other a rod were synthesized. TEM and SEM imaging were used for the morphological characterization of the shape and XPS was used to confirm the chemical composition. Investigation of the protein corona by LC-MS and SDS – PAGE revealed very small amounts of adsorbed abundant proteins such as albumin and fibrinogen on both shapes. A significantly larger amount of protein adsorption from plasma and serum were observed on the rod-like particles compared to the spheres. Investigation of the protein corona by LC-MS and SDS – PAGE revealed shape-dependent differences in the adsorption of immunoglobulins on both protein solutions and albumin proteins from serum. This result suggests that there is a group of specialized proteins that can recognise and clear foreign objects simply based on invading objects' shape. Therefore, there is a need for further detailed studies to understand the

specific protein adsorption patterns on nanoparticles of different shapes and the conformational state of these proteins when they encounter objects of a certain geometry. Understanding these phenomena and the underlying process can have a profound implication on how we design nanoparticles for medical therapies.

8.1. Limitations and Future Work

Overall, this thesis demonstrates the importance of understanding the mechanism of interaction between surface -protein-cells for the successful designing of biomaterial surfaces. The systematic evaluation of various modifications such as those outlined in this thesis can endow development of advanced biomaterials with favourable biological responses.

In this thesis, THP-1 cell line was used as a macrophage model with which to study the immune responses from modifies biomaterials surfaces. Future studies should include primary macrophages and other cell types such as dendritic cells, lymphocytes, and neutrophils to be able to draw more general conclusions.

In **chapter 5**, serum protein adsorption on different chemistry's demonstrated a high amount of albumin and immunoglobulin adsorption. In **chapter 4**, the role of nanotopography in fibrinogen unfolding and subsequent immune response was reported. Therefore, future studies should aim to investigate the conformational changes of abundant serum proteins such as albumin and immunoglobulins and their role in modulating immune responses with different surface properties.

Furthermore, **chapter 6** demonstrated the combinational effect of nanoporous and different surface chemistry in modulating the immune responses. However, the synergetic effect of the well-defined nanotopography surface of different height reported in **chapter 3** needs to be studied for the combinational effect with different surface chemistries. These additional studies will provide more insight on the synergetic effect of chemistry and nanotopography in modulating macrophages response. Finally, in **chapter 7** the role of shape in protein adsorption was studied, additional experiments should be conducted to investigate the effect of shape in cellular uptake and immune responses. In addition to the immune system, osteoblast responses and osteointegration should be studied for the development of better biomaterial surfaces that provide favourable immune response and better bone or tissue integration.

Ultimately, this thesis begins working towards a catalogue of the effect of chemistry and nanostructures on protein interactions and subsequent biological responses. As research into the field continues, a substantial index of how chemistry and nanotopography can be applied in the biomaterial field to help modulate immune responses at the site of implant to enhance patient outcomes.

Chapter 9. Reference

1. Franz, S., et al., *Immune responses to implants – A review of the implications for the design of immunomodulatory biomaterials.* Biomaterials, 2011. **32**(28): p. 6692-6709.
2. Anderson, J.M., A. Rodriguez, and D.T. Chang, *Foreign body reaction to biomaterials.* Seminars in Immunology, 2008. **20**(2): p. 86-100.
3. Sheikh, Z., et al., *Macrophages, Foreign Body Giant Cells and Their Response to Implantable Biomaterials.* Materials, 2015. **8**(9): p. 5269.
4. Luttikhuizen, D.T., M.C. Harmsen, and M.J.V. Luyn, *Cellular and molecular dynamics in the foreign body reaction.* Tissue engineering, 2006. **12**(7): p. 1955-1970.
5. Anderson, J.M., *Multinucleated giant cells.* Current opinion in hematology, 2000. **7**(1): p. 40-47.
6. Anderson, J.M., *Biological responses to materials.* Annual Review of Materials Research, 2001. **31**(1): p. 81-110.
7. Gretzer, C., et al., *The inflammatory cell influx and cytokines changes during transition from acute inflammation to fibrous repair around implanted materials.* Journal of Biomaterials Science, Polymer Edition, 2006. **17**(6): p. 669-687.
8. Rajesh, P., et al., *Host Response of Implanted Biomaterials.* Biosurfaces: A Materials Science and Engineering Perspective, 2015: p. 106-125.
9. Thevenot, P., W. Hu, and L. Tang, *SURFACE CHEMISTRY INFLUENCE IMPLANT BIOCOMPATIBILITY.* Current topics in medicinal chemistry, 2008. **8**(4): p. 270-280.
10. Chen, Z., et al., *Nanotopography-based strategy for the precise manipulation of osteoimmunomodulation in bone regeneration.* Nanoscale, 2017.
11. Zheng, K., M. Kapp, and A.R. Boccaccini, *Protein interactions with bioactive glass surfaces: A review.* Applied Materials Today, 2019. **15**: p. 350-371.
12. Blaszykowski, C., S. Sheikh, and M. Thompson, *Surface chemistry to minimize fouling from blood-based fluids.* Chemical Society Reviews, 2012. **41**(17): p. 5599-5612.
13. Lord, M.S., M. Foss, and F. Besenbacher, *Influence of nanoscale surface topography on protein adsorption and cellular response.* Nano Today, 2010. **5**(1): p. 66-78.
14. Ngo, B.K.D. and M.A. Grunlan, *Protein Resistant Polymeric Biomaterials.* ACS Macro Letters, 2017: p. 992-1000.
15. Williams, D.F., *On the nature of biomaterials.* Biomaterials, 2009. **30**(30): p. 5897-5909.
16. Bagnall, R.D., *Implant biocompatibility.* Biomaterials, 1980. **1**(2): p. 97-99.
17. Khan, W., et al., *Implantable medical devices*, in *Focal controlled drug delivery*. 2014, Springer. p. 33-59.
18. Mariani, E., et al., *Biomaterials: Foreign Bodies or Tuners for the Immune Response?* International journal of molecular sciences, 2019. **20**(3): p. 636.
19. *Orthopedic implants market analysis, by application (spinal fusion, long bone, foot & ankle, craniomaxillofacial, joint replacement, dental), and segment forecasts to 2024*, in *Orthopedic Implants Market Size, Industry Report, 2024*. 2016, Grand View Research: San Francisco, United States. p. 80.
20. *Biomaterials market for implantable devices (material type-metals, polymers, ceramics and natural; applications-cardiology, orthopedics, dental, ophthalmology and others)global industry analysis, size, share, growth, trends and forecast 2013-2019.*, in *Biomaterials Market*. May 2014, Transparency Market ResearchMay 2014: United States. p. 117.
21. Saini, M., et al., *Implant biomaterials: A comprehensive review.* World Journal of Clinical Cases: WJCC, 2015. **3**(1): p. 52.
22. Boni, B.O.O., et al., *Immunomodulation and cellular response to biomaterials: the overriding role of neutrophils in healing.* Materials Horizons, 2019.
23. Vishwakarma, A., et al., *Engineering Immunomodulatory Biomaterials To Tune the Inflammatory Response.* Trends in Biotechnology, 2016. **34**(6): p. 470-482.

24. Vroman, L., et al., *Interaction of high molecular weight kininogen, factor XII, and fibrinogen.* Blood, 1980. **55**(1): p. 156-9.
25. Jenney, C.R. and J.M. Anderson, *Adsorbed IgG: a potent adhesive substrate for human macrophages.* Journal of biomedical materials research, 2000. **50**(3): p. 281-290.
26. Brodbeck, W.G., E. Colton, and J.M. Anderson, *Effects of adsorbed heat labile serum proteins and fibrinogen on adhesion and apoptosis of monocytes/macrophages on biomaterials.* Journal of Materials Science: Materials in Medicine, 2003. **14**(8): p. 671-675.
27. Jenney, C.R. and J.M. Anderson, *Adsorbed serum proteins responsible for surface dependent human macrophage behavior.* Journal of Biomedical Materials Research, 2000. **49**(4): p. 435-447.
28. Milleret, V., et al., *Protein adsorption steers blood contact activation on engineered cobalt chromium alloy oxide layers.* Acta biomaterialia, 2015. **24**: p. 343-351.
29. Sridharan, R., et al., *Biomaterial based modulation of macrophage polarization: a review and suggested design principles.* Materials Today, 2015. **18**(6): p. 313-325.
30. Zdolsek, J., J.W. Eaton, and L. Tang, *Histamine release and fibrinogen adsorption mediate acute inflammatory responses to biomaterial implants in humans.* J Transl Med, 2007. **5**(1): p. 31-36.
31. Tang, L., T.A. Jennings, and J.W. Eaton, *Mast cells mediate acute inflammatory responses to implanted biomaterials.* Proceedings of the National Academy of Sciences, 1998. **95**(15): p. 8841-8846.
32. Chomarat, P. and J. Banchereau, *Interleukin-4 and Interleukin-13: Their Similarities and Discrepancies.* International reviews of immunology, 1998. **17**(1-4): p. 1-52.
33. Murthy, T., et al., *Biological response modifiers.* Int J Pharm Tech Res, 2010. **2**: p. 2152-2160.
34. Kwee, B.J. and D.J. Mooney, *Manipulating the Intersection of Angiogenesis and Inflammation.* Annals of biomedical engineering, 2015. **43**(3): p. 628-640.
35. Hu, W.-J., et al., *Molecular basis of biomaterial-mediated foreign body reactions.* Blood, 2001. **98**(4): p. 1231-1238.
36. Wooley, P.H. and N.J. Hallab, *Wound Healing, Chronic Inflammation, and Immune Responses*, in *Metal-on-Metal Bearings*. 2014, Springer. p. 109-133.
37. Grainger, D.W., *All charged up about implanted biomaterials.* Nat Biotech, 2013. **31**(6): p. 507-509.
38. Williams, D., *Tissue-biomaterial interactions.* Journal of Materials science, 1987. **22**(10): p. 3421-3445.
39. Donnelly, H., et al., *Current approaches for modulation of the nanoscale interface in the regulation of cell behavior.* Nanomedicine: Nanotechnology, Biology and Medicine, 2017.
40. Kunzler, T.P., et al., *Systematic study of osteoblast and fibroblast response to roughness by means of surface-morphology gradients.* Biomaterials, 2007. **28**(13): p. 2175-2182.
41. Dalby, M.J., et al., *Changes in fibroblast morphology in response to nano-columns produced by colloidal lithography.* Biomaterials, 2004. **25**(23): p. 5415-5422.
42. Christo, S.N., et al., *Innate immunity and biomaterials at the nexus: friends or foes.* BioMed research international, 2015. **2015**.
43. Rostam, H.M., et al., *Impact of surface chemistry and topography on the function of antigen presenting cells.* Biomaterials Science, 2015. **3**(3): p. 424-441.
44. Chen, Z., et al., *Tuning chemistry and topography of nanoengineered surfaces to manipulate immune response for bone regeneration applications.* ACS nano, 2017. **11**(5): p. 4494-4506.

45. Scatena, M., et al., *Macrophages: The bad, the ugly, and the good in the inflammatory response to biomaterials*, in *The immune response to implanted materials and devices*. 2017, Springer. p. 37-62.
46. Rayahin, J.E. and R.A. Gemeinhart, *Activation of Macrophages in response to biomaterials*, in *Macrophages*. 2017, Springer. p. 317-351.
47. Brown, B.N., et al., *Macrophage polarization: an opportunity for improved outcomes in biomaterials and regenerative medicine.* Biomaterials, 2012. **33**(15): p. 3792-3802.
48. Janeway Jr, C.A. and R. Medzhitov, *Innate immune recognition.* Annual review of immunology, 2002. **20**(1): p. 197-216.
49. Koh, T.J. and L.A. DiPietro, *Inflammation and wound healing: the role of the macrophage.* Expert reviews in molecular medicine, 2011. **13**.
50. Martinez, F.O., et al., *Macrophage activation and polarization.* Front Biosci, 2008. **13**(1): p. 453-461.
51. Mosser, D.M. and J.P. Edwards, *Exploring the full spectrum of macrophage activation.* Nature reviews immunology, 2008. **8**(12): p. 958.
52. Rahmati, M. and M. Mozafari, *Protein adsorption on polymers.* Materials Today Communications, 2018. **17**: p. 527-540.
53. Lord, M.S., et al., *Fibrinogen adsorption and platelet adhesion to silica surfaces with stochastic nanotopography.* Biointerphases, 2014. **9**(4): p. 1-11.
54. Anderson, J.M., T.L. Bonfield, and N.P. Ziats, *Protein adsorption and cellular adhesion and activation on biomedical polymers.* Int J Artif Organs, 1990. **13**(6): p. 375-82.
55. Shen, M., et al., *Effects of adsorbed proteins and surface chemistry on foreign body giant cell formation, tumor necrosis factor alpha release and procoagulant activity of monocytes.* J Biomed Mater Res A, 2004. **70**(4): p. 533-41.
56. Andrade, J.D. and V. Hlady, *Plasma protein adsorption: the big twelve.* Ann N Y Acad Sci, 1987. **516**: p. 158-72.
57. Nath, N., et al., *Surface engineering strategies for control of protein and cell interactions.* Surface Science, 2004. **570**(1): p. 98-110.
58. Pankowsky, D.A., et al., *Morphologic characteristics of adsorbed human plasma proteins on vascular grafts and biomaterials.* J Vasc Surg, 1990. **11**(4): p. 599-606.
59. Heuberger, M., T. Drobek, and N.D. Spencer, *Interaction forces and morphology of a protein-resistant poly(ethylene glycol) layer.* Biophys J, 2005. **88**(1): p. 495-504.
60. Evans-Nguyen, K.M., et al., *Changes in adsorbed fibrinogen upon conversion to fibrin.* Langmuir, 2006. **22**(11): p. 5115-21.
61. Collier, T.O. and J.M. Anderson, *Protein and surface effects on monocyte and macrophage adhesion, maturation, and survival.* J Biomed Mater Res, 2002. **60**(3): p. 487-96.
62. Lu, D.R. and K. Park, *Effect of surface hydrophobicity on the conformational changes of adsorbed fibrinogen.* Journal of colloid and interface science, 1991. **144**(1): p. 271-281.
63. Lenk, T.J., et al., *Infrared spectroscopic studies of time-dependent changes in fibrinogen adsorbed to polyurethanes.* Langmuir, 1991. **7**(8): p. 1755-1764.
64. Chinn, J.A., et al., *Postadsorptive transitions in fibrinogen adsorbed to polyurethanes: changes in antibody binding and sodium dodecyl sulfate elutability.* J Biomed Mater Res, 1992. **26**(6): p. 757-78.
65. Rapoza, R.J. and T.A. Horbett, *Changes in the SDS elutability of fibrinogen adsorbed from plasma to polymers.* J Biomater Sci Polym Ed, 1989. **1**(2): p. 99-110.
66. Takahara, A., et al., *Plasma protein adsorption behavior onto the surface of phase-separated organosilane monolayers on the basis of scanning force microscopy.* Colloids and Surfaces B: Biointerfaces, 2002. **23**(2): p. 141-152.

67. Gettens, R.T., Z. Bai, and J.L. Gilbert, *Quantification of the kinetics and thermodynamics of protein adsorption using atomic force microscopy.* J Biomed Mater Res A, 2005. **72**(3): p. 246-57.
68. Schaaf, P. and P. Dejardin, *Structural changes within an adsorbed fibrinogen layer during the adsorption process: a study by scanning angle reflectometry.* Colloids and surfaces, 1988. **31**: p. 89-103.
69. Ladam, G., et al., *Protein adsorption onto auto-assembled polyelectrolyte films.* Biomol Eng, 2002. **19**(2-6): p. 273-80.
70. Deng, Z.J., et al., *Nanoparticle-induced unfolding of fibrinogen promotes Mac-1 receptor activation and inflammation.* Nature nanotechnology, 2011. **6**(1): p. 39-44.
71. Blaszykowski, C., S. Sheikh, and M. Thompson, *Biocompatibility and antifouling: is there really a link?* Trends in biotechnology, 2014. **32**(2): p. 61-62.
72. Sheikh, Z., et al., *Macrophages, Foreign Body Giant Cells and Their Response to Implantable Biomaterials.* Materials, 2015. **8**(9): p. 5671-5701.
73. Shiba, E., et al., *Antibody-detectable changes in fibrinogen adsorption affecting platelet activation on polymer surfaces.* Am J Physiol, 1991. **260**(5 Pt 1): p. C965-74.
74. Deng, Z.J., et al., *Nanoparticle-induced unfolding of fibrinogen promotes Mac-1 receptor activation and inflammation.* Nat Nano, 2011. **6**(1): p. 39-44.
75. Ugarova, T.P., et al., *Conformational changes in fibrinogen elicited by its interaction with platelet membrane glycoprotein GPIIb-IIIa.* J Biol Chem, 1993. **268**(28): p. 21080-7.
76. Tang, L. and W. Hu, *Molecular determinants of biocompatibility.* Expert Rev Med Devices, 2005. **2**(4): p. 493-500.
77. Wang, Y.X., et al., *Effects of the chemical structure and the surface properties of polymeric biomaterials on their biocompatibility.* Pharm Res, 2004. **21**(8): p. 1362-73.
78. Horbett, T.A. and K.R. Lew, *Residence time effects on monoclonal antibody binding to adsorbed fibrinogen.* J Biomater Sci Polym Ed, 1994. **6**(1): p. 15-33.
79. Wilson, C.J., et al., *Mediation of biomaterial-cell interactions by adsorbed proteins: a review.* Tissue Eng, 2005. **11**(1-2): p. 1-18.
80. Roach, P., D. Farrar, and C.C. Perry, *Interpretation of protein adsorption: surface-induced conformational changes.* Journal of the American Chemical Society, 2005. **127**(22): p. 8168-8173.
81. Clarke, M.L., J. Wang, and Z. Chen, *Conformational changes of fibrinogen after adsorption.* J Phys Chem B, 2005. **109**(46): p. 22027-35.
82. Gallagher, W.M., et al., *Molecular basis of cell-biomaterial interaction: insights gained from transcriptomic and proteomic studies.* Biomaterials, 2006. **27**(35): p. 5871-82.
83. Andorko, J.I. and C.M. Jewell, *Designing biomaterials with immunomodulatory properties for tissue engineering and regenerative medicine.* Bioengineering & translational medicine, 2017. **2**(2): p. 139-155.
84. Nair, A. and L. Tang. *Influence of scaffold design on host immune and stem cell responses*. in *Seminars in immunology*. 2017. Elsevier.
85. Mosesson, M., *Fibrinogen and fibrin structure and functions.* Journal of Thrombosis and Haemostasis, 2005. **3**(8): p. 1894-1904.
86. Lomakina, E.B. and R.E. Waugh, *Micromechanical tests of adhesion dynamics between neutrophils and immobilized ICAM-1.* Biophysical journal, 2004. **86**(2): p. 1223-1233.
87. Jhunjhunwala, S., *Neutrophils at the biological–material interface.* ACS Biomaterials Science & Engineering, 2017. **4**(4): p. 1128-1136.
88. Morais, J.M., F. Papadimitrakopoulos, and D.J. Burgess, *Biomaterials/tissue interactions: possible solutions to overcome foreign body response.* Aaps j, 2010. **12**(2): p. 188-96.
89. Papenburg, B.J., et al., *Insights into the role of material surface topography and wettability on cell-material interactions.* Soft Matter, 2010. **6**(18): p. 4377-4388.

90. Christo, S.N., et al., *Innate Immunity and Biomaterials at the Nexus: Friends or Foes.* BioMed Research International, 2015. **2015**: p. 23.
91. Tang, L., P. Thevenot, and W. Hu, *Surface chemistry influences implant biocompatibility.* Current topics in medicinal chemistry, 2008. **8**(4): p. 270-280.
92. Wang, W., et al., *Predicting Nano–Bio Interactions by Integrating Nanoparticle Libraries and Quantitative Nanostructure Activity Relationship Modeling.* ACS Nano, 2017.
93. Liu, X., et al., *Surface Chemical Gradient Affects the Differentiation of Human Adipose-Derived Stem Cells via ERK1/2 Signaling Pathway.* ACS applied materials & interfaces, 2015. **7**(33): p. 18473-18482.
94. Hartvig, R.A., et al., *Protein Adsorption at Charged Surfaces: The Role of Electrostatic Interactions and Interfacial Charge Regulation.* Langmuir, 2011. **27**(6): p. 2634-2643.
95. Lu, H.H., S.R. Pollack, and P. Ducheyne, *45S5 Bioactive glass surface charge variations and the formation of a surface calcium phosphate layer in a solution containing fibronectin.* Journal of Biomedical Materials Research: An Official Journal of The Society for Biomaterials and The Japanese Society for Biomaterials, 2001. **54**(3): p. 454-461.
96. Lee, W.-H., C.-Y. Loo, and R. Rohanizadeh, *A review of chemical surface modification of bioceramics: effects on protein adsorption and cellular response.* Colloids and Surfaces B: Biointerfaces, 2014. **122**: p. 823-834.
97. Rabe, M., D. Verdes, and S. Seeger, *Understanding protein adsorption phenomena at solid surfaces.* Advances in Colloid and Interface Science, 2011. **162**(1–2): p. 87-106.
98. Mano, J.F., *Stimuli-responsive polymeric systems for biomedical applications.* Advanced Engineering Materials, 2008. **10**(6): p. 515-527.
99. Kessel, A. and N. Ben-Tal, *Introduction to proteins: structure, function, and motion*. 2010: CRC Press.
100. Krajewski, A., R. Malavolti, and A. Piancastelli, *Albumin adhesion on some biological and non-biological glasses and connection with their Z-potentials.* Biomaterials, 1996. **17**(1): p. 53-60.
101. Wang, K., et al., *A review of protein adsorption on bioceramics.* Interface focus, 2012. **2**(3): p. 259-277.
102. Wilson, C.J., et al., *Mediation of biomaterial–cell interactions by adsorbed proteins: a review.* Tissue engineering, 2005. **11**(1-2): p. 1-18.
103. Dalton, B.A., et al., *Polymer surface chemistry and bone cell migration.* Journal of Biomaterials Science, Polymer Edition, 1998. **9**(8): p. 781-799.
104. Damsky, C.H., et al., *The solid state environment orchestrates embryonic development and tissue remodeling.* Kidney international, 1997. **51**(5): p. 1427-1433.
105. Seiffert, D. and J.W. Smith, *The cell adhesion domain in plasma vitronectin is cryptic.* Journal of Biological Chemistry, 1997. **272**(21): p. 13705-13710.
106. Ruckenstein, E. and Z.F. Li, *Surface modification and functionalization through the self-assembled monolayer and graft polymerization.* Adv Colloid Interface Sci, 2005. **113**(1): p. 43-63.
107. Arima, Y. and H. Iwata, *Effect of wettability and surface functional groups on protein adsorption and cell adhesion using well-defined mixed self-assembled monolayers.* Biomaterials, 2007. **28**(20): p. 3074-82.
108. Michelmore, A., et al., *Surface Morphology in the Early Stages of Plasma Polymer Film Growth from Amine-Containing Monomers.* Plasma Processes and Polymers, 2011. **8**(5): p. 367-372.
109. Vasilev, K., et al., *Early stages of growth of plasma polymer coatings deposited from nitrogen-and oxygen-containing monomers.* Plasma Processes and Polymers, 2010. **7**(9-10): p. 824-835.

110. Macgregor, M. and K. Vasilev, *Perspective on Plasma Polymers for Applied Biomaterials Nanoengineering and the Recent Rise of Oxazolines.* Materials, 2019. **12**(1): p. 191.
111. Vasilev, K., et al., *Substrate influence on the initial growth phase of plasma-deposited polymer films.* Chem. Commun., 2009(24): p. 3600-3602.
112. Ostrikov, K.K., U. Cvelbar, and A.B. Murphy, *Plasma nanoscience: setting directions, tackling grand challenges.* Journal of Physics D: Applied Physics, 2011. **44**(17): p. 174001.
113. Friedrich, J., *Mechanisms of plasma polymerization–reviewed from a chemical point of view.* Plasma Processes and Polymers, 2011. **8**(9): p. 783-802.
114. Vasilev, K., *Nanoengineered plasma polymer films for biomaterial applications.* Plasma Chemistry and Plasma Processing, 2014. **34**(3): p. 545-558.
115. Ramiasa, M., et al., *Plasma polymerised polyoxazoline thin films for biomedical applications.* Chemical Communications, 2015. **51**(20): p. 4279-4282.
116. Hegemann, D., et al., *Stable, nanometer-thick oxygen-containing plasma polymer films suited for enhanced biosensing.* Plasma Processes and Polymers, 2018. **15**(11): p. 1800090.
117. Christo, S.N., et al., *The role of surface nanotopography and chemistry on primary neutrophil and macrophage cellular responses.* Advanced healthcare materials, 2016. **5**(8): p. 956-965.
118. Coad, B.R., et al., *Functionality of proteins bound to plasma polymer surfaces.* ACS applied materials & interfaces, 2012. **4**(5): p. 2455-2463.
119. Harding, F.J., et al., *Assessing embryonic stem cell response to surface chemistry using plasma polymer gradients.* Acta biomaterialia, 2012. **8**(5): p. 1739-1748.
120. Murray, P., et al., *The potential of small chemical functional groups for directing the differentiation of kidney stem cells*. 2010, Portland Press Limited.
121. Bachhuka, A., et al., *Nanotopography mediated osteogenic differentiation of human dental pulp derived stem cells.* Nanoscale, 2017. **9**(37): p. 14248-14258.
122. Bachhuka, A., et al., *Effect of surface chemical functionalities on collagen deposition by primary human dermal fibroblasts.* ACS applied materials & interfaces, 2015. **7**(42): p. 23767-23775.
123. Delalat, B., et al., *Materials displaying neural growth factor gradients and applications in neural differentiation of embryoid body cells.* Advanced Functional Materials, 2015. **25**(18): p. 2737-2744.
124. Vasilev, K., et al., *Creating gradients of two proteins by differential passive adsorption onto a PEG-density gradient.* Biomaterials, 2010. **31**(3): p. 392-397.
125. Goreham, R.V., R.D. Short, and K. Vasilev, *Method for the generation of surface-bound nanoparticle density gradients.* The Journal of Physical Chemistry C, 2011. **115**(8): p. 3429-3433.
126. Taheri, S., et al., *Binding of nanoparticles to aminated plasma polymer surfaces is controlled by primary amine density and solution PH.* The Journal of Physical Chemistry C, 2018. **122**(26): p. 14986-14995.
127. Christo, S., et al., *The contribution of inflammasome components on macrophage response to surface nanotopography and chemistry.* Scientific reports, 2016. **6**.
128. Bazaka, K., et al., *Plasma-assisted surface modification of organic biopolymers to prevent bacterial attachment.* Acta biomaterialia, 2011. **7**(5): p. 2015-2028.
129. Vasilev, K., S.S. Griesser, and H.J. Griesser, *Antibacterial surfaces and coatings produced by plasma techniques.* Plasma Processes and Polymers, 2011. **8**(11): p. 1010-1023.
130. Dalby, M.J., et al., *Increasing Fibroblast Response to Materials Using Nanotopography: Morphological and Genetic Measurements of Cell Response to 13-nm-High Polymer Demixed Islands.* Experimental Cell Research, 2002. **276**(1): p. 1-9.

131. Emerich, D.F. and C. Halberstadt, *32 - Nanotechnology's Impact on Cell Transplantation*, in *Cellular Transplantation*. 2007, Academic Press: Burlington. p. 611-627.
132. Zhang, L. and T. Webster, *17 - Nanotopography of biomaterials for controlling cancer cell function A2 - Park, Kinam*, in *Biomaterials for Cancer Therapeutics*. 2013, Woodhead Publishing. p. 461-488e.
133. Park, J., et al., *Directed migration of cancer cells guided by the graded texture of the underlying matrix.* Nature materials, 2016. **15**(7): p. 792-801.
134. Tsui, J.H., et al., *Harnessing Sphingosine-1-Phosphate Signaling and Nanotopographical Cues To Regulate Skeletal Muscle Maturation and Vascularization.* ACS Nano, 2017.
135. Wang, P.-Y., et al., *Modulation of PEI-Mediated Gene Transfection through Controlling Cytoskeleton Organization and Nuclear Morphology via Nanogrooved Topographies.* ACS Biomaterials Science & Engineering, 2017.
136. Song, H., et al., *Plasmid DNA Delivery: Nanotopography Matters.* Journal of the American Chemical Society, 2017.
137. Korrapati, P.S., et al., *Recent advancements in nanotechnological strategies in selection, design and delivery of biomolecules for skin regeneration.* Materials Science and Engineering: C, 2016. **67**(Supplement C): p. 747-765.
138. Venugopal, J. and S. Ramakrishna, *Biocompatible nanofiber matrices for the engineering of a dermal substitute for skin regeneration.* Tissue engineering, 2005. **11**(5-6): p. 847-854.
139. Onesto, V., et al., *Nano-topography Enhances Communication in Neural Cells Networks.* Scientific Reports, 2017. **7**(1): p. 9841.
140. Chang, Y.-C., et al., *Multichanneled Nerve Guidance Conduit with Spatial Gradients of Neurotrophic Factors and Oriented Nanotopography for Repairing the Peripheral Nervous System.* ACS Applied Materials & Interfaces, 2017. **9**(43): p. 37623-37636.
141. MacGregor-Ramiasa, M., et al., *Surface nanotopography guides kidney-derived stem cell differentiation into podocytes.* Acta Biomaterialia, 2017. **56**: p. 171-180.
142. Qian, W., et al., *Nanotopographic Regulation of Human Mesenchymal Stem Cell Osteogenesis.* ACS Applied Materials & Interfaces, 2017.
143. Nobbs, A.H., et al., *Towards the cell-instructive bactericidal substrate: exploring the combination of nanotopographical features and integrin selective synthetic ligands.* Scientific Reports, 2017. **7**(1): p. 16363.
144. Chowdhury, N.R., et al., *Influence of nanotopography and chemistry on bacterial surface colonisation.* Chemeca 2016: Chemical Engineering-Regeneration, Recovery and Reinvention, 2016: p. 745.
145. Yang, G., et al., *Capturing Circulating Tumor Cells through a Combination of Hierarchical Nanotopography and Surface Chemistry.* ACS Biomaterials Science & Engineering, 2017.
146. Tsai, Y.-T., et al., *Topologically Controlled Cell Differentiation Based on Vapor-Deposited Polymer Coatings.* Langmuir, 2017. **33**(36): p. 8943-8949.
147. Deng, J., et al., *Nanopatterned Adhesive, Stretchable Hydrogel to Control Ligand Spacing and Regulate Cell Spreading and Migration.* ACS Nano, 2017. **11**(8): p. 8282-8291.
148. Charras, G. and E. Sahai, *Physical influences of the extracellular environment on cell migration.* Nature reviews Molecular cell biology, 2014. **15**(12): p. 813-824.
149. Taskin, M.B., et al., *Nanotopography Featured Polycaprolactone/Polyethyleneoxide Microfibers Modulates Endothelial Cell Response.* Nanoscale, 2017.
150. Harvey, A.G., E.W. Hill, and A. Bayat, *Designing implant surface topography for improved biocompatibility.* Expert Review of Medical Devices, 2013. **10**(2): p. 257-267.

151. Christo, S.N., et al., *The Role of Surface Nanotopography and Chemistry on Primary Neutrophil and Macrophage Cellular Responses.* Advanced healthcare materials, 2016.
152. Gonzalez Garcia, L.E., et al., *Protein Interactions with Nanoengineered Polyoxazoline Surfaces Generated via Plasma Deposition.* Langmuir, 2017. **33**(29): p. 7322-7331.
153. Lord, M., et al., *The effect of silica nanoparticulate coatings on serum protein adsorption and cellular response.* Biomaterials, 2006. **27**(28): p. 4856-4862.
154. Dolatshahi-Pirouz, A., et al., *The influence of glancing angle deposited nano-rough platinum surfaces on the adsorption of fibrinogen and the proliferation of primary human fibroblasts.* Nanotechnology, 2009. **20**(9): p. 095101.
155. Dolatshahi-Pirouz, A., et al., *Bovine serum albumin adsorption on nano-rough platinum surfaces studied by QCM-D.* Colloids and Surfaces B: Biointerfaces, 2008. **66**(1): p. 53-59.
156. Ainslie, K.M., et al., *Attenuation of protein adsorption on static and oscillating magnetostrictive nanowires.* Nano letters, 2005. **5**(9): p. 1852-1856.
157. Ainslie, K.M., et al., *In vitro inflammatory response of nanostructured titania, silicon oxide, and polycaprolactone.* Journal of Biomedical Materials Research Part A: An Official Journal of The Society for Biomaterials, The Japanese Society for Biomaterials, and The Australian Society for Biomaterials and the Korean Society for Biomaterials, 2009. **91**(3): p. 647-655.
158. Smith, B.S., et al., *Reduced in vitro immune response on titania nanotube arrays compared to titanium surface.* Biomaterials Science, 2013. **1**(3): p. 322-332.
159. Lü, W.L., et al., *Effects of anodic titanium dioxide nanotubes of different diameters on macrophage secretion and expression of cytokines and chemokines.* Cell Proliferation, 2015. **48**(1): p. 95-104.
160. Jin, S., et al., *Macrophage inflammatory response to TiO 2 nanotube surfaces.* Journal of Biomaterials and Nanobiotechnology, 2011. **2**(03): p. 293.
161. Mohiuddin, M., et al., *Control of growth and inflammatory response of macrophages and foam cells with nanotopography.* Nanoscale Research Letters, 2012. **7**(1): p. 1-9.
162. Bachhuka, A., et al., *The interplay between surface nanotopography and chemistry modulates collagen I and III deposition by human dermal fibroblasts.* ACS applied materials & interfaces, 2017. **9**(7): p. 5874-5884.
163. Macgregor-Ramiasa, M.N., A.A. Cavallaro, and K. Vasilev, *Properties and reactivity of polyoxazoline plasma polymer films.* Journal of Materials Chemistry B, 2015. **3**(30): p. 6327-6337.
164. Li, D., et al., *Combining surface topography with polymer chemistry: exploring new interfacial biological phenomena.* Polymer Chemistry, 2014. **5**(1): p. 14-24.
165. Nguyen, V.H. and B.-J. Lee, *Protein corona: a new approach for nanomedicine design.* International Journal of Nanomedicine, 2017. **12**: p. 3137-3151.
166. Huang, Y., et al., *Competitive protein adsorption on biomaterial surface studied with reflectometric interference spectroscopy.* Acta Biomaterialia, 2010. **6**(6): p. 2083-2090.
167. Smith, B.S., et al., *Hemocompatibility of titania nanotube arrays.* Journal of biomedical materials research Part A, 2010. **95**(2): p. 350-360.
168. Chen, Z., et al., *Nanoporous microstructures mediate osteogenesis by modulating the osteo-immune response of macrophages.* Nanoscale, 2017. **9**(2): p. 706-718.
169. Pujari, S., et al., *Effects of nanoporous alumina on inflammatory cell response.* Journal of Biomedical Materials Research Part A, 2014. **102**(11): p. 3773-3780.
170. Anderson, J.M., A. Rodriguez, and D.T. Chang. *Foreign body reaction to biomaterials*. in *Seminars in immunology*. 2008. Elsevier.
171. Morais, J.M., F. Papadimitrakopoulos, and D.J. Burgess, *Biomaterials/tissue interactions: possible solutions to overcome foreign body response.* The AAPS journal, 2010. **12**(2): p. 188-196.

172. Hernandez-Lopez, J., et al., *Functional polymers as nanoscopic building blocks.* Materials Science and Engineering: C, 2003. **23**(1): p. 267-274.
173. Chu, P.K., et al., *Plasma-surface modification of biomaterials.* Materials Science and Engineering: R: Reports, 2002. **36**(5–6): p. 143-206.
174. Wang, T.F., et al., *Corrosion protection of cold-rolled steel by low temperature plasma interface engineering.* Progress in Organic Coatings, 1996. **28**(4): p. 291-297.
175. Farrugia, B.L., et al., *Poly (2-oxazoline) hydrogels for controlled fibroblast attachment.* Biomacromolecules, 2013. **14**(8): p. 2724-2732.
176. Konradi, R., C. Acikgoz, and M. Textor, *Polyoxazolines for nonfouling surface coatings—a direct comparison to the gold standard PEG.* Macromolecular rapid communications, 2012. **33**(19): p. 1663-1676.
177. Adams, N. and U.S. Schubert, *Poly (2-oxazolines) in biological and biomedical application contexts.* Advanced Drug Delivery Reviews, 2007. **59**(15): p. 1504-1520.
178. Cavallaro, A.A., M.N. Macgregor-Ramiasa, and K. Vasilev, *Antibiofouling Properties of Plasma-Deposited Oxazoline-Based Thin Films.* ACS Applied Materials & Interfaces, 2016. **8**(10): p. 6354-6362.
179. Bachhuka, A., et al., *Hybrid core/shell microparticles and their use for understanding biological processes.* Journal of Colloid and Interface Science, 2015. **457**: p. 9-17.
180. Turkevich, J., P.C. Stevenson, and J. Hillier, *A study of the nucleation and growth processes in the synthesis of colloidal gold.* Discussions of the Faraday Society, 1951. **11**: p. 55-75.
181. Zhu, T., et al., *Surface Modification of Citrate-Reduced Colloidal Gold Nanoparticles with 2-Mercaptosuccinic Acid.* Langmuir, 2003. **19**(22): p. 9518-9525.
182. MacNeil, S., J. Shepherd, and L. Smith, *Production of tissue-engineered skin and oral mucosa for clinical and experimental use.* 3D Cell Culture: Methods and Protocols, 2011: p. 129-153.
183. Taheri, S., et al., *Substrate independent silver nanoparticle based antibacterial coatings.* Biomaterials, 2014. **35**(16): p. 4601-4609.
184. Hazrati, H.D., J.D. Whittle, and K. Vasilev, *A mechanistic study of the plasma polymerization of ethanol.* Plasma Processes and Polymers, 2014. **11**(2): p. 149-157.
185. Michelmore, A., et al., *The link between mechanisms of deposition and the physico-chemical properties of plasma polymer films.* Soft Matter, 2013. **9**(26): p. 6167-6175.
186. Lv, L., et al., *Biomaterial Cues Regulate Epigenetic State and Cell Functions—A Systematic Review.* Tissue Engineering Part B: Reviews, 2017.
187. Anselme, K., A. Ponche, and M. Bigerelle, *Relative influence of surface topography and surface chemistry on cell response to bone implant materials. Part 2: biological aspects.* Proceedings of the Institution of Mechanical Engineers, Part H: Journal of Engineering in Medicine, 2010. **224**(12): p. 1487-1507.
188. Schulte, C., et al., *Quantitative Control of Protein and Cell Interaction with Nanostructured Surfaces by Cluster Assembling.* Accounts of Chemical Research, 2017. **50**(2): p. 231-239.
189. Biggs, M.J.P., R.G. Richards, and M.J. Dalby, *Nanotopographical modification: a regulator of cellular function through focal adhesions.* Nanomedicine: Nanotechnology, Biology and Medicine, 2010. **6**(5): p. 619-633.
190. Sato, M. and T.J. Webster, *Nanobiotechnology: implications for the future of nanotechnology in orthopedic applications.* Expert review of medical devices, 2004. **1**(1): p. 105-114.
191. Ngandu Mpoyi, E., et al., *Protein Adsorption as a Key Mediator in the Nanotopographical Control of Cell Behavior.* ACS Nano, 2016. **10**(7): p. 6638-6647.

192. Malekian, B., et al., *A Method for Investigation of Size-Dependent Protein Binding to Nanoholes Using Intrinsic Fluorescence of Proteins.* ACS Omega, 2017. **2**(8): p. 4772-4778.
193. Macgregor, M., et al., *The Role of Controlled Surface Topography and Chemistry on Mouse Embryonic Stem Cell Attachment, Growth and Self-Renewal.* Materials, 2017. **10**(9): p. 1081.
194. Bettinger, C.J., R. Langer, and J.T. Borenstein, *Engineering substrate topography at the micro-and nanoscale to control cell function.* Angewandte Chemie International Edition, 2009. **48**(30): p. 5406-5415.
195. Guadarrama Bello, D., et al., *A nanoporous titanium surface promotes the maturation of focal adhesions and formation of filopodia with distinctive nanoscale protrusions by osteogenic cells.* Acta Biomaterialia, 2017. **60**(Supplement C): p. 339-349.
196. Kim, H.N., et al., *Artificial Slanted Nanocilia Array as a Mechanotransducer for Controlling Cell Polarity.* ACS Nano, 2017. **11**(1): p. 730-741.
197. Chaudhuri, P.K., et al., *Differential Depth Sensing Reduces Cancer Cell Proliferation via Rho-Rac-Regulated Invadopodia.* ACS Nano, 2017. **11**(7): p. 7336-7348.
198. Ko, J.-Y., et al., *Nanotopographic Influence on the In Vitro Behavior of Induced Pluripotent Stem Cells.* Tissue Engineering Part A, 2017.
199. Bachhuka, A., et al., *Nanotopography mediated osteogenic differentiation of human dental pulp derived stem cells.* Nanoscale, 2017.
200. Bhardwaj, G. and T.J. Webster, *Reduced bacterial growth and increased osteoblast proliferation on titanium with a nanophase TiO2 surface treatment.* International journal of nanomedicine, 2017. **12**: p. 363.
201. Mano, J.F., I.S. Choi, and A. Khademhosseini, *Biomimetic Interfaces in Biomedical Devices.* Advanced Healthcare Materials, 2017. **6**(15): p. 1700761-n/a.
202. Norman, J.J. and T.A. Desai, *Methods for fabrication of nanoscale topography for tissue engineering scaffolds.* Annals of biomedical engineering, 2006. **34**(1): p. 89-101.
203. MacGregor-Ramiasa, M.N. and K. Vasilev, *Questions and Answers on the Wettability of Nano-Engineered Surfaces.* Advanced Materials Interfaces, 2017.
204. Arregui, F.J., et al., *Optical fiber sensors based on nanostructured coatings*, in *Sensors Based on Nanostructured Materials*. 2009, Springer. p. 275-301.
205. Zhang, J., et al., *Nanostructured Materials for Room-Temperature Gas Sensors.* Advanced Materials, 2016. **28**(5): p. 795-831.
206. Arico, A.S., et al., *Nanostructured materials for advanced energy conversion and storage devices.* Nature materials, 2005. **4**(5): p. 366.
207. Visalakshan, R.M., et al., *Downstream influences of oxazoline plasma polymerisation conditions on chemical and biological interactions.* Chemeca 2016: Chemical Engineering-Regeneration, Recovery and Reinvention, 2016: p. 840.
208. MacGregor-Ramiasa, M., et al., *Plasma deposited polyoxazoline coatings, a versatile new class of biomaterials.* Chemeca 2016: Chemical Engineering-Regeneration, Recovery and Reinvention, 2016: p. 302.
209. Zanini, S., et al., *Plasma polymerized 2-ethyl-2-oxazoline: Chemical characterization and study of the reactivity towards different chemical groups.* Materials & Design, 2016. **108**: p. 791-800.
210. Goreham, R.V., et al., *A substrate independent approach for generation of surface gradients.* Thin Solid Films, 2013. **528**: p. 106-110.
211. Vasilev, K., et al., *Solvent-Induced Porosity in Ultrathin Amine Plasma Polymer Coatings.* The Journal of Physical Chemistry B, 2008. **112**(35): p. 10915-10921.
212. Goreham, R.V., et al., *Small surface nanotopography encourages fibroblast and osteoblast cell adhesion.* Rsc Advances, 2013. **3**(26): p. 10309-10317.

213. Levich, V.G. and R.J. Seeger, *Physicochemical hydrodynamics.* American Journal of Physics, 1963. **31**(11): p. 892-892.
214. Collins, F.C. and G.E. Kimball, *Diffusion-controlled reaction rates.* Journal of colloid science, 1949. **4**(4): p. 425-437.
215. Gregory, J., *Approximate expressions for retarded van der waals interaction.* Journal of Colloid and Interface Science, 1981. **83**(1): p. 138-145.
216. Hogg, R., T.W. Healy, and D.W. Fuerstenau, *Mutual coagulation of colloidal dispersions.* Transactions of the Faraday Society, 1966. **62**(0): p. 1638.
217. Ruckenstein, E. and D.C. Prieve, *Adsorption and desorption of particles and their chromatographic separation.* AIChE Journal, 1976. **22**(2): p. 276-283.
218. Van Oss, C.J., M.K. Chaudhury, and R.J. Good, *Interfacial Lifshitz-van der Waals and polar interactions in macroscopic systems.* Chemical Reviews, 1988. **88**(6): p. 927-941.
219. Bradford, S.A., et al., *Contributions of Nanoscale Roughness to Anomalous Colloid Retention and Stability Behavior.* Langmuir, 2017. **33**(38): p. 10094-10105.
220. Sasidharan, S., et al., *Coupled effects of hydrodynamic and solution chemistry on long-term nanoparticle transport and deposition in saturated porous media.* Colloids and Surfaces a-Physicochemical and Engineering Aspects, 2014. **457**: p. 169-179.
221. Królikowska, A. and J. Bukowska, *Self-assembled monolayers of mercaptosuccinic acid on silver and gold surfaces designed for protein binding. Part I: structure of the monolayer.* Journal of Raman Spectroscopy, 2007. **38**(7): p. 936-942.
222. Pfeiffer, C., et al., *Interaction of colloidal nanoparticles with their local environment: the (ionic) nanoenvironment around nanoparticles is different from bulk and determines the physico-chemical properties of the nanoparticles.* Journal of The Royal Society Interface, 2014. **11**(96): p. 20130931.
223. Liu, X.-Q. and R.-Z. Tang, *Biological responses to nanomaterials: understanding nano-bio effects on cell behaviors.* Drug delivery, 2017. **24**(2): p. 1-15.
224. Onesto, V., et al., *Nano-topography Enhances Communication in Neural Cells Networks.* Scientific reports, 2017. **7**(1): p. 9841.
225. Gerecht, S., et al., *The effect of actin disrupting agents on contact guidance of human embryonic stem cells.* Biomaterials, 2007. **28**(28): p. 4068-4077.
226. Rebollar, E., et al., *Proliferation of aligned mammalian cells on laser-nanostructured polystyrene.* Biomaterials, 2008. **29**(12): p. 1796-1806.
227. Anderson, J.M. and S. Jiang, *Implications of the Acute and Chronic Inflammatory Response and the Foreign Body Reaction to the Immune Response of Implanted Biomaterials*, in *The Immune Response to Implanted Materials and Devices: The Impact of the Immune System on the Success of an Implant*, B. Corradetti, Editor. 2017, Springer International Publishing: Cham. p. 15-36.
228. Lynch, I., A. Salvati, and K.A. Dawson, *Protein-nanoparticle interactions: what does the cell see?* Nature nanotechnology, 2009. **4**(9): p. 546-547.
229. Serpooshan, V., et al., *Protein Corona Influences Cell–Biomaterial Interactions in Nanostructured Tissue Engineering Scaffolds.* Advanced Functional Materials, 2015. **25**(28): p. 4379-4389.
230. Mahmoudi, M., et al., *Irreversible changes in protein conformation due to interaction with superparamagnetic iron oxide nanoparticles.* Nanoscale, 2011. **3**(3): p. 1127-1138.
231. Walczyk, D., et al., *What the Cell "Sees" in Bionanoscience.* Journal of the American Chemical Society, 2010. **132**(16): p. 5761-5768.
232. Simon, J., et al., *Hydrophilicity Regulates the Stealth Properties of Polyphosphoester-Coated Nanocarriers.* Angewandte Chemie International Edition, 2018. **57**(19): p. 5548-5553.
233. Ramiasa-MacGregor, M., et al., *Tuning and predicting the wetting of nanoengineered material surface.* Nanoscale, 2016. **8**(8): p. 4635-4642.

234. Ngo, B.K.D. and M.A. Grunlan, *Protein Resistant Polymeric Biomaterials.* ACS Macro Letters, 2017. **6**(9): p. 992-1000.
235. Hench, L.L. and I. Thompson, *Twenty-first century challenges for biomaterials.* Journal of the Royal Society Interface, 2010. **7**(suppl_4): p. S379-S391.
236. Thiele, L., et al., *Competitive adsorption of serum proteins at microparticles affects phagocytosis by dendritic cells.* Biomaterials, 2003. **24**(8): p. 1409-1418.
237. Warkentin, P., et al., *Differential surface binding of albumin, immunoglobulin G and fibrinogen.* Biomaterials, 1994. **15**(10): p. 786-795.
238. Zhang, Z., et al., *Blood compatibility of surfaces with superlow protein adsorption.* Biomaterials, 2008. **29**(32): p. 4285-4291.
239. Fabrizius-Homan, D.J. and S.L. Cooper, *A comparison of the adsorption of three adhesive proteins to biomaterial surfaces.* Journal of Biomaterials Science, Polymer Edition, 1992. **3**(1): p. 27-47.
240. Bale, M., et al., *Identification of vitronectin as a major plasma protein adsorbed on polymer surfaces of different copolymer composition.* Blood, 1989. **74**(8): p. 2698-2706.
241. Horbett, T.A., *Principles underlying the role of adsorbed plasma proteins in blood interactions with foreign materials.* Cardiovascular Pathology, 1993. **2**(3): p. 137-148.
242. Visalakshan, R.M., et al., *Nanotopography-Induced Unfolding of Fibrinogen Modulates Leukocyte Binding and Activation.* Advanced Functional Materials, 2019: p. 1807453.
243. Christo, S., et al., *The contribution of inflammasome components on macrophage response to surface nanotopography and chemistry.* Scientific reports, 2016. **6**: p. 26207.
244. Visalakshan, R.M., et al., *Creating Nano-engineered Biomaterials with Well-Defined Surface Descriptors.* ACS Applied Nano Materials, 2018. **1**(6): p. 2796-2807.
245. Mierczynska-Vasilev, A., et al., *Magnetic separation technology: Functional group efficiency in the removal of haze-forming proteins from wines.* Food Chemistry, 2019. **275**: p. 154-160.
246. Smith, L.E., et al., *Haptotatic Plasma Polymerized Surfaces for Rapid Tissue Regeneration and Wound Healing.* ACS applied materials & interfaces, 2016. **8**(48): p. 32675-32687.
247. Mei, K.C., et al., *Protein-Corona-by-Design in 2D: A Reliable Platform to Decode Bio–Nano Interactions for the Next-Generation Quality-by-Design Nanomedicines.* Advanced Materials, 2018. **30**(40): p. 1802732.
248. Schöttler, S., et al., *Protein adsorption is required for stealth effect of poly (ethylene glycol)-and poly (phosphoester)-coated nanocarriers.* Nature nanotechnology, 2016. **11**(4): p. 372-377.
249. Tenzer, S., et al., *Rapid formation of plasma protein corona critically affects nanoparticle pathophysiology.* Nature nanotechnology, 2013. **8**(10): p. 772.
250. Ritz, S., et al., *Protein Corona of Nanoparticles: Distinct Proteins Regulate the Cellular Uptake.* Biomacromolecules, 2015. **16**(4): p. 1311-1321.
251. Jeyachandran, Y.L., et al., *Quantitative and Qualitative Evaluation of Adsorption/Desorption of Bovine Serum Albumin on Hydrophilic and Hydrophobic Surfaces.* Langmuir, 2009. **25**(19): p. 11614-11620.
252. Kim, J. and G.A. Somorjai, *Molecular packing of lysozyme, fibrinogen, and bovine serum albumin on hydrophilic and hydrophobic surfaces studied by infrared− visible sum frequency generation and fluorescence microscopy.* Journal of the American Chemical Society, 2003. **125**(10): p. 3150-3158.
253. Krisdhasima, V., P. Vinaraphong, and J. McGuire, *Adsorption Kinetics and Elutability of α-Lactalbumin, β-Casein, β-Lactoglobulin, and Bovine Serum Albumin at Hydrophobic and Hydrophilic Interfaces.* Journal of Colloid and Interface Science, 1993. **161**(2): p. 325-334.

254. Brynda, E., N. Cepalova, and M. Štol, *Equilibrium adsorption of human serum albumin and human fibrinogen on hydrophobic and hydrophilic surfaces.* Journal of biomedical materials research, 1984. **18**(6): p. 685-693.
255. Wertz, C.F. and M.M. Santore, *Effect of surface hydrophobicity on adsorption and relaxation kinetics of albumin and fibrinogen: single-species and competitive behavior.* Langmuir, 2001. **17**(10): p. 3006-3016.
256. Malmsten, M., *Ellipsometry studies of the effects of surface hydrophobicity on protein adsorption.* Colloids and Surfaces B: Biointerfaces, 1995. **3**(5): p. 297-308.
257. Chanput, W., et al., *Transcription profiles of LPS-stimulated THP-1 monocytes and macrophages: a tool to study inflammation modulating effects of food-derived compounds.* Food & Function, 2010. **1**(3): p. 254-261.
258. Chanput, W., J.J. Mes, and H.J. Wichers, *THP-1 cell line: An in vitro cell model for immune modulation approach.* International Immunopharmacology, 2014. **23**(1): p. 37-45.
259. Leonard, F., et al., *Macrophage polarization contributes to the anti-Tumoral efficacy of Mesoporous Nanovectors loaded with albumin-bound Paclitaxel.* Frontiers in immunology, 2017. **8**: p. 693.
260. Yang, J., et al., *Monocyte and macrophage differentiation: circulation inflammatory monocyte as biomarker for inflammatory diseases.* Biomarker research, 2014. **2**(1): p. 1.
261. Absolom, D.R., *[13] Opsonins and dysopsonins: An overview*, in *Methods in Enzymology*. 1986, Academic Press. p. 281-318.
262. Newton, K. and V.M. Dixit, *Signaling in innate immunity and inflammation.* Cold Spring Harbor perspectives in biology, 2012. **4**(3): p. a006049.
263. Saha, K., et al., *Regulation of macrophage recognition through the interplay of nanoparticle surface functionality and protein corona.* ACS nano, 2016. **10**(4): p. 4421-4430.
264. Lundqvist, M., et al., *Nanoparticle size and surface properties determine the protein corona with possible implications for biological impacts.* Proc Natl Acad Sci, 2008. **105**(38): p. 14265-70.
265. Vu, V.P., et al., *Immunoglobulin deposition on biomolecule corona determines complement opsonization efficiency of preclinical and clinical nanoparticles.* Nature Nanotechnology, 2019. **14**(3): p. 260-268.
266. Torché, A.-M., et al., *PLGA Microspheres Phagocytosis by Pig Alveolar Macrophages: Influence of Polyvinyl alcohol) Concentration, Nature of Loaded-Protein and Copolymer Nature.* Journal of drug targeting, 1999. **7**(5): p. 343-354.
267. Matsuda, T., et al., *the Blood Interface With Segmented Polyurethanes::"multilayered Protein Passivation Mechanism".* ASAIO Journal, 1984. **30**(1): p. 353-358.
268. Chang, T., *Platelet–surface interaction: effect of albumin coating or heparin complexing on thrombogenic surfaces.* Canadian journal of physiology and pharmacology, 1974. **52**(2): p. 275-285.
269. Chanput, W., et al., *Characterization of polarized THP-1 macrophages and polarizing ability of LPS and food compounds.* Food & Function, 2013. **4**(2): p. 266-276.
270. Vroman, L., et al., *Interaction of high molecular weight kininogen, factor XII, and fibrinogen in plasma at interfaces.* Blood, 1980. **55**(1): p. 156-159.
271. Hirsh, S.L., et al., *The Vroman effect: Competitive protein exchange with dynamic multilayer protein aggregates.* Colloids and Surfaces B: Biointerfaces, 2013. **103**: p. 395-404.
272. Nimeri, G., et al., *The influence of plasma proteins and platelets on oxygen radical production and F-actin distribution in neutrophils adhering to polymer surfaces.* Biomaterials, 2002. **23**(8): p. 1785-1795.

273. Nimeri, G., et al., *Oxygen radical production in neutrophils interacting with platelets and surface-immobilized plasma proteins: Role of tyrosine phosphorylation.* Journal of Biomedical Materials Research Part A, 2003. **67A**(2): p. 439-447.
274. Wetterö, J., T. Bengtsson, and P. Tengvall, *Complement activation on immunoglobulin G-coated hydrophobic surfaces enhances the release of oxygen radicals from neutrophils through an actin-dependent mechanism.* Journal of Biomedical Materials Research, 2000. **51**(4): p. 742-751.
275. Lynn, A.D., T.R. Kyriakides, and S.J. Bryant, *Characterization of the in vitro macrophage response and in vivo host response to poly(ethylene glycol)-based hydrogels.* Journal of Biomedical Materials Research Part A, 2010. **93A**(3): p. 941-953.
276. Zhao, Q., et al., *Foreign-body giant cells and polyurethane biostability: In vivo correlation of cell adhesion and surface cracking.* Journal of Biomedical Materials Research, 1991. **25**(2): p. 177-183.
277. Martinez, F.O., et al., *Macrophage activation and polarization.* Front Biosci, 2008. **13**: p. 453-61.
278. Mosser, D.M., *The many faces of macrophage activation.* Journal of Leukocyte Biology, 2003. **73**(2): p. 209-212.
279. Mantovani, A., et al., *The chemokine system in diverse forms of macrophage activation and polarization.* Trends in Immunology, 2004. **25**(12): p. 677-686.
280. Martinez, F.O., L. Helming, and S. Gordon, *Alternative Activation of Macrophages: An Immunologic Functional Perspective.* Annual Review of Immunology, 2009. **27**(1): p. 451-483.
281. Ferraz, N., et al., *Nanoporosity of alumina surfaces induces different patterns of activation in adhering monocytes/macrophages.* International journal of biomaterials, 2010. **2010**.
282. Lamers, E., et al., *In vitro and in vivo evaluation of the inflammatory response to nanoscale grooved substrates.* Nanomedicine : nanotechnology, biology, and medicine, 2012. **8**(3): p. 308-317.
283. Rosso, F., et al., *Smart materials as scaffolds for tissue engineering.* Journal of Cellular Physiology, 2005. **203**(3): p. 465-470.
284. Santos, A., et al., *Drug-releasing implants: current progress, challenges and perspectives.* Journal of Materials Chemistry B, 2014. **2**(37): p. 6157-6182.
285. La Flamme, K.E., et al., *Biocompatibility of nanoporous alumina membranes for immunoisolation.* Biomaterials, 2007. **28**(16): p. 2638-2645.
286. Popat, K.C., et al., *Influence of nanoporous alumina membranes on long-term osteoblast response.* Biomaterials, 2005. **26**(22): p. 4516-4522.
287. Swan, E.E.L., K.C. Popat, and T.A. Desai, *Peptide-immobilized nanoporous alumina membranes for enhanced osteoblast adhesion.* Biomaterials, 2005. **26**(14): p. 1969-1976.
288. Popat, K.C., et al., *Osteogenic differentiation of marrow stromal cells cultured on nanoporous alumina surfaces.* Journal of biomedical materials research Part A, 2007. **80**(4): p. 955-964.
289. Karlsson, M., et al., *Initial in vitro interaction of osteoblasts with nano-porous alumina.* Biomaterials, 2003. **24**(18): p. 3039-3046.
290. Michelmore, A., et al., *Surface Morphology in the Early Stages of Plasma Polymer Film Growth from Amine-Containing Monomers.* Plasma Processes and Polymers, 2011. **8**(5): p. 367-372.
291. Vasilev, K., et al., *Substrate influence on the initial growth phase of plasma-deposited polymer films.* Chemical communications, 2009(24): p. 3600-3602.

292. von Keudell, A. and J. Benedikt, *A physicist's perspective on "views on macroscopic kinetics of plasma polymerisation".* Plasma Processes and Polymers, 2010. **7**(5): p. 376-379.
293. Gleason, K.K., *A chemical engineering perspective on "Views on macroscopic kinetics of plasma polymerisation".* Plasma Processes and Polymers, 2010. **7**(5): p. 380-381.
294. Rinsch, C.L., et al., *Pulsed radio frequency plasma polymerization of allyl alcohol: Controlled deposition of surface hydroxyl groups.* LANGMUIR, 1996. **12**(12): p. 2995-3002.
295. Michelmore, A., et al., *Nanoscale deposition of chemically functionalised films via plasma polymerisation.* Rsc Advances, 2013. **3**(33): p. 13540-13557.
296. Masuda, H. and K. Fukuda, *Ordered metal nanohole arrays made by a two-step replication of honeycomb structures of anodic alumina.* science, 1995. **268**(5216): p. 1466-1468.
297. Nielsch, K., et al., *Self-ordering regimes of porous alumina: the 10 porosity rule.* Nano letters, 2002. **2**(7): p. 677-680.
298. Lee, W. and S.-J. Park, *Porous anodic aluminum oxide: anodization and templated synthesis of functional nanostructures.* Chemical reviews, 2014. **114**(15): p. 7487-7556.
299. Santos, A., T. Kumeria, and D. Losic, *Nanoporous anodic aluminum oxide for chemical sensing and biosensors.* TrAC Trends in Analytical Chemistry, 2013. **44**: p. 25-38.
300. Kamath, S., et al., *Surface chemistry influences implant-mediated host tissue responses.* Journal of Biomedical Materials Research Part A, 2008. **86**(3): p. 617-626.
301. Barbosa, J.N., et al., *The influence of functional groups of self-assembled monolayers on fibrous capsule formation and cell recruitment.* Journal of Biomedical Materials Research Part A: An Official Journal of The Society for Biomaterials, The Japanese Society for Biomaterials, and The Australian Society for Biomaterials and the Korean Society for Biomaterials, 2006. **76**(4): p. 737-743.
302. Damanik, F.F.R., et al., *Towards an in vitro model mimicking the foreign body response: tailoring the surface properties of biomaterials to modulate extracellular matrix.* Scientific Reports, 2014. **4**: p. 6325.
303. Roach, P., et al., *Modern biomaterials: a review—bulk properties and implications of surface modifications.* Journal of Materials Science: Materials in Medicine, 2007. **18**(7): p. 1263-1277.
304. Chen, C.Z. and M. Raghunath, *Focus on collagen: in vitro systems to study fibrogenesis and antifibrosis _ state of the art.* Fibrogenesis & Tissue Repair, 2009. **2**(1): p. 7.
305. Holt, D.J. and D.W. Grainger, *Multinucleated giant cells from fibroblast cultures.* Biomaterials, 2011. **32**(16): p. 3977-3987.
306. Kamath, S., et al., *Surface chemistry influences implant-mediated host tissue responses.* Journal of Biomedical Materials Research Part A, 2008. **86A**(3): p. 617-626.
307. Eaton, J.W. and L. Tang, *Inflammatory Responses to Biomaterials.* American Journal of Clinical Pathology, 1995. **103**(4): p. 466-471.
308. Moreira, M., et al., *The effect of liposome-delivered prednisolone on collagen density, myofibroblasts, and fibrous capsule thickness around silicone breast implants in rats.* Wound Repair and Regeneration, 2010. **18**(4): p. 417-425.
309. Avula, M., et al., *Local release of masitinib alters in vivo implantable continuous glucose sensor performance.* Biosensors and Bioelectronics, 2016. **77**: p. 149-156.
310. Kastellorizios, M., F. Papadimitrakopoulos, and D.J. Burgess, *Multiple tissue response modifiers to promote angiogenesis and prevent the foreign body reaction around subcutaneous implants.* Journal of Controlled Release, 2015. **214**: p. 103-111.
311. Shin, Y.N., et al., *Adhesion comparison of human bone marrow stem cells on a gradient wettable surface prepared by corona treatment.* Applied Surface Science, 2008. **255**(2): p. 293-296.

312. Liu, X., et al., *Surface modification by allylamine plasma polymerization promotes osteogenic differentiation of human adipose-derived stem cells.* ACS applied materials & interfaces, 2014. **6**(12): p. 9733-9741.
313. Liu, X., et al., *Surface chemical functionalities affect the behavior of human adipose-derived stem cells in vitro.* Applied Surface Science, 2013. **270**: p. 473-479.
314. Hulander, M., et al., *Immune complement activation is attenuated by surface nanotopography.* International Journal of Nanomedicine, 2011. **2011**(Journal Article): p. 2653-2666.
315. Liu, X., et al., *The co-effect of surface topography gradient fabricated via immobilization of gold nanoparticles and surface chemistry via deposition of plasma polymerized film of allylamine/acrylic acid on osteoblast-like cell behavior.* Applied Surface Science, 2019. **473**: p. 838-847.
316. De Jong, W.H. and P.J. Borm, *Drug delivery and nanoparticles: applications and hazards.* International journal of nanomedicine, 2008. **3**(2): p. 133.
317. Petros, R.A. and J.M. DeSimone, *Strategies in the design of nanoparticles for therapeutic applications.* Nature reviews Drug discovery, 2010. **9**(8): p. 615.
318. Wang, Y., et al., *Mesoporous silica nanoparticles in drug delivery and biomedical applications.* Nanomedicine: Nanotechnology, Biology and Medicine, 2015. **11**(2): p. 313-327.
319. Ma, Z., et al., *Impact of shape and pore size of mesoporous silica nanoparticles on serum protein adsorption and RBCs hemolysis.* ACS applied materials & interfaces, 2014. **6**(4): p. 2431-2438.
320. Tang, F., L. Li, and D. Chen, *Mesoporous silica nanoparticles: synthesis, biocompatibility and drug delivery.* Advanced materials, 2012. **24**(12): p. 1504-1534.
321. Johnston, H.J., et al., *A review of the in vivo and in vitro toxicity of silver and gold particulates: particle attributes and biological mechanisms responsible for the observed toxicity.* Critical reviews in toxicology, 2010. **40**(4): p. 328-346.
322. Mo, J., et al., *Revealing the immune perturbation of black phosphorus nanomaterials to macrophages by understanding the protein corona.* Nature communications, 2018. **9**(1): p. 2480.
323. Escamilla-Rivera, V., et al., *Protein corona acts as a protective shield against Fe3O4-PEG inflammation and ROS-induced toxicity in human macrophages.* Toxicology letters, 2016. **240**(1): p. 172-184.
324. Lazarovits, J., et al., *Nanoparticle–blood interactions: the implications on solid tumour targeting.* Chemical Communications, 2015. **51**(14): p. 2756-2767.
325. Tenzer, S., et al., *Nanoparticle Size Is a Critical Physicochemical Determinant of the Human Blood Plasma Corona: A Comprehensive Quantitative Proteomic Analysis.* ACS Nano, 2011. **5**.
326. Gräfe, C., et al., *Intentional formation of a protein corona on nanoparticles: serum concentration affects protein corona mass, surface charge, and nanoparticle–cell interaction.* The international journal of biochemistry & cell biology, 2016. **75**: p. 196-202.
327. Kurtz-Chalot, A., et al., *Impact of silica nanoparticle surface chemistry on protein corona formation and consequential interactions with biological cells.* Materials Science and Engineering: C, 2017. **75**: p. 16-24.
328. Schöttler, S., et al., *Protein source and choice of anticoagulant decisively affect nanoparticle protein corona and cellular uptake.* Nanoscale, 2016. **8**(10): p. 5526-5536.
329. Dasgupta, S., T. Auth, and G. Gompper, *Shape and orientation matter for the cellular uptake of nonspherical particles.* Nano letters, 2014. **14**(2): p. 687-693.
330. Truong, N.P., et al., *The importance of nanoparticle shape in cancer drug delivery.* Expert opinion on drug delivery, 2015. **12**(1): p. 129-142.

331. Cho, E.C., et al., *The effects of size, shape, and surface functional group of gold nanostructures on their adsorption and internalization by cells.* Small, 2010. **6**(4): p. 517-522.
332. Geng, Y., et al., *Shape effects of filaments versus spherical particles in flow and drug delivery.* Nature nanotechnology, 2007. **2**(4): p. 249.
333. Champion, J.A. and S. Mitragotri, *Role of target geometry in phagocytosis.* Proceedings of the National Academy of Sciences, 2006. **103**(13): p. 4930-4934.
334. Florez, L., et al., *How shape influences uptake: interactions of anisotropic polymer nanoparticles and human mesenchymal stem cells.* Small, 2012. **8**(14): p. 2222-2230.
335. Janát-Amsbury, M., et al., *Geometry and surface characteristics of gold nanoparticles influence their biodistribution and uptake by macrophages.* European Journal of Pharmaceutics and Biopharmaceutics, 2011. **77**(3): p. 417-423.
336. Gratton, S.E., et al., *The effect of particle design on cellular internalization pathways.* Proceedings of the National Academy of Sciences, 2008. **105**(33): p. 11613-11618.
337. Trewyn, B.G., et al., *Biocompatible mesoporous silica nanoparticles with different morphologies for animal cell membrane penetration.* Chemical Engineering Journal, 2008. **137**(1): p. 23-29.
338. Benzigar, M.R., et al., *Highly Crystalline Mesoporous C60 with Ordered Pores: A Class of Nanomaterials for Energy Applications.* Angewandte Chemie, 2018. **130**(2): p. 578-582.
339. Lakhi, K.S., et al., *Morphological control of mesoporous CN based hybrid materials and their excellent CO 2 adsorption capacity.* RSC Advances, 2015. **5**(50): p. 40183-40192.
340. Gagner, J.E., et al., *Effect of gold nanoparticle morphology on adsorbed protein structure and function.* Biomaterials, 2011. **32**(29): p. 7241-7252.
341. Cedervall, T., et al., *Understanding the nanoparticle–protein corona using methods to quantify exchange rates and affinities of proteins for nanoparticles.* Proceedings of the National Academy of Sciences, 2007. **104**(7): p. 2050-2055.
342. Lindman, S., et al., *Systematic investigation of the thermodynamics of HSA adsorption to N-iso-propylacrylamide/N-tert-butylacrylamide copolymer nanoparticles. Effects of particle size and hydrophobicity.* Nano letters, 2007. **7**(4): p. 914-920.
343. Moghimi, S.M. and A.C. Hunter, *Recognition by macrophages and liver cells of opsonized phospholipid vesicles and phospholipid headgroups.* Pharmaceutical research, 2001. **18**(1): p. 1-8.
344. Lesniak, A., et al., *Effects of the Presence or Absence of a Protein Corona on Silica Nanoparticle Uptake and Impact on Cells.* ACS Nano, 2012. **6**.
345. Van Hong Nguyen, B.-J.L., *Protein corona: a new approach for nanomedicine design.* International journal of nanomedicine, 2017. **12**: p. 3137.
346. Cai, R. and C. Chen, *The Crown and the Scepter: Roles of the Protein Corona in Nanomedicine.* Advanced Materials, 2018: p. 1805740.
347. Vu, V.P., et al., *Immunoglobulin deposition on biomolecule corona determines complement opsonization efficiency of preclinical and clinical nanoparticles.* Nature Nanotechnology, 2019.
348. Gao, H. and Q. He, *The interaction of nanoparticles with plasma proteins and the consequent influence on nanoparticles behavior.* Expert Opinion on Drug Delivery, 2014. **11**(3): p. 409-420.
349. Göppert, T. and R. Müller, *Adsorption kinetics of plasma proteins on solid lipid nanoparticles for drug targeting.* International journal of pharmaceutics, 2005. **302**(1-2): p. 172-186.
350. Camner, P., et al., *Experimental and calculated parameters on particle phagocytosis by alveolar macrophages.* Journal of Applied Physiology, 2002. **92**(6): p. 2608-2616.
351. Benzigar, M.R., et al., *Ordered Mesoporous C70 with Highly Crystalline Pore Walls for Energy Applications.* Advanced Functional Materials, 2018. **28**(35): p. 1803701.

352. Lakhi, K.S., et al., *Energy efficient synthesis of highly ordered mesoporous carbon nitrides with uniform rods and their superior CO 2 adsorption capacity.* Journal of Materials Chemistry A, 2017. **5**(31): p. 16220-16230.
353. Benzigar, M.R., et al., *Recent advances in functionalized micro and mesoporous carbon materials: synthesis and applications.* Chemical Society Reviews, 2018. **47**(8): p. 2680-2721.